AJNTS

ALBANIAN JOURNAL OF NATURAL AND TECHNICAL SCIENCES

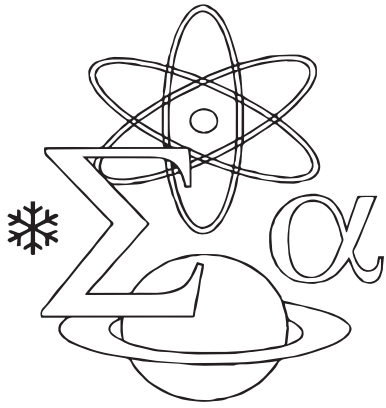

2026

30 (**2**)

PUBLISHED BY ACADEMY OF SCIENCES OF ALBANIA

PUBLISHED BY THE ACADEMY OF SCIENCES OF ALBANIA

AJNTS

ALBANIAN JOURNAL OF NATURAL AND TECHNICAL SCIENCES

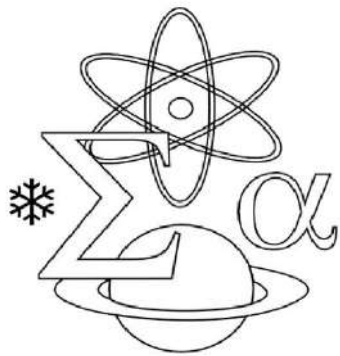

2026
30 (2)

Aims and Scope
This Journal is a multidisciplinary publication devoted to all field of Natural and Technical Sciences. The Editor of AJNTS invites original contributions which should comprise previously unpublished results, data and interpretations. Types of contributions to be published are: (1) research papers; (2) shorts communications; (3) reviews; (4) discussions; (5) book reviews;(6) announcements

ISSN 2074-0867

EISSN 3135-1115

Graphic by: Dorina Muka, Printed by “Akademia”

C O N T E N T S

ROBOT MOTION PLANNING WITH LARGE LANGUAGE MODELS: LANGUAGE-TO-PATHS GUIDANCE OVER SUPERFACETS

Evis PLAKU[1] **and Nikolla CIVICI**[2]

[1,2] Faculty of Computer Sciences and IT, University Metropolitan Tirana, Albania

Author for correspondence: evis.plaku@umt.edu.al

EP, 0009-0002-4042-2673; NC, 0000-0002-0378-8783

ABSTRACT

Robots operating in cluttered environments must compute collision-free motions under nonholonomic dynamics while maintaining fast, reliable planning. This article presents a language-guided motion-planning framework built on a visibility-aware superfacet decomposition, which partitions free space into navigable regions connected by a region graph. A large language model (LLM) converts natural-language preferences into a constrained domain-specific language (DSL) containing route, waypoint, constraint, and parameter hints. Each hint is validated by an affordance/feasibility gate that enforces connectivity and visibility, rejects unreachable suggestions, accounts for recent failures, and bounds updates. Validated hints softly bias inter-region costs and sampling priorities, while kinodynamic rollouts and collision checking determine final feasibility. Experiments with car-like and snake-like robots in cluttered 2D scenes show an approximately 18% reduction in mean planning time and fewer dead-end explorations relative to the superfacet baseline. The framework maintains comparable success rates and path quality, demonstrating that natural-language guidance can be integrated without increasing computational overhead. This makes the framework practical for non-expert operators to direct robot navigation without knowledge of the underlying planning mechanics.

***Keywords*:** language-guided motion planning, superfacet decomposition, sampling-based planning

Publisher: Academy of Sciences of Albania

Citation: **Plaku E, Civici N. 2026.** Robot motion planning with large language models: Language-to-paths guidance over superfacets *Albanian Journal of Natural and Technical Sciences* (*AJNTS),* **2 (30),**
Journal URL: https://journals-akad.gov.al/magazines/1
Classification: Research
Subject Category: Formal sciences + Applied Sciences subject areas: Robotics + Autonomous Systems

1. INTRODUCTION

Robot motion planning computes collision-free trajectories from a start state to a goal state while respecting a robot's dynamics and actuator limits (LaValle, 2006). This differs from the narrower problem of path planning, which ignores dynamics; kinodynamic planning specifically requires that the computed trajectory be physically executable under the robot's equations of motion. In many practical settings—such as ground robots, mobile manipulators, and articulated robots—these constraints are nonholonomic, and the environment often contains narrow passages that trap naïve exploration (Donald *et al*. 1993). Sampling-based kinodynamic planners address these challenges by exploring the state space through forward simulation. However, they may spend significant time expanding motions in regions that do not lead to a solution (Choset *et al*. 2005).

To reduce search effort, an intermediate geometric abstraction of free space is often used (Choset *et al.* 2005). In a visibility-aware superfacet decomposition, free space is triangulated and merged into larger regions (superfacets) based on visibility. This produces a compact region graph capturing which parts of the environment connect through collision-free, mutually visible transitions. Shortest-path search on this graph provides a high-level route-to-goal estimate, guiding sampling and region expansion while underlying kinodynamic rollouts verify feasibility (Plaku *et al.* 2016). Building on this prior work, this paper extends the framework with a language guidance layer that allows natural-language preferences to safely influence search over the region graph.

At the same time, many navigation tasks are naturally described at a higher level than geometry or controls. Humans often express preferences such as "go through the wide corridor," "avoid tight turns," or "pass near a landmark before entering the goal area." Large language models (LLMs) are attractive for converting such natural-language preferences into planning guidance; however, they may produce suggestions that are not grounded in the actual geometry or that conflict with the robot's dynamics (Wang *et al*. 2024). Recent work has explored several strategies for integrating LLMs into robot planning. Navigation agents such as NavGPT (Zhou *et al*. 2024) use LLMs to generate sequential action decisions for vision-and-language navigation, demonstrating strong high-level reasoning but lacking kinodynamic feasibility enforcement. Structured prompting approaches, such as ProgPrompt (Singh *et al*. 2023), constrain LLM output to program-like formats that are easier to validate and execute,

thereby reducing free-form hallucinations. Additionally, LLM-augmented search methods like LLM-A* (Meng *et al.* 2024) use language priors to guide heuristic search over discrete grids, showing that language-based guidance can accelerate search when properly bounded. A consistent finding across these directions is that language must be grounded in the robot's physical and environmental affordances: unvalidated suggestions reliably degrade performance. For motion planning, this is a critical issue; an ungrounded hint can bias search toward infeasible transitions, increase collision-driven backtracking, and reduce overall reliability (Liang *et al.* 2023). Consequently, language guidance must be constrained, checked, and limited to improve efficiency without compromising safety or correctness (Ichter *et al*. 2022).

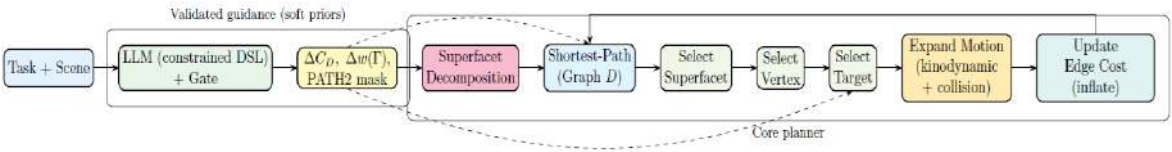

Fig. 1: System architecture. Natural-language task and scene pass through an LLM (constrained DSL) with affordance/feasibility gating; accepted hints softly bias superfacet costs and sampling, while shortest-path over superfacets guides sampling and kinodynamic rollouts with collision checks.

This work proposes a structured integration framework that extends our superfacet kinodynamic planner with language guidance, treated as a soft prior rather than a replacement for classical planning. The key premise is that the LLM does not generate trajectories or determine feasibility; instead, it outputs guidance in a constrained, interpretable domain-specific language (DSL). The DSL supports a discrete set of hint types: route hints (preferring specific region-to-region corridors), waypoint hints (suggesting intermediate targets), constraint hints (discouraging narrow gaps or high-curvature turns), and parameter hints (adjusting decomposition and sampling settings).

These hints are filtered by an affordance-feasibility gate that verifies graph connectivity and visibility, enforces waypoint reachability, incorporates recent collision/failure statistics, and clips bias magnitudes to predefined bounds (Meng *et al.* 2024). Only validated hints are applied to adjust high-level quantities, such as inter-region costs and sampling

priorities on the superfacet graph. Crucially, the underlying kinodynamic rollout and collision checking remain unchanged and authoritative.

This article makes these three contributions:

1. A gated DSL interface: An extension of the visibility-aware superfacet framework that provides an auditable, limited channel for language guidance grounded in the planner's region graph and failure feedback.
2. Structured region-level hints: The definition of specific hint types that operate directly on the superfacet abstraction, enabling language to bias search in a verifiable way. Unlike pure LLM-based planners, this approach delegates kinodynamic feasibility entirely to the classical planning core.
3. Empirical validation: An evaluation using car-like and snake-like robots in cluttered 2D scenes, demonstrating that language-guided extensions reduce planning time and dead-end exploration while maintaining the success rates and path quality of the superfacet-only baseline and classical sampling-based planners.

2. BACKGROUND AND RELATED WORK

Motion planning addresses the problem of finding a collision-free motion that moves a robot from a start state to a goal state while respecting geometric obstacles and, in many systems, dynamic and control constraints. A standard formulation models the robot state as $x \in \mathcal{X}$ (e.g., position, orientation, velocities), controls as $u \in \mathcal{U}$, and evolution through dynamics $\dot{x} = f(x, u)$ (or a discrete-time variant). The goal is to find a trajectory $x(t)$ and control $u(t)$ that avoid obstacles (remain in the free space $\mathcal{X}_{\text{free}}$), satisfy bounds on controls and states, and optimize a cost such as time, path length, energy, or clearance. In cluttered environments with narrow passages, the difficulty is not only to ensure feasibility but also to guide search efficiently toward regions that can connect start and goal.

2.1. Motion Planning Foundations

Classical approaches can be broadly grouped into combinatorial methods and sampling-based methods. Combinatorial methods discretize

the space (exactly or approximately) and then solve a graph search problem (e.g., grid-based search and incremental replanning algorithms such as D* Lite (Koenig and Likhachev, 2002)), which can be effective in low-dimensional settings but can become expensive as the dimension grows. Sampling-based planners instead build an implicit representation of connectivity by sampling states and extending motions, which scales better to higher-dimensional systems and complex constraints (Latombe, 1991; LaValle, 2006).

Two widely used families are probabilistic roadmaps (PRMs) and rapidly-exploring random trees (RRTs) (Kavraki *et al.* 1996; LaValle and Kuffner, 2001). PRM-style methods sample many collision-free configurations, connect nearby samples with local planners, and then query a path on the resulting graph; they are especially effective for multi-query settings (Kavraki *et al*. 1996). RRT-style methods grow a tree from the start (or from start and goal) by repeatedly sampling targets and extending toward them; they are often used in single-query problems and can quickly explore large spaces (LaValle and Kuffner 2001; Karaman & Frazzoli, 2011; Webb 2013). Many planners also incorporate heuristics (e.g., goal biasing) and informed sampling to focus exploration as soon as a partial solution becomes available (Gammell *et al*. 2014, Siciliano & Khatib, 2016).

When dynamics and nonholonomic constraints matter, planners must reason about motions, not only configurations. Kinodynamic planning addresses this case by using forward simulation to propagate states under sampled controls for a duration, followed by collision checking of the resulting motion segment (LaValle, 2006). This approach is general but can be computationally demanding: many rollouts may be rejected due to collision, and narrow passages can cause repeated failures. Practical kinodynamic planners therefore rely on guidance mechanisms, such as heuristics, cost-to-go approximations, or intermediate abstractions, to reduce time spent in unproductive regions (LaValle, 2006).

2.2. Abstractions, Guidance, And Language Grounding

A recurring idea in motion planning is to use an intermediate representation that captures the global structure of free space while keeping the underlying planner responsible for feasibility (Choset *et al.* 2005; LaValle, 2006). Cell decompositions partition the environment into

regions and convert navigation into graph search over region adjacency, while roadmaps capture connectivity through sampled nodes and edges (Kavraki *et al*. 1996). These abstractions can drastically reduce planning complexity by turning a continuous search into a discrete search at a higher level, then refining to continuous motions locally (Choset *et al*. 2005).

Visibility-based decompositions are particularly natural in cluttered 2D or 2.5D navigation settings. The intuition is that regions of free space with good mutual visibility often allow robust local manoeuvring and are less likely to create dead-ends, while transitions across occlusions or tight gaps are riskier (Brock and Kavraki, 2001; Choset *et al*. 2005). In visibility-aware approaches, the environment is first discretized into small primitives (often triangles in 2D) and then merged into larger navigable regions according to visibility criteria, producing a compact region graph (Plaku *et al.* 2016). Shortest-path computations on this graph provide a global "route-to-goal" signal that can guide sampling and expansion decisions. This type of representation is especially useful for sampling-based kinodynamic planners: it does not replace motion-level simulation and collision checking, but it provides a global structure that makes search more directed (Plaku *et al*. 2016).

Guidance mechanisms in sampling-based planning aim to change the order in which the planner explores the space without changing the definition of feasibility (LaValle, 2006). Common strategies include: i) changing the sampling distribution (biasing samples toward the goal, toward low-cost regions, or toward a corridor), ii) changing which nodes/regions are expanded first (priority queues, multi-heuristic search ideas), and iii) adapting costs when repeated failures occur (penalizing transitions that often collide) (LaValle, 2006; Gammell *et al*. 2014). A key design principle is to ensure that guidance remains "soft": it can prioritize promising regions, but it must not bypass collision checking or dynamics constraints. This principle is important when guidance is imperfect or noisy, because the planner should be able to recover and explore alternatives. In practice, many systems combine soft biasing with feedback: when an attempted motion fails, costs are increased or priorities are reduced so the search shifts away from that transition.

Natural language provides an intuitive way for humans to specify preferences, constraints, or task context that may not be captured by geometric cost functions alone. Recent work in robotics has explored the use of large language models as interfaces that translate language into structured actions, plans, or policy parameters (Wang *et al.* 2024). Two

recurring lessons from this literature are: i) language must be grounded in the robot's actual capabilities and environment; and ii) the output should be constrained to a verifiable format, rather than unconstrained free text, to support safety and auditability (Ichter *et al*. 2022; Liang *et al*. 2023).

Several representative directions are relevant to this article. First, "language grounded in affordances" emphasizes that a system should only propose actions that are feasible given what the robot can do in the current world state. Second, "language as programs/policies" shows that LLM outputs can be structured as code-like representations (or DSLs) that are easier to validate, debug, and integrate with classical pipelines (Liang *et al*. 2023; Singh *et al*. 2023; Izquierdo-Badiola *et al*. 2024; Wolber *et al*. 2025). Third, LLM-augmented search approaches demonstrate that language models can provide priors for exploration (e.g., which route is likely better) while retaining a classical planner/search algorithm for correctness and fallback behavior (Ichter *et al*. 2022; Liang *et al*. 2023; Meng *et al*. 2024). These directions motivate using language not as a trajectory generator, but as a source of hints that shape the planner's priorities.

Existing approaches in these three categories each address a part of the integration problem but leave gaps that are relevant to kinodynamic planning. LLM-as-planner systems such as SayCan (Ichter *et al*. 2022) and ProgPrompt (Singh *et al*. 2023) generate action or task-level sequences grounded in affordances, but they operate at a symbolic level and do not enforce geometric connectivity or kinodynamic feasibility: a suggested action sequence may be logically coherent yet physically unexecutable under nonholonomic dynamics. Navigation agents such as NavGPT (Zhou *et al*. 2024) demonstrate that LLMs can reason about routes and landmarks effectively, but they rely on visual observations and discrete action sets rather than a continuous kinodynamic planner with collision-checked rollouts. Code-as-policies approaches (Liang *et al*. 2023) constrain LLM output to executable programs, which improves structure and debuggability, but the generated code is typically not gated against a planner's internal state, there is no mechanism that rejects a suggestion because the corresponding region transition has a high recent failure rate or is geometrically disconnected. LLM-augmented heuristic search methods such as LLM-A* (Meng *et al*. 2024) are perhaps closest in spirit: they use language priors to bias search costs, preserving a classical algorithm for correctness. However, LLM-A* operates over discrete grid graphs, without kinodynamic rollouts or failure-driven cost inflation. The

approach presented in this article addresses precisely this gap: gated, bounded DSL hints that are explicitly validated against a visibility-aware region graph and recent collision feedback, while a kinodynamic planning core retains sole authority over trajectory feasibility.

This article builds on these foundations by combining i) an intermediate free-space abstraction (a visibility-aware region graph), ii) a sampling-based kinodynamic planner that remains responsible for feasibility through rollout simulation and collision checking, and iii) language guidance expressed in a constrained DSL and filtered through explicit feasibility checks. The goal is to obtain the practical benefits of language, such as capturing high-level route preferences and avoiding likely dead-ends, while maintaining the robustness of classical motion planning. Unlike approaches that attempt to directly generate trajectories from language, the emphasis here is on safe integration: language is allowed to bias costs and sampling within fixed bounds, and any suggestion that cannot be grounded in the region graph or recent planning feedback is rejected or clipped.

3. PROPOSED METHOD

The framework operates under the following assumptions. The workspace W is a bounded $2D$ environment with a known, static obstacle map; obstacle geometry is available before planning begins and does not change during execution. Dynamic obstacles are outside the scope of this work. The robot's state space S, control space U, and equations of motion f are known and fixed. These assumptions are standard for offline kinodynamic planning and are shared by the baselines used in the evaluation.

We propose a language-guided motion planning framework that combines a visibility-aware superfacet abstraction with a kinodynamic, collision-checked planning core. The central design choice is to treat language as a soft prior: the large language model (LLM) never generates trajectories and never decides feasibility. Instead, it outputs structured hints that can only bias high-level search over a region graph, while kinodynamic rollout and collision checking remain the sole authority for validity. Figure 1 summarizes the overall pipeline and the separation of responsibilities between language guidance and motion-level feasibility.

3.1. Visibility-Aware Superfacet Representation

Given an obstacle map, the planner first builds a decomposition of free space into compact, navigable regions called *superfacets*. As shown in Figure 2, in 2D environments, free space is triangulated into small triangles and adjacent triangles are merged based on visibility tests, producing a set of regions that are large enough for navigation while still capturing connectivity through narrow passages. Two triangles are considered mutually visible if the line segment joining their centers does not intersect any obstacle boundary. Visibility polygons are computed from each region center using the VisiLibity library (Obermeyer and Contributors 2008) and cached so that subsequent checks require only a point-in-polygon test rather than a full recomputation. The decomposition induces a weighted region graph $D = (V_D, E_D, C_D)$, where V_D is the set of superfacets, E_D connects adjacent regions that pass visibility/connectivity checks, and $C_D(\Gamma, \Gamma')$ is the edge cost defined as the shortest-path distance in the triangulation Λ from $CENTER(\Gamma)$ to $CENTER(\Gamma')$, approximating the geometric effort to navigate between neighboring regions.

Refinement proceeds iteratively until convergence. At each iteration, the centre of each group is recomputed as the triangle closest to the group's centroid. Triangles are then reassigned to the nearest visible centre using a modified Dijkstra expansion that only relaxes edges to triangles visible from the current centre, ensuring that every triangle in a group has an unobstructed line of sight to its centre. Because the visibility criterion can cause a group to be split by another group during reassignment, a breadth-first search is run from each centre to identify the connected component that contains it; triangles outside this component are detached. Any detached or unassigned triangle seeds a new group and triggers a local Dijkstra expansion from that triangle, which continues until all triangles have been assigned. This cycle of centre adjustment, visibility-guided reassignment, split repair, and new-group seeding repeats until no triangle changes its group assignment between consecutive iterations. A shortest-path computation on D provides a coarse route-to-goal signal that guides search at the region level, reducing exploration in parts of the environment that are unlikely to lead to the goal.

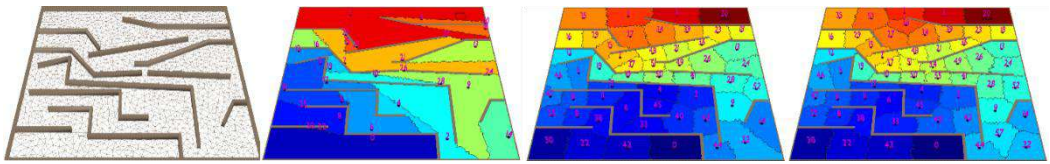

Fig. 2: Triangulation (left), superfacet initialization (centre-left), refinement (centre-right), and convergence (right). Regions are color-coded by shortest-path distance to the goal (red = close, blue = far); the goal region is marked with a square (□). The start position is indicated by the initial robot placement visible in the overlaid solution path. Note that refinement can introduce new superfacets as the visibility criterion resolves group splits.

3.2. Superfacet-Guided Kinodynamic Planning Core

The baseline planner combines region-level guidance with motion-level simulation. First, it uses the superfacet region graph to choose where to focus exploration next. At each iteration, the planner selects a promising superfacet Γ based on the current shortest-path information on D, which estimates which regions are most likely to lead toward the goal. Region selection is governed by a weight

$$w(\Gamma) = h(\Gamma)^{\alpha} \cdot \left(SEL(\Gamma)\right)^{\beta}$$

where $h(\Gamma) \in [\varepsilon, 1]$ is the normalized inverse path cost, approaching 1 as the shortest-path cost to the goal approaches zero; $\alpha \geq 1$ controls the strength of the shortest-path heuristic, $SEL(\Gamma)$ is the number of times Γ has previously been selected for expansion, and $\beta \in (0,1)$ is a penalty exponent that progressively down-weights regions that have been expanded many times, preventing the search from becoming permanently stuck in any single region. Among all regions currently reached by the motion tree, the region with the highest weight is selected. After selecting Γ, the planner generates candidate motions by sampling one or more target points inside that region. Each kinodynamic rollout applies a PID controller to steer the robot from a frontier state toward the sampled target, integrating the robot's equations of motion using fourth-order Runge-Kutta for up to 20 steps of duration $dt = 0.5\ s$ each, and halting immediately if any intermediate state is found to be in collision. Each rollout is then

checked for collisions along the entire simulated motion segment, so only dynamically valid and collision-free motions are accepted and added to the planner's search structure.

A key feature of the baseline is its failure-driven feedback. If rollouts repeatedly fail when attempting to move through a particular region-to-region transition (often because the boundary between regions lies near obstacles or a narrow passage) the planner treats that transition as less promising. Specifically, when a rollout attempting to cross the transition from Γ to Γ' results in collision, the edge cost $C_D(\Gamma, \Gamma')$ is multiplied by an inflation factor $\gamma = 1.1$ and shortest paths over D are immediately recomputed. As a result, the high-level route-to-goal preference shifts away from the repeatedly failing transition and toward alternative corridors that are more likely to be traversable. This mechanism keeps the planner robust: the region graph provides global direction, but motion-level simulation and collision checking decide feasibility, and repeated failures automatically reshape the high-level guidance without changing the underlying dynamics model.

3.3. Language Guidance with Gated, Constrained Hints

We employ a Large Language Model (LLM) as a source of high-level priors capable of interpreting semantic user preferences, such as "use wider corridors" or "avoid sharp turns." However, free-form linguistic input is inherently difficult to validate and introduces critical safety risks if permitted to directly manipulate low-level planning execution. To address this issue, the LLM does not generate arbitrary text; instead, it outputs a compact Domain-Specific Language (DSL) that encodes heuristic hints within a fixed schema. This constraint ensures that every language-derived output can be systematically verified, logged, and safely integrated into the pipeline.

The proposed DSL supports four specialized hint types, each designed to modify only abstract, high-level structural quantities. Table 1 defines the formal schema. Each hint is structured as a typed record containing an invariant set of fields; the LLM is prompted to generate outputs strictly conforming to this architecture, and any malformed string that fails parsing is rejected before reaching the affordance and feasibility gate.

Table 1. DSL Hint Schema for the Language Guidance Layer

Hint Type	Fields	Field Types	Constraints
Route	from, to, preference, weight	RegionID, RegionID, {prefer|avoid}, float	from, to ∈ V_D; (from,to) ∈ E_D; weight ∈ [0,1]
Waypoint	region, priority	RegionID, float	region ∈ V_D; priority ∈ [0,1]
Constraint	transition_type, penalty	{narrow|sharp_turn|low_clearance}, float	penalty ∈ [0,1]
Parameter	param_name, value	string, float	param_name ∈ allowed set; value within safe range

Each hint is a typed record with fixed fields; any LLM output that does not conform to this schema is rejected prior to gate evaluation. *RegionID* denotes an identifier drawn from the superfacet graph V_D; the Constraints column defines the validity conditions enforced by the affordance/feasibility gate.

These categories correspond to: (i) **Route hint**: expresses a mandate to prefer (or avoid) specific region-to-region corridors within D; (ii) **Waypoint hint**: proposes an intermediate region or target area that should be reached next; (iii) **Constraint hint**: penalizes undesirable transitions such as narrow gaps or sharp turns; (iv) **Parameter hint**: bounded adjustments to global planner parameters governing decomposition or sampling resolutions. Importantly, these hints generate strictly bounded updates applied exclusively to: (a) edge costs $C_D(\Gamma, \Gamma')$, (b) region-selection weights $w(\Gamma)$, and (c) target sampling within the next expansion region, without modifying dynamics, controllers, or collision checks

Because the LLM output functions strictly as a heuristic recommendation, every parsed hint passes through an explicit feasibility gate that enforces spatial grounding. This design adheres to the core principle that language-based commands must be bounded by what is physically executable in the current environmental state. The validation gate executes checks sequentially via the following protocol:

Hard rejection (hint is discarded entirely):

a) Any referenced region ID is not in V_D , or any referenced edge is not in E_D.
b) A proposed transition (Γ, Γ') fails the connectivity or visibility checks used to construct the superfacet graph.
c) A proposed waypoint region is not reachable from the currently selected expansion context, i.e., it does not appear in the next-region set along any shortest path from the current frontier.

Soft clipping (hint is retained but its magnitude is reduced):

d) The transition (Γ, Γ') has a recent collision history above a threshold. The proposed update is scaled by a collision-history factor $\alpha(\Gamma, \Gamma')$ before any bounds are applied:

$$\alpha(\Gamma, \Gamma') = max(0, 1 - k \cdot f(\Gamma, \Gamma'))$$

where $f(\Gamma, \Gamma')$ = failures / attempts is the recent failure rate for the transition and k is a constant (set to 2.0 in the experiments). A transition with a 50% recent failure rate therefore receives at most half the proposed update magnitude.

e) After scaling by α, the update magnitude is clipped to the predefined bounds ε_C and ε_w (see below).

Logging: the raw hint, the outcome of each check in order, the value of α(Γ, Γ'), and the final applied update are recorded for every planning episode, making the influence of language fully auditable.

Bounded update rule. Let $\Delta\, C_D$ and $\Delta\, w$ be the changes proposed by the validated hint(s). The gate enforces bounds such as

$$\Delta C_D(\Gamma, \Gamma') = clip(\, \tilde{\Delta} C_D(\Gamma, \Gamma'), -\varepsilon_C, +\varepsilon_C) \text{ and } \Delta w(\Gamma) = clip(\, \Delta w(\Gamma), -\varepsilon_w, +\varepsilon_w)$$

Updates are applied as $C_D \leftarrow C_D + \Delta C_D$ and $w \leftarrow w + \Delta w$, after which C_D is clipped to a predefined range $[C_D, min, C_D, max]$ to prevent edge costs from growing unboundedly or collapsing to zero. These are soft priors: the collision-driven inflation and all kinodynamic feasibility checks remain entirely unchanged. The LLM is queried with a structured prompt consisting of a fixed system message and a per-episode user message. The system message provides the full DSL schema and output constraints; the user message is generated per episode and supplies i) a text description of the scene including obstacle layout and goal location, ii) current region

graph statistics including the number of regions and shortest-path cost, and iii) any recent failure transitions. The complete prompt template is shown in Figure 3.

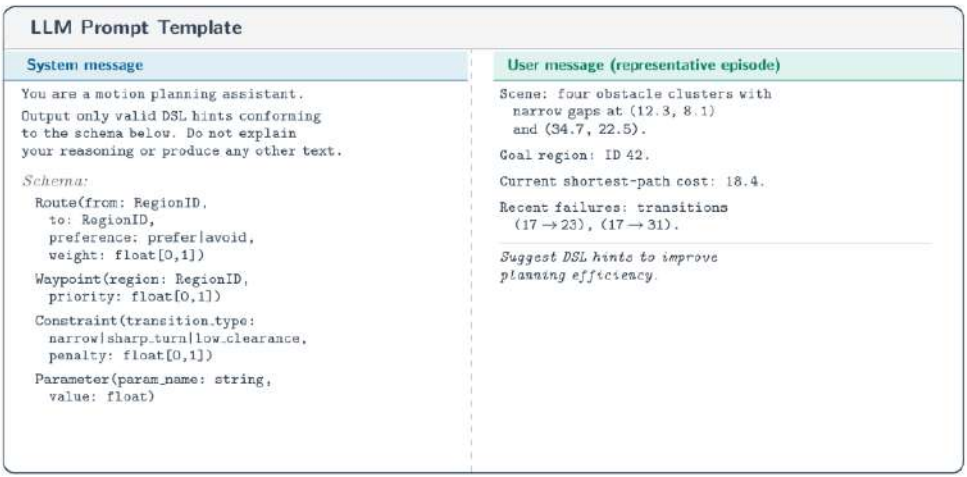

Fig. 3: LLM prompt template used in experiments. The system message (left) is fixed across all planning episodes and specifies the DSL schema and output constraints. The user message (right) is generated per episode from the current scene state, including obstacle layout, region graph statistics, and recent failure transitions.

Algorithm 1: Language-guided superfacet motion planning (gated DSL)

Input: Obstacle map, robot dynamics, start state x_s, goal x_g, time budget T_{max}, bias bounds ε_C, ε_w
Output: Collision-free dynamically-feasible trajectory (if found)
Build/refine superfacet decomposition and region graph $D = (V_D, E_D, C_D)$
Initialize region weights $w(\Gamma)$ and compute shortest-path route-to-goal on D
Initialize motion-planner structure; start timer
while elapsed time < T_{max} **and** goal not reached **do**
    Select expansion region Γ using shortest-path signal and $w(\cdot)$
    if *language guidance enabled* **then**
        Query LLM and obtain DSL hints H
        Validate H with the feasibility gate (reject infeasible hints, clip updates using ε_C, ε_w)
        Convert validated hints into bounded updates (ΔC_D, Δw)
        Update guidance: $C_D \leftarrow C_D + \Delta C_D$; $w \leftarrow \text{clip}(w + \Delta w)$

Sample target points inside Γ according to the current sampling distribution
Simulate kinodynamic rollouts toward sampled targets and collision-check each segment
if *a feasible rollout is found* **then**
Add the new state and motion segment to the planner structure
if *goal reached* **then**
return reconstructed trajectory
if *repeated failures for transition* (Γ, Γ') **then**
Inflate edge cost C_D(Γ, Γ')
Recompute shortest paths on D
return failure

Algorithm 1 outlines the complete runtime planning loop. The planner initially constructs or dynamically refines the superfacet decomposition and its associated region graph $D = (V_D, E_D, C_D)$. It computes shortest paths on D to obtain a route-to-goal signal and region priorities. When the language guidance module is activated, the planner queries the LLM for structured DSL hints that reflect semantic user preferences adapted to the current task and workspace topography. The affordance and feasibility gate subsequently processes these suggestions, executing validation checks and clipping updates to conservative, pre-defined boundaries. The planner applies the resulting bounded updates to the region-graph costs C_D, the region-selection weights $w(\Gamma)$, and the sampling distribution used to generate targets in the next selected region. Utilizing these modulated priorities, the planning core isolates a target region for expansion, executes continuous kinodynamic rollouts toward the sampled target coordinates, and subjects each trajectory segment to localized collision-checking routines. If rollouts repeatedly fail for a transition, the planner inflates the corresponding edge cost, recomputes shortest paths, and continues exploration with updated guidance. Crucially, if no generated hint passes the grounding checks, the system seamlessly falls back to the baseline superfacet planner without language biasing. This fail-safe architecture ensures that linguistic feedback cannot degrade safety margins or bypass physical feasibility protocols; its influence is restricted exclusively to optimizing the order in which topological regions are explored.

4. EXPERIMENTAL EVALUATION

4.1. Experimental Setup

All experiments were conducted on a standard laptop computing platform (Intel Core i7, 16 GB RAM) utilizing a native C++ implementation for the motion planning core and GPT-4o-mini for Large Language Model inference. We evaluated the framework across two distinct robot morphologies: i) a car-like differential-drive robot operating in a 3D state space (2D position coordinates accompanied by a single heading angle with bounded translational and angular velocity constraints, and ii) an articulated snake robot consisting of multiple linked segments governed by local nonholonomic constraints.

The evaluation was performed within four distinct navigation scenes obtained from established motion planning benchmarks. Each scene was validated across 60 randomized start-and-goal configuration pairs to ensure statistical reliability over diverse initial geometric distributions.

Table 2 summarizes the key geometric and topological properties of the four evaluation environments.

Scene 1 (Concentric Rings): Consists of nested, concentric obstacle rings featuring narrow radial gaps. This environment requires the robot to systematically thread through successive bottlenecks, where a single sub-optimal region-selection choice traps the search tree within a dead-end ring.

Scene 2 (Cluttered Field): Formed by an open, cluttered field containing high-density, randomly distributed convex obstacles. The dominant challenge in this environment is managing the expansive number of near-equal-cost path alternatives and the total absence of clear topological corridors.

Scene 3 (Mixed Structure): Combines a highly structured lower workspace section with a cluttered upper section, segregated by a sparse row of bottlenecks. This layout evaluates whether the planner can effectively exploit the low-complexity lower section while accurately identifying the single viable crossing point.

Scene 4 (Maze Corridors): Presents a maze-like configuration composed of orthogonal rectangular corridors with multiple deep dead-ends and forced backtracking profiles. This environment serves as a rigorous stress-test for the failure-driven cost-inflation feedback mechanism.

Table 2. Properties of the four navigation scenes used in the evaluation.

Scene	Obstacles	Density (%)	Dominant Challenge
Rings	6 (concentric)	22	Sequential bottlenecks
Cluttered	47	31	High obstacle density, many near-equal paths
Mixed	35	25	Mixed structured/cluttered, single crossing
Maze	24	28	Dead-ends, forced backtracking

All scenes share an 80 × 80 m workspace. Obstacle density is measured as the percentage of workspace area occupied by obstacles.

The planning pipeline operates via the following execution sequence: given a cluttered environmental map, the planner first constructs a visibility-aware superfacet decomposition to generate the primary region graph $D = (V_D, E_D, C_D)$. For each individual start-to-goal query, the planner is allocated a strict, fixed computational time budget of 30 seconds per run.

At the initiation of each planning episode, the Large Language Model (LLM) is queried exactly once with a structured textual description of the task and workspace layout (detailing obstacle topologies and goal coordinates). The model returns a sequence of specialized DSL hints—categorized into *route*, *waypoint*, *constraint*, and *parameter* adjustments—conforming to the architecture detailed in Section 2.3. These hints are dynamically passed through the validation gate, which filters out invalid references and clips acceptable values within conservative bounds. Approved hints are applied as soft adjustments to the edge costs C_D and region weights $w(\Gamma)$, and the planner then executes the integrated planning loop (superfacet graph search, kinodynamic rollouts, collision checking, and cost inflation on failure).

Key planner parameters held constant across all baseline and guided evaluations include:

- **Triangulation resolution:** 0.2m fine grid spacing.
- **Superfacet refinement threshold:** 0.5m^2 minimum region area.

- **Kinodynamic rollout horizon:** 0.5s duration with 20 control inputs sampled per expansion.
- **Collision checking resolution:** 0.01m localized interpolation intervals along each simulated trajectory segment.

For language guidance, the bias bounds were set to ε_C = 0.2 (edge cost adjustment) and $\varepsilon_w = 0.15$ (region weight adjustment), chosen conservatively to ensure soft influence and recovery via collision-driven inflation. The LLM temperature was set to 0.7 to balance creativity and consistency in hint generation.

4.2. Baselines and Metrics

To ensure a rigorous and unbiased evaluation, we compare four distinct planning methodologies under identical operational conditions, utilizing the same robot dynamics models, low-level kinodynamic tracking controllers, collision-checking routines, and scene geometries under a uniform 30-second runtime budget. The evaluated methods are categorized as follows: i) **rapidly-exploring random tree (RRT):** A foundational sampling-based planner that incrementally constructs a search tree by sampling state-space configurations—augmented with standard goal biasing—and extending tree branches toward them, ii) **kinodynamic planning by interior-exterior boundary expansion (KPIECE):** A widely deployed kinodynamic sampling-based planner from the open motion planning library (OMPL), implemented here using its default parameter configurations, iv) **superfacets (Baseline):** The visibility-aware abstraction framework without linguistic input, which relies exclusively on the topological region graph combined with failure-driven cost-inflation feedback to guide state-space exploration, and v) **superfacets + LLM (Proposed):** Our complete framework, which augments the core superfacet backbone with gated, DSL-based linguistic hints to softly bias edge costs and region-selection weights, leaving absolute feasibility verification to the underlying kinodynamic core.

The first baseline is Rapidly-exploring Random Tree (RRT), a classical sampling-based planner that grows a tree by repeatedly sampling targets (often with some goal bias) and extending toward them. The second baseline is Kinodynamic Planning by Interior-Exterior Boundary Expansion (KPIECE), a widely used kinodynamic sampling-based planner available in the Open Motion Planning Library (OMPL), used here with default settings. The third method is the visibility-aware Superfacets

planner without language guidance, which relies only on the superfacet region graph together with collision-driven cost inflation feedback to guide exploration. The fourth method is our proposed Superfacets + LLM system, which augments the same superfacet backbone with gated, DSL-based language hints that softly bias costs and sampling while leaving feasibility checks to the underlying kinodynamic planner.

Performance is quantified across several primary evaluation metrics: i) **Planning time (seconds):** Measures the absolute elapsed time from the initiation of a start-to-goal query to the discovery of the first feasible solution (defined as a continuous, collision-free trajectory that respects all dynamic constraints), ii) **Success rate (percentage):** Defined as the fraction of the 60 randomized start-to-goal queries per scene successfully solved within the allocated 30-second budget, iii) **Edge-cost inflations (count):** Tracks the frequency with which the planner increments inter-region edge costs in response to localized rollout failures; a lower count indicates minimized entrapment within dead-ends and reduced computational redundancy, iv) **Normalized path length:** Computed as the cumulative executed trajectory length divided by the straight-line Euclidean distance between the start and goal states, assessing whether search acceleration degrades downstream path quality, and v) **LLM inference time (milliseconds):** Quantifies the precise computational overhead required to generate and parse the structured DSL hints, capturing the latency introduced by the language guidance layer.

To determine whether the performance discrepancies between the *Superfacets* baseline and the *Superfacets + LLM* framework are statistically significant, we apply the **Wilcoxon signed-rank test** to paired per-run observations across all 60 configurations per scene, utilizing a significance threshold of $\alpha = 0.05$. This non-parametric test is appropriate for this domain because planning-time distributions typically exhibit heavy right-skewness, violating standard normality assumptions.

The pronounced performance disparity between the classical sampling planners (RRT and KPIECE) and the superfacet-based variants is directly attributable to the structural abstraction layer; the visibility-aware region graph provides explicit global directionality that neither RRT's Voronoi bias nor KPIECE's boundary-cell expansion can replicate. Consequently, the incremental performance gain demonstrated by *Superfacets + LLM* over the *Superfacets* baseline successfully isolates the specific algorithmic contribution of natural language guidance, independent of the underlying environmental decomposition. The

comprehensive ablation results presented later in Table 4 further validate this attribution, demonstrating that these performance benefits collapse when semantic hints bypass the feasibility validation gate.

4.3. Results and Analysis

Table 3 reports aggregated experimental results across all four benchmark environments and both robot models. The values represent sample means ± standard deviation calculated over a total of 480 runs (4 scenes × 2 robots × 60 runs). The *p*-value column reports the Wilcoxon signed-rank test result for each method compared against Superfacets + LLM framework. The proposed language-guided variant (Superfacets + LLM) achieves the lowest mean planning time at 1.4 ± 0.3 s, a modest but consistent reduction of approximately 18% (1.7 ± 0.3 s). This reduction does not come at the expense of reliability: success rate is slightly higher with language guidance (99.6% vs. 99.1%), and the number of edge-cost inflations is lower (3.1 ± 0.4 vs. 3.4 ± 0.5), indicating fewer dead-end explorations and fewer collision-driven recoveries. Path quality remains essentially unchanged, as the normalized path length is nearly identical for the two superfacet variants (1.24 ± 0.08 with LLM guidance versus 1.23 ± 0.07 without LLM guidance), suggesting that language primarily reduces unproductive exploration rather than encouraging shorter but riskier routes.

Table 3. Aggregated planning results across all evaluation environments

Method	Time (s) ↓	Success (%) ↑	Inflations ↓	Path Length (norm.) ↓	LLM Inference (ms)	p-value
RRT	41.8 ± 5.1	58.1 ± 3.8	9.8 ± 1.3	1.52 ± 0.18	N/A	< 0.001
KPIECE	33.7 ± 4.2	83.6 ± 3.2	6.5 ± 1.0	1.38 ± 0.12	N/A	< 0.001
Superfacets (no LLM)	1.7 ± 0.3	99.1 ± 0.4	3.4 ± 0.5	1.23 ± 0.07	N/A	0.031
Superfacets + LLM	1.4 ± 0.3	99.6 ± 0.2	3.1 ± 0.4	1.24 ± 0.08	210 ± 35	—

Aggregated planning results across all four scenes and both robot morphologies (480 runs per method). Planning time and inflations are mean ±

standard deviation. Path length is normalized by straight-line start-to-goal distance. The p-value column reports the Wilcoxon signed-rank test comparing each method to Superfacets + LLM on planning time ($\alpha = 0.05$). LLM inference time is reported only for Superfacets + LLM. N/A indicates the metric does not apply to that method.

From a practical perspective, achieving planning performance that meets or exceeds a highly optimized geometric baseline while seamlessly incorporating natural-language input is a significant milestone for human-robot interaction. It demonstrates that non-expert operators can successfully steer complex robotic assets using intuitive linguistic commands without incurring structural computational penalties. This is a critical prerequisite for tactical deployments where operators lack deep technical insight into the underlying nonholonomic kinodynamic mechanics. The minimal computational overhead introduced by the language layer (210 ± 35 ms LLM inference against a mean planning time of 1.4 s further confirms the viability of this methodology for real-time field deployments.

Figure 4 provides an intuitive visualization of how semantic guidance alters the exploration profile of the search trees. Within each scene, the decomposed superfacet regions are color-coded based on their distance-to-goal metrics, while the white overlapping traces illustrate the actual motion tree expansions. This visualization clearly illustrates the structural transition from a broad, unconstrained search to focused exploration within a viable corridor. With language guidance enabled, the motion tree branches cluster early along broader, structurally sound corridors instead of repeatedly probing narrow, high-risk apertures. This behavior is quantitatively detailed in Figure 5, which plots individual planning times and edge-cost inflation counts across each specific benchmark scene. The per-environment metrics verify that the ~18% performance benefit is robust across all tested configurations. While the benefits of language guidance remain constant across environments, its exact magnitude depends directly on the topological constraints of the workspace: the most significant reductions in search time are achieved within the most tightly constrained, complex layouts.

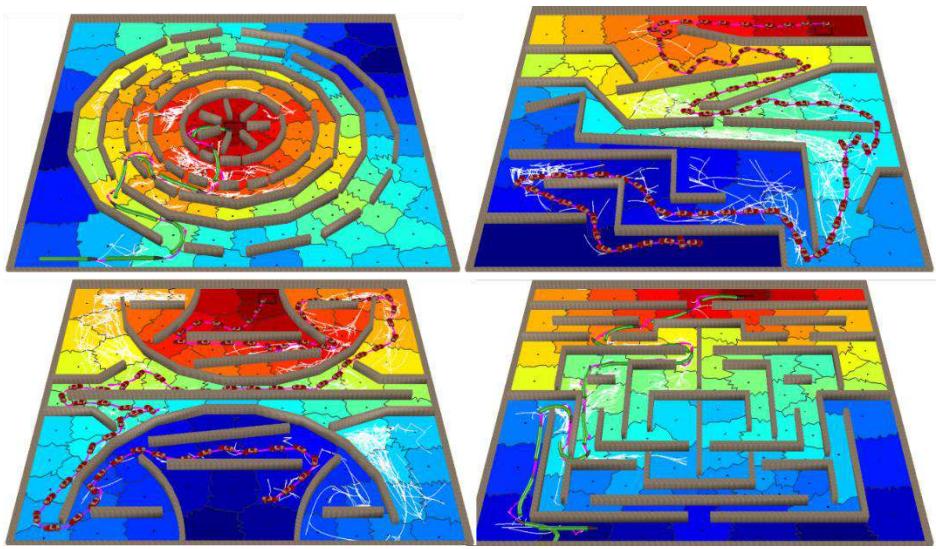

Fig. 4: Qualitative results in four scenes. Scenes 1 and 4 show the snake robot; Scenes 2 and 3 show the car robot. Superfacets are color-coded by shortest-path distance to the goal (red = close, blue = far). White traces indicate motion-tree expansions; the final feasible path is overlaid in magenta. The goal region is marked with a square (□) and the start position is indicated by the initial robot placement.

Compared to classical sampling baselines (RRT and KPIECE), the superfacet methods are dramatically faster and more reliable in these cluttered testing environments. While RRT solves only 58% of the configuration queries within the allocated time budget and KPIECE reaches an 84% success rate, both superfacet variants exceed a 99% success rate. This stark contrast reflects the clear advantage of utilizing a compact, region-level topological abstraction combined with shortest-path guidance in environments dominated by complex narrow passages.

The Wilcoxon signed-rank test confirms that the performance profiles of both RRT and KPIECE differ significantly from Superfacets + LLM ($p < 0.001$). Furthermore, the discrepancy between the baseline Superfacets (no LLM) and the guided Superfacets + LLM framework is also statistically significant ($p = 0.031$). This statistical validation supports the conclusion that semantic language guidance provides a consistent, mathematically meaningful benefit beyond that of the superfacet structural abstraction alone. In scenes characterized by wider free spaces and fewer tight transitions, the observed search time reduction is smaller but still

noticeable. This pattern suggests that language guidance remains useful even when the underlying geometric superfacet heuristic already provides strong directionality. The inflation plots referenced in Figure 5 follow the same qualitative distribution: the Superfacets + LLM method produces fewer cost-inflation events in each scene, indicating a lower frequency of collision-driven recoveries and minimized backtracking. Collectively, these results support the interpretation that gated language guidance improves runtime efficiency primarily by reducing unproductive or redundant state-space exploration, while absolute feasibility and safety margins remain rigidly enforced by the unchanged kinodynamic rollout and collision-checking core.

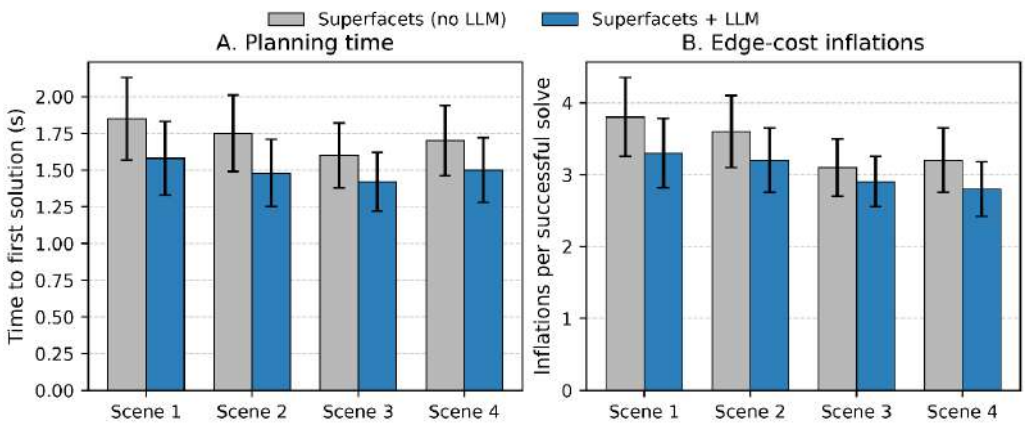

Fig. 5: Per-scene time and inflations. Mean planning time (A) and edge-cost inflations (B) per scene for Superfacets (no LLM) vs. Superfacets + LLM; error bars show ± s.e.m. over 60 start/goal pairs per scene.

4.4. Ablation Studies

Table 4 evaluates the individual and combined impacts of each DSL hint type across all four benchmark environments and both robot morphologies, compiled over 480 runs per configuration. The Maze and Rings environments, representing the most spatially constrained layouts, exhibit the largest absolute performance gains. Conversely, the Cluttered Field and Mixed scenes show smaller but highly consistent improvements, confirming that the algorithmic benefits generalize well beyond heavily

bottlenecked topologies. Analyzing the hint types individually reveals distinct contributions to the system's efficiency: Route-Only Guidance: Effectively reduces planning times by biasing early state-space exploration toward structurally viable corridors. Waypoint-Only Guidance: Decreases search times by approximately 10% by tightly focusing target selection variables within the next scheduled expansion region. Constraint-Only Hints: Consistently minimize search latency by discouraging exploration near narrow apertures or failure-prone transitions. Parameter-Only Hints: Yield the most modest efficiency gains in this specific experimental configuration, indicating that the default triangulation resolution and sampling densities are already operating near a localized optimum. The highest performance optimization is achieved when all four hint modalities are enabled concurrently. This full configuration yields a combined reduction of approximately 19% in planning time and a 14% decrease in cost-inflation counts relative to the baseline Superfacets (no LLM) framework. These findings demonstrate that the distinct semantic components of the DSL are complementary rather than redundant, each targeting a separate layer of the hierarchical motion-planning problem.

Table 4. Hint-type ablation across all four scenes and both robot morphologies (mean ± s.e.m., 480 runs per configuration). Lower is better for Time and Inflations; higher is better for Success.

Hint Configuration	Time (s) ↓	Inflations ↓	Success (%) ↑
Baseline (no LLM)	1.71 ± 0.30	3.6 ± 0.5	99.0 ± 0.5
Route hints only	1.60 ± 0.20	3.4 ± 0.4	99.2 ± 0.4
Waypoint hints only	1.54 ± 0.25	3.2 ± 0.5	99.4 ± 0.3
Constraint hints only	1.61 ± 0.22	3.3 ± 0.4	99.1 ± 0.4
Parameter hints only	1.67 ± 0.28	3.5 ± 0.5	99.0 ± 0.6
All hint types (full system)	**1.39 ± 0.28**	**3.1 ± 0.4**	**99.4 ± 0.3**
LLM without gate (ungated)	4.2 ± 1.1	8.3 ± 1.7	87.0 ± 2.1

To assess whether explicit semantic grounding and bounding are structurally necessary, we evaluated an ungated variant ("LLM without gate") in which hint validation was completely bypassed and saturation bounds were not enforced. Table 4 includes the aggregate results for this

configuration across all four benchmark environments, revealing a consistent and severe performance degradation: the mean planning time escalates to 4.2 pm 1.1s, edge-cost inflation events rise to 8.3 ± 1.7, and the overall success rate drops to 87.0%. This profile is significantly worse than even the baseline Superfacets (no LLM) framework, demonstrating that invalidated linguistic guidance acts as an active impediment rather than a neutral fallback. In contrast, the complete gated framework maintains a high success rate (99.4%) and low planning latency (1.4 ± 0.3 s) across all environments, proving that bounding and verifying language is a core architectural necessity even when prompt heuristics are well-intentioned. Qualitatively, ungated system failures occurred when the language model proposed region-to-region corridors that were unsupported by the underlying workspace geometry. This caused the planning core to execute repeated, colliding rollouts before the tree expansion could eventually abandon the heavily biased path. Conversely, with the validation gate enabled, such anomalous hints were systematically rejected or clipped, allowing the planner to instantly fall back to the baseline superfacet heuristic without compromising physical feasibility. Taken together, these ablation studies establish three definitive conclusions: each hint modality contributes independently, the distinct hint types are complementary when executed concurrently, and the validation gate functions as an indispensable safety barrier required to preserve system reliability.

5. CONCLUSIONS

This article presented a language-guided motion planning framework that seamlessly integrates Large Language Model guidance with a visibility-aware superfacet decomposition layer and a kinodynamic, collision-checked planning core. The foundational architecture treats linguistic input strictly as a soft, bounded prior: the LLM produces structured recommendations using a constrained Domain-Specific Language, and an explicit feasibility gate validates these suggestions against a topological region graph and real-time failure feedback before they are permitted to influence the search space. Consequently, language can safely bias abstract edge costs, region-selection weights, and local target sampling distributions, while continuous kinodynamic rollouts and

explicit collision-checking routines retain ultimate veto authority over trajectory feasibility.

Experimental evaluations utilizing car-like and articulated snake-like robot morphologies within cluttered benchmark environments demonstrate that the proposed method achieves a consistent reduction in both planning time and redundant space exploration (manifested as a reduction in cost-inflation cycles). Crucially, these efficiency gains are realized while preserving exceptionally high success rates and maintaining comparable downstream path quality relative to the unguided baseline. These findings support the broader conclusion that structured, grounded language can provide an interpretable and auditable guidance channel, provided it functions as a constrained search heuristic rather than a direct trajectory generator. Furthermore, this framework allows non-expert operators to articulate navigational preferences using natural language without imposing additional planning penalties, offering a practical interface for real-world human-robot interaction in field deployments.

While the proposed framework demonstrates clear advantages, several open limitations suggest directions for future research:

Adaptive Gating and Semantics: The validation gate can be made more adaptive by incorporating learned affordance models and structural uncertainty estimates. This modification would enable aggressive language-driven guidance when semantic confidence is high, and conservative geometric fallback behaviour when confidence is low. Additionally, expanding the DSL to incorporate richer task semantics—such as clearance preferences, risk-sensitivity metrics, or explicit "must-pass/must-avoid" constraints—will improve expressiveness while preserving formal verifiability.

Dynamic Environments and Scale: Extending the framework to high-dimensional 3D environments, multi-agent cooperative settings, and long-horizon tasks represents a vital direction for future validation. A particularly promising avenue involves adapting the pipeline to dynamic environments where obstacles move, requiring online region-graph updates, analogous to incremental replanning methods such as D* Lite (Koenig and Likhachev, 2002) that efficiently repair shortest paths when edge costs change. Language guidance could prioritize re-planning efforts within newly altered spaces. For example, maintaining a dynamic version of the superfacet graph that automatically flags regions with recently detected obstacle variations as high-priority zones for LLM re-querying

would focus computational replanning effort strictly on affected corridors while leaving undisturbed spaces intact.

Prompt and Language Robustness: The current evaluation queries the LLM exactly once per planning episode under a fixed temperature parameter. System robustness against prompt variations, adversarial inputs, or ambiguous spatial language remains unassessed. Future empirical studies should involve systematic evaluations over a broader spectrum of bias bounds, prompt structural styles, and adversarial instructions to precisely map the practical speed–safety–interpretability trade-offs.

Ethical Statement. This study involves computational simulation only. No human subjects, live animals, or personal data were involved in any part of this research. No formal ethical approval was required.

Data Accessibility. The data, source code, and simulation materials that support the findings of this study are available from the corresponding author upon reasonable request, subject to applicable institutional and intellectual property considerations.

Conflict of Interest. The authors declare that they have no conflicts of interest.

Originality and Authorship. This work is based on original data and conceptual ideas developed entirely by the authors. No artificial intelligence (AI) technologies or automated tools were employed in the generation of the data, analysis, or manuscript preparation.

The authors have read and approved the final version of this manuscript for publication.

Authors' Contributions. E.P.: conceptualization, methodology, engineered the software implementation, designed and performed the simulation experiments, analysed the aggregate results, and wrote the manuscript text. N.C.: institutional supervision, scientific guidance, reviewing, editing the manuscript draft, supported the contextual interpretation of the planning results.

Funding. This research received no external funding or financial support.

REFERENCES

Brock O, Kavraki LE. 2001. Decomposition-based motion planning: A framework for real-time motion planning in high-dimensional configuration spaces. In Proceedings of the 2001 *IEEE International Conference on Robotics and Automation* (ICRA) (pp. 1469–1475). IEEE. https://doi.org/10.1109/ROBOT.2001.932817.

Choset H, Lynch KM, Hutchinson S, Kantor G, Burgard W, Kavraki LE, Thrun S. 2005. *Principles of Robot Motion: Theory, Algorithms, and Implementations*. Cambridge, MA: MIT Press.

Donald B, Xavier P, Canny J, Reif J. 1993. Kinodynamic motion planning. *Journal of the Association for Computing Machinery (ACM),* **40(5):**1048–1066. https://doi.org/10.1145/174147.174150.

Gammell JD, Srinivasa SS, Barfoot TD. 2014. Informed RRT*: Optimal sampling-based path planning focused via direct sampling of an admissible ellipsoidal heuristic. In 2014 IEEE/RSJ International Conference on Intelligent Robots and Systems (IROS) (pp. 2997–3004). *IEEE*. https://doi.org/10.1109/IROS.2014.6942976.

Ichter B, Brohan A, Chebotar Y, Finn C, Hausman K, Herzog A, Ho D, Ibarz J, Irpan A, Jang E, Julian R, Kalashnikov D, Levine S, Lu Y, Parada C, Rao K, Sermanet P, Toshev AT, Vanhoucke V, Xia F, Xiao T, Xu P, Yan M, Brown N, Ahn M, Cortes O, Sievers N, Tan C, Xu S, Reyes D, Rettinghouse J, Quiambao J, Pastor P, Luu L, Lee K-H, Kuang Y, Jesmonth S, Joshi NJ, Jeffrey K, Ruano RJ, Hsu J, Gopalakrishnan K, David B, Zeng A, Fu CK. 2023. Do as I can, not as I say: Grounding language in robotic affordances. *In Proceedings of the 6th Conference on Robot Learning* (pp. 287-318). PMLR. https://proceedings.mlr.press/v205/ichter23a.html.

Izquierdo-Badiola S, Canal G, Rizzo C, Alenyà G. 2024. PlanCollabNL: Leveraging large language models for adaptive plan generation in human-robot collaboration. IEEE Robotics and Automation Letters.

Karaman S, Frazzoli E. 2011. Sampling-based algorithms for optimal motion planning. *The International Journal of Robotics Research*, **30(7):**846–894. SAGE Publications. https://doi.org/10.1177/0278364911406761.

Kavraki LE, Švestka P, Latombe J-C, Overmars MH. 1996. Probabilistic roadmaps for path planning in high-dimensional configuration spaces. *IEEE Transactions on Robotics and Automation,* **12(4):**566–580. https://doi.org/10.1109/70.508439.

Koenig S, Likhachev M. 2002. D* Lite. In Proceedings of the 18th National Conference on Artificial Intelligence (AAAI) (pp. 476–483). AAAI Press.

Latombe J-C. 1991. *Robot Motion Planning*. Boston: Kluwer Academic Publishers.

LaValle SM. 2006. *Planning Algorithms*. Cambridge: Cambridge University Press.

LaValle SM, Kuffner JJ. 2001. Rapidly-exploring random trees: Progress and prospects. *In algorithmic and computational robotics: New Directions* (pp. 293–308). A K Peters.

Liang J, Huang W, Xia F, Xu P, Hausman K, Ichter B, Florence P, Zeng A. 2023. Code as policies: Language model programs for embodied control. *In 2023 IEEE International Conference on Robotics and Automation* (ICRA) (pp. 9493–9500). IEEE. https://doi.org/10.1109/ICRA48891.2023.10160591.

Meng S, Wang Y, Yang C-F, Peng N, Chang K-W. 2024. LLM-A*: Large language model enhanced incremental heuristic search on path planning. In *Findings of the Association for Computational Linguistics: EMNLP* 2024 (pp. 1087-1102). Association for computational linguistics. https://doi.org/10.18653/v1/2024.findings-emnlp.60.

Obermeyer KJ, Contributors. 2008. The VisiLibity library [Software]. Retrieved from http://www.VisiLibity.org.

Plaku E, Plaku E, Simari P. 2016. Direct path superfacets: An intermediate representation for motion planning. *IEEE Robotics and Automation Letters*, **2:**350-357. https://doi.org/10.1109/LRA.2016.2619381.

Siciliano B, Khatib O (eds.). 2016. Springer Handbook of Robotics. 2nd ed. Cham: Springer.

Singh I, Blukis V, Mousavian A, Goyal A, Xu D, Tremblay J, Fox D, Thomason J, Garg A. 2023. ProgPrompt: Generating situated robot task plans using large language models. In *2023 IEEE International Conference on Robotics and Automation (ICRA)* (pp. 11523–11530). IEEE. https://doi.org/10.1109/ICRA48891.2023.10161317.

Wang J, Shi E, Hu H, Chong M, Liu Y, Wang X, Yao Y, Liu X, Ge B, Zhang S. 2024. Large language models for robotics: Opportunities, challenges, and perspectives. *Journal of Automation and Intelligence,* 4. https://doi.org/10.1016/j.jai.2024.12.003.

Webb D, van den Berg J. 2013. Kinodynamic RRT*: Asymptotically optimal motion planning for robots with linear dynamics. In *2013 IEEE International Conference on Robotics and Automation* (ICRA). IEEE. https://doi.org/10.1109/ICRA.2013.6631022.

Wolber J, Lv M, Koch D, Bretz L, Lanza G, Baer F. 2025. Large language models for robotics: A systematic literature review on prompt engineering. *In Mining Science,* (pp. 201–213). Springer. https://doi.org/10.1007/978-3-031-84744-8_17.

Zhou G, Hong Y, Wu, Q. 2024. NavGPT: Explicit reasoning in vision-and-language navigation with large language models. In *Proceedings of the Thirty-Eighth AAAI Conference on Artificial Intelligence (AAAI'24/IAAI'24/EAAI'24)*, **38: 849** (pp. 7641–7649). AAAI Press. https://doi.org/10.1609/aaai.v38i7.28597.

GEOLOGICAL AND TECTONIC CHARACTERISTICS AND SEISMICITY OF THE KURBNESH–KUKËS–PRIZREN FAULT

Naser PECI[1], Rrapo ORMENI[2], Behxhet SHALA[3], Petraq NAQO[4], Dionald MUÇAJ[5]

[1,2,3]University, Isa Boletini, Mitrovica, Kosovo,

[2,4,5]Temporary Research Unit for Geosciences and Geoengineering, Academy of Sciences of Albania

Author for correspondence: naser.peci@umib.net

NP, 0009-0006-3887-7192; RrO, 0000-0002-5514-2204; BSh, 0000-0002-7242-3526

ABSTRACT

Albania and Kosovo are situated within the seismically active Alpine–Mediterranean belt, where significant crustal deformation results from the ongoing convergence between the Adria microplate and the Eurasian plate. Within this geodynamic framework, the Kurbnesh–Kukës–Prizren fault zone constitutes a geotectonic structure of paramount importance for understanding regional tectonics and seismicity in northern Albania and southwestern Kosovo. This SW–NE-trending fault segment represents one of the principal active tectonic zones in the Western Balkans and plays a fundamental role in both landscape evolution and the spatial distribution of regional seismicity. The area has undergone a complex, prolonged tectonic evolution characterized by multiple deformation phases associated with successive Alpine orogenic events. Contemporary tectonic activity, driven by neotectonic stress regimes, has reactivated these inherited fault systems, thereby exerting a direct control over the present-day seismic hazard. Seismological records from local and regional monitoring networks indicate that the Kurbnesh–Kukës–Prizren fault zone experiences moderate-to-high levels of seismic activity. This study aims to characterize the geological and tectonic framework of this fault as an active transboundary structure between Albania and Kosovo, while analyzing its seismic behavior to enhance understanding of the region's geodynamic evolution. To quantify the seismic characteristics of the fault zone, we employed standard statistical seismological parameters, including temporal histograms of earthquake occurrence, spatiotemporal variations in the seismotectonic *b*-value, annual probabilities of occurrence, and earthquake recurrence intervals. The results underscore the necessity for a more detailed assessment of geological and seismic risk, particularly regarding urban expansion, critical infrastructure planning, and natural hazard risk management.

***Keywords*:** active faults; neotectonics; seismicity; seismotectonic *b*-value; transboundary tectonics

Publisher: Academy of Sciences of Albania
License: Creative Commons Attribution License (CC BY 4.0)
Citation: **Peci N, Ormeni Rr, Shala B, Naqo P, Muçaj D. 2026. Geological and tectonic characteristics and seismicity of the Kurbnesh–Kukës–Prizren fault.** *Albanian Journal of Natural and Technical Sciences* (*AJNTS*), **2 (30),**
Journal URL: https://journals-akad.gov.al/magazines/1
Classification: Research
Subject Category Natural / Earth Sciences subject areas: Seismotectonics & Neotectonics

1.INTRODUCTION

The convergence between the African and Eurasian plates in the Mediterranean region is accommodated by several intervening microplates, among which the Adriatic plate plays a central role. This plate is characterized by arcuate and, in many areas, diffuse boundaries, where subduction processes and convergence rates exhibit significant spatial variability (Faccenna *et al.* 2003; Handy *et al*. 2019).

The Albanides constitute the principal geological units forming the structural framework of Albania. Owing to their complex tectonostratigraphic architecture, these units were collectively termed the "Albanides" by Peza (1967) and were subsequently further refined and described by Aliaj (2010).

The geological framework of the Kurbnesh–Kukës–Prizren fault zone, spanning northern Albania and southern Kosovo, belongs to the folded Alpine–Mediterranean belt of the Dinaride–Albanide–Hellenide orogenic system, which forms part of the western sector of the Eastern Mediterranean orogenic domain.

Neotectonic deformation in Albania is predominantly expressed by thrust faulting, reflecting the overall compressional tectonic regime of the region. However, normal faults, mainly oriented NE–SW, are also widely developed, particularly in central and eastern Albania, indicating the superposition of extensional deformation on the prevailing compressional stress field (Sulstarova, 1986; Muço 2007; Kiratzi, 2011; Ormeni *et al.* 2013). Within this framework, the Kurbnesh–Kukës–Prizren (KKP) fault extends for approximately 90 km in a SW–NE direction and dips toward the northwest.

The historical earthquake of 1456, with an epicentral intensity of MMI VI (Elezaj, 2002), represents one of the strongest seismic events affecting northern Albania, although its epicentre was located just across the present-day border in Kosovo. This event is estimated to have had a magnitude of approximately M_w 6.3, based on historical macroseismic data.

Extensive international research has demonstrated that seismic activity varies systematically across different tectonic environments, reflecting the underlying geodynamic processes that control stress accumulation and release. In this context, the present study examines the geological setting and structural framework of the Kurbnesh–Kukës–Prizren fault as an active transboundary tectonic structure between Albania and Kosovo, with the aim of providing an integrated interpretation of the region's tectonic evolution and seismicity.

2. MATERIALS AND METHODS

The study area encompasses the Kurbnesh–Kukës–Prizren (KKP) fault zone and its adjacent geological units in northeastern Albania and western Kosovo. To characterize the structural and seismotectonic framework of the region, an integrated methodological approach was adopted, combining geological, geophysical, and seismological analyses. Quantitative statistical methods, including earthquake magnitude–frequency distributions and *b*-value calculations, were applied to evaluate spatial and temporal variations in seismicity along individual fault segments. In addition, earthquake focal mechanism solutions compiled from multiple sources and research groups (Muço, 1994; Ormeni *et al.* 2013; 2022) were analyzed to constrain the stress regime and fault kinematics. Collectively, these multidisciplinary datasets provide a robust framework for interpreting fault segmentation, segment-specific seismic behaviour, and the role of transverse structures in controlling the regional seismotectonic architecture.

2.1 GEOLOGICAL–TECTONIC CHARACTERISTICS OF ALBANIA–KOSOVO AND THE KURBNESH–KUKËS–PRIZREN ZONE

From a geological standpoint, Albania and Kosovo form part of the Dinaric–Albanide–Hellenide orogenic arc (Fig. 1). The fundamental

geological characteristics of the broader region are primarily controlled by the tectonic position of the Albanides within the Alpine–Mediterranean belt, as well as by the evolutionary history of adjacent orogenic domains. Accordingly, the Albanides and the surrounding geological framework are conventionally subdivided into two principal tectonostratigraphic domains: The External Albanides, comprising the Krasta–Cukali Zone and the Albanian Alps, and the Internal Albanides, including the Gashi, Mirdita, and Korabi zones (Fig. 2). These units consist of a wide range of metamorphic, magmatic, and sedimentary lithologies, spanning an age interval from the Ordovician to the Quaternary, and reflecting the long and complex geodynamic evolution of the region.

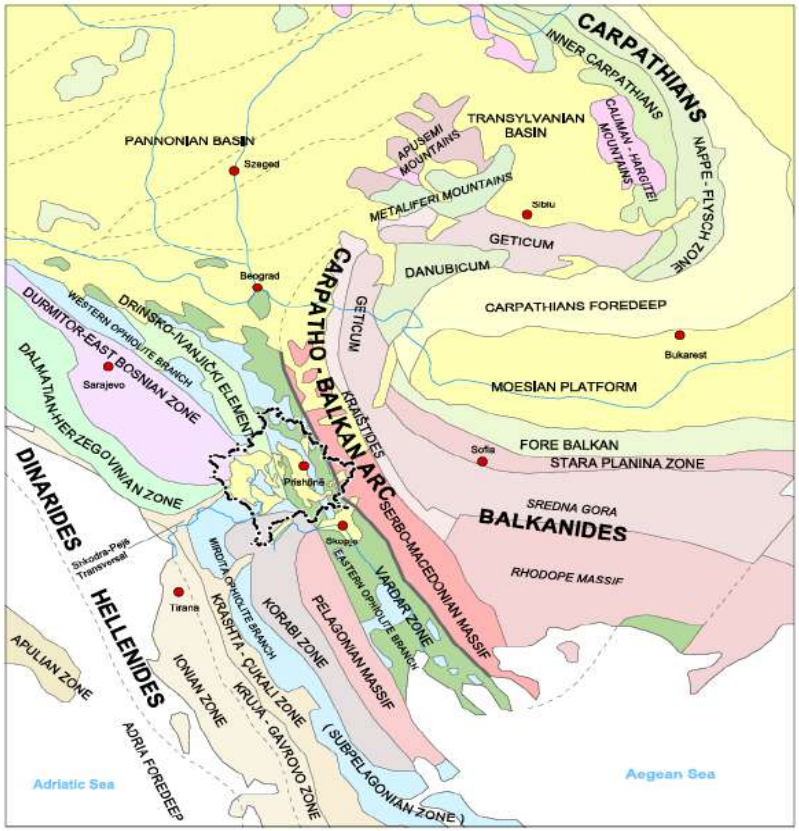

Fig.1. Geotectonic units of the Balkan Peninsula (Beak, 2005; modified after Schönenberg *and Neugebauer 1997; Dimitrijević, 1999; Meço and Aliaj, 2000.)*

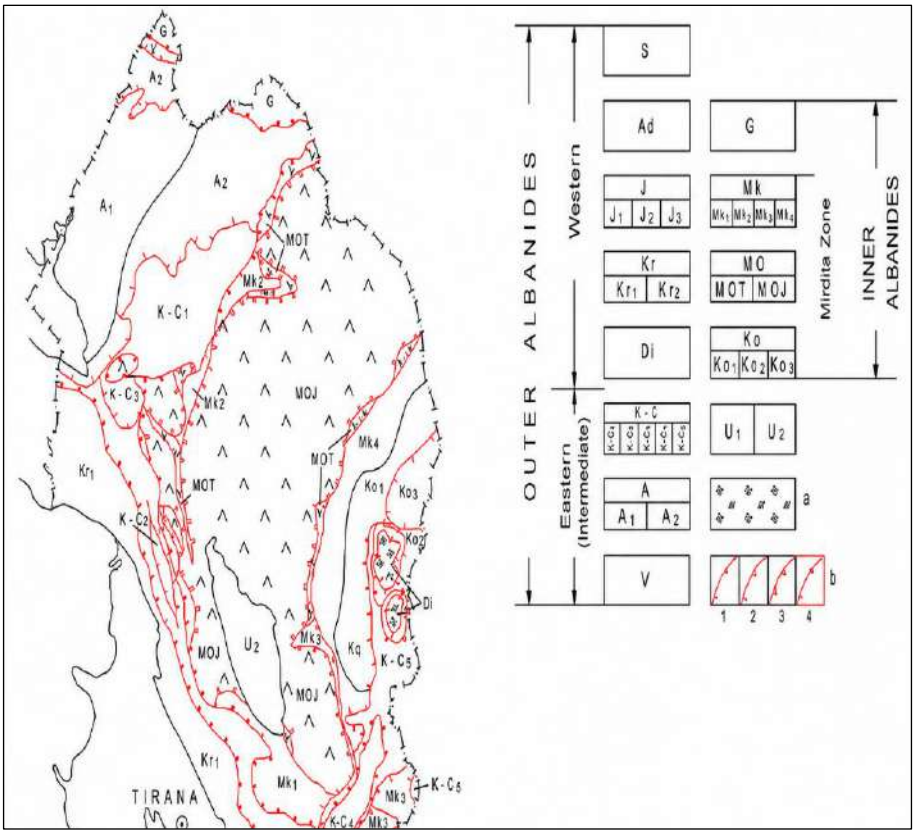

Fig. 2. Fragment from the tectonic map of the Albanides (Xhomo et al. 2002).

From a geological perspective, Kosovo is characterized by a highly diverse assemblage of lithological units, ranging from Proterozoic crystalline basement complexes to Quaternary sedimentary deposits. These include sedimentary, magmatic, and metamorphic rocks, reflecting a complex tectonostratigraphic evolution. Tectonically, Kosovo comprises structural elements of both the Dinaride and Albanide–Hellenide orogenic systems. The principal tectonic zones that define the regional geological framework and extend from northern Albania into Kosovo include the Korabi zone (referred to in Kosovo as the Sharr–Korabi zone), the Mirdita zone (known in Kosovo as the Gjakova zone), and the Prizren basin (Fig. 3) (Legler *et al.* 2003; Elezaj and Kodra, 2008).

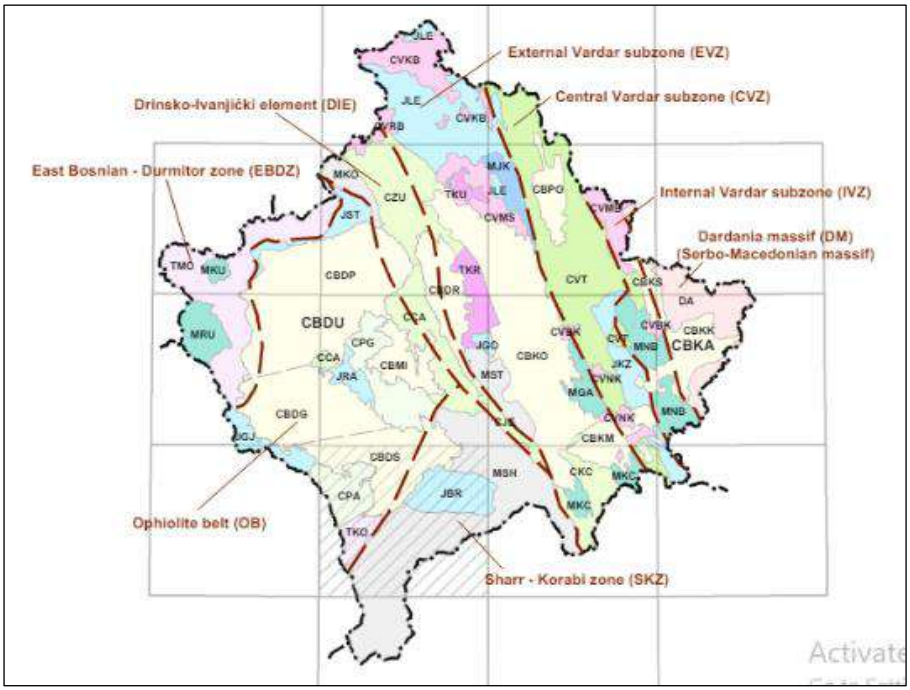

Fig. 3. Geological units within the geotectonic regionalization of Kosovo (Legler et al. 2003) .

2.2 TECTONICS

The broader Kurbnesh–Kukës–Prizren (KKP) fault zone is situated within the Internal Albanides, which, south of the Shkodër–Pejë transverse structure, are represented by the Mirdita and Korabi zones and extend into Kosovo. Each of these zones exhibits a complex internal structure and comprises several distinct subzones (Fig. 4). The Internal Albanides, together with their associated ophiolitic sequences, form part of an orogenic system characterized by an intricate tectonic history. This evolution is recorded through a series of major tectonic phases spanning from the Jurassic and Cretaceous to the Paleogene and Neogene. As a result, the region has undergone multiphase deformation, with each successive tectonic event superimposed on the structural framework established by earlier phases.

The KKP fault zone exhibits a combination of strike-slip and reverse (transpressional) motion, whereas the Shkodër–Pejë zone accommodates both lateral and compressional stresses, functioning as a major transverse shear corridor. The interaction between these structures localizes deformation and plays a significant role in the elevated seismicity observed in northeastern Albania and western Kosovo.

3. RESULTS AND DISCUSSIONS

The Kurbnesh–Kukës–Prizren (KKP) fault system exhibits distinct structural and kinematic characteristics along its three principal segments (Kiratzi and Dimakis, 2013; Ormeni and Hoxha, 2019). Interaction with the Shkodër–Pejë transverse structure further influences fault kinematics, localizing deformation and generating a structural knot associated with enhanced earthquake clustering (Gürbüz *et al*. 2024). Overall, the observed variations in fault geometry, focal mechanisms, and seismicity across these segments indicate a heterogeneous kinematic regime. Strike-slip, reverse, and locally developed normal faulting coexist within the system, reflecting the combined effects of regional plate convergence and structural intersections on the spatial distribution of seismic hazard (Kiratzi and Dimakis, 2013; Ormeni *et al*. 2024).

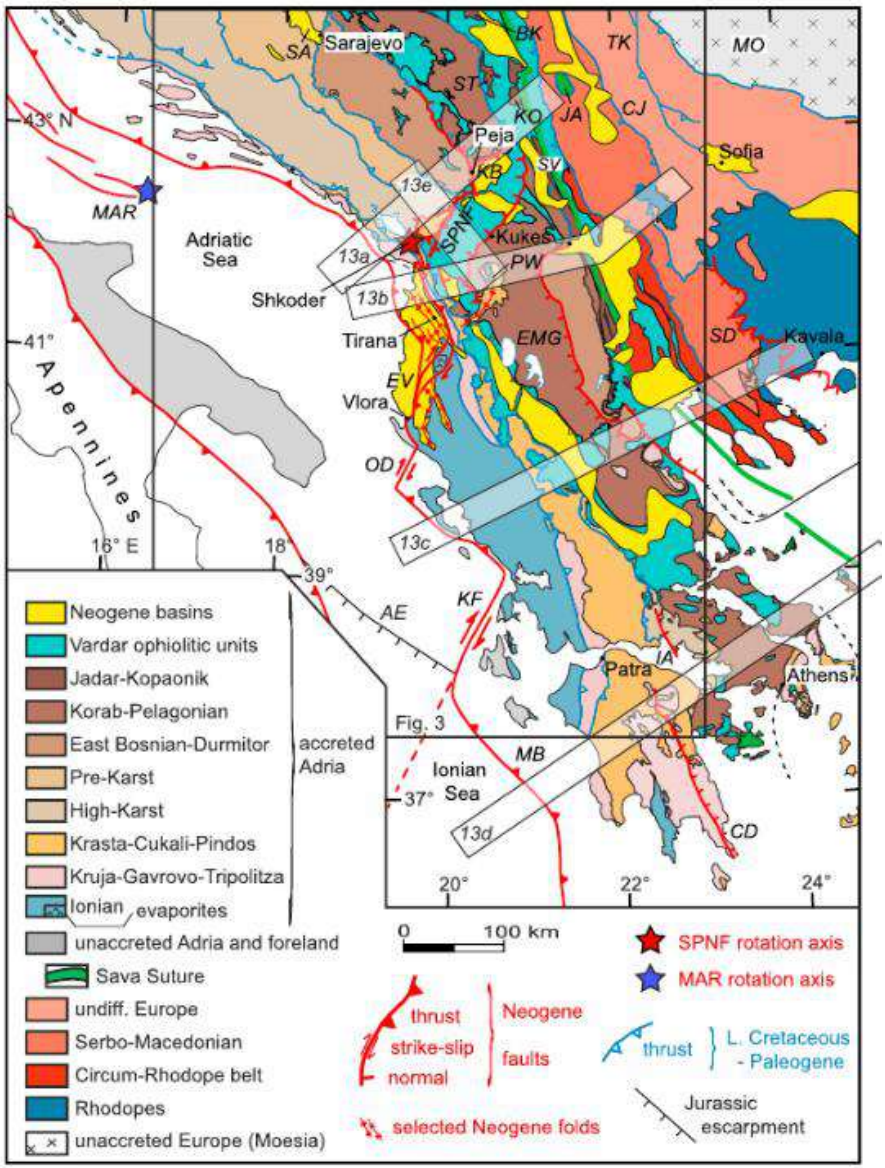

Fig. 4. Tectonic map of the Dinarid–Albanid–Hellenid orogen and Neogene faults (Schmid *et al*. 2008; 2011; Brun and Soukoutis, 2010; Georgiev *et al.* 2012; Van Hinsbergen and Schmid, 2012; Handy *et al.* 2019).

3.1 THE KURBNESH–KUKËS–PRIZREN ZONE

The Kurbnesh–Kukës–Prizren (KKP) fault zone forms part of the Albanides and extends into Kosovo. This transverse fault system is considered a primary source of seismic activity in the region. The average focal depth of the 2,355 recorded earthquakes is approximately 11 km. A total of 20 moderate-magnitude earthquakes (M = 4.0–5.2) have been identified, with an average focal depth of about 13 km. Within the broader seismic framework of eastern Albania, earthquake depths in this area are comparable to the typical depth distribution observed across the region.

The fault zone exhibits a NE–SW orientation and has an overall length of approximately 90 km (Fig. 5). It is subdivided into three main segments: (1) Kurbnesh–Skavicë, (2) Skavicë–Kukës, and (3) Kukës–Prizren (Ormeni *et al.* 2019). The southwestern continuation of the KKP fault system remains uncertain, as its morphological expression becomes increasingly diffuse toward the Burrel basin.

Analysis of the available data indicates that the transverse KKP fault system, specifically along the segment between Arrë-Mollë and Skavicë, intersects a longitudinal fault that extends from Tërnova (near Bulqizë) through Qafë Murrë and Lurë, terminating in Kukës. This configuration represents a structural fault junction where two fault systems with distinct kinematic characteristics interact.

The interpretation of an intersection between the proposed transverse KKP zone and the longitudinal structure originating near Tërnova is based primarily on seismological data rather than on direct surface-mapped geological evidence (Fig. 6).

Focal mechanism solutions indicate that, along most of its length, the Kurbnesh–Kukës–Prizren (KKP) transverse fault system predominantly exhibits normal faulting, which is consistent with a local extensional tectonic regime (Kiratzi and Dimakis, 2013; Ormeni *et al.* 2024). However, in the vicinity of the structural fault junction—where the Kurbnesh–Skavicë segment intersects the longitudinal fault bounding the western margin of the Lurë–Gjallica–Koritnik carbonate massif—focal mechanisms shift predominantly to thrust faulting, which is frequently accompanied by a minor strike-slip component (Ormeni and Hoxha, 2019).

This structural configuration suggests that under specific tectonic stress conditions, extension along the transverse KKP fault system may induce compressional stress responses in adjacent longitudinal fault systems near the junction. The spatial juxtaposition of normal and thrust

faulting indicates that this tectonic intersection functions as a strain transfer zone, where deformation is partitioned differently compared to other segments of the system (Ormeni *et al*. 2024).

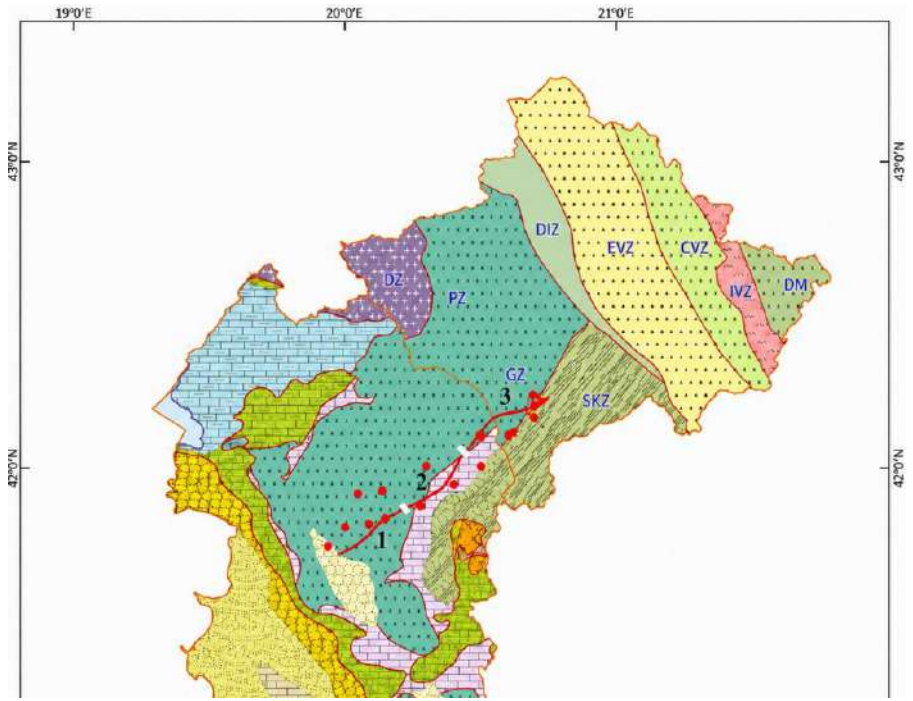

Fig. 5. Schematic tectonic map and epicenters of earthquakes (ML ≥ 4.5) in the Kurbnesh–Kukës–Prizren fault zone during the period 1954–2023.Legend: Three main segments of Kurbnesh–Kukës–Prizren fault: (1) Kurbnesh–Skavicë; (2) Skavicë–Kukës, and (3) Kukës–Prizren.

Field observations along the KKP fault zone reveal surficial structural expressions of thrusting, providing clear evidence of earlier contractional phases. This indicates that the initial stages of regional deformation were closely associated with thrust tectonics, which drove the formation of local fold-and-thrust structures. At present, however, seismological data and focal mechanism analyses demonstrate that the region is characterized by a contemporary extensional regime, reflecting the cumulative effects of its complex geodynamic evolution (Kiratzi and Dimakis, 2013; Ormeni *et al*. 2024).

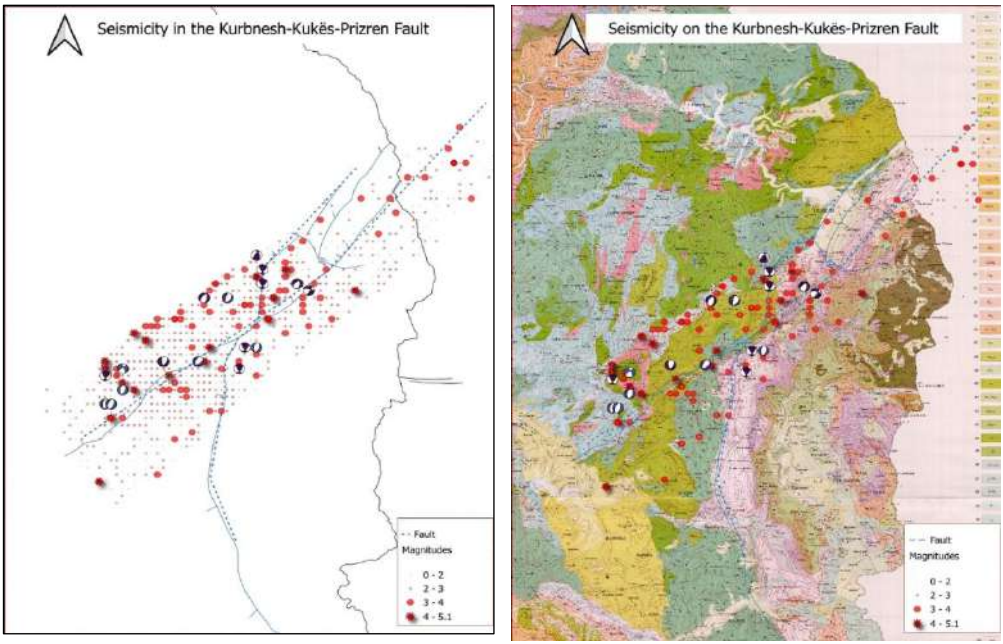

Fig.6. a) Seismicity of the Kurbnesh–Kukës–Prizren fault; b) Seismicity of the Kurbnesh–Kukës–Prizren fault shown on Geologic Map of Albania (1978).

The coexistence of normal and thrust faulting at structural junctions is a phenomenon well-documented in other orogenic belts. In the Albanides, the deformation regime is characterized by a combination of extensional and contractional structures, where rheological and geological contrasts between carbonate mountain massifs and adjacent basins play a key role in the spatial partitioning of tectonic stress (Copley *et al.* 2009). Focal mechanism solutions along major fault segments, particularly at intersections with longitudinal systems in northeastern Albania, indicate a dominance of thrust or reverse faulting, whereas adjacent segments exhibit normal faulting consistent with regional extension (Muço, 1994; Ormeni *et al*. 2022). The most recent focal mechanism catalogue for Albania confirms this complexity, showing that although normal faulting dominates contemporary deformation, oblique-slip and strike-slip mechanisms occur frequently, clustered primarily at structural intersections and zones of high topographic or lithological contrast (Ormeni, 2022).

3.2 SEISMIC ACTIVITY ANALYSIS IN THE ALBANIA–KOSOVO REGION ALONG THE TRANSVERSAL K–K–P ZONE

The seismic activity of the region was analyzed through a comprehensive spatiotemporal assessment of earthquake catalogs along the Kurbnesh–Kukës–Prizren (KKP) fault zone. The earthquake database compiled for this study spans the period 1968–2023 and comprises 2,355 events along the KKP fault system. Epicentral locations of earthquakes with magnitudes in the range1.0 ≤ ML ≤ 5.2, as well as significant events with ML > 4.0, are illustrated in Figures 7a and 7b. To characterize seismic behavior along the KKP fault zone, key statistical parameters were calculated, including temporal histograms of earthquake occurrence, spatiotemporal variations in the seismotectonic *b*-value, annual probabilities of occurrence, and recurrence intervals (Ormeni *et al*. 2024). The structural interpretation is based on an integrated analysis of multiple seismotectonic parameters, including the spatial distribution of epicenters, their linear alignment, the distribution of aftershock sequences of moderate-magnitude earthquakes along the structural trend, spatial variations in the *b*-value, and the kinematic orientations of focal mechanisms.

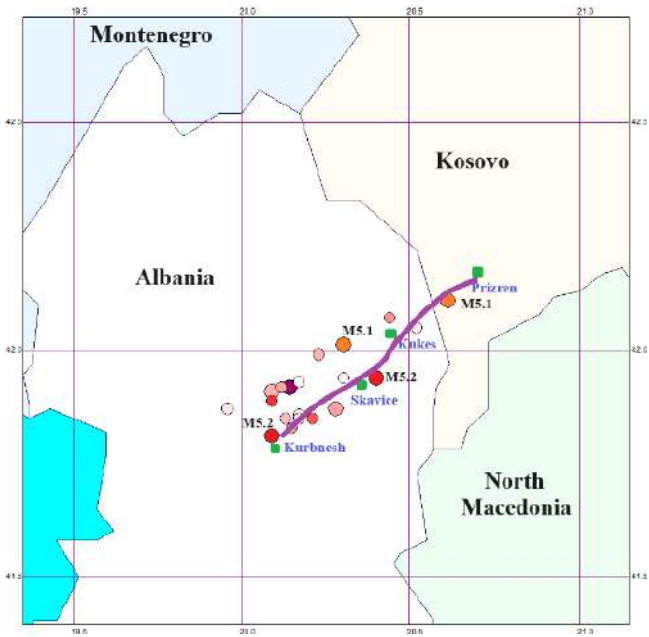

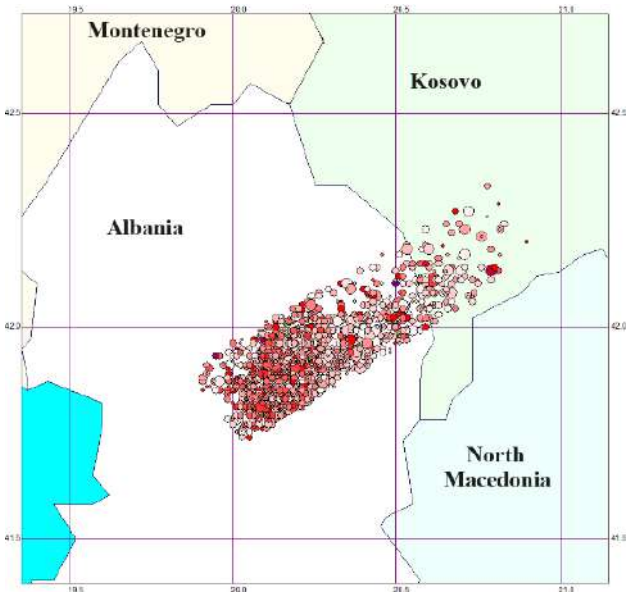

Fig.7. (a) Epicentral distribution of all events with M_L > 4.0, **(b)** epicentral distribution of all events with ML > 0.5 in the K–K–P fault zone, 1968–2023 (Ormeni et al. 2024).

Magnitude histograms for the Kurbnesh–Kukës–Prizren (KKP) fault zone indicate a magnitude range of 0.4 to 5.2, with earthquake frequency exhibiting an exponential decay. The majority of events fall within the magnitude range of 1.6 to 2.7 (Fig. 8), whereas the highest frequency occurs within the ML = 2.1–2.4 interval (Ormeni, 2024).

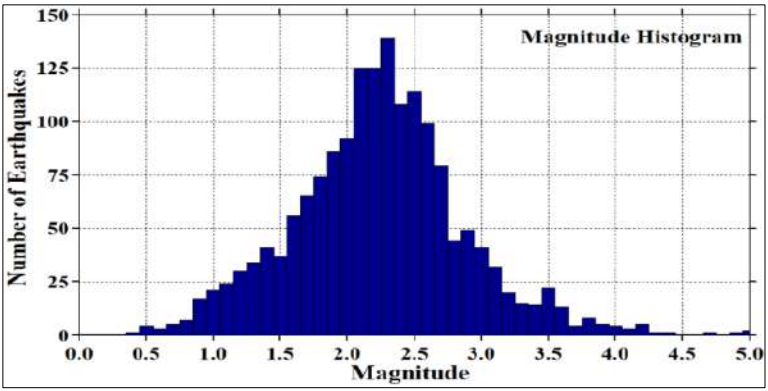

Fig. 8. Earthquake magnitude histograms in and around the K–K–P fault zone (Ormeni et al. 2024).

Temporal variations in the completeness magnitude (*Mc*) are a means to address an accurate estimation of the seismotectonic *b*-value the annual probabilities of occurrence and recurrence intervals (Öztürk and Ormeni, 2021). In the study area, *Mc* ranged between 2.1 and 2.5 until 2012, decreased to approximately 1.2 at the beginning of 2022, and subsequently fluctuated between 1.2 and 2.4 after 2023. It is well established that temporal variations in *Mc* are often unstable; therefore, its evaluation represents a fundamental first step in seismic analysis, as it is a key parameter for reliable *b*-value estimation (Ormeni *et al.* 2023).

The frequency–magnitude distribution of earthquakes is effectively described by the Gutenberg–Richter (G–R) relationship. For the Kurbnesh–Kukës–Prizren (KKP) fault, the *b*-value was determined to be 0.87 ± 0.08 with *Mc* = 2.3 (Ormeni *et al.* 2023). Globally, *b*-values range between 0.3 and 2.0 across various tectonic settings. The mean *b*-value is typically close to 1.0 (Frohlich and Davis, 1993), with tectonic earthquakes generally exhibiting values between 0.5 and 1.5. Lower *b*-values are commonly associated with low crustal heterogeneity and higher stress concentrations in the region (Ormeni *et al.* 2025; Frohlich and Davis, 1993).

Spatial variations in the *b*-value along the KKP fault zone were estimated to range between 0.83 and 1.04 (Fig. 9). Higher b-values (>0.96) occur in the northeastern Kishaj–Nashec segment and along the Kukës–Vërmic–Prizren belt, whereas lower values (less than 1.0) are observed in the southwestern Kurbnesh–Skavicë segment. The lowest values, ranging from 0.80 to 0.86, are identified in the Fushë-Lurë–Lajthizë–Rreps area and the Skavicë–Harren–Domgjon belt. In other segments, *b*-values range from 0.90 to 0.95.

Fault segments characterized by lower *b*-values indicate zones where larger-magnitude earthquakes are more likely to occur, potentially reflecting low structural heterogeneity combined with elevated tectonic stress accumulation along the KKP fault zone. Monitoring regions with anomalously low *b*-values can therefore provide critical insights into seismic potential along the fault system. Accordingly, particular attention should be given to these segments in regional seismic hazard assessments (Ormeni *et al.* 2023; 2025) (Fig. 9).

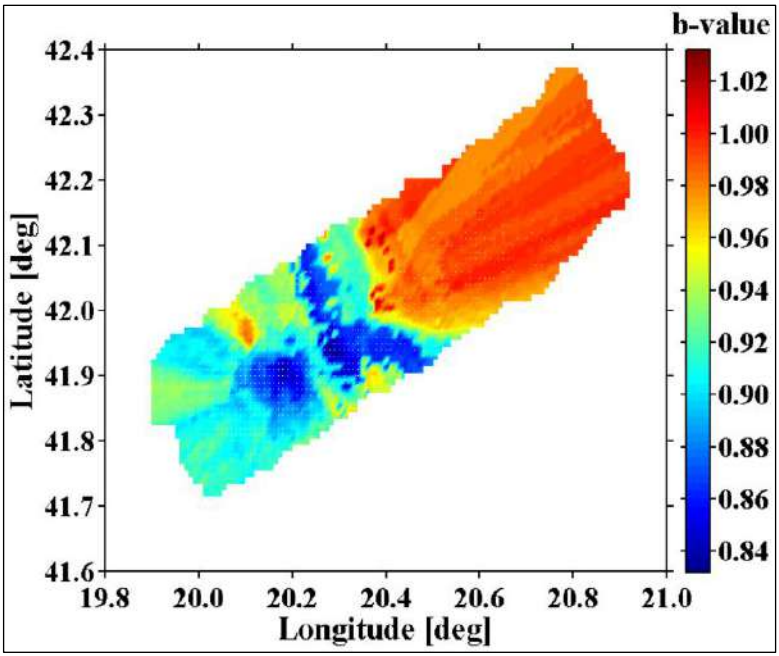

Fig. 9. Map of the b value in the K–K–P fault zone, estimated using the maximum likelihood method (Ormeni, 2024).

4. CONCLUSIONS

The following conclusions could be drawn:

Geodynamic and Structural Framework: The geologic–tectonic framework of Albania and Kosovo is governed by the complex evolution of the Dinaric–Albanide–Hellenide arc. Within this framework, the Albanides are subdivided into External and Internal units characterized by diverse lithological compositions and multiphase tectonic histories. The Kurbnesh–Kukës–Prizren (KKP) fault zone occupies a central position within the Internal Albanides, linking the Mirdita and Korabi zones across the transboundary region into Kosovo. This fault zone has experienced successive orogenic phases spanning from the Jurassic to the Cenozoic (Paleogene–Neogene), resulting in highly overprinted structural architectures.

Kinematic Heterogeneity and Strain Partitioning: The KKP fault system constitutes a major active tectonic structure in northeastern Albania

and western Kosovo, where geological, structural, and seismological datasets collectively define its role within the regional deformation framework. The fault system is segmented into distinct sections with varying orientations and kinematic behaviours, reflecting a complex interplay of strike-slip, reverse, and locally developed normal faulting.

Stress Intersection Mechanics: Along most of its length, the KKP transverse fault system predominantly exhibits normal faulting, which is indicative of the contemporary extensional stress regime in the region. However, at its structural junction with the Tërnovë–Qafë Murrë–Lurë–Kukës longitudinal fault system, local strain transfer results in localized contractional thrust and strike-slip mechanisms that act as localized stress adjustments to the regional extension. This demonstrates that the intersection functions as a critical strain transfer zone.

Tectonic Inversion: Historically, the region evolved from an ancestral contractional regime—responsible for the development of major fold-and-thrust structures—to the contemporary extensional regime, reflecting a clear tectonic inversion and the changing geodynamics of the Western Balkans.

Seismotectonic Parameters: Statistical seismological analysis yields a Gutenberg–Richter *b*-value of 0.87±0.08 with a completeness magnitude (M_c) of 2.3. Spatial variations reveal pockets of anomalously low *b*-values (down to 0.80), suggesting elevated crustal stress accumulation along locked segments of the KKP fault zone. Contemporary assessments indicate that the KKP fault system is capable of generating earthquakes of higher magnitude than those accommodated in existing seismic hazard maps.

Geodetic Constraints: Geodynamic models and contemporary GNSS/GPS velocity vectors confirm slow but continuous relative plate motion across the region, directly driving the crustal stress accumulation responsible for modern earthquake generation.

Hazard Mitigation Implications: A detailed, high-resolution re-evaluation of localized geological and seismic hazards along the KKP fault system is strongly recommended. These updated hazard parameters are critical for directing safe urban expansion, evaluating critical infrastructure planning, and updating natural hazard risk management models across both nations.

Data accessibility. The datasets generated and analysed during the current study are available from the corresponding author upon reasonable request.

Conflict of interest declaration. The authors declare that they have no competing financial interests or personal relationships that could have appeared to influence the work reported in this paper.

Declaration of AI use. During the preparation of this work, the authors utilized artificial intelligence (AI) tools solely to improve the English language expression, syntax, and clarity of the manuscript. Following the use of this service, the authors reviewed and edited the content as necessary and take full responsibility for the entirety of the scientific content and conclusions presented in the manuscript.

Author contributions. N.P.: conceptualizing- study design, methodology, structural/seismological interpretation - results; **Rr.O.:** conceptualizing- study design, methodology, structural/seismological interpretation - results; **B.Sh.:** geological analyzing- Quaternary stratigraphy and neotectonic evolution; **P.N.:** structural interpretation - geological configurations - fault zone- bounding relationships within the broader tectonic units of the Albanides; **D.M.:** investigating -field mapping, structural geology data acquisition; primary data processing.

All authors contributed to the drafting, critical revision, and final approval of the manuscript.

Funding. This research was financially supported by the bilateral project *"Seismic hazard assessment of an active tectonic fault system for a safer life."* The funding agency had no role in the study design, data collection, statistical analysis, geodynamic interpretation, or the decision to submit the manuscript for publication.

REFERENCES:

Aliaj S, Koçiu S, Muço B, Sulstarova E. 2010. *Seismicity, seismotectonic and seismic hazard assessment in Albania*. Published by Albanian Academy of Sciences, 100 pp.

BEAK. 2005. *The Compilation of Geo-Scientific Maps of Kosovo. The Compilation of Geo-Scientific Maps of Kosovo General Map of Minerals of Kosovo* (1:200 000). 200,000) Report – description of the map compilation. Independent Commission for Mines and Minerals. Prishtinë.2005. (www.kosovo-mining.org.).

Elezaj Z, Kodra A. 2008. *Gjeologjia e Kosovës*.Universiteti Prishtinës – Fakulteti Xehetarisë dhe Metalurgjisë, Mitrovicë. Book; ISBN: 978-9951-00-068-0.

Geozavod – Geološki Institut. 1982. Osnovna geološka karta SFRJ, /Sheet K34-66 Prizren, 1: 100,000. Beograd.

Gürbüz A, Shala A, Mustafa S, Erten A. 2024. Active tectonics of western Kosovo: Insights from geomorphic and structural analyses. *Bulletin of the Mineral Research and Exploration*, **173**, 153–173.https://doi.org/10.19111/bulletinofmre.1364807.

Handy MR, Giese J, Schmid SM, Pleuger J, Spakman W, Onuzi K, Ustaszewski K. 2019. Coupled crust–mantle response to slab tearing, bending, and rollback along the Dinaride–Hellenide orogeny. *Geochemistry, Geophysics, Geosystems*, **20(11):** 5367–5394. https://doi.org/10.1029/2019GC008505.

Hoxha I, Ormeni R, Peci N, Mustafa S. 2019. Seismotectonic activity of the Kurbnesh-Kukes-Prizren transversal fault zone. IMGC2019 proceedings, pp 68-73. https://umib.net/wp-content/uploads/2020/03/11.5.1-Conference-2019-Proceedings-IMGC-2019.pdf.

Kiratzi A, Dimakis E. 2013. Focal mechanisms and slip models of moderate-size earthquakes in Albania and adjacent countries. *Italian Journal of Geosciences*, **132(2):** 186–193. https://doi.org/10.3301/IJG.2011.33.

Muço B. 2007. Focal mechanism solutions and stress field distribution in Albania. *Albanian Journal of Natural & Technical Sciences*, **1**, 129–138. *https://akad.gov.al/ajnts-papers/.*

Naço P, Peci N, Shala B, Muçaj D. 2025. Raport studimor mbi vrojtimet e kryera ne terren në kuadrin e projektit. ASHSH-UIBM, Maj 2025, Tiranë-Mitrovicë.

Ormeni R, Hasimi A, Öztürk S, Çomo E. 2023. Correlations between seismic b-value and heat flow density in Vlora-Lushnja-Elbasani-Dibra Fault Zone in Elbasani area, central Albania. *BALTICA*, **36(2):** 176–189. https://doi.org/10.5200/baltica.2023.2.7.

Ormeni R, Hoxha I, Gjuzi O, Bozo R, Gega D, Kanani X, Muca D, Piccardi L, Vittori E, Blumetti AM, Di Manna P, Comerci V. 2022. *The catalogue of earthquakes focal mechanism occurred in Albania and its surrounding during 1948 to 2022*. In NSG2022 – 28th European Meeting of Environmental and Engineering

Geophysics, 18–22 September 2022, Belgrade, Serbia. ISSN 2214-4609. https://doi.org/10.3997/2214-4609.202220159.

Ormeni R, Koçiaj S, Fundo A, Daja S, Doda V. 2013. Moderate earthquakes in Albania during 2009 and their associated seismogenic zones. *Italian Journal of Geosciences*, **132(2)**: 203–212. https://doi.org/10.3301/IJG.2012.45.

Ormeni R, Mustafa S, Lule, A, Muçaj D. 2024. *Analiza hapësinore kohore e sizmicitetit aktual në zonën e thyerjeve Kurbnesh -Kukës-Prizren.* Forum Shkencor 22 Maj 2024, Mitrovicë.https://umib.net/u-mbajt-forumi-shkencor-per-zonat-e-thyerjeve-tektonike-terthore-kurbnesh-kukes-prizren-dhe-shkoder-peje/ .

Ormeni R, Öztürk S, Silo E, Bozo R, Hoxha I, Muçaj D. 2025. Spatial and temporal analysis of seismicity and seismotectonic parameters in Albania region. *BALTICA*, **38(2):** 130–142. Doi https://doi.org/10.5200/baltica.2025.2.2.

Ormeni R, Peci N, Hoxha I, Skrame K, Doda V, Hasim A. 2023. *Vlerësimi i shtresave sizmoaktive në zonën e thyerjeve tektonike Kurbnesh-Kukës-Prizren. I*nternational Multidisciplinary Geo-Science Conference - IMGC2023, 19 - 20 October 2023, Mitrovicë, Republic of Kosovo (https://umib.net/filloi-punimet-konferenca-v-nderkombetare-multidiciplinare-per-gjeoshkence/).

Öztürk S, Ormeni, R. 2021. A comprehensive spatiotemporal evaluation of the current earthquake activity in different parts of the Frakull-Durrës fault zone, Albania. *BALTICA*, **34(1):** 58–70. https://doi.org/10.5200/baltica.2021.1.5.

Peci N, Lule A. 2024. Ndërtimi gjeologjik zonës Kurbnesh-Kukës-Prizren. Forum Shkencor 22 Maj 2024, Mitrovicë (https://umib.net/u-mbajt-forumi-shkencor-per-zonat-e-thyerjeve-tektonike-terthore-kurbnesh-kukes-prizren-dhe-shkoder-peje/).

Schmid SM, Handy MR, Onuzi K., Giese J, Pleuger J, Ustaszewski K. 2017. *Tectonics and geodynamics of the Dinarides and Hellenides: similarities and differences.* Workshop proceedings. 13th Workshop on Alpine Geological Studies Zlatibor Serbia September 7-18. (https://www.researchgate.net/profile/Stefan-Schmid-4/publication/320015193_Tectonics_and_geodynamics_of_the_Dinarides_and_Hellenides_similarities_and_differences/links/59c8b87e458515548f3c4616/Tectonics-and-geodynamics-of-the-Dinarides-and-Hellenides-similarities-and-differences.pdf.)

Xhomo A, Kodra A, Xhafa Z, Shallo M, Nazaj Sh, Nakuçi V, Yzeiraj D, Lula F, Vranaj A, Melo V, Dimo Ll, Sadushi P. 2002. *Gjeologjia e Shqipërisë, Stratigrafia, Magmatizmi, Metamorfizmi, Tektonika dhe Evolucioni Paleogjeografik dhe Evolucioni Paleogjeografik dhe Gjeodinamik (Geology of Albania, text of geological map of Albania), scale 1:200 000).* Tiranë: Albanian Geological Survey.

MORPHOTECTONIC EVIDENCE OF MAJOR ACTIVE FAULTS IN WESTERN ALBANIA: A CONTRIBUTION FOR SEISMIC HAZARD ASSESSMENT

Pio DI MANNA[1], Luigi PICCARDI[2], Eutizio VITTORI[3], Anna Maria BLUMETTI[4], Valerio COMERCI[5], Ismail HOXHA[6], Rrapo ORMENI[7], Rrezart BOZO[8], Olgert GJUZI[9], Petraq NACO[10], Dashamir GEGA[11]

[1]Geological Survey of Italy, ISPRA, Rome, Italy
[2,3,4,5] CNR, Institute of Geosciences and Earth Resources, Florence, Italy
[7,8,9,10]Temporary research unit for geosciences and geoengineering, Academy of Sciences of Albania
[11]Geological Survey of Albania, Tirana, Albania

Author for correspondence: pio.dimanna@isprambiente.it

DiMP,0000-0003-3486-5136; LP,0000-0001-6964-3205; EV, 0000-0003-0653-8437; AMB, 0000-0002-5331-9379; VC, 0000-0002-1022-9488; IH, 0000-0002-4505-3128; RrO, 0000-0002-5514-2204; OGj, 0000-0002-5163-157X

ABSTRACT

The Albanides form a segment of the southern Alpine orogenic belt, connecting the northern Dinarides to the southern Hellenides. These NW–SE-trending, predominantly west-verging chains border the eastern Adriatic Basin, where thrust and strike-slip structures influence coastal and offshore sectors, necessitating accurate seismic potential estimates. While historical and instrumental data confirm intense seismicity in western Albania and its offshore areas, gaps remain in current seismic hazard models. To better characterize potential seismogenic sources, we analyzed the region's principal tectonic features, emphasizing surface evidence and potential surface-faulting effects. The study focuses on the highly exposed sector between the Kruja thrust front, the Tirana Plain, and the Adriatic coast—an area marked by significant urban, commercial, and touristic development. This seismic landscape is shaped by Quaternary-to-recent activity along the Shijak thrust and Vora backthrust, which have disrupted and reorganized the fluvial network, as evidenced by multiple river diversions and wind gaps. Although previous studies consider the Kruja thrust front sealed by Upper Miocene molasse and Pliocene sequences, we identified evidence of potential Quaternary activity along its front, likely associated with secondary gravity-driven processes. Additional Quaternary-to-recent compressional deformation and localized uplift are documented along the Makaresh anticline and Fushë-Kruja hills, indicated by an endorheic basin and both local- and basin-scale

fluvial diversions. Our data suggest that historical and instrumental seismicity may not capture the maximum seismic and surface-faulting potential of the area. This underscores the necessity of integrating surface geological evidence into seismic hazard models to improve risk assessment and mitigation strategies for communities exposed to earthquake and potential tsunami hazards.

***Keywords*:** seismic landscape; tectonic uplift; drainage control; fluvial diversion; wind gap; uplift-driven relief

Citation: Di Manna P, Piccardi L, Vıttorı E, Blumetti AM, Comercı V, Hoxha I, Ormeni Rr, Bozo Rr, Gjuzı O, Naco P, Gega D. 2026. Morphotechtonic evidence of major active faults in western Albania: A contribution for seismic hazard assessment. *Albanian Journal of Natural and Technical Sciences* (AJNTS), **2 (30),**
Journal URL: https://journals-akad.gov.al/magazines/1
Classification: Research
Subject Category: Natural / earth sciences subject area: morphotectonics & paleoseismology

1. INTRODUCTION

Western Albania represents a highly seismically active region within the broader Dinarides–Albanides–Hellenides orogenic belt, shaped by ongoing convergence between the Adriatic microplate and the Eurasian plate. This convergence, active since the Jurassic, has driven the formation of the south-eastern branch of the Alpine orogen, expressed as a NW–SE-trending, southwest-verging thrust-and-fold belt system, and continues to control present-day tectonic activity. This geodynamic framework has resulted in a complex geological and tectonic setting, which is clearly reflected in recent morphotectonic features observable at the surface. These structures provide critical insights for seismic hazard assessment and the identification of active tectonic processes.

Despite the increasing attention given to active tectonics in the region, significant gaps remain in the systematic identification and characterization of active fault systems and associated surface deformations—data that are essential for improving seismic hazard assessment.

In this study, we focus on the western sector of Albania, while complementary contributions within the same volume address the southern

and eastern seismic provinces (Piccardi *et al*. 2025). In addition, a new comprehensive seismic catalogue covering Albania and the surrounding regions is presented by Vittori *et al*. (2025).

The objective of this study is to investigate the morphotectonic signatures of active tectonics in western Albania, with particular emphasis on identifying active faults and folds capable of generating near-surface deformation or surface ruptures. The recognition of such features is crucial for improving the understanding of seismotectonic behaviour and for refining regional seismic hazard models.

Major urban centres within the study area—including Tirana, Kruja, and Durrës—characterized by historical cores and densely populated districts, have undergone rapid industrial, commercial, and tourism-driven development in recent decades, substantially increasing their exposure to seismic hazards. However, much of this expansion has occurred without adequate risk mitigation strategies. In particular, tourism has driven extensive construction along coastal zones, further increasing exposure to natural hazards, including tsunamis. This additional risk must be incorporated into a comprehensive disaster mitigation framework. Raising awareness among residents and tourists, alongside the implementation of effective early warning systems and evacuation plans, is essential to ensure timely response and to minimize potential human and material losses.

To investigate active tectonic structures, we adopt an integrated approach that combines geological and tectonic data, seismicity analysis, remote sensing techniques, geomorphological interpretation, and field verification. Particular emphasis is placed on morphotectonic analysis, which highlights the strong tectonic control on landscape evolution associated with active faulting. This approach involves the identification of key geomorphic indicators, including fault scarps, uplifted sectors, structurally controlled drainage patterns, and deflected channels along active faults. It also documents features such as closed basins, abandoned stream channels, river capture and diversion processes, and drainage damming, all of which are used to evaluate the influence of tectonics on drainage organization and landscape development.

This integrated methodology enables the identification of long-term evidence of tectonic activity, supports the recognition and characterization of major active faults—including a preliminary assessment of their seismic potential—and facilitates the delineation of zones of ongoing deformation. The results suggest that historical and recent seismic events may not fully represent the maximum seismic hazard potential of the area.

Morphotectonic evidence points to the presence of additional seismic sources whose capacity may be underestimated. Further refinement of this assessment requires detailed field investigations and paleoseismological studies.

1.2 Geological and tectonic framework

The study area extends from the relief bordering the eastern margin of the Tirana–Kruja plain to Durrës and the Adriatic coast (Fig. 1). The region lies within the external Albanides and is affected by long-term convergence between the Adriatic (Adria) microplate and Eurasia. This convergence is generally interpreted as part of the closure of the Neotethys (Western Vardar–Meliata ocean), which began during the Mesozoic (Late Jurassic; Bortolotti *et al.* 2005; Schmid *et al.* 2008; Richter *et al.* 2025), marking the onset of oceanic subduction. However, the external Albanides—including the Tirana–Kruja–Durrës sector—were involved only in the later stages of this convergence, particularly during the Miocene, when continental collision led to the development of the fold-and-thrust belt (Velaj *et al.* 1999; Nieuwland *et al*. 2001; Roure *et al.* 2004; Mazzoli *et al*. 2008; 2022; Aliaj *et al.* 2010; Velaj, 2012; Handy *et al.* 2019). Continental subduction has driven NE–SW shortening since the Late Cretaceous, resulting in the decoupling of Meso–Cenozoic sedimentary sequences along Triassic evaporites and the development of thin-skinned thrusting and frontal accretion. In addition, deeper involvement of continental lithospheric slices within the orogenic wedge occurred through crustal underplating (thick-skinned tectonics), particularly during slab rollback, with crustal-scale ramps mainly developing over the last 6–5 Ma (Rossetti *et al*. 2024).

Sedimentary and compressional processes have led to the definition of three main tectonic units, bounded by regional thrust systems: the Krasta–Cukali, Kruja, and Ionian zones (Fig. 1). In the coastal sector, the Peri-Adriatic Depression developed as a foredeep in front of the external Albanides thrust belt (Fig. 1).

The active NE–SW compressional regime, possibly related to slab break-off processes (Handy et al., 2019 and references therein), is expressed by a NW–SE-trending fold-and-thrust belt characterized by predominantly SW-verging thrusts and subordinate backthrusts (Caporali *et al*. 2009; Jouanne *et al.* 2012; Vittori *et al*. 2021). Along the contractional front of the southern Dinarides fold-and-thrust belt in

Montenegro, active normal faults with well-preserved bedrock scarps have also been documented (Biermanns *et al.* 2022), indicating that extensional structures may coexist with a dominantly compressional regime.

The continuity of the Albanides along strike is disrupted by three major transverse, roughly NE–SW-trending lineaments whose tectonic significance remains debated: the Shkodër–Peja, Lezha, and Vlora–Elbasan fault zones. Seismological, GPS, and field data suggest that normal faulting along the Shkodër–Peja zone since the Neogene was preceded by earlier right-lateral strike-slip kinematics (Frashëri *et al*. 2012; Jouanne *et al*. 2012). Schmitz *et al.* (2025) further document post-Eocene brittle normal faulting along this zone, identifying two main phases of activity: one in the Early Oligocene and another in the Late Miocene. It has been proposed that the Shkodër–Peja transverse zone is controlled by slab geometry and tearing of the subducting Adriatic lithosphere (Handy *et al*. 2019), whereas D'Agostino *et al*. (2020) interpret it as a long-lived strike-slip transfer zone marking the northern limit of Aegean rotation, acting as a stable hinge between the rigid Adriatic–Dinaride lithosphere and the deforming Hellenic back-arc system since the Miocene. The Lezha fault zone (Aliaj *et al.* 2000) separates Plio–Quaternary thrust-and-fold belts with different structural orientations: NW–SE in the north (Dinaride trend) and NNW–SSE in the south. It also coincides with a sharp gradient in the GPS velocity field (Jouanne *et al*. 2012). Farther south, the SW–NE-trending Vlora–Elbasan lineament (VEL) (e.g., Roure *et al*. 2004) approximately marks the boundary between the Ionian domain and the Peri-Adriatic Basin of the external Albanides. The tectonic framework is locally influenced by evaporite diapirism, which acts both as an autonomous geodynamic process and as a factor interacting with major tectonic structures at the local scale (Velaj *et al*. 1999; Velaj, 2001; Prifti *et al*. 2018).

Deformation is mainly accommodated by blind reverse faults affecting Pliocene–Quaternary sediments, consistent with a thin-skinned tectonic style (Velaj, 2001; 2011; Roure *et al*. 2004; Mazzoli *et al*. 2008, 2022; Rossetti *et al*. 2024). Seismological and geodetic evidence, particularly from the 2019 Durrës earthquake (Mw 6.4), indicates that this compressional regime remains active, with strain accumulating and being episodically released along buried thrust systems at low but persistent convergence rates of a few mm/yr (D'Agostino *et al*. 2008; Jouanne *et al*. 2012; Govorčin *et al*. 2020; Teloni *et al*. 2021; Vittori *et al*. 2021; Theodoulidis *et al*. 2022; Matraku *et al*. 2023). Accordingly, the present-

day tectonic framework of the western Albanian margin is dominated by southwest-directed crustal shortening, which controls ongoing seismicity concentrated mainly within the external compressional structures of the Ionian and Adriatic domains.

1.3. Historical and instrumental seismicity

The intense seismicity characterizing Albania is well documented by historical catalogues (Aliaj *et al.* 2010; Guidoboni *et al*. 2019; Vittori *et al*. 2025) and instrumental records (e.g., Ormeni *et al.* 2022). Within the study area, twelve earthquakes with magnitude M > 6 have been identified since Roman times, seven of which occurred during the last two centuries. The 1270 earthquake represents the earliest sufficiently documented event of this magnitude, causing severe damage and numerous casualties in Dyrrachium (modern Durrës), with an intensity of IX–X on the MCS scale. For this event, Guidoboni *et al.* (2019) estimated an equivalent magnitude (Me) of 6.2, derived from macroseismic observations (Fig. 1). Contemporary accounts describing "violent vertical movements" suggest that the causative fault was located very close to the city. A less well-documented earthquake (Me 6.2) struck Kruja in 1617, reaching intensity VIII (MCS; Sulstarova and Kociu, 1975). Subsequently, several earthquakes with Mw > 6 affected the Durrës–Tirana region during the nineteenth century, the strongest occurring in 1870 (Mw 6.7; Papazachos and Papazachou, 2003). The most recent major seismic events occurred near Durrës in 1926 (IX MSK, Mw 6.1) and 2019 (VIII–IX EMS, Mw 6.4) (IGEWE, 2019; Ganas *et al*. 2020; Vittori *et al*. 2021; 2025).

During the 2019 earthquake, the relatively deep hypocenter (≥ 20 km) prevented the development of coseismic surface faulting; instead, tectonic uplift/subsidence and westward displacement were the primary effects (Vittori *et al*. 2021). Field investigations (Lekkas *et al*. 2019; Papadopoulos *et al.* 2020; Mavroulis *et al*. 2021; Vittori *et al*. 2021) documented widespread secondary phenomena, including ground fissuring, liquefaction, and lateral spreading. Focal mechanism solutions consistently indicate a predominance of compressional tectonics (Ormeni *et al.* 2022, and references therein).

According to the EMTC tsunami catalogue (version 2; Maramai *et al*. 2019), no tsunami events have been recorded in northwestern Albania. In contrast, six events are documented in southern Albania, associated with onshore earthquakes in 1833, 1851, January 1866, March 1866, 1893, and

1920. These events are primarily linked to ruptures along the Vlorë–Elbasan line and to thrusting within the Ionian Zone over the Sazani Zone (Maramai *et al.* 2019; Piccardi *et al.* 2025). Notably, the 1920 event is described as very strong and "heavily damaging," reaching intensity VIII on the Papadopoulos–Imamura tsunami intensity scale, and causing significant coastal damage, including inundation of the Gulf of Vlorë and Sazani Island (Morelli, 1942).

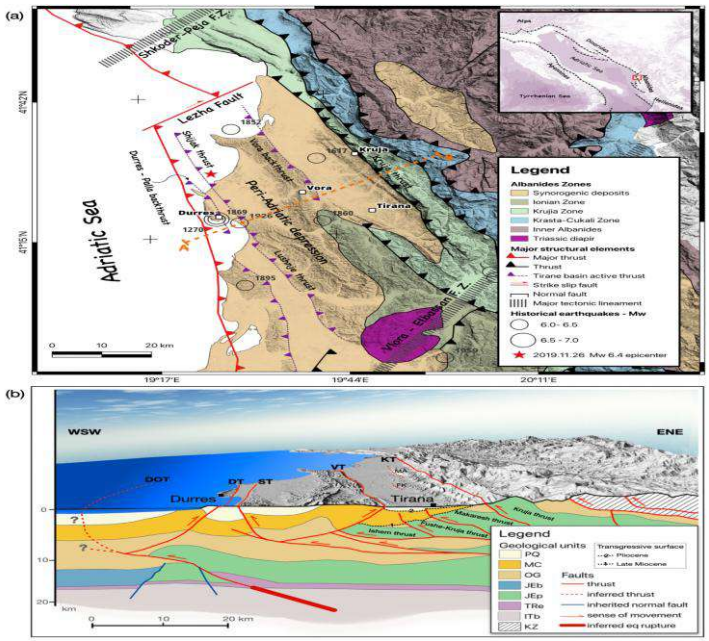

Fig. 1. (a) Simplified geological map of northwestern Albania showing major historical earthquakes, modified from Vittori et al. (2021). (b) Tectonic cross-section of northwestern Albania illustrating the complex structural framework dominated by the interaction of the Krasta–Cukali, Kruja, and Ionian zones within a compressional regime associated with southwest-directed crustal shortening. PQ – Pliocene–Quaternary; MC – Miocene terrigenous deposits; OG – Oligocene terrigenous deposits; JEb – Jurassic–Eocene carbonates (Albanian Basin); JEp – Jurassic–Eocene carbonates (platform); TRe – Triassic evaporites; ITb – Infra-Triassic basement; KZ – Krasta Zone (ultramafic rocks). KT – Kruja Thrust; VT – Vorë Thrust; ST – Shijak Thrust; DT – Durrës Thrust; DOT – Durrës Offshore Thrust; MA – Makaresh Anticline; FK – Fushë-Kruja Anticline. The bold red line represents the inferred rupture zone of the 2019 Mw 6.4 Durrës earthquake.

2. METHODOLOGY

Seismic hazard assessment is primarily based on the analysis of both historical and instrumental seismicity. Although recent earthquakes often attract greater attention and shape the perception of regional hazard, a comprehensive evaluation requires consideration of the complete seismic record of the area. However, the limited temporal coverage and incompleteness of historical datasets represent significant constraints for robust hazard assessment and risk mitigation planning. In this context, geological, morphotectonic, and paleoseismological investigations—capable of identifying and characterizing past earthquake evidence preserved in the geological record—provide essential constraints for extending seismic histories beyond instrumental and historical observations. In western Albania, several major active structures, predominantly thrust and transfer faults, have been identified; nevertheless, their seismogenic potential remains insufficiently constrained.

To address this gap, we first conducted a critical review of available geological and tectonic data and analyzed the spatial distribution and characteristics of both historical and instrumental seismicity derived from national and international seismic catalogues. This analysis enabled the identification of spatial patterns and the recognition of potential seismogenic sources, including the main active fault systems documented in the literature.

To improve the identification and characterization of active faults and folds capable of generating earthquakes and associated surface or near-surface deformation, we adopted an integrated, multi-disciplinary approach combining geological and tectonic data, geospatial analysis, remote sensing, morphotectonic investigation, and field observations. Particular attention was devoted to the identification of neotectonic features within the landscape and to the mapping and characterization of active structures in the western sector of Albania.

The initial phase consisted of a tectonic–geomorphological analysis based on remote sensing techniques, including the detailed interpretation of satellite and aerial imagery, supported by the processing of Digital Elevation Models (DEMs). This phase also involved the review and comparative analysis of existing topographic maps, historical aerial photographs, and geological maps. The preliminary interpretations derived from remote sensing were subsequently validated through targeted

morphostructural field surveys aimed at refining and verifying the identified features. Multiple DEM datasets of varying spatial resolution were collected and processed, including the ALOS 3D World DEM (30 m resolution), the SRTM DEM (30 m resolution; NASA JPL, 2013), and the Copernicus EU-DEM (10 m and 30 m resolution). In selected areas—particularly low-relief sectors such as the Erzen and Ishëm river plains—high-resolution LiDAR data were obtained from the ASIG (Albanian State Authority for Geospatial Information) geoportal. These high-resolution datasets enabled detailed mapping of subtle geomorphological features, such as fault scarps, displaced fluvial terraces, and drainage anomalies. Topographic maps and aerial photographs from different periods and scales were analyzed to detect recent landscape changes and geomorphic indicators of tectonic activity. All datasets were processed within a GIS environment to derive morphometric parameters, including slope, aspect, curvature, and drainage network configurations, which are indicative of active tectonics. These analyses contributed to reconstructing the morphotectonic evolution of the study area and to validating observed deformation features.

Finally, geological and morphostructural field investigations conducted in selected key areas confirmed the presence of active faults and provided critical constraints on their geometry, kinematics, and seismic potential. A specific morphometric analysis was performed along the exposed Kruja thrust front and across the main river valleys intersecting it, following the methodology proposed by Bull (2007). This analysis included the calculation of the mountain-front sinuosity index (J) and the valley floor width-to-height ratio (Vf), which are widely used proxies for assessing the relative tectonic activity of mountain fronts.

3. RESULTS

The results presented in this section illustrate representative examples of the major tectonic lineaments affecting the area between the Kruja thrust front, the Tirana Basin, and the Adriatic coast. The landscape extending from the Kruja thrust front to the coastline is characterized by NW–SE-trending active folding, expressed as narrow anticlines and broad synclines. This structural configuration gives rise to a series of alternating, sub-parallel ridges and lowlands that exert a strong control on the hydrographic network (Fig. 2a). Thrust-related ridges are commonly bounded by active thrust faults along their western flanks and/or by

backthrusts on their eastern sides, reflecting the overall compressional tectonic regime. The Tirana–Thumanë synform, infilled by Late Miocene–Pliocene molasse deposits and overlain by Quaternary fluvial sediments, forms a wide depression structurally controlled by the interaction between the frontal structures of the Kruja thrust system to the east and the Vorë backthrust to the west. Further west of the Vorë ridge, the course of the Erzen River is locally deflected and structurally guided by the shallow (sub-cropping) trace of the Shijak thrust, highlighting the ongoing influence of active tectonics on fluvial dynamics.

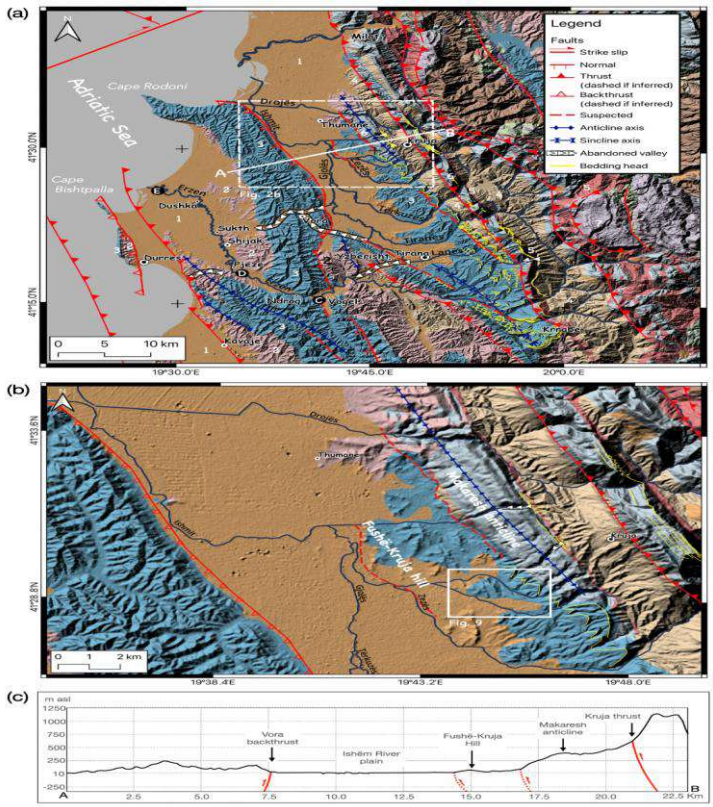

Fig. 2: *(a)* Morphological evidence of active tectonics in W Albania. Red lines: thrusts (empty teeth: backthrusts). Geological Units from https://geoportal.asig.gov.al/en/data: 1-Holocene. Alluvial sediments: silts, sands, gravels; 2 - Lower Pliocene. Clays, siltstones, sandstones; 3 - Tortonian- Messinian. Sandstones, clays, conglomerates, limestones, and evaporites; 4- Lower Oligocene. Clay-siltstone-sandstone flysch with slumping layers and limestone olistoliths; 5 - Eocene. Biomicritic and turbidite limestones in the Ionian and Kruja zones; 6 -

Upper Cretaceous. Limestones with rudists and dolomitized limestones in the Sazani, Kruja, Mirdita zones; 7 - Upper Triassic-Lower Jurassic. Limestones with megalodontes. (b) Copernicus 10 m DTM detailing the morphotectonic features of the anticlines in front of Kruja thrust. The white box locates the area of Fig 9. (c) Topographic profile across the Tirana Basin (trace A-B in *(a)*). Vertical exaggeration 4:1.

3.1. Kruja Zone thrust front

The Kruja Zone is mainly composed of Cretaceous platform carbonates and Paleocene–Eocene shallow-water deposits, detached along weak horizons (Aptian shales or anhydrites levels) and organized into a stack of duplexes (Roure *et al.* 2004; Velaj, 2012). These structures are constrained by drilling and seismic data and are also expressed at the surface in the Makaresh and Dajti anticlines (Roure *et al.* 2004; Aliaj, 2006; Silo *et al.* 2010; Velaj, 2011; Bega, 2013). Oligocene flysch deposits record the flexure of the Adriatic foreland and the incorporation of the Kruja domain into the Albanides foredeep. The Kruja carbonate units were transported southwestward and emplaced over the Oligocene flysch and the Ionian unit during the Burdigallian (Nieuwland *et al.* 2001; Roure *et al.* 2004; Jardin *et al.* 2011).

Tortonian to Pliocene transgressive unconformity sediments, deposited in piggyback basins, indicate thrust emplacement in the Outer Albanides continuing during the Neogene. The main activity of the Kruja thrust system is considered sealed by the Tortonian–Messinian unconformity (Nieuwland *et al.* 2001; Roure *et al.* 2004), followed by an out-of-sequence phase of activity along the internal Kruja thrust (Jardin *et al.* 2011). Aliaj (2006), Silo *et al.* (2010), and Meçaj *et al.* (2018) report significant deformation and displacement of the Miocene molasse deposits associated with the activity of the buried Makaresh and Fushe-Kruja thrusts, as well as more subtle deformation and offset affecting the base of the Pliocene transgressive sequence in the Tirana piggyback basin succession. This confirms the activity of the Kruja thrust system at least up to the early Pliocene, while also suggesting a progressive decrease in tectonic activity and a transition toward a more stable or less intense deformation regime during post-Miocene times. Quaternary activity along the Kruja thrust front is inferred to be limited to deep seismicity, as no clear surface evidence has been identified by now. This study aims to evaluate the presence of evidence for such recent activity.

In detail, the Kruja thrust front consists of four main imbricate thrusts, including an outcropping internal thrust and a basal thrust, which enclose a stack of thrusts buried beneath the Tirana wedge-top basin deposits (Fig. 1B). These deposits are deformed at the surface by the NW–SE-oriented Makaresh anticline, and at depth by the Fushë-Kruja and Ishëm thrusts (Silo *et al*. 2010). The main outcropping thrust (Dajti-Kruja) bounds with a NW-trending rectilinear front the Dajti mountain ridge for ca. 50 km (Fig. 2, 3a). The very steep and rectilinear fault scarp, located just above the tectonic contact between the Mesozoic limestones and the underlying Oligocene flysch deposits, suggests that neotectonic activity plays a significant role in shaping the present-day morphology, slope evolution, and geomorphic expression of the fault zone.

Morphometric analysis carried out on the thrust front and the major river valleys crossing it appears to confirm this role, as indicated by the low value of the mountain-front sinuosity index (J = 1.1) and the mean valley floor width-to-valley height ratio (Vf = 0.25), both estimated according to Bull (2007). The mean Vf index was calculated from Vf values derived for 10 river valleys crossing the Kruja thrust (Fig. 3). The most representative valleys are those associated with major rivers (Lanes, Tiranes, Terkuzes, Drojes), where erosional processes are expected to be more active (Sectors 1- 6 in Fig. 3). However, to ensure a more objective assessment, minor river valleys were also included as additional indicators of tectonic activity (Sectors 7-10 in Fig. 3). A series of topographic profiles was analyzed across selected major valleys intersecting the Kruja thrust. The analysis was conducted from SE to NW. In each sector, valleys were examined over a 1 km stretch upstream of the thrust, ensuring lithological consistency, with cross-sectional profiles spaced at 50 m intervals. Topographic profiles were traced over lengths of approximately 4 km in sectors 1 to 6 and 2 km in sectors 8 to 10, ensuring that both the right and left drainage divides were crossed. Profiles were spaced at 50 m intervals, yielding a total of 210 profiles (Fig. 3 and 4). For each topographic profile, the parameters required to calculate the Vf index were extracted, as reported in Table 01. In addition, the J index was calculated as the ratio between the length of the Kruja thrust trace and the total linear length of the thrust front between the same reference points (Kruja thrust line), yielding a value indicative of a highly linear fault scarp associated with the Kruja thrust (Fig. 4).

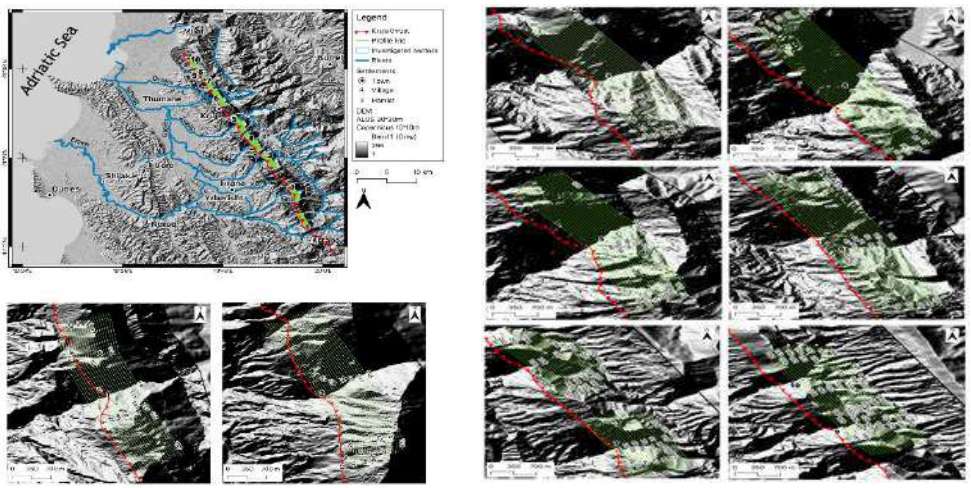

Fig. 3 - Location of the ten investigated river valleys crossing the Kruja thrust front, indicated as sectors 1 to 10. Each close-up panel shows the trace of the topographic profiles used for extracting the parameters defining the Vf index. A series of profiles were traced across the main valleys intersecting the Kruja thrust, starting from the thrust trace and extending 1 km upstream, ensuring consistent lithology along each profile. The profiles were traced over lengths of approximately 4 km in sectors 1 to 6 and 2 km in sectors 7 to 10, ensuring that both the right and left drainage divides were crossed. Profiles were spaced at 50 m intervals. The number shown on each profile line represents the profile ID and corresponds to the list in Table 01. Parameter extraction was performed using the Copernicus 10 m resolution DTM; a dedicated QGIS tool, developed as a Python script, was used to analyse the DTM along the profile lines.

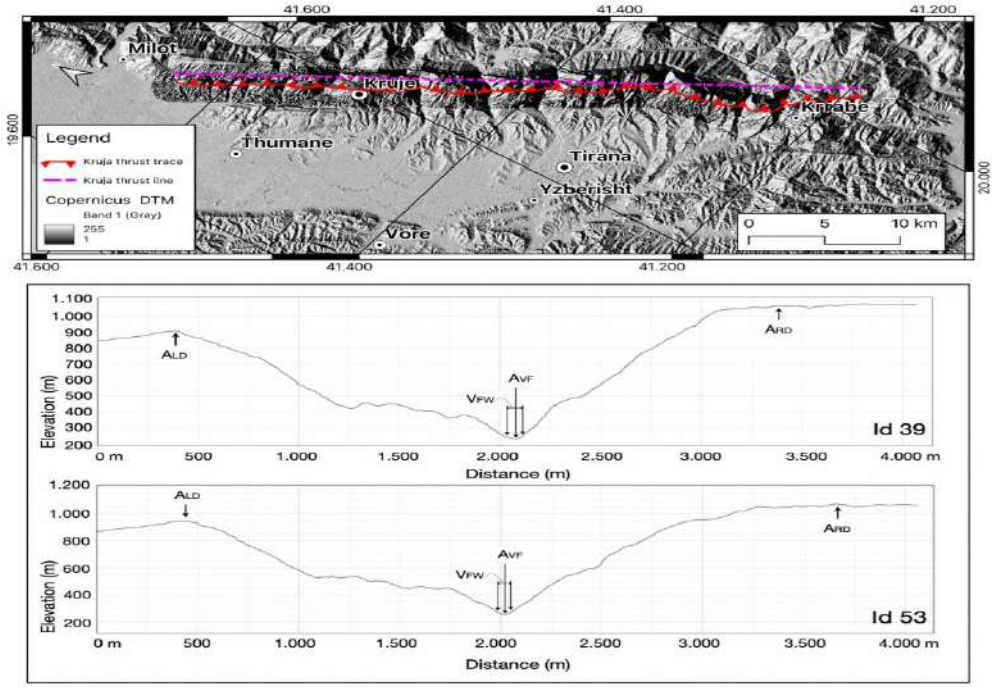

Fig. 4 - a) Comparison between the length of the Kruja thrust trace (red line, about 58 km in length) and the total linear length of the thrust front (Kruja thrust line; purple dashed line, about 54 km in length), measured between the same reference points. **b)** Example of two topographic profiles identified as Id39 and Id53 (the full list of profiles and related parameters is provided in Table 01), with an indication of the measured parameters used for the calculation of the Vf index. **Id** – identifier of the profile line; $\mathbf{A_{VF}}$ – altitude of the valley floor; $\mathbf{A_{LD}}$ – altitude on the left watershed divide; $\mathbf{A_{RD}}$ – altitude on the right watershed divide; $\mathbf{V_{FW}}$– valley-floor width, defined as the distance between the two valley flanks; measured based on slope breaks identified from variations in the tangent of the slope angle; $\mathbf{V_{FR}}$ – Vf index—valley-floor width-to-mean height ratio, defined as the ratio between valley-floor width and the mean relief between the valley floor and the watershed divides.

Table 01 - List of profile lines with the corresponding extracted parameters for the calculation of the Vf index. The locations of the profile lines are shown in Fig. 3. Distance and altitude values are in meters.

Id	Avf	Ald	Ard	Vfw	Vfr	Id	Avf	Ald	Ard	Vfw	Vfr	Id	Avf	Ald	Ard	Vfw	Vfr	Id	Avf	Ald	Ard	Vfw	Vfr
0	263,45	538,26	497,26	70,00	0,28	53	254,77	946,02	1073,65	80,00	0,11	106	264,94	929,34	1128,34	70,00	0,09	158	139,71	371,90	414,39	60,00	0,24
1	193,67	627,91	747,49	60,00	0,12	54	695,23	934,94	1036,20	70,00	0,24	107	270,24	1047,94	1120,26	60,00	0,07	159	147,73	402,17	399,86	60,00	0,24
2	223,97	843,68	782,67	60,00	0,10	55	236,51	688,89	717,81	70,00	0,15	108	219,62	1130,21	1116,93	60,00	0,07	160	148,56	347,04	425,95	70,00	0,29
3	164,98	932,06	804,77	60,00	0,09	56	367,21	728,07	714,89	80,00	0,23	109	253,65	1125,50	1219,11	60,00	0,07	161	184,12	424,18	353,67	60,00	0,29
4	213,02	882,33	1014,73	60,00	0,08	57	241,46	880,56	1066,78	60,00	0,08	110	761,72	1103,18	1291,26	60,00	0,14	162	198,88	410,42	340,41	60,00	0,34
5	615,25	790,67	818,87	60,00	0,32	58	252,62	1075,3	1074,20	60,00	0,07	111	256,13	826,77	856,14	60,00	0,10	163	161,88	426,11	387,67	60,00	0,24
6	222,85	552,67	574,41	70,00	0,21	59	197,23	1058,4	951,93	60,00	0,07	112	517,83	762,81	762,49	60,00	0,25	164	171,18	434,18	373,87	60,00	0,26
7	279,07	560,15	523,30	60,00	0,23	60	245,29	969,75	1086,79	60,00	0,08	113	271,01	913,16	1115,31	70,00	0,09	165	315,13	379,84	364,14	60,00	1,06
8	199,05	665,80	771,26	60,00	0,12	61	702,91	958,74	1057,45	80,00	0,26	114	272,85	1016,23	1138,24	60,00	0,07	166	316,96	351,31	375,19	60,00	1,30
9	224,55	886,54	802,70	60,00	0,10	62	237,25	726,18	750,87	60,00	0,12	115	214,99	1155,25	1146,19	60,00	0,06	167	303,37	365,16	374,85	70,00	1,05
10	173,32	970,40	829,50	70,00	0,10	63	378,82	743,40	745,51	70,00	0,19	116	255,67	1157,03	1244,61	60,00	0,06	168	309,34	373,44	377,02	70,00	1,06
11	214,14	887,43	1063,36	70,00	0,09	64	240,37	890,41	1111,67	100,00	0,13	117	770,93	1132,83	1335,39	60,00	0,13	169	357,57	383,78	475,31	60,00	0,83
12	627,20	812,24	860,81	60,00	0,29	65	257,95	1052,0	1086,97	60,00	0,07	118	249,34	811,71	850,66	60,00	0,10	170	361,61	386,49	479,39	70,00	0,98
13	223,89	562,73	598,35	80,00	0,22	66	198,23	1039,9	968,74	60,00	0,07	119	545,13	752,81	753,75	70,00	0,34	171	266,30	391,23	550,58	60,00	0,29
14	295,74	598,03	550,46	60,00	0,22	67	242,42	987,05	1090,56	60,00	0,08	120	274,34	897,42	1094,78	60,00	0,08	172	274,24	393,65	535,53	60,00	0,32
15	211,80	710,31	803,26	60,00	0,11	68	713,14	992,34	1095,42	60,00	0,18	121	275,17	993,48	1159,99	60,00	0,07	173	245,85	400,97	544,98	80,00	0,35
16	230,99	927,04	829,80	70,00	0,11	69	236,56	753,31	807,70	60,00	0,11	122	219,71	1180,56	1174,92	60,00	0,06	174	258,61	397,76	548,17	60,00	0,28
17	179,31	1001,27	853,56	60,00	0,08	70	393,00	756,36	761,76	80,00	0,22	123	260,98	1183,12	1265,20	60,00	0,06	175	302,74	376,78	455,94	60,00	0,53
18	219,81	901,46	1077,37	60,00	0,08	71	245,73	895,23	1140,67	80,00	0,10	124	779,10	1152,63	1341,61	60,00	0,13	176	310,45	387,72	415,46	60,00	0,66
19	629,33	832,72	898,55	60,00	0,25	72	258,60	1074,7	1070,39	60,00	0,07	125	272,30	791,27	844,04	60,00	0,11	177	287,88	387,80	515,09	70,00	0,43
20	223,40	580,15	608,40	80,00	0,22	73	202,30	1029,5	989,89	60,00	0,07	126	554,30	738,37	734,96	60,00	0,33	178	296,05	375,49	487,23	60,00	0,44
21	310,71	635,47	580,68	60,00	0,20	74	243,24	1009,9	1106,35	70,00	0,09	127	277,39	894,42	1082,86	80,00	0,11	179	188,19	414,27	484,03	60,00	0,23
22	220,41	765,44	836,57	60,00	0,10	75	722,67	1025,5	1119,10	60,00	0,17	128	307,16	963,57	1189,44	70,00	0,09	180	200,81	408,43	505,37	60,00	0,23
23	233,71	960,15	859,36	60,00	0,09	76	232,35	766,16	841,55	60,00	0,10	129	222,43	1184,17	1199,64	60,00	0,06	181	178,70	425,49	457,98	60,00	0,23
24	185,81	1016,30	869,39	60,00	0,08	77	408,70	759,26	771,89	60,00	0,17	130	261,67	1205,44	1289,93	80,00	0,08	182	222,86	405,80	548,07	70,00	0,28
25	223,03	905,70	1080,06	60,00	0,08	78	244,22	894,99	1140,08	60,00	0,08	131	787,65	1173,18	1318,19	80,00	0,17	183	233,82	401,38	545,45	60,00	0,25
26	648,71	853,78	928,47	60,00	0,25	79	259,69	1104,1	1055,48	60,00	0,07	132	264,29	770,71	833,49	60,00	0,11	184	210,80	410,54	522,23	70,00	0,27
27	229,34	598,49	615,12	60,00	0,16	80	204,36	1024,0	1011,15	60,00	0,07	133	569,72	725,18	700,26	70,00	0,49	185	216,11	409,48	538,53	60,00	0,23
28	322,92	666,98	615,06	60,00	0,19	81	245,02	1031,8	1125,02	60,00	0,07	134	281,35	891,18	1097,58	60,00	0,08	186	346,33	355,84	444,52	70,00	1,30
29	223,66	808,08	873,60	60,00	0,10	82	730,81	1055,6	1165,41	60,00	0,16	135	292,94	928,62	1207,13	70,00	0,09	187	353,32	373,97	453,00	60,00	1,00
30	245,52	1004,90	894,47	60,00	0,09	83	238,05	779,71	849,99	60,00	0,10	136	221,21	1199,87	1225,50	60,00	0,06	188	330,35	397,90	393,76	60,00	0,92
31	192,74	1034,96	882,69	70,00	0,09	84	424,57	760,99	774,21	60,00	0,17	137	263,07	1224,79	1312,88	60,00	0,06	189	339,81	340,65	414,58	40,00	1,06
32	223,92	907,59	1083,38	60,00	0,08	85	251,76	909,84	1135,82	60,00	0,08	138	798,89	1197,58	1326,17	60,00	0,13	190	411,04	475,27	551,72	70,00	0,68
33	664,48	869,62	958,31	60,00	0,24	86	261,76	1105,2	1055,70	60,00	0,07	139	262,56	746,21	819,35	60,00	0,12	191	419,92	472,96	564,72	70,00	0,71
34	225,74	616,50	627,72	60,00	0,15	87	205,45	1045,2	1041,54	60,00	0,07	140	361,61	386,49	563,87	70,00	0,62	192	330,18	554,14	486,30	60,00	0,32
35	333,97	705,64	653,19	60,00	0,17	88	247,81	1057,6	1142,71	70,00	0,08	141	580,04	714,13	665,74	70,00	0,64	193	344,43	549,93	453,01	60,00	0,38
36	230,34	823,06	917,62	60,00	0,09	89	738,55	1080,1	1202,63	60,00	0,15	142	284,15	897,88	1116,10	60,00	0,08	194	278,07	544,98	546,61	60,00	0,22
37	243,43	1037,26	927,52	60,00	0,08	90	236,47	811,82	854,04	60,00	0,10	143	286,29	887,43	1211,76	60,00	0,08	195	316,44	548,17	529,63	60,00	0,27
38	198,97	1053,30	897,28	60,00	0,08	91	452,39	766,83	791,99	70,00	0,21	144	226,32	1218,27	1227,54	70,00	0,07	196	331,16		577,98	30,00	NUL
39	227,09	909,04	1078,08	80,00	0,10	92	251,88	920,88	1137,49	60,00	0,08	145	267,00	1220,61	1331,47	60,00	0,06	197	312,82		580,67	30,00	NUL
40	676,41	898,80	996,55	60,00	0,22	93	262,50	1098,1	1072,30	90,00	0,11	146	806,86	1216,52	1338,95	60,00	0,13	198	363,39	551,44	419,52	60,00	0,49
41	226,47	640,72	652,42	60,00	0,14	94	208,74	1077,3	1065,85	60,00	0,07	147	257,51	720,93	801,62	60,00	0,12	199	348,42		569,52	30,00	NUL
42	344,84	727,73	683,78	60,00	0,17	95	248,71	1080,8	1167,45	60,00	0,07	148	322,32	337,72	383,78	80,00	2,08	200	199,34	484,03	548,81	60,00	0,19
43	236,75	846,60	953,00	60,00	0,09	96	745,75	1083,0	1226,13	60,00	0,15	149	325,97	355,42	385,08	100,00	2,26	201	219,45	505,37	592,96	60,00	0,18
44	242,65	1048,39	963,37	60,00	0,08	97	234,57	823,79	854,50	80,00	0,13	150	254,63	377,35	321,68	80,00	0,84	202	178,46	457,10	525,42	60,00	0,19
45	199,41	1059,89	915,79	60,00	0,08	98	467,70	770,70	794,19	60,00	0,19	151	262,00	371,18	344,70	70,00	0,73	203	260,38	548,07	575,75	80,00	0,27
46	232,29	921,22	1072,79	60,00	0,08	99	256,78	934,60	1137,47	80,00	0,10	152	222,91	399,03	325,24	60,00	0,43	204	268,93	545,45	545,87	70,00	0,25
47	685,63	920,66	1014,91	60,00	0,21	100	271,11	1085,4	1096,08	60,00	0,07	153	237,92	387,10	321,44	60,00	0,52	205	234,40	522,23	606,57	70,00	0,21
48	234,55	863,21	684,56	70,00	0,16	101	216,93	1107,5	1088,57	60,00	0,07	154	289,80	362,12	364,94	60,00	0,81	206	246,74	537,61	595,93	60,00	0,19
49	356,42	725,58	692,09	80,00	0,23	102	252,05	1101,5	1188,23	60,00	0,07	155	298,17	359,41	370,92	60,00	0,90	207	386,43	432,08	560,76	60,00	0,55
50	232,27	864,29	993,13	60,00	0,09	103	752,17	1083,7	1262,21	70,00	0,17	156	273,55	369,26	355,86	70,00	0,79	208	399,69	453,51	538,99	60,00	0,62
51	247,90	1049,91	1019,20	70,00	0,09	104	249,24	832,74	849,18	70,00	0,12	157	281,79	367,42	357,98	60,00	0,74	209	337,00	371,56	584,29	70,00	0,50
52	200,47	1063,93	925,47	60,00	0,08	105	488,31	770,52	777,82	60,00	0,21	158	139,71	371,90	414,39	60,00	0,24	210	364,31	399,67	581,78	70,00	0,55

Field survey observations confirm the rectilinear morphology of the Dajti Mountain slope, particularly in the sector southeast of the town of Kruja, where a pronounced morphological scarp is evident (Fig. 5a). This scarp is locally accentuated by extensional fault planes associated with the gravitational evolution of the Kruja thrust front. The contact with the underlying flysch deposits in the footwall is mantled by breccia deposits containing large carbonate boulders, generated by rockfall, toppling, and rock avalanche processes. These slope deposits are characteristic of the geomorphic evolution of an active thrust front. However, no direct evidence was observed indicating that these deposits are currently involved in thrust activity. A possible exception occurs at the outlet of the Tirana River, where it intersects the thrust front and forms a prominent gorge (Fig. 5b). At this location, the structural relationship between the thrust surface and the overlying Quaternary deposits, which rest upon folded and steeply inclined Oligocene flysch, remains insufficiently constrained based on the available data and field observations.

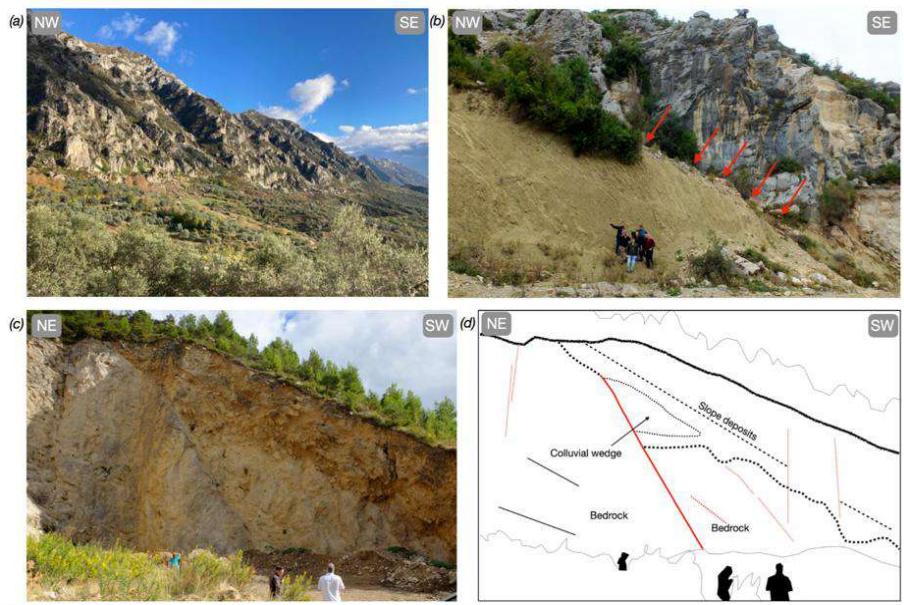

Fig. 5: (a) Landscape view of the Dajti Mountain slope, southeast of the town of Kruja. The view is from NW. (b) The Kruja-Dajti thrust front at the outlet of the Tirana River, showing the contact between the Upper Cretaceous carbonate rocks in the hanging wall and the Oligocene flysch deposits in the footwall. Red arrows mark the sector where potential involvement of slope deposits in the thrusting process

needs to be verified through further investigation. (c) Quaternary normal fault observed along the road "Rruga e Malit", from Kruja to Mount Flamurit (culmination of the ridge back to Kruja town;(Lat 41.517145°N, Lon.19.794541°E). (d) Line drawing of the photo in the panel (c) showing the trace of the normal fault and the triangular geometry of the Quaternary deposits against the fault suggesting the occurrence of a "Colluvial wedge". The bedrock consists of Upper Cretaceous limestones.

In the frontal zone northwest of Kruja, along "Rruga e Malit" (the road connecting Kruja to Mount Flamurit, marking the culmination of the ridge behind the town), just outside the historical center, a southwest-dipping Quaternary normal fault has been identified (Figs. 5c and d). This structure is interpreted as a secondary feature within the thrust system, likely related to gravitational collapse processes affecting the thrust front. The fault offsets both the Upper Cretaceous limestone bedrock and the overlying Quaternary breccia deposits, indicating activity during the Quaternary. The wedge-shaped geometry of the Quaternary deposits adjacent to the fault is consistent with the presence of a colluvial wedge, interpreted as material derived from the progressive degradation of a fault scarp generated by coseismic surface faulting (Fig. 5d). However, no evidence of fault displacement is observed within the most recent slope deposits, and no clear surface scarp is currently preserved, suggesting a lack of recent reactivation. In the surrounding area, localized warping or gentle folding of slope breccia deposits points to possible structural complexity. Further detailed investigations are required to better constrain their geometry and to assess any potential relationship with recent or ongoing activity along the thrust system

Conversely, the morphological connection between the emergence of the thrust and the top surface of old Quaternary breccias outcropping under the old castle, now largely eroded, may suggest sealing and an overall uplift (Fig. 6). Overall, the available data appear to support limited Quaternary activity of the thrust, possibly expressed through secondary structures associated with frontal collapse processes; however, data are insufficient to either rule out or confirm ongoing activity, which may instead be associated with younger structures to the west. At the foot of the Dajti-Kruja main thrust, an Early Oligocene-Late Miocene succession of mainly clay and sandstone deposits crops out, with a prominent bedding steeply dipping SW. The tectonic uplift has generated well-developed flatirons at the base of the ridge just NE of Tirana (Fig. 2).

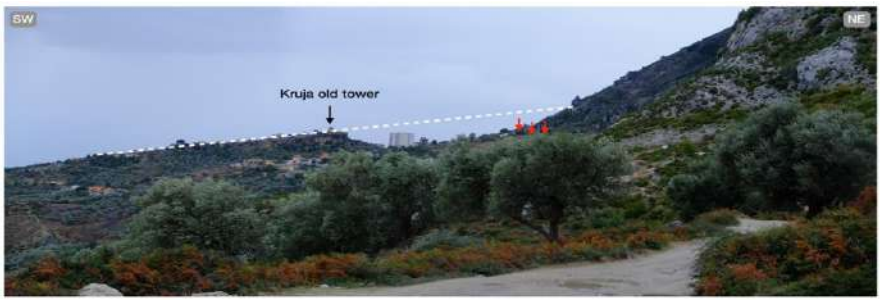

Fig.6. Ancient breccia paleosurface connected to the present slope, showing no significant evidence of tectonic displacement. The morphological relationship between the emergence of the thrust and the upper surface of the older Quaternary breccias—exposed beneath the Kruja castle and now largely eroded—may indicate progressive sealing of the structure and overall uplift, rather than ongoing thrust activity. The viewpoint is located southeast of the Kruja historical center, along a track at the base of the thrust front escarpment. View direction: SE–NW. Coordinates: 41.502468° N, 19.804391° E.

3.2. Makaresh anticline

West of Kruja, crustal shortening associated with a more internal, buried thrust has generated the NW–SE-trending Makaresh anticline. Its growth is evidenced by significant disruption of the hydrographic network, including the development of small endorheic basins along its eastern flank, locally dammed drainage systems, and abandoned stream channels (Figs. 7 and 8). To the west, a smaller anticline likely represents the surface expression of a minor splay of the Makaresh thrust (Fig. 1b). In this sector, a hummocky topography may reflect a relative decrease in folding rates, while still indicating ongoing uplift (Figs. 2b and 2c). The hypothesis of continued uplift is further supported by local drainage anomalies. In particular, the drainage pattern shows a clockwise curvature and a northwestward diversion, as highlighted in Fig. 2b (white box) and detailed in Fig. 9. The river (orange arrows in Fig. 9), which originally flows southwestward from Makaresh Hill, is abruptly deflected by approximately 90° toward the north-northwest. This deflection is interpreted as a response to uplift of a topographic ridge located farther west. Additional support for this interpretation is provided by the presence of a wind gap (brown arrows in Fig. 9), marking a former (abandoned) fluvial pathway, indicative of drainage reorganization driven by tectonic processes.

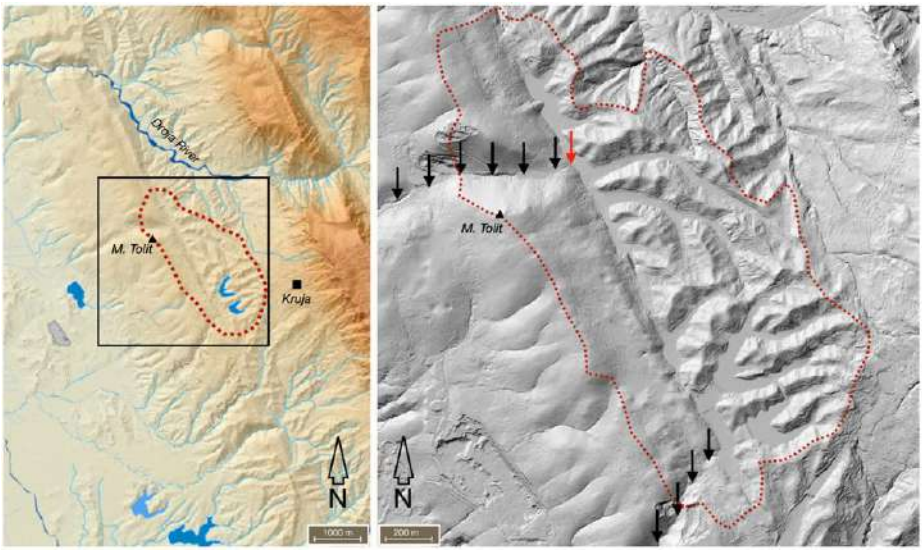

Fig. 7: Left: Influence on drainage by growth of the Makaresh anticline. The drainage pattern in the sector between the Kruja thrust front and the culmination of the ridge of Mount Tolit, associated with the Makaresh anticline, is characterized by a large area with disorganized and endorheic drainage. This area is enclosed within the dotted red line. The black box indicates the area covered by the DEM shown in the figure on the right. Right: Close-up view of the endorheic area, showing two major abandoned stream beds (black arrows) and clear evidence of drainage damming (red arrow).

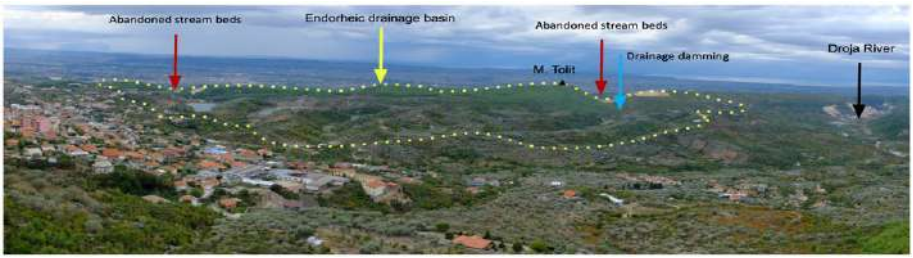

Fig. 8: Panoramic view toward the west showing the endorheic basin, the two major abandoned stream beds, and the dammed drainage. The main river, the Droja River, is deeply incised into the sedimentary deposits, however due to tectonic control, the drainage flows in the opposite direction, toward the endorheic area. The endorheic basin exhibits a SE–NW elongated morphology, extending approximately 4 km in length and 1.7 km in width, with an estimated total area of 7.5 km².

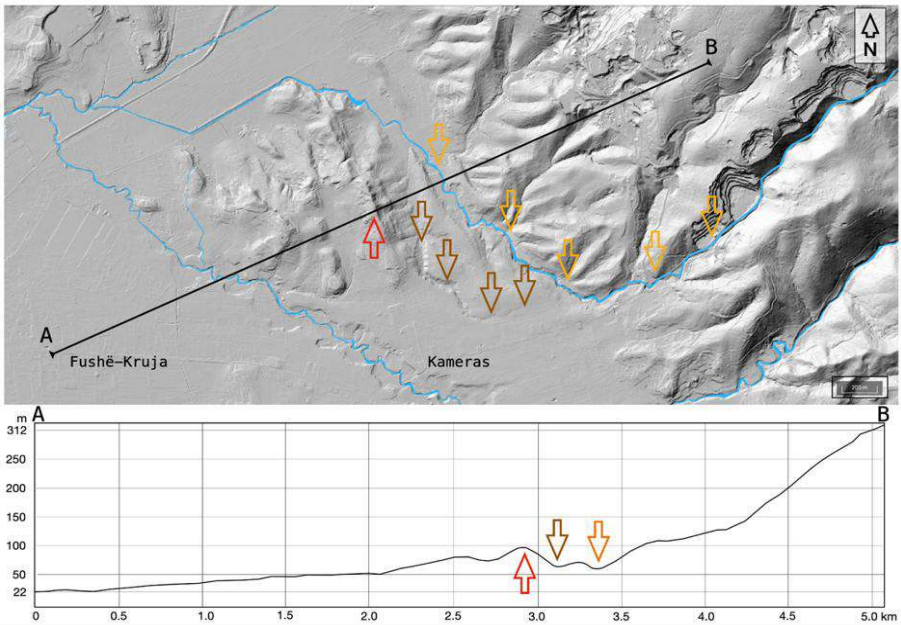

Fig. 9: Topographic profile across the Fushë-Kruja hills showing the effects of tectonic uplift on the local drainage network. The black line represents the trace of topographic profile A–B. The red arrow indicates tectonic uplift, the orange arrow marks fluvial diversion, and the brown arrow highlights a wind gap. Vertical exaggeration of the topographic profile is 4:1.

The course of the Ishëm River, which constitutes the main drainage system of the Tirana–Thumanë synform, is strongly influenced by the Holocene activity of the principal tectonic structures (Fig. 2). In particular, its right-bank tributaries exhibit a marked deflection from an approximately E–W to a SE–NW orientation. This change in direction is interpreted as the result of a barrier effect produced by the uplift of the Vorë Ridge, coupled with subsidence in its footwall within the Tirana syncline. The western margin of the Ishëm River plain is bounded by the NW–SE-trending Vorë Ridge, whose uplift is associated with the activity of the NE-vergent Vorë backthrust. This structure is, in turn, linked to the deeper tectonic framework and is driven by the propagation of the buried thrust system of the Kruja thrust front (Fig. 1).

3.3. Vora backthrust

The Vorë backthrust extends for approximately 25–30 km and is expressed by a remarkably continuous, rectilinear, and steep escarpment, despite being developed within relatively soft clastic lithologies (Fig. 2). The ridge crest corresponds to an uplifted and tilted paleosurface of the hanging wall, separating the Tirana–Thumanë syncline from the coastal Shijak syncline. Quaternary and ongoing uplift of the ridge is evidenced by a series of abandoned valleys. One of the most prominent is the valley currently occupied by the SH2 highway between Tirana and Durrës. This valley was initially incised during the Pleistocene by the Tërkuza River and later by the Tirana River, which once joined the Erzen River near Sukth (Fig. 2a). Subsequently, the valley was largely abandoned following drainage diversion toward the Ishëm River. A second major abandoned valley (wind gap), extending from Yzberisht to southwest of Vokël across the Yzberisht ridge, was formerly used by the Tirana and Lana rivers to flow southwestward into what is now the lower course of the Erzen River. These features indicate that both the Vorë–Sukth and Yzberisht–Vokël corridors once provided direct drainage pathways from the Dajti ridge to the Adriatic Sea.

Additional evidence of backthrust activity is observed farther west, where the north–south flowing Peza River (location C in Fig. 2) is diverted westward as it becomes incised into the uplifting thrust front. Along the Erzen River, in the sector where it crosses the Vorë backthrust, a long-term incision rate of up to ~0.5 mm yr^{-1} has been estimated, whereas the vertical offset of a paleoriver profile across the structure indicates a deformation rate of approximately 0.4 mm yr^{-1} (Mugnier *et al.* 2024). Moreover, a major deviation of the Erzen River southwest of Tirana (the Tirana wind gap) has been attributed to drainage reorganization during the Holocene Climatic Optimum (Guzmán *et al.* 2023).

The interaction between the Vorë backthrust and adjacent structures is further highlighted by the activity of the Shijak thrust. Uplift along this structure forces the Erzen River to flow along the eastern flank of the Shijak syncline, producing a sharp deviation near Pezë (location C in Fig. 2). In the same area, a narrow, dry incision cuts across a small anticline developed on the hanging wall of the Shijak thrust. The progressive growth of this anticline has contributed to local damming effects, diverting the Erzen River from an original NE–SW course to a NW–SE orientation downstream of its confluence with the Peza River. The long-term eastward

migration of the Erzen River is further evidenced by the systematic bypassing of its meanders, particularly near the villages of Shijak and Dushk. In this sector, a splay of the Shijak thrust likely uplifts a series of aligned hills that control the river's northeastward shift, preventing its probable capture by the nearby Juba River (Fig. 2). Further downstream, minor compressional folds deform Early Pliocene silty–clay deposits at the mesoscale within the Erzen alluvial plain near its mouth (Fig. 10; location D in Fig. 2). The axial planes of these structures generally strike N40W, consistent with the regional structural trend. These observations indicate that, despite high sedimentation rates typical of alluvial environments, active compressional tectonics associated with the Shijak thrust continues to deform the surface and significantly influence landscape evolution. Notably, this area coincides with a zone of measurable uplift (up to ~11 cm) detected by InSAR following the 2019 Durrës earthquake (Fig. 10; Vittori *et al*. 2021). This evidence suggests recent reactivation of the Shijak thrust and, together with the geometry and extent of the uplifted area, indicates that this structure may have acted as a secondary fault during the 2019 event, whose main seismic source is inferred at a depth of approximately 25 km (Fig. 1).

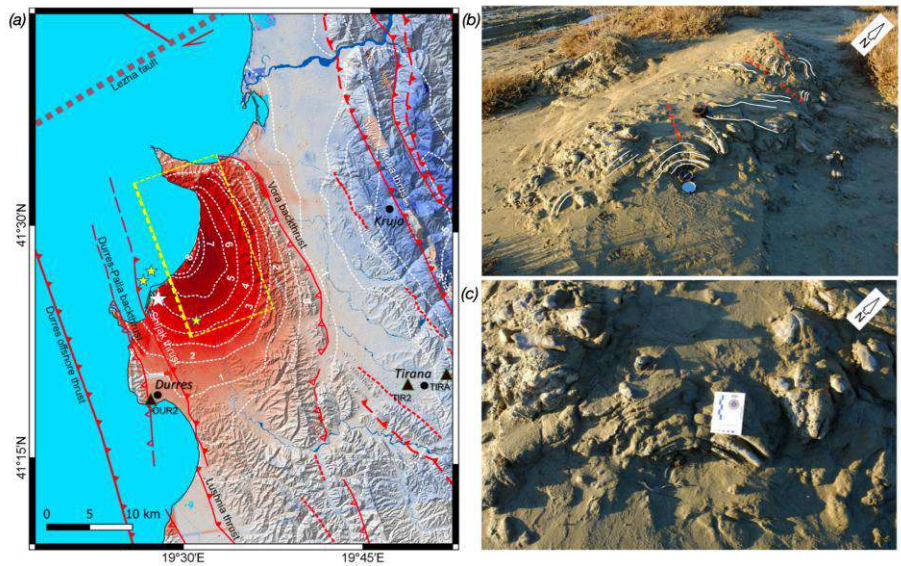

Fig. 10: (a) Surface deformation produced by 2019 Mw 6.4 Durres earthquake calculated from InSAR data (Vittori et al., 2021). Red colour indicates uplift, blue indicates lowering; white dashed lines represent deformation isolines (in cm);

yellow stars mark the epicentres of major events; the yellow box outlines the hypothesized source; the white star marks the outcrop of the folded deposits shown in panels (b) and (c). (b) Meso-scale folds deform Early Pliocene silty-clay deposits in the alluvial plain of the Erzen River, near its mouth (E in Fig. 2; white star in Fig 10a). The axial planes generally strike N40W, consistent with the regional structural trend. (c) A close-up view of the fold.

4. DISCUSSION

Our analysis highlights evidence of active tectonics in the sector between the Kruja thrust front, the Tirana Plain, and the Adriatic Sea, based on the identification of several major, well-documented structures and their associated surface expressions of tectonic activity. We attempt to summarize, albeit somewhat speculatively, the possible significance of this evidence in terms of its contribution to seismic hazard assessment.

Stratigraphic and structural constraints indicate that the Kruja thrust system was predominantly active during the Neogene (Roure *et al*. 2004), with deformation continuing into the early Pliocene (Aliaj, 2006; Silo *et al*. 2010). Regional seismic profiles suggest that major thrust activity was largely sealed by the Tortonian–Messinian unconformity, whereas out-of-sequence deformation and post-Miocene reactivation are mainly confined to more internal structures (e.g., the Kruja–Dajti and Makaresh thrusts).

Despite this, the pronounced morphological expression—characterized by an approximately 50 km-long, abrupt scarp along the exposed Kruja thrust front—together with morphometric indices (J = 1.1; Vf = 0.25; Bull, 2007), indicates a well-preserved, linear structure consistent with sustained tectonic control on landscape evolution. Although such indices are not diagnostic on their own and may reflect lithological or erosional influences, their consistency across multiple catchments (ten river valleys crossing the thrust front), combined with the homogeneous lithology of Upper Cretaceous limestones, supports a dominant tectonic control on present-day morphology.

Nevertheless, evidence for Quaternary activity along this tectonic element is very sparse and largely indirect. The absence of clear offsets in Quaternary slope deposits and the lack of related reverse fault scarps argue against sustained surface-breaking activity in the recent past. However, the occurrence of a SW-dipping normal fault affecting Quaternary breccias in the frontal zone is consistent with secondary deformation processes,

potentially related to frontal collapse and gravitational readjustment of the thrust front.

Nevertheless, direct evidence for Quaternary activity along this structure remains sparse and largely indirect. The absence of clear offsets in Quaternary slope deposits and the lack of well-defined reverse-fault scarps argue against persistent surface-breaking activity in recent times. However, the presence of a SW-dipping normal fault affecting Quaternary breccias in the frontal zone is consistent with secondary deformation processes, possibly related to gravitational readjustment and frontal collapse of the thrust front. Alternatively, these structures may represent extensional faulting that postdates the growth of fault-related anticlines, as documented in Montenegro (Biermanns *et al*. 2022). This hypothesis warrants further investigation along the frontal scarp and may help explain the observed morphological features. At the same site, localized warping and folding of slope breccias suggest near-surface structural complexity; however, their origin remains uncertain and may reflect either tectonic deformation or gravitational processes. The lack of significant displacement affecting the Quaternary breccia paleosurface exposed beneath the old Kruja Castle, and extending along the present slope, suggests sealing and regional uplift rather than post-breccia fault activity.

Overall, Quaternary deformation within the Kruja thrust system appears to be limited to secondary structures, although it is not negligible. While there is no clear evidence of an active, surface-breaking thrust, secondary processes related to thrust-front evolution and regional uplift appear to be ongoing.

The Makaresh anticline exhibits geomorphic features consistent with active fold growth, including disrupted drainage, endorheic basins, and channel reorganization, indicating ongoing tectonic influence west of Kruja. A smaller adjacent structure (Fushë-Kruja Hill) likely reflects distributed shortening within the same thrust system, together with localized uplift affecting the drainage network. Strong structural control on drainage is further evidenced by abrupt (~90°) channel deflections from NE–SW to SE–NW orientations, as well as the presence of wind gaps, indicating tectonic forcing of fluvial systems at both local and basin scales (e.g., within the Ishëm River system).

Farther west, the Ishëm River records the interaction between uplift at the Vora Ridge and relative subsidence within the Tirana–Thumanë synform. The ridge is interpreted as a backthrust-related structure linked to deeper deformation within both the Kruja and Ionian systems. Overall,

the geomorphic evidence supports Quaternary deformation and ongoing tectonic activity localized along fold-and-thrust structures, particularly the Makaresh thrust and the Vora backthrust. The Vora backthrust represents a major active structure in the study area, characterized by a pronounced geomorphic expression, including a rectilinear scarp extending up to 30 km, an uplifted ridge, and a tilted crest interpreted as a hanging-wall paleosurface. Regional drainage reorganization—evidenced by abandoned valleys and wind gaps (e.g., Vora–Sukth and Yzberisht–Vogel)—indicates significant Quaternary uplift and progressive river capture, reflecting sustained tectonic forcing. Estimated incision and offset rates (up to ~0.4–0.5 mm yr^{-1}; Mugnier *et al*. 2024) further support ongoing deformation.

To the west, the Shijak thrust system exerts additional control on drainage evolution within the Erzen River basin. River diversions, incision patterns, and progressive meander abandonment reflect uplift-driven obstruction and lateral channel migration. The growth of associated anticlines and local thrust splays further contributes to drainage reorganization and potential capture processes.

Deformation also affects smaller-scale geomorphic features, including the mouth of the Erzen River, where compressional disharmonic folding within Early Pliocene deposits indicates ongoing tectonic activity despite high sedimentation rates. The spatial correspondence between these structures and InSAR-derived coseismic uplift from the 2019 Durrës earthquake (~11 cm; Vittori *et al.* 2021) suggests possible involvement or triggered reactivation of the Shijak thrust system, although its precise seismogenic role remains uncertain given the inferred deeper earthquake source (~25 km).

In summary, the Vora backthrust and Shijak thrust systems accommodate spatially distributed Quaternary deformation expressed through active uplift and localized folding, which strongly controls drainage evolution. These structures likely represent the shallow expression of deeper active thrusting, while also potentially contributing to the seismic behaviour of the region. They may act as secondary structures accommodating deformation from major deep-seated thrusts, although an independent seismogenic role cannot be excluded.

Steep, rectilinear fault scarps are associated with major NW–SE-striking thrusts and back-thrusts, extending 30 to 50 km along the Kruja Mountain front and the margins of the Durrës and Vora Hills. A comparable extent is observed for the shallowly outcropping Shijak thrust.

Fluvial diversions and wind gaps provide some of the most compelling evidence of the ongoing compressional regime, reflecting thrusting and folding processes that govern landscape evolution between the Kruja thrust front and the coastline. These surface features ultimately reflect the activity of deeper-seated structures identified through geophysical investigations, which drive shallow deformation and control regional uplift rates, thereby shaping large-scale morphology. Morphotectonic evidence, combined with empirical scaling relationships (e.g., Wells and Coppersmith, 1994; Pavlides and Caputo, 2004), suggests that historical earthquakes—including the November 2019 event—likely underestimate the maximum seismic and surface-faulting potential of the region. The studied fault systems may be capable of generating stronger and/or shallower earthquakes than those recorded in 2019, with magnitudes potentially reaching Mw ~7. This is consistent with the DISS 3.3.1 estimate of Mw 6.8 for the Shijak source, based on Leonard's (2014) scaling relations. Such large-magnitude earthquakes may generate both primary and secondary hazards, including surface faulting, landslides, and liquefaction, underscoring the need for a comprehensive multi-hazard approach to risk assessment and mitigation.

5. CONCLUSIONS

Our analysis highlights clear evidence of active tectonics in the sector between the Kruja thrust front, the Tirana Plain, and the Adriatic Sea, based on the identification of several major, well-documented structures and their associated surface expressions. We present a synthesis—while acknowledging some degree of uncertainty—of the implications of this evidence for seismic hazard assessment.

These findings are also highly relevant for tsunami hazard assessment. Tsunamis occur less frequently than earthquakes, and coastal areas may have been sparsely populated in the past, resulting in a limited historical record. This lack of data underscores the need for further investigation and for improved characterization of seismic sources located near coastal zones.

The Mw 6.4 earthquake of 26 November 2019, which struck northwestern Albania, renewed concerns regarding the level of seismic hazard in this region. This area hosts significant industrial and commercial development, a rich natural and cultural heritage, and rapidly expanding

tourism. Major urban centers—including Tirana, Kruja, and Durrës—comprise historical cores as well as densely populated zones of recent urban expansion, increasing overall exposure to seismic risk.

To contribute to a more comprehensive characterization of potential seismogenic sources in western Albania, we analysed the seismic landscape with the aim of identifying active structures capable of generating deformation and/or surface rupture.

Morphotectonic analysis confirms ongoing tectonic deformation under a compressional regime, expressed by NW–SE-trending thrusts and backthrusts that exert strong control on landscape evolution and drainage patterns. Key evidence includes uplift- and subsidence-driven relief and basin formation, structurally aligned landforms, tectonically controlled sedimentation and erosion, and drainage disruption and reorganization (e.g., fluvial diversions and wind gaps), as well as the presence of endorheic basins. Overall, the region exhibits clear signatures of active tectonics shaping both geomorphology and the hydrological network.

Comparison between morphotectonic evidence from the investigated active faults and the effects of the 2019 Durrës earthquake suggests that historical events do not fully represent the maximum seismic and surface-faulting potential of the region. The studied structures may be capable of generating more energetic (Mw up to ~7) and/or shallower earthquakes than the 2019 event, potentially leading to more complex multi-hazard scenarios.

These findings highlight the need for detailed investigations of active tectonics and paleoseismology to better characterize seismogenic sources and improve estimates of their seismic potential, ultimately supporting more robust risk mitigation strategies. Future studies should focus on reconstructing the complete seismic history of key tectonic structures, including the estimation of long-term slip rates, the number and magnitude of past seismic events, coseismic displacement, maximum expected slip, recurrence intervals, and overall seismic and surface-faulting potential.

Acknowledgements

The authors gratefully acknowledge the Albanian colleagues from the IGEO – Institute of Geosciences and the AGS – Albanian Geological Survey for their collaboration and support throughout this study. The authors also thank the two anonymous reviewers for their careful and constructive comments, which significantly improved the manuscript.

Data Accessibility: No dedicated repository hosts the data presented in this manuscript. Information regarding the project and the broader framework within which these activities are conducted is available at: https://seismotectonics-albania.com/about/.

Declaration of AI Use: The authors declare that no artificial intelligence (AI) or AI-assisted technologies were used in the preparation of this manuscript.

Authors' Contributions: * **PDM:** conceptualizing, writing – original draft, validating, writing – reviewing, editing; L.P.: conceptualizing, validating, writing—review and editing; EV: conceptualizing, validating, writing—review and editing; AMB: validating, reviewing and editing; VC: validation, review and editing; IH: validation, review and editing; Rr.O.: validating, review and editing; RB: validation, review and editing; OG: validation, review and editing; PN: validation, review and editing; DG: validation, review and editing.

REFERENCES

Aliaj S, Sulstarova E, Muço B, Koçiu S. 2000. *Seismotectonic Map of Albania, scale 1:500,000*. Institute of Seismology, Albanian Academy of Sciences, Tirana.

Aliaj Sh. 2006. The Albanian orogen: convergence zone between the Eurasia and Adria Microplate. In: Pinter N. et al. (eds). The Adria Microplate: GPS, Geodesy, Tectonics and Hazards. 133-149. 2006 Springer. Printed in the Netherlands.

Aliaj Sh, Koçiu S, Muço B, Sulstarova E. 2010. Seismicity, seismotectonics and seismic hazard assessment in Albania. (In Albanian with English extended summary) The Academy of Sciences of Albania, Tirana, 97 p. ISBN: 978-99956-10-26-5

ALOS Global Digital Surface Model "ALOS World 3D - 30m (AW3D30)". **https://www.eorc.jaxa.jp/ALOS/en/dataset/aw3d30/aw3d30_e.htm .** Date Accessed: 2026-04-14

ASIG Geoportal. http://geoportal.asig.gov.al/map/?auto=true and http://www.gsa.gov.al/en. Date Accessed: 2026-04-14.

Bega Z. 2013. Deep seated platform carbonate reservoirs as new hydrocarbon plays in the NW Albania-Montenegro segment of the Adriatic region: AAPG European regional conference & exhibition, Barcelona, Spain, April 8-10, 2013, 3 AAPG Conference,

Barcelona, 8-10 April 2013. https://www.searchanddiscovery.com/documents/2013/10497bega/ndx_bega.pdf. Website accessed April 2026.

Biermanns P, Schmitz B, Silke Mechernich S, Weismüller C, Onuzi K, Ustaszewski K, Reicherter K. 2022. Aegean-style extensional deformation in the contractional southern Dinarides: incipient normal fault scarps in Montenegro. *Solid Earth*, **13**, 957–974, https://doi.org/10.5194/se-13-957-2022.

Bortolotti V, Marroni M, Pandolfi L, Principi G. 2005. Mesozoic to Tertiary tectonic history of the Mirdita ophiolites, northern Albania. *Island Arc*, **14**: 471-493. https://doi.org/10.1111/j.1440-1738.2005.00479.x

Caporali A, Aichhorn C, Barlik M, Becker M, Fejes I, Gerhatova L, Ghitau D, Grenerczy G, Hefty J, Krauss S, Medak D, Milev G, Mojzes M, Mulic M, Nardo A, Pesec P, Rus T, Simek J, Sledzinski J, Solaric M, Stangl G, Stopar B, Vespe F, Virag G. 2009. Surface kinematics in the Alpine–Carpathian–Dinaric and Balkan region inferred from a new multi-network GPS combination solution. *Tectonophysics*, **474 (1–2),** 295-321, ISSN 0040-1951, https://doi.org/10.1016/j.tecto.2009.04.035 .

Copernicus EU-DEM (30 m and 10 m resolution). https://documentation.dataspace.copernicus.eu/Data/Others/CCM.html#copernicus-dem. Date Accessed: 2026-04-14.

Bull WB. 2007. Tectonic geomorphology of mountains: A new approach to paleoseismology. Oxford - Wiley-Blackwell. 328 pages. ISBN: 978-0-470-69155-7.

D'Agostino N, Avallone A, Cheloni D, D'Anastasio E, Mantenuto S, Selvaggi G. 2008. Active tectonics of the Adriatic region from GPS and earthquake slip vectors. *Journal of Geophysical Research: Solid Earth*, **113, B12413**, https://doi.org/10.1029/2008JB005860.

D'Agostino N, Métois M, Koci R, Duni L, Kuka N, Ganas A, Georgiev I, Jouanne F, Kaludjerovic N, Radovan Kandić R. 2020. Active crustal deformation and rotations in the southwestern Balkans from continuous GPS measurements. *Earth and Planetary Science Letters*, **539**: 116246, ISSN 0012-821X, https://doi.org/10.1016/j.epsl.2020.116246.

DISS Working Group 2025. Database of individual seismogenic sources (DISS), Version 3.3.1: A compilation of potential sources for earthquakes larger than M 5.5 in Italy and surrounding areas. Istituto

Nazionale di Geofisica e Vulcanologia (INGV). https://doi.org/10.13127/diss3.3.1.

Frashëri A, Bushati S, Frashëri N, Dema Sh. 2012. Generalized geophysical overview on Shkoder-Peje deep transversal fracture. Jubilee Conference "90 Years of the Albanian geology", Tirana, 26-28 October 2012.

Ganas A, Elias P, Briole P, Cannavo F, Valkaniotis S, Tsironi V, Partheniou E. 2020. Ground deformation and seismic fault model of the M 6.4 Durres (Albania) Nov. 26, 2019, Earthquake, Based on GNSS/INSAR Observations. Geosciences, Geological Survey of Iran, 2020, 10 (6), pp. 210. https://doi.org/10.3390/geosciences10060210.

Govorčin M, Wdowinski S, Matoš B, Funning G J. 2020. Geodetic source modeling of the 2019 Mw 6.3 Durrës, Albania, earthquake: Partial rupture of a blind reverse fault. *Geophysical Research Letters*, **47**: e2020GL088990. https://doi.org/10.1029/2020GL088990.

Guidoboni E, Ferrari G, Tarabusi G, Sgattoni G, Comastri A, Mariotti D, Ciuccarelli C, Bianchi MG, Valensise G. 2019. CFTI5Med, the new release of the catalogue of strong earthquakes in Italy and in the Mediterranean area. Scientific Data 6, 80. https://storing.ingv.it/cfti/cfti5/.

Guzmán O, Mugnier JL, Vassallo R, Koçi R, Julien Carcaillet J, François Jouanne F. 2023. Fluvial terrace formation in mountainous areas: (1) Influence of climate changes during the last glacial cycle in Albania. *Comptes Rendus Géoscience*, **355**: 331-353 Published online: 9 January 2024. https://doi.org/10.5802/crgeos.251.

Handy MR, Giese J, Schmid SM, Pleuger J, Spakman W, Onuzi K, Ustaszewski K. 2019. Coupled crust-mantle response to slab tearing, bending, and rollback along the Dinaride-Hellenide orogen. Tectonics, 38. https://doi.org/10.1029/2019TC005524.

IGEWE 2019. Monthly Bulletin of Seismology, 5, November 2019. Universiteti Politeknik i Tiranës, Institute of Geosciences, Energy, Water and Environment, Tirana, 336 p. ISSN: 2664 – 410X (in Albanian, with summary in English).

Jardin A, Roure F, Nikolla L. 2011. Subsalt Depth Seismic Imaging and Structural Interpretation in Dumre Area, Albania. Oil & Gas Science and Technology – Rev. IFP Energies nouvelles, Vol. 66 (2011), No.

6, pp. 911-929 Copyright © 2011, IFP Energies nouvelles. https://doi.org/10.2516/ogst/2011100.

Jouanne F, Mugnier JL, Koci R, Bushati S, Matev K, Kuka N, Shinko I, Kociu S, Duni L. 2012. GPS constraints on current tectonics of Albania. *Tectonophysics*, **554-557**: 50-62. https://doi.org/10.1016/j.tecto.2012.06.008 .

Lekkas E, Mavroulis S, Papa D, Carydis P. 2019. The November 26, 2019, Mw 6.4 Durrës (Albania) earthquake. *Newsletter of environmental, disaster and crisis management strategies*, **15**: 1-80, National and Kapodistrian University of Athens. https://doi.org/10.13140/RG.2.2.23801.29281.

Leonard M. 2014. Self-consistent earthquake fault-scaling relations: Update and extension to stable continental strike-slip faults. *Bulletin of the Seismological Society of America*, **104(6):** 2953–2965. https://doi.org/10.1785/0120140087.

Maramai A, Graziani L, Brizuela B. 2019. Euro-Mediterranean tsunami catalogue (EMTC), version 2.0. Istituto Nazionale di Geofisica e Vulcanologia (INGV). https://doi.org/10.13127/tsunami/emtc.2.0.

Matraku K, Jouanne F, Dushi E, Koçi R, Kuka N, Grandin R, Bascou P. 2023. The 26 November 2019 Durrës earthquake, Albania: Coseismic displacements and occurrence of slow slip events in the year following the earthquake, *Geophysical Journal International*, **234 (2):** August 2023, Pages 807–838, https://doi.org/10.1093/gji/ggad101.

Mavroulis S, Lekkas E, Carydis P. 2021. Liquefaction phenomena induced by the 26 November 2019, Mw = 6.4 Durrës (Albania) Earthquake and liquefaction susceptibility assessment in the affected area. *Geosciences*, **11(5):** 215; https://doi.org/10.3390/geosciences11050215.

Mazzoli S, Pierantoni PP, Borraccini F. 2008. Structural evolution of the outer Albanides: constraints from cross-section balancing. *Geological Society of America Bulletin*, **120**, pp.123–140.

Mazzoli S, Basilici M, Spina V, Pierantoni PP, Tondi E. 2022. Space and time variability of detachment-versus ramp-dominated thrusting: Insights from the outer Albanides. *Tectonics*, **41,** e2022TC007274. https://doi.org/10.1029/2022TC007274.

Meçaj M, Durmishi Ç, Pritfi I. 2018. Back thrust of molasse deposits in western Albania / For a din spate a depozitelor de molasă din vestul Albaniei. *Muzeul Olteniei Craiova. Oltenia. Studii şi comunicări.*

Ştiinţele Naturii, **34(1):** ISSN 1454-6914. Ştiinţele Naturii with full text articles available on-line: http://www.olteniastudii.3x.ro/ .

Morelli C. 1942. Carta sismica dell'Albania. Reale Accademia d'Italia, Commissione Italiana di Studio per i problemi del soccorso alle popolazioni, vol. X, Firenze: Le Monnier, 120 p.

Mugnier JL, Guzmán O, Vassallo R, Matraku K, Jouanne F. 2024. Fluvial terrace formation in a mountainous area (2): influence of eustatism, tectonics and altitudinal distribution of watersheds based on an allostratigraphic study (Albania). *Comptes Rendus Géoscience*, 2024, **356 (G1):** pp.211-230. https://doi.org/10.5802/crgeos.278 .

NASA JPL. 2013. NASA Shuttle Radar Topography Mission Global 1 arc second [Data set]. NASA Land Processes Distributed Active Archive Center. https://doi.org/10.5067/MEASURES/SRTM/SRTMGL1.003 . Date Accessed: 2026-04-14.

Nieuwland A, Oudmayer BC, Valbona U. 2001. The tectonic development of Albania: explanation and prediction of structural styles. *Marine and Petroleum Geology***, 18 (1):** 2001, Pages 161-177, ISSN 0264-8172, https://doi.org/10.1016/S0264-8172(00)00043-X.

Ormeni R, Hoxha I, Gjuzi O, Bozo R, Gega D, Kanani X, Mucaj D, Piccardi L, Vittori E, Blumetti AM, Di Manna P, Comerci V. 2022. The catalogue of earthquake focal mechanisms occurred in Albania and its surrounding during 1948 to 2022. EAGE NSG2022, 28th European meeting environmental and engineering geophysics, **1–5**. https://doi.org/10.3997/2214-4609.202220159.

Papadopoulos GA, Agalos A, Carydis P, Lekkas E, Mavroulis S, Triantafyllou I. 2020. The 26 November 2019 Mw 6.4 Albania Destructive Earthquake. *Seismological Research Letters*, **91(6):** 3129-3138. doi.org/10.1785/0220200207.

Papazachos BC, Papazachou C. 2003. The earthquakes of Greece. Ziti publications, Thessaloniki, Greece, 286 pp. (in Greek).

Pavlides S, Caputo R. 2004. Magnitude versus faults' surface parameters: quantitative relationships from the Aegean Region. *Tectonophysics*, **380(3–4)**: pp. 159–188. https://doi.org/10.1016/j.tecto.2003.09.019.

Piccardi L, Di Manna P, Vittori E, Hoxha I, Ormeni R, Comerci V, Blumetti AM, Gega D, Naco P, D'Alessandro A. 2025. Migrating earthquake sequences on major fault systems in southern and eastern

Albania. *Albanian Journal of Natural and Technical Sciences*, (*AJNTS*) **63** (**2**)**:21-42**. https://akad.gov.al/albanian-journal-of-natural-and-technical-sciences-ajnts-2025-2-vol-xxx-63/ .

Prifti I, Durmishi Ç, Dorre P, Boçari A. 2013. Evaporite diapirism and its contribution to the tectonic regime of Albania. Muzeul Olteniei Craiova. *Oltenia Journal for Studies in Natural Sciences*, (**29): 2**/2013 ISSN 1454-6914.

Rossetti F, Fellin MG, Ballato P, Faccenna C, Balestrieri M L, Muceku B, Rondenay S, Maesano F E, Crosetto S, Durmischi C, Bazzucchi C, Maden C. 2024. *Building* the Albanides by deep underplating. *Tectonics*, **43**, **e2024TC008506**. https://doi.org/10.1029/2024TC008506.

Roure F, Nazaj S, Mushka K, Fili I, Cadet JP, Bonneau M. 2004. Kinematic evolution and petroleum systems: an appraisal of the outer Albanides, in Thrust Tectonics and Hydrocarbon Systems. 474–493, ed. McClay, K.R., 82, AAPG Memoir. https://doi.org/10.1306/M82813C25.

Richter M, Pollok K, Onuzi K, Ustaszewski K. 2025. Tectonometamorphic evolution of a subduction plate interface at the base of the Mirdita Ophiolite (Bajram Curri, northeastern Albania). *Swiss Journal of Geosciences*, **118 (4):**https://doi.org/10.1186/s00015-024-00472-5.

Schmid SM, Bernoulli D, Fügenschuh B, Matenco L, Schefer S, Schuster R, Tischler M, Ustaszewski K. 2008. The Alpine-Carpathian-Dinaridic orogenic system: correlation and evolution of tectonic units. *Swiss Journal of Geosciences*, **101:** 139–183 (2008). https://doi.org/10.1007/s00015-008-1247-3.

Schmitz B, Biermanns P, Hueck M, Wemmer K, Schmid SM, Onuzi K, Reicherter K, Ustaszewski K. 2025. Kinematics and age of the orogen-perpendicular Shkoder-Peja Normal Fault in north Albania constrained by fault-slip data, Raman spectroscopy and K-Ar fault-gouge dating. *Tectonics*, **44**: e2024TC008660. https://doi.org/10.1029/2024TC008660**.**

Silo V, Pertef Nishani P, Erald Silo E. 2010. Hydrocarbon exploration under Kruja zone in Tirana-Rodon area, Albania. *Journal of the Balkan Geophysical Society*, **13(1):** February 2010, p. 9-16, 13 figs.

Sulstarova E, Kociu S. 1975. The catalogue of Albanian earthquakes. Botim i Qendrës Sizmologjike. Tiranë, 223 pp.

Teloni S, Invernizzi C, Mazzoli S, Pierantoni PP, Vincenzo Spina V. 2021. Seismogenic fault system of the M_w 6.4 November 2019 Albania earthquake: new insights into the structural architecture and active tectonic setting of the outer Albanides. *Journal of the Geological Society* **202; 178 (2):** jgs2020–193. doi: https://doi.org/10.1144/jgs2020-193.

Theodoulidis N, Dushi E, Duni L, Grendas i, Panou A, Hajrullai A, Kuka N, Koci R. 2022. Local Site Effects Investigation in Durres City (Albania) Using ambient noise, after the 26 November 2019 (M6.4) Destructive Earthquake. *Applied Sciences*, **12(22):** 11309; https://doi.org/10.3390/app122211309.

Velaj T, Davison I, Serjani A, Alsop I. 1999. Thrust Tectonics and the Role of Evaporites in the Ionian Zone of the Albanides. *AAPG Bulletin*, **83(9):** (September 1999), P. 1408–1425.

Velaj T. 2001. Evaporite in Albania and their impact on the thrusting processes. Journal of the Balkan Society, vol 4, no 1, February 2001, pp 9–18

Velaj T. 2011. Tectonic style in Western Albania Thrustbelt and its implication on hydrocarbon exploration. AAPG search and discovery Article #10371. November 2011

Velaj T. 2012. Tectonic style and hydrocarbon exploration evaluation of duplex Kruja zone in Albania. Nafta J Nr. 63, no 7–8, Zagreb, Croatia, pp 236–242

Vittori E, Blumetti AM, Comerci V, Di Manna P, Piccardi L, Gega D, Hoxha I. 2021. Geological effects and tectonic environment of the 26 November 2019, Mw 6.4 Durres earthquake (Albania). Geophysical Journal International, 225, 2, 1174–1191. https://doi.org/10.1093/gji/ggaa582

Vittori E, Di Manna P, Piccardi L, Blumetti AM, Comerci V, Hoxha I, Ormeni R, Mucaj D, Gjuzi O, Naco P, Gega D. 2025. A working earthquake catalogue for seismic and fault hazard in Albania. *Albanian Journal of Natural and Technical Sciences*, AJNTS No 63 / 2025 (XXX).

Wells DL, Coppersmith KJ. 1994. New empirical relationships among magnitude, rupture length, rupture width, rupture area, and surface displacement. *Bulletin of the Seismological Society of America*, **84:** 974–1002. https://doi.org/10.1785/BSSA0840040974.

OBSERVATIONS AND MULTIVARIATE ANALYSES OF AVIATION CONTRAILS AND CIRRUS CLOUDS CONDUCTED BY LATMOS, OPGC AND LAMP IN FRANCE

Florian MANDIJA[1], Philippe KECKHUT[2], Dunya ALRADDAWI[3], Alain SARKISSIAN[4], Abdenour IRBAH[5], Sergey KHAYKIN[6], Frédéric PEYRIN[7], Jean-Luc BARAY[8,]

[1,2,3,4,5,6]Laboratoire Atmosphères, Observations Spatiales (LATMOS), Institut Pierre-Simon Laplace (IPSL), Université de Versailles-Saint-Quentin-en-Yvelines (UVSQ)/Paris-Saclay University, Sorbonne University, Centre National de la Recherche Scientifique (CNRS), 78280 Guyancourt, France. [2,8]Observatoire de Physique du Globe de Clermont-Ferrand (OPGC), UAR 833, CNRS, Université Clermont Auvergne, 63000 Clermont-Ferrand, France

[3,8]Laboratoire de Météorologie Physique (LaMP), UMR 6016, CNRS, Université Clermont Auvergne, 63000 Clermont-Ferrand, France

Author for correspondence: florian.mandija@latmos.ipsl.fr

FM, 0000-0002-9324-9440; PhK, 0000-0002-8110-4148; DA, 0009-0004-5889-7735; AS, 0000-0002-7041-6197; AI,0000-0003-3265-3148; SK, 0000-0002-54661096; FP, 0000-0001-8054-4144; J-LB, 0000-0003-4711-6310;

ABSTRACT

Over recent decades, condensation trails (contrails), have attracted special interest in the worldwide scientific community. Their impact on radiative balance, as one of the most significant anthropogenic non-CO_2 emissions, has been extensively investigated using a wide range of observational and modelling approaches. The Laboratoire Atmosphères, Observations Spatiales (LATMOS), Observatoire de Physique du Globe de Clermont-Ferrand (OPGC), and Laboratoire de Météorologie Physique (LaMP) operate several ground-based remote sensing instruments dedicated to the monitoring of cirrus clouds and contrails, including Lidar , radar, all-sky cameras, Automatic Dependent Surveillance–Broadcast ADS-B, and radiosondes. These facilities enable the reliable detection and detailed characterization of contrail properties and their temporal evolution. In this paper, we present a comprehensive overview of our group's recent investigations on contrails, including results on cirrus cloud climatology, multivariate analyses of contrails, and case studies.

Keywords: aviation contrails, cirrus clouds, Lidar measurement, ERA5 dataset, southern France

Citation: **Mandija F, Keckhut Ph, Alraddawi D, Sarkissian A, Irbah A, Khaykin S, Peyrin F, Baray J-L. 2026.** Observations and multivariate analyses of aviation contrails and cirrus clouds conducted by LATMOS, OPGC and LAMP in France**.** *Albanian Journal of Natural and Technical Sciences* (*AJNTS),* **2 (30)**
Journal URL: https://journals-akad.gov.al/magazines/1
Classification: Research
Subject Category: Natural / Applied Sciences subject areas: Atmospheric Physics & Climatology

1. INTRODUCTION

Contrails are formed when the hot and humid exhaust of an aircraft is mixed with cold air at high altitudes. These aircraft products consist of water vapour, soot, and other components. For contrails to form, they must encounter favourable environmental conditions to freeze the exhaust water vapour into ice crystals. The principal thermodynamic condition for contrail formation is the Schmidt-Appleman criterion (SAC) (Schmidt, 1941; Appleman, 1953).

If the contrails evolve within ice-super saturation regions (ISSR: $100\% < RH_{ice} < 150\%$), they become persistent and, live more than 10 min (Schumann and Heymsfield, 2017). Otherwise, the short-lived contrails disperse and vanish within a few minutes (Wolf *et al*. 2023; 2024).

The critical values of temperature (T_{crit}) and relative humidity with respect to liquid water ($RH_{crit,\,liq}$) depend on the temperature, atmospheric pressure level, aircraft, and fuel type (Sonntag, 1994; Murphy and Koop, 2005). Both SAC and ISSR criteria are summarized in Table 1.

Table 1. Criteria for contrail formation and persistence: Schmidt–Appleman contrail formation (SAC) and ice super saturation (ISSR) criteria (Mandija *et al*. 2025).

Temp	**RH_{liq}**	**RH_{ice}**	**SAC**	**ISSR**	**Characteristic**
$T < T_{crit}$	$RH_{liq} > RH_{crit,liq}$	$RH_{ice} > 100\%$	√	√	Persistent
$T < T_{crit}$	$RH_{liq} > RH_{crit,liq}$	$RH_{ice} < 100\%$	√	x	Non-persistent
$T < T_{crit}$	$RH_{liq} < RH_{crit,liq}$	$RH_{ice} > 100\%$	**x**	√	Potential
$T > T_{crit}$	$RH_{liq} <> RH_{crit,liq}$	$RH_{ice} <> 100\%$	**x**	–	No-contrail

In particular, persistent contrails play an important role in radiative balance (Kärcher, 2018; Singh *et al.* 2024; Teoh *et al*.2024). When these

contrails age, they lose their linear geometrical features and, develop into artificial cirrus clouds called contrail cirrus. Figure 1 presents examples of natural cirrus clouds, freshly formed contrails, aged contrails, and fully developed contrail cirrus, which illustrate the transformation process.

Fig. 1. Examples of natural cirrus clouds, fresh and old contrails, and contrail cirrus.

In addition, Figure 2 presents the effective radiative forcing (ERF) of various aviation-related components, indicating that contrail cirrus exhibits the highest ERF (57.4±40 $\mu W \cdot m^{-2}$) and radiative forcing (RF) (111.4±78 $\mu W \cdot m^{-2}$) among all components. The substantial uncertainty associated with these estimates highlights the need for further investigation into the respective roles of young and mature contrails in the climate budget.

LATMOS has conducted continuous research on cirrus cloud and contrail characterisation, mainly using Lidar measurements, but also meteorological reanalysis data (Keckhut *et al*. 2005; 2006; 2013; Alraddawi *et al*. 2025; Mandija *et al*. 2024-2026).

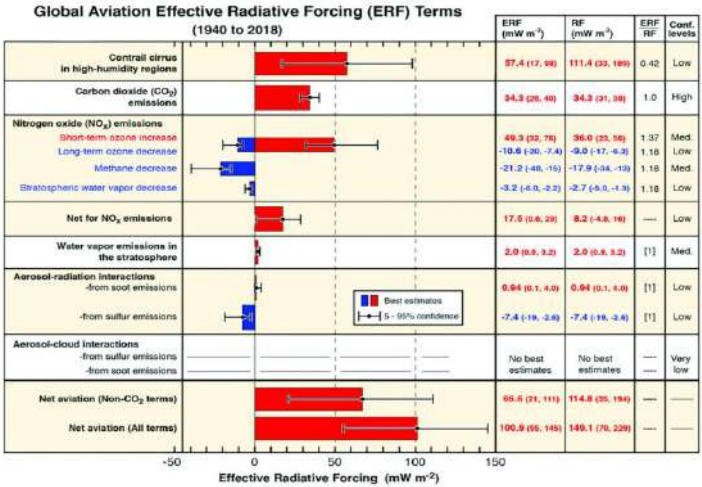

Fig. 2. Climate forcing terms of historic global aviation emissions from 1940 to 2018 (EASA, 2018).

Among the primary tasks undertaken by our working groups within Laboratoire Atmosphères, Observations Spatiales (LAMOS), Observatoire de Physique du Globe de Clermont-Ferrand (OPGC) and Laboratoire de Météorologie Physique (LaMP), part of the Centre National de la Recherche Scientifique (CNRS) are:

- Development and optimization of detection algorithms for contrails to reduce false positives and false negatives;
- Determination of contrail morphological, optical and microphysical properties, as well as their vertically resolved altitude profiles;
- Investigation of contrail evolution, from line-shaped fresh contrails to their persistent phase and eventual transition into contrail cirrus clouds.

The comprehensive dataset obtained provides a robust foundation for further investigation of the climate impact of both natural and anthropogenic thin cirrus clouds. This contributes to reducing existing knowledge gaps in understanding and quantifying the effects of non-CO_2 aviation-induced radiative forcing.

Current knowledge gaps in contrail research are primarily related to the quantification and understanding of the conditions governing their formation, persistence, and radiative forcing. Limitations include insufficient high-resolution and potentially biased relative humidity measurements at flight altitudes, incomplete satellite observational coverage (with fresh contrails often undetected), and uncertainties in the processes by which persistent contrails evolve into contrail cirrus. These factors complicate the accurate modelling of their net radiative effect and hinder the development of effective mitigation strategies.

Although contrail research has intensified over the past decade using a variety of observational and modelling tools, the synergistic integration of Lidar measurements, satellite imagery, ground-based camera observations, meteorological reanalysis data, and radiosonde measurements provides a comprehensive and robust framework for such investigations, significantly improving detection capability and parameter retrieval accuracy.

2. METHODS AND INSTRUMENTS

The Laboratoire Atmosphères, Observations Spatiales (LATMOS) is equipped with a comprehensive suite of atmospheric measurement instruments. These include ground-based systems, remote sensing techniques, Automatic Dependent Surveillance–Broadcast (ADS-B) data (Peyrin *et al.* 2023), visible and thermal infrared cameras, and numerical modelling tools, enabling detailed analysis of the geometrical and optical properties of contrails (Irbah *et al.* 2025).

Among these, Lidar (Light Detectin and Ranging) systems provide vertically resolved profiles of atmospheric backscatter signals, allowing the detection and characterization of cirrus clouds and contrails. A Rayleigh–Mie–Raman Lidar operated by LATMOS is located at the Haute-Provence Observatory (OHP) in southern France and is used to measure atmospheric temperature, ozone, aerosols, and water vapour.

Among these, Lidar (Light Detection and Ranging) systems provide vertically resolved profiles of atmospheric backscatter signals, allowing the detection and characterization of cirrus clouds and contrails. A Rayleigh–Mie–Raman Lidar operated by LATMOS is located at the Haute-Provence Observatory (OHP) in southern France and is used to measure atmospheric temperature, ozone, aerosols, and water vapour.

Among these, Lidar (Light Detection and Ranging) systems provide vertically resolved profiles of atmospheric backscatter signals, allowing the detection and characterization of cirrus clouds and contrails. A Rayleigh–Mie–Raman Lidar operated by LATMOS is located at the Haute-Provence Observatory (OHP) in southern France and is used to measure atmospheric temperature, ozone, aerosols, and water vapour.

In addition, radar observations are used to investigate contrail microphysical properties. Satellite-based instruments, including those from MODIS, CALIPSO, and Sentinel missions, provide large-scale observations of contrail and contrail cirrus coverage, as well as their optical characteristics.

At the OHP site, two hemispherical cameras (visible and infrared) have been installed to record contrail imagery for both daytime and night-time observations (Fig. 3).

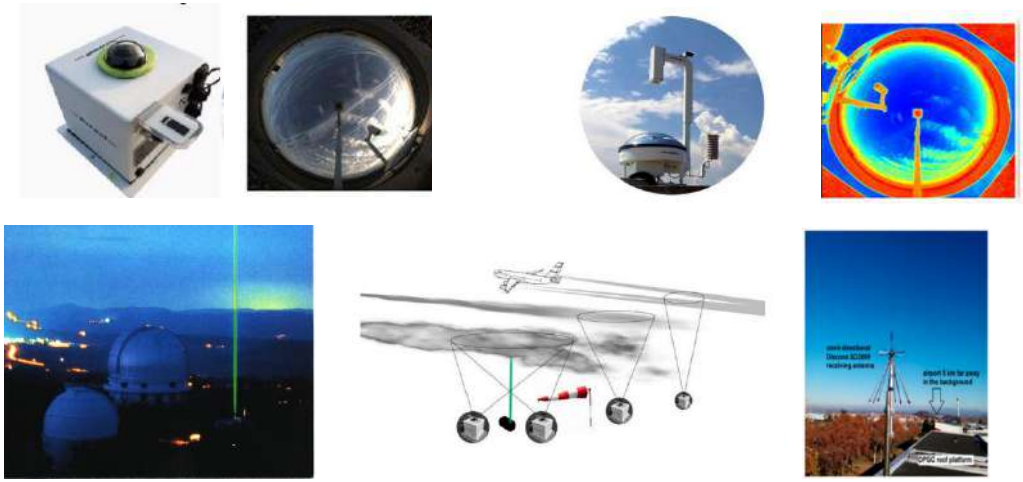

Fig. 3. upper-left: Sky Cam Vision™: Visible-range all-sky imager and visible contrails; upper-right: Sky InSight™: Thermal infrared all-sky imager and infrared view of contrails. The lower-left; view of the Lidar system operated by LATMOS in Observatory of Haute-Provence, France. The lower-middle figure is a schematic presentation of combination of camera with Lidar. Lower-right figure represents the schema of ADS-B system.

Lidar systems play a crucial role in altitude-resolved profiles of optical and geometrical contrails and cirrus properties. The backscattering Lidar profiles analysed in this study have been provided by the Rayleigh–Mie–Raman Lidar system (Sherlock *et al*. 1999; Keckhut *et al*. 2006; 2013). The Lidar system employed a frequency-doubled Nd: YAG laser emitting at 532 nm, operating at a repetition rate of 30 Hz with an average pulse energy of 300 mJ. Backscattered signals were collected by a telescope with an 800 mm diameter primary mirror and a field of view of 1mrad (Khaykin *et al*. 2018 The cirrus detection channel includes a primary lens and an interference filter. The vertical resolution of the Lidar measurements is 15 m, while the temporal resolution is 60 s, enabling the detection of both fresh contrails and evolved contrail cirrus (Mandija *et al*. 2024).

The contrail optical depth (COD) at a certain altitude z is given by integrating the total volume scattering coefficient β(z):

$$\mathrm{COD}(\lambda, z) = \int_{zmin}^{zmax} \beta(\lambda, z)\mathrm{d}z$$

where the total volume scattering coefficient β(z) is given as the product of the total scattering cross-section per molecule σ(z) and the molecular number density $n_{air}(z)$ ($\sigma = 5.4 \times 10^{-31}$ m^2).

The Lidar scattering ratio (SR) is calculated using the Mie and Rayleigh scattering coefficients and is defined as the ratio of the particulate backscattering to the total backscattering:

$$SR = \frac{\beta_{aerosol}(\lambda, z) + \beta_{Rayleigh}(\lambda, z)}{\beta_{Rayleigh}(\lambda, z)}$$

The Automatic Dependent Surveillance–Broadcast (ADS-B) system deployed at COPLid near Clermont-Ferrand consists of a low-cost software-defined radio (SDR) receiver (RTL-SDR R820T2) coupled with a Discone SD3000 antenna and operated via a Raspberry Pi 3B running the DUMP1090 decoding software. Operating at 1090 MHz, the system decodes aircraft transponder signals and, when an aircraft is detected within a 2 km radius, transmits an alert via TCP/IP to the LabVIEW-based Lidar supervisory system, triggering an automatic shutdown of laser emissions for safety purposes (Peyrin *et al*. 2023).

In addition, radiosondes have been systematically deployed at different sites to validate different sensors and models, such the recent measurement campaign conducted in May and June 2025 (Alraddawi *et al*. 2025).

In addition, auxiliary datasets such as meteorological reanalysis data, were used to assess environmental conditions. The ERA5, which represents the 5th generation of the European Center for Medium-Range Weather Forecasts (ECMWF), is extensively used for these purposes (Hersbach *et al*. 2020). The ERA5 biases were treated using methods applied in (Teoh *et al*. 2022; 2024; Wolf *et al*. 2025). To address the issues regarding RH_{ice} biases, a correction of this parameter is proposed (Teoh *et al*. 2022).

$$RH_{ice}^{*} = \begin{cases} \dfrac{RH_{ice}}{a} \; for \; \left(\dfrac{RH_{ice}}{a}\right) \leq 1 \\ min\left(\left(\dfrac{RH_{ice}}{a}\right)^{b}\right), RH_{ice}^{max}, for \; \left(\dfrac{RH_{ice}}{a}\right) > 1 \end{cases}$$

The RH bias correction was performed using optimised coefficients: $a = 0.9587$ and $b = 1.796$,meanwhile threshold value of RH_{ice} is given by

$$RH_{ice}^{max} = \begin{cases} \dfrac{e_{liq}(T)}{e_{ice}(T)}, T > 235\ K \\ 1.67 + (1.45 - 1.67) \times \dfrac{(T - 190)}{(235 - 190)}, T \leq 235\ K \end{cases}$$

where e_{ilq} and e_{ice} are the saturation vapour pressure over liquid and ice.

The threshold temperature $T(p)_{crit}$ and relative humidity related to liquid $RH(T)_{crit}^{liq}$ for contrail formation are expressed as follows:

$$T(p)_{crit} = \begin{cases} 226.69 + 9.43ln(G - 0.053) + 0.72\big(ln(G - 0.053)\big)^2 \\ for\ T < 233K\ or\ G \leq 2PaK^{-1} \\ 26.03 + 10.22lnG + 0.355(lnG)^2 + 0.0642(lnG)^3 \\ for\ 2.38PaK^{-1} \geq G > 2PaK^{-1} \\ 235.15 \\ for\ G > 2.38PaK^{-1} \end{cases}$$

$$RH(T)_{crit}^{liq} = \frac{G \cdot (T - T_{crit}) + e(T_{crit})_{sat}^{liq}}{e(T)_{sat}^{liq}}$$

where $e(T_{crit})_{sat}^{liq}$ is given in hPa and G is the slope of the isobaric mixing line:

$$G = \frac{EI_{H2O}c_p p}{\varepsilon Q(1 - \eta)} = \frac{1.2232 \cdot 1004}{0{,}622 \cdot 43.2 \cdot 10^6 \cdot 0.7} p = 65.6 \cdot 10^{-6} p$$

and atmospheric pressure p, as given in (Pa).

The uncertainty associated with the identification of ice-supersaturated regions (ISSRs) primarily arises from the limited availability of high-resolution upper-tropospheric water vapour measurements, which affects the accuracy of modelled humidity fields

(Teoh *et al*. 2022; Alraddawi *et al*. 2025). In addition, the vertical discretisation of pressure levels in the ERA5 reanalysis may further contribute to representation errors. Figure 4 shows a schematic illustration of the contrail detection process.

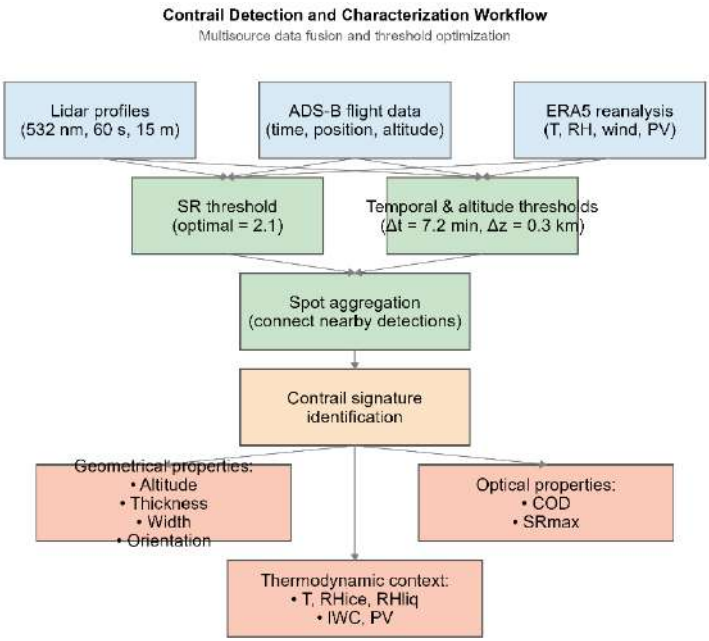

Fig. 4. Multisource contrail detection using Lidar , ADS-B, and ERA5 data was performed to assess their morphological and optical properties and thermodynamic environment.

Flights overpassing the site were tracked using ADS-B or any other flight provider. Collocated Lidar backscatter altitude profiles were checked for possible abrupt anomalies or “spots”. To form contrails, the Schmidt-Appleman criteria were verified using a meteorological dataset provided by ERA5 reanalysis. Once such features were identified and their contrail origin confirmed, threshold-based aggregation methods were applied to group individual detections into coherent contrail signatures. The final step involves the retrieval of morphological and optical properties of the detected contrails, along with the characterization of the thermodynamic state of the surrounding atmosphere, which provides an indication of their persistence.

3. General results and discussions

3.1. Cirrus clouds climatology

Recent analyses include climatological investigations of cirrus clouds based on their geometrical and optical properties derived from Lidar measurements, multivariate analyses of potential contrail formation and persistence using the ERA5 dataset, and detailed case studies of contrail occurrences over the Haute-Provence Observatory (OHP).

Four primary geometrical classes and three optical groups of cirrus clouds have been identified based on their morphological and optical characteristics over OHP. Table 2 presents the mean values of the principal cirrus cloud variables corresponding to these classifications.

Table 2. Geometric properties of cirrus cloud classes and the optical properties of cirrus cloud groups: cloud base, middle, and top heights, optical depth, mid-cloud temperature, type, and position.

Class	CBH (km)	CMH (km)	CTH (km)	CGT (km)	COD	T (°C)	Type	Position
1	11.7	12.2	12.7	1.06	0.20	−61.3	Thin	Tropopause
2	9.0	10.7	12.5	3.49	1.39	−55.7	Thick	Upper troposphere
3	10.0	10.6	11.4	1.43	0.24	−54.7	Moderate	Upper troposphere
4	8.1	8.8	9.6	1.57	0.40	−44.2	Moderate	Mid-troposphere
1	11.4	11.7	11.9	0.5	0.02	−58.8	SVC	Tropopause
2	10.3	11.0	11.6	1.2	0.15	−54.9	Thin	Upper troposphere
3	9.3	10.5	11.6	2.3	0.81	−54.3	Opaque	Upper troposphere

In addition, Fig. 5 visualizes the altitude profiles of the four cirrus clouds, indicating also their thickness and their occurrences.

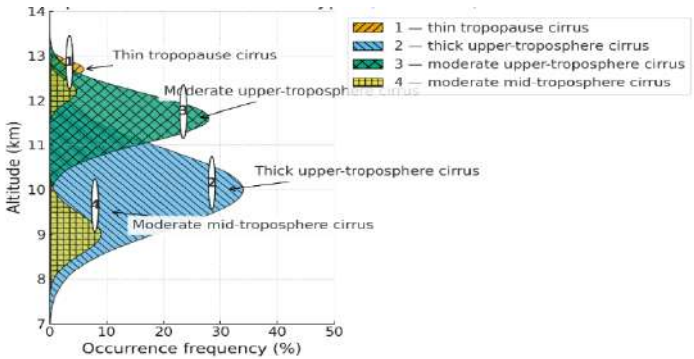

Fig. 5. Schematic representation of the four cirrus classes: moderate/thick mid/upper tropospheric and thin tropopause cirrus clouds.

To investigate the relationships among cirrus cloud properties, a principal component analysis (PCA) was performed. The first two components capture most of the variance, providing a clear visualization of how individual observations group into clusters and how different variables contribute to their separation (Fig. 6).

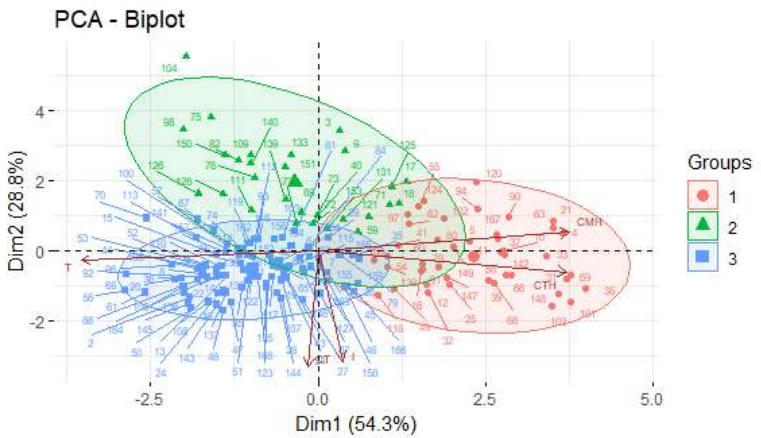

Fig. 6. Principal-component biplot of cirrus cloud properties showing individual observations (points) and variable loadings (arrows) projected on PC1 (Dim1 = 54.3%) and PC2 (Dim2 = 28.8%), explaining 83.1% of the total variance.

To investigate the relationships among cirrus cloud properties, a principal component analysis (PCA) was performed. The first two principal components account for the majority of the variance, enabling clear visualization of the clustering of individual observations and the contribution of each variable to their separation (Fig. 6).

3.2. Contrail's multivariate analyses

Application of the Schmidt–Appleman criterion (SAC) and ice-supersaturated region (ISSR) criteria to the ERA5 dataset for the period 2021–2023 enabled comprehensive statistical analyses of contrail properties (Mandija *et al*. 2025). Environmental conditions were classified into four categories according to their potential for contrail formation and persistence: persistent contrails (PC), non-persistent contrails (NPC), no-contrail conditions (NoC), and potential contrail cases (Pot).

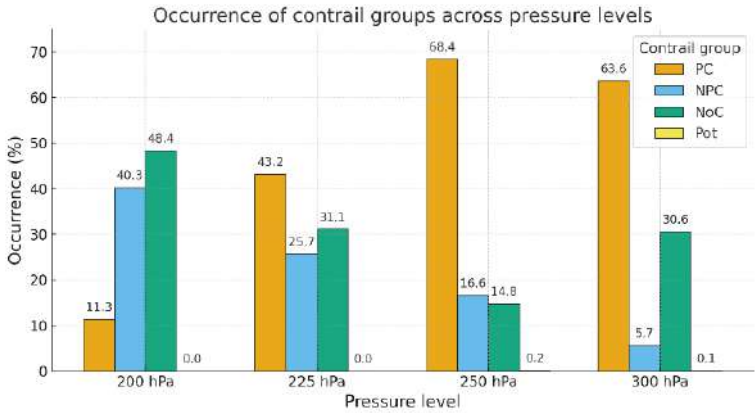

Chart 1. Distribution of contrail group occurrences at various pressure levels: 200 hPa, 225, hPa, 250 hPa, and 300 hPa.

Chart 1 shows that persistent contrail cases over this mid-latitude region occur predominantly at pressure levels between 250 and 300 hPa. At higher altitudes, non-persistent contrail cases become more prevalent.

The four pressure levels are characterized by distinct distributions of the principal meteorological parameters governing contrail formation and persistence. Figure 7 presents the probability distributions of temperature (T), RH_{liq} and RH_{ice}, also indicating their critical values.

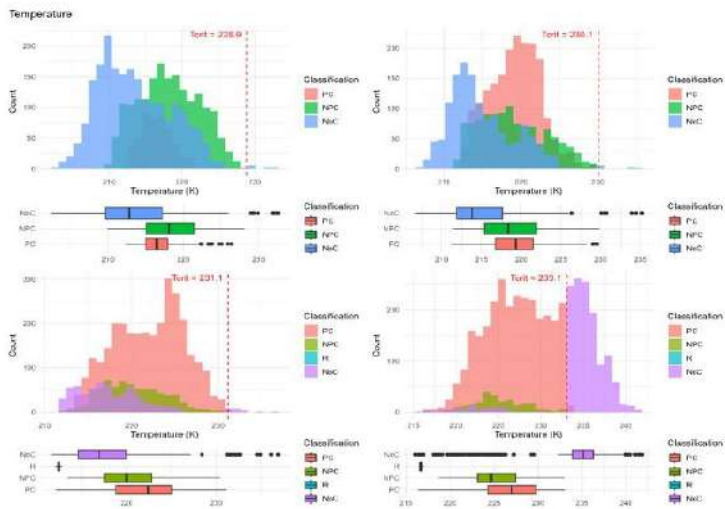

a)

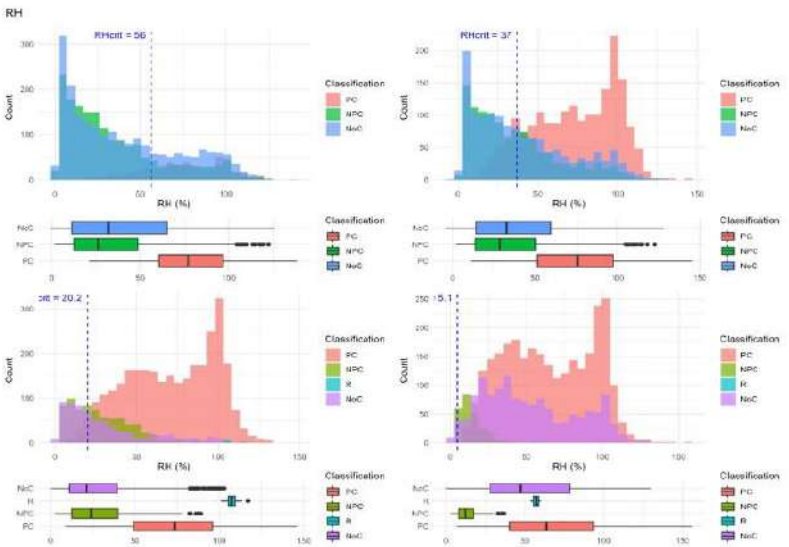

b)

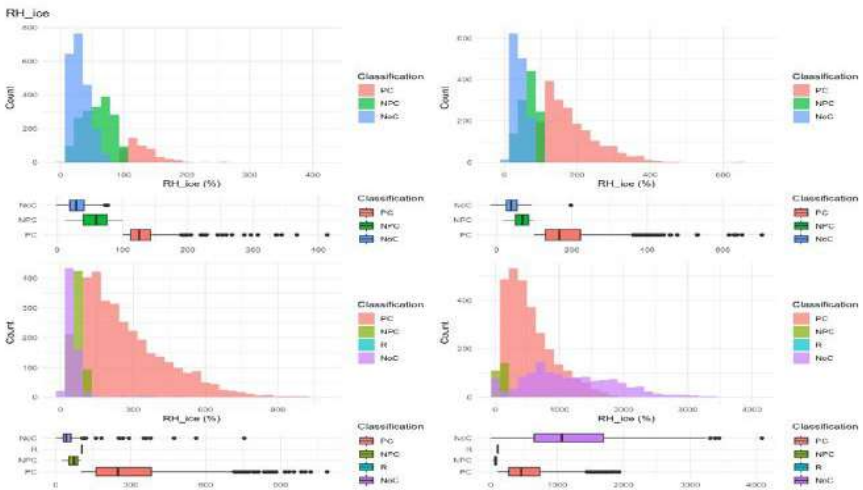

c)

Fig.7. Statistical distributions of the a) Temperature, b) Relative humidity over liquid (RH_{liq}), c) Relative humidity over ice (RH_{ice}), at four pressure levels; 200, 225, 250 and 300 hPa.

The distributions shown in Figure 7 indicate that contrail formation is constrained by the critical thresholds of temperature (T_{crit}) and relative humidity with respect to liquid water ($RH_{liq,crit}$). Persistent contrails are primarily concentrated within the low-temperature and high-RH_{liq} regime, typically between 200 and 300 hPa. At higher altitudes (200–225 hPa), persistent contrails are associated with ice supersaturation (RH_{ice} > 100%) combined with elevated RH_{liq}, while lower levels (250–300 hPa) near-saturation conditions prevail. These lower levels coincide with major flight corridors over the observation site, further favoring contrail occurrence.

3.3. Contrail special cases

By combining aircraft trajectory data, Lidar observations, and ERA5 reanalysis fields, specific contrail events during nighttime conditions have been identified (Fig. 8). Here, we present a representative contrail case observed over the Haute-Provence Observatory (OHP) on 13 January 2023.

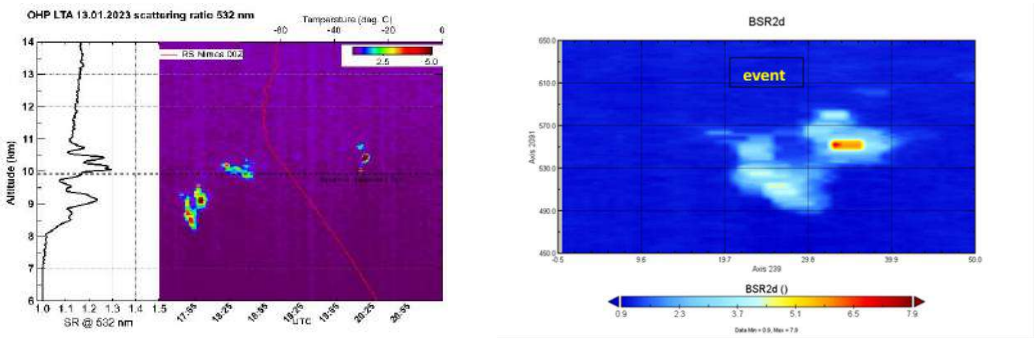

Fig. 8. Left part: Altitude-resolved profiles of the Lidar scattering ratio during 13 January 2023. Four contrail principal events have been identified. Right part shows, zoomed in, the first contrail during the time-interval 17:28-17:35.

In addition to the ADS-B information about the aircraft passage, Planefinder (https://planefinder.net/) provides worth images and aircraft details, such as type, speed, altitude and direction over the site (Fig. 9).

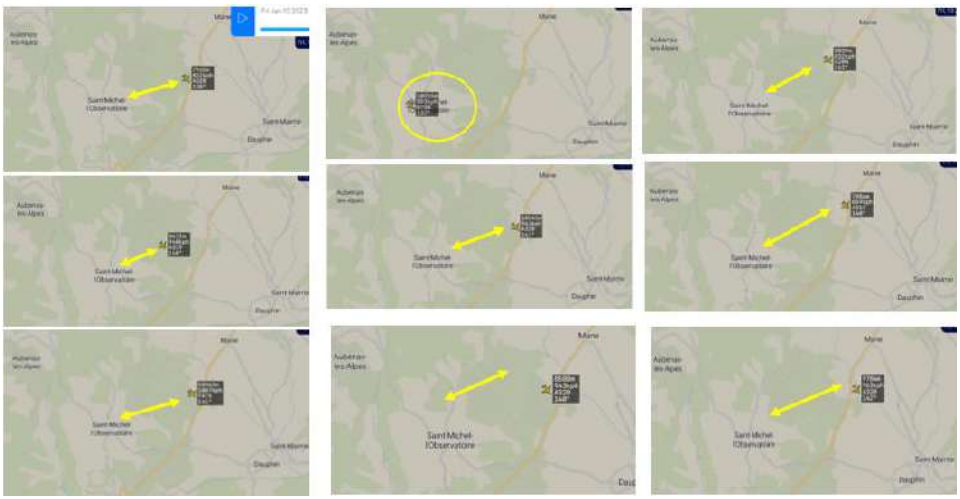

Fig. 9. Flight Data Provider "Planefinder" images over OHP during a case study, on 13 January 2023.

Following contrail detection using aircraft flight tracking data, Lidar profiles are used to determine their geometrical properties. In a second step, meteorological variables—such as temperature, relative humidity with respect to liquid water and ice, and ice water content—are incorporated to retrieve additional geometrical, optical, and microphysical contrail properties. Furthermore, using ERA5-derived values of RH_{ice} in the surrounding environment, contrail persistence is assessed. The spot-like structure of these contrails is further approximated using a linear model to determine the orientation of their principal axis.

Individual Lidar -detected spots are subsequently aggregated using an automated algorithm developed in this study. The algorithm applies scattering ratio (SR) thresholds for contrail identification, together with spatio-temporal constraints to minimize false positives and false negatives. A schematic representation of the algorithm is provided in Figure 10.

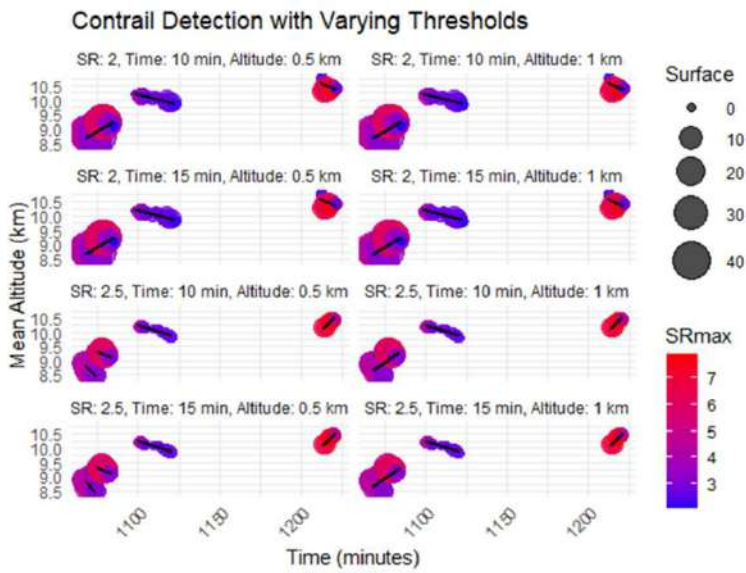

Fig.10. Contrail signatures were grouped into four classes by varying optimal detection and discrimination thresholds. Linear trend lines show their principal spacetime–altitude axes; the legend reports each contrail's peak mid-contrail backscattering ratio and its spatio-temporal area.

Differentiating the thresholds values, several contrail signatures have been obtained (Fig. 10). Those thresholds that minimize false positive/negatives in contrail detection have been taken into account.

3.4 Discussions about general results

Contrail detection and characterization have been extensively investigated in recent studies, particularly over the last decade (Iwabuchi *et al*. 2012; Lamquin *et al.* 2012; Keckhut *et al*. 2013; Schumann *et al*. 2017; Kärcher, 2018; Duda *et al.* 2019; Petzold *et al*. 2020; Lee *et al.* 2021; Gierens, 2021; Voigt *et al*. 2021; Wilhelm *et al*. 2022; Agarwal *et al*. 2022; Dischl *et al*. 2022; Roosenbrand *et al*. 2022; 2023; Groß *et al*. 2024; Martin Frias *et al*. 2024; Gryspeerdt *et al*. 2024; Hofer *et al*. 2024; Megill and Grewe, 2025; Low *et al.* 2025). Overall, the results of this study are

consistent with previous findings, although differences arise due to regional variability and methodological approaches.

In this study, persistent contrails (PC) over southern France are most frequently observed at 250–300 hPa, accounting for approximately 36% of cases, while non-persistent contrails (NPC) represent about 33%. These fractions are higher than those reported over the North Atlantic by Wolf *et al*. (2025), based on ERA5 and IAGOS data (~11–12% PC, ~44–47% NPC) and by Agarwal *et al*. (2022) (~3–6% PC). However, they align more closely with Wolf *et al*. (2023) over Paris (~29% PC, ~52% NPC) and Teoh *et al*. (2024) (~20% of flights form PC). The potential contrail fraction (R ~2.7%) agrees with Wolf *et al*. (2023) (~1.2%). The mean PC temperature (~−56°C) matches Iwabuchi *et al*. (2012) (−54°C) and Schumann et al. (2017), while mean PC altitude (~10.6 km) aligns with both Iwabuchi *et al*. (2012) (10.7 km) and Dischl *et al*. (2022). However, this study's PC mean RHice (147%) exceeds Iwabuchi *et al*. 2012 (126%), suggesting regional or methodological differences in supersaturation characterization. These comparisons validate the multivariate approach while highlighting regional variability in contrail-favourable conditions.

The study retrieves contrail geometrical and optical properties over southern France using a novel multisource methodology combining Lidar , ADS-B flight data, and ERA5 reanalysis. Optimal detection thresholds (scattering ratio = 2.1, temporal separation = 7.2 min, altitude separation = 0.3 km) enable reliable contrail identification. Retrieved contrail altitudes (8.7–10.3 km) align with previous Lidar -based observations (Keckhut *et al*. 2013; Xu *et al*. 2023) and satellite-derived climatologies (Lamquin *et al*. 2012; Duda *et al*. 2019). Geometrical thicknesses (0.1–1.1 km) and widths (2–28 km) fall within ranges reported by Freudenthaler *et al*. (1995) and Poellot *et al*. (1999) for contrails aged 15–30 min. Optical depths (0.05–0.40) are consistent with Sassen (1997) (0.1–0.5) and Atlas and Wang (2010) (mean ~0.2). The thermodynamic conditions ($T < -41°C$, $RH_{ice} > 100\%$) confirm persistent contrail formation criteria established by Kärcher (2018) and Schumann *et al*. (2017). These comparisons validate the methodological framework while demonstrating its capability to characterize individual contrails with high precision.

4. CONCLUSIONS

This study summarizes recent research activities on cirrus clouds and contrails conducted at the Laboratoire Atmosphères, Observations

Spatiales (LATMOS), the Observatoire de Physique du Globe de Clermont-Ferrand (OPGC), and the Laboratoire de Météorologie Physique (LaMP).

The main research efforts focus on multivariate statistical analyses, including descriptive statistics, principal component analysis, clustering methods, and correlation analyses of the geometrical and optical properties of cirrus clouds and contrails over the Haute-Provence Observatory (OHP). The objective is to identify distinct clusters of cirrus and contrail populations based on shared physical characteristics, to assess the influence of contrails on natural cirrus clouds, and to improve understanding of the evolution from fresh linear contrails to aged contrail cirrus.

The goal is to identify the corresponding clusters of cirrus and contrails based on the matching properties, to evaluate the extent of contrail impacts on natural cirrus, and to provide insights into the evolution of fresh line-shaped contrails into aged contrail cirrus.

The integrated use of Lidar observations, ADS-B flight data, and ERA5 reanalysis fields provides a robust framework for contrail detection and characterization. The application of optimized detection thresholds significantly reduces false positives and negatives, enabling reliable identification of individual contrail events. Retrieved geometrical properties, including altitudes (8.7–10.3 km) and optical depths (0.05–0.40), are consistent with previous Lidar and satellite-based studies, confirming the validity of the multisource approach.

Multivariate statistical analyses further reveal distinct climatological patterns in both cirrus clouds and contrails. Cirrus clouds, classified into four geometrical classes and three optical groups using PCA-derived features, show that optically thicker cirrus are generally associated with lower altitudes and higher optical depths, while optically thinner cirrus are more frequent near the tropopause. For contrails, application of the Schmidt–Appleman criterion and ISSR conditions to ERA5 data indicates that persistent contrail formation occurs predominantly between 250 and 300 hPa, corresponding to major flight corridors. The mean temperature (~−56 °C) and mean RH_{ice} (~147%) further highlight the importance of cold, ice-supersaturated environments in contrail formation and persistence.

The synergistic integration of ground-based remote sensing, satellite observations, flight tracking data, and reanalysis products provides a

powerful framework for improving contrail parameterizations in climate models.

Future work will focus on expanding the contrail case-study database, further statistical analysis of water vapour variability and contrail occurrence, intercomparison of Lidar with additional sensors, improved tracking of contrails using satellite and ground-based imagery, and enhanced prediction of ice-supersaturated regions.

Data accessibility:

The study uses ERA5 reanalysis data from the European Centre for Medium-Range Weather Forecasts (ECMWF), aircraft tracking data from ADS-B sources, flight information from Planefinder, and ground-based Lidar and all-sky camera observations. Processed data and derived results are available from the corresponding author upon reasonable request.

Declaration of AI use:

The authors declare that no artificial intelligence tools were used in the preparation, analysis, interpretation, or writing of this manuscript.

Author contributions:

P.K: conceptualization; F.M. compilation and preparation of the manuscript; F.M. P.K. F.P. J-L.B. writing and original draft preparation; D. A. A. S. A. I. S. K. writing and review and editing.

Authors' approval:

All authors have read and approved the final version of the manuscript and consent to its publication.

Conflict of interest declaration:

The authors declare that they have no conflicts of interest.

Funding:

This project has received funding from the French government in the framework of France 735 2030 under Grant DOS0182433/00 and from the Horizon Europe Research and Innovation 736 Actions program under Grant Agreement N°101056885.

Ethics: Not applicable.

REFERENCES:

Agarwal A, Meijer V R, Eastham S D, Speth RL, Barrett SRH. 2022. Reanalysis-driven simulations may overestimate persistent contrail formation by 100%–250%. *Environmental Research Letters*, **17**:**014045** . doi:10.1088/1748-9326/ac38d9.

Alraddawi D, Keckhut P, Mandija F, Sarkissian A, Pietras C, Dupont J-C, Farah A, Hauchecorne A, Porteneuve J. 2025. Calibration of upper air water vapour profiles using the IPRAL Raman Lidar and ERA5 model results and comparison to GRUAN radiosonde observations. *Atmosphere* **16**: **351**. doi:10.3390/atmos16030351.

Appleman H. 1953. The formation of exhaust condensation trails by jet aircraft. *Bulletin of the American Meteorological Society*, **34**, **14**–**20** . doi:10.1175/1520-0477-34.1.14.

Atlas D, Wang Z. 2010. Contrails of small and very large optical depth. *Journal of Atmospheric Sciences*, **67:** 3065–3073. doi:10.1175/2010JAS3403.1.

Dischl R, Kaufmann S, Voigt C. 2022. Regional and seasonal dependence of the potential contrail cover and the potential contrail cirrus cover over Europe. *Aerospace* **9**:**485**. doi:10.3390/aerospace9090485.

Duda D P, Bedka S T, Minnis P, Spangenberg D, Khlopenkov K, Chee T, Smith WL Jr. 2019. Northern Hemisphere contrail properties derived from Terra and Aqua MODIS data for 2006 and 2012. *Atmospheric Chemistry and Physics* **19**: 5313–5330. doi:10.5194/acp-19-5313-2019.

Freudenthaler V, Homburg F, Jäger H. 1995. Contrail observations by ground-based scanning Lidar : cross-sectional growth. *Geophysical Research Letters*, **22**: 3501–3504. doi:10.1029/95GL03549

Gierens K. 2021. Theory of contrail formation for fuel cells. *Aerospace*, **8 (6)**:164. doi:10.3390/aerospace8060164.

Groß S, Jurkat-Witschas T, Li Q, Wirth M, Urbanek B, Krämer M, Weigel R, Voigt C. 2023. Investigating an indirect aviation effect on mid-latitude cirrus clouds – linking Lidar -derived optical properties to in situ measurements. *Atmospheric Chemistry and Physics*, **23**: 8369–8381. doi:10.5194/acp-23-8369-2023.

Gryspeerdt E, Stettler MEJ, Teoh R, Burkhardt U, Delovski T, Driver OGA, Painemal D. 2024. Operational differences lead to longer lifetimes of satellite detectable contrails from more fuel efficient aircraft. *Environmental Research Letters*, **19**: **084059**. doi:10.1088/1748-9326/AD5B78.

Hersbach H, Bell B, Berrisford P, Hirahara S, Horányi A, Muñoz-Sabater J, Nicolas J, Peubey C, Radu R, Schepers D, Simmons A, Soci C, Abdalla S, Abellan X, Balsamo G, Bechtold P, Biavati G, Bidlot J, Bonavita M, De Chiara G, Dahlgren P, Dee D,

Diamantakis M, Dragani R, Flemming J, Forbes R, Fuentes M, Geer A, Haimberger L, Healy S, Hogan R J, Hólm E, Janisková M, Keeley S, Laloyaux P, Lopez P, Lupu C, Radnoti G, de Rosnay P, Rozum I, Vamborg F, Villaume S, Thépaut J-N. 2020. The ERA5 global reanalysis. *Quarterly Journal of the Royal Meteorological Society*, **146**: **1999**–**2049**. doi:10.1002/qj.3803

Hofer S, Gierens K, Rohs S. 2024. How well can persistent contrails be predicted? An update. *Atmospheric Chemistry and Physics*, **24**: **7911**–**7925**. doi:10.5194/acp-24-7911-2024.

Iwabuchi H, Yang P, Liou K, Minnis P. 2012. Physical and optical properties of persistent contrails: climatology and interpretation. *Journal of Geophysical Research: Atmospheres*, **117**: **D06215**. doi:10.1029/2011JD017020.

Kärcher B. 2018. Formation and radiative forcing of contrail cirrus. *Nature Communications*, **9**: **1824**. doi:10.1038/s41467-018-04068-0.

Keckhut P, Borchi F, Bekki S, Hauchecorne A, Silaouina M. 2006. Cirrus classification at midlatitude from systematic Lidar observations. *Journal of Applied Meteorology and Climatology*, **45**: **249**–**258**. doi:10.1175/JAM2348.1.

Keckhut P, Hauchecorne A, Bekki S, Colette A, David C, Jumelet J. 2005. Indications of thin cirrus clouds in the stratosphere at mid-latitudes. *Atmospheric Chemistry and Physics*, **5**: **3407**–**3414**. doi:10.5194/acp-5-3407-2005.

Keckhut P, Perrin J-M, Thuillier G, Hoareau C, Porteneuve J, Montoux N. 2013. Subgrid-scale cirrus observed by Lidar at mid-latitude: variability effects of the cloud optical depth. *Journal of Applied Remote Sensing*, **7**(**1**): **073530** . doi:10.1117/1.JRS.7.073530.

Khaykin S, Godin-Beekmann S, Hauchecorne A, Pelon J, Ravetta F, Keckhut P. 2018. Stratospheric smoke layer with unprecedentedly high backscatter observed by Lidar s above southern France. *Geophysical Research Letters*, **45**: **1639**–**1646**. doi:10.1002/2017GL076763.

Lamquin N, Stubenrauch C J, Gierens K, Burkhardt U, Smit H. 2012. A global climatology of upper-tropospheric ice supersaturation occurrence inferred from the Atmospheric Infrared Sounder calibrated by MOZAIC. *Atmospheric Chemistry and Physics*, **12**, **381**–**405**. doi:10.5194/acp-12-381-2012

Lee D, Fahey D, Skowron A, Allen M, Burkhardt U, Chen Q, Doherty S, Freeman S, Forster P, Fuglestvedt J, Owen B, Stefanidis G P, Tsimplis M N. 2021. The contribution of global aviation to anthropogenic climate forcing for 2000 to 2018. *Atmospheric Environment,* **244**: **117834**. doi:10.1016/j.atmosenv.2020.117834.

Low J, Teoh R, Ponsonby J, Gryspeerdt E, Shapiro M, Stettler MEJ. 2025. Ground-based contrail observations: comparisons with reanalysis weather data and contrail model simulations. *Atmospheric Measurement Techniques,* **18**, **37**–**56**. doi:10.5194/amt-18-37-2025.

Mandija F, Keckhut P, Alraddawi D, Irbah A, Sarkissian A, Khaykin S, Peyrin F, Baray J-L. 2026. Nighttime contrail characterization from multisource Lidar and meteorological observations. *Remote Sensing,* **18**: **210**. doi:10.3390/rs18020210.

Mandija F, Keckhut P, Alraddawi D, Khaykin S, Sarkissian A. 2024. Climatology of cirrus clouds over the Observatory of Haute-Provence (France) using multivariate analyses on Lidar profiles. *Atmosphere,* **15**(**10**):**1261**. doi:10.3390/atmos15101261.

Megill L, Grewe V. 2025. Investigating the limiting aircraft-design-dependent and environmental factors of persistent contrail formation. *Atmospheric Chemistry and Physics,* **25**, **4131**–**4149**. doi:10.5194/acp-25-4131-2025.

Murphy D M, Koop T. 2005. Review of the vapour pressures of ice and supercooled water for atmospheric applications. *Quarterly Journal of the Royal Meteorological Society,* **131**, **1539**–**1565**. doi:10.1256/qj.04.94

Petzold A, Neis P, Rütimann M, Rohs S, Berkes F, Smit HGJ, Krämer M, Spelten N, Spichtinger P, Nédélec P, Wahner A. 2020. Ice-supersaturated air masses in the northern mid-latitudes from regular in situ observations by passenger aircraft: vertical distribution, seasonality and tropospheric fingerprint. *Atmospheric Chemistry and Physics,* **20**: **8157**–**8179**. doi:10.5194/acp-20-8157-2020.

Peyrin F, Fréville P, Montoux N, Baray J-L. 2023. Original and low-cost ADS-B system to fulfill air traffic safety obligations during high power Lidar operation. *Sensors,* **23**: **2899**. doi:10.3390/s23062899

Poellot MR, Arnott WP, Hallett J. 1999. In situ observations of contrail microphysics and implications for their radiative impact. *Journal of Geophysical Research: Atmospheres,* **104**: **12077**–**12084**. doi:10.1029/1999JD900109.

Roosenbrand E, Sun J, Hoekstra J. 2023. Contrail minimization through altitude diversions: a feasibility study leveraging global data. *Transportation Research Interdisciplinary Perspectives*, **22**:**100953**. doi:10.1016/j.trip.2023.100953.

Sassen K. 1997. Contrail-cirrus and their potential for regional climate change. *Bulletin of the American Meteorological Society*, **78**: **1885**–**1903**.

Schumann U, Baumann R, Baumgardner D, Bedka ST, Duda D P, Freudenthaler V, Gayet J-F, Heymsfield AJ, Minnis P, Quante M, Raschke E, Schlager H, Vázquez-Navarro M, Voigt C, Wang Z. 2017. Properties of individual contrails: a compilation of observations and some comparisons. *Atmospheric Chemistry and Physics*, **17**: **403**–**438**. doi:10.5194/acp-17-403-2017.

Sherlock V, Garnier A, Hauchecorne A, Keckhut P. 1999. Implementation and validation of a Raman Lidar measurement of middle and upper tropospheric water vapour. *Applied Optics*, **38**, **5838**–**5850**.

Singh D K, Sanyal S, Wuebbles D J. 2024. Understanding the role of contrails and contrail cirrus in climate change: a global perspective. *Atmospheric Chemistry and Physics*, **24**, **9219**–**9262**. doi:10.5194/acp-24-9219-2024

Sonntag D. 1994. Advancements in the field of hygrometry. *Meteorologische Zeitschrift*, **3**: **51**–**66**. doi:10.1127/metz/3/1994/51.

Teoh R, Engberg Z, Schumann U, Voigt C, Shapiro M, Rohs S, Stettler MEJ. 2024. Global aviation contrail climate effects from 2019 to 2021. *Atmospheric Chemistry and Physics*, **24**: **6071**–**6093**. doi:10.5194/acp-24-6071-2024.

Teoh R, Schumann U, Gryspeerdt E, Molloy J, Koudis G, Voigt C, Stettler MEJ. 2022. Aviation contrail climate effects in the North Atlantic from 2016 to 2021. *Atmospheric Chemistry and Physics*, **22**: **10919**–**10935**. doi:10.5194/acp-22-10919-2022.

Voigt C, Kleine J, Sauer D, Moore R H, Bräuer T, Le Clercq P, Kaufmann S, Scheibe M, Jurkat-Witschas T, Aigner M, Bauder U, Boose Y, Borrmann S, Crosbie E, Diskin G S, DiGangi J, Hahn V, Heckl C, Huber F, Nowak J B, Rapp M, Rauch B, Robinson C, Schripp T, Shook M, Winstead E, Ziemba L, Schlager H, Anderson BE. 2021. Cleaner burning aviation fuels can reduce contrail cloudiness. *Communications Earth & Environment*, **2**: **1**–**10**. doi:10.1038/s43247-021-00174-y.

Wilhelm L, Gierens K, Rohs S. 2022. Meteorological conditions that promote persistent contrails. *Applied Sciences*, **12**:**4450**. doi:10.3390/app12094450.

Wolf K, Bellouin N, Boucher O, Rohs S, Li Y. 2025. Correction of ERA5 temperature and relative humidity biases by bivariate quantile mapping for contrail formation analysis. *Atmospheric Chemistry and Physics*, **25**: **157**–**181**. doi:10.5194/acp-25-157-2025.

Wolf K, Bellouin N, Boucher O. 2023. Long-term upper-troposphere climatology of potential contrail occurrence over the Paris area derived from radiosonde observations. *Atmospheric Chemistry and Physics*, **23**: **287**–**309**. doi:10.5194/acp-23-287-2023.

Wolf K, Bellouin N, Boucher O. 2024. Distribution and morphology of non-persistent contrail and persistent contrail formation areas in ERA5. *Atmospheric Chemistry and Physics*, **24**: **5009**–**5024**. doi:10.5194/acp-24-5009-2024.

FEASIBILITY ASSESSMENT OF NANOPESTICIDES AND NANOFERTILIZERS FOR SUSTAINABLE AGRICULTURE IN ALBANIA

Magdalena CARA[1,2], Florida GASHI[3], Orges CARA[4,2], Klevis HOXHALLARI[1,2,6], Nensi ISAK[5,2], Kledi XHAXHIU[5,2]

[1]Department of Plant Protection, Faculty of Agriculture and Environment, Agricultural University of Tirana, Albania
[2]NanoAlb/Nanobalkan - Regional Center of Nanotechnology, Academy of Sciences of Albania.
[3]Department of Natural Resources Institute, Agriculture for Sustainable Development, University of Greenwich, UK
[4]International Centre for Advanced Mediterranean Agronomic Studies (CIHEAM of Bari), Valenzano, Italy
[5] Department of Chemistry, Faculty of Natural Sciences, University of Tirana, Albania
Author for correspondence: magdacara@ubt.edu.al

MC, 0000-0002-1715-8635; FG, 0009-0009-9451-4232; OC, 0009-0000-0682-0796; KH, 0009-0002-7618-7660; NI, 0009-0005-5531-3471; KXh, 0000-0002-1798-3141

ABSTRACT

This study evaluates the feasibility of nano-enabled agrochemicals, including nanopesticides and nanofertilizers, for sustainable agricultural applications, with a particular focus on Albania. A structured literature-based approach was employed to assess agronomic, environmental, economic, and regulatory dimensions. The findings indicate that nano-enabled formulations offer potential advantages, including improved input efficiency and reduced environmental losses. However, their performance remains variable across agro-ecological conditions, and their environmental fate and long-term impacts are not yet fully understood. In the Albanian context, factors such as agro-climatic variability, soil heterogeneity, smallholder-dominated farm structures, and limited institutional capacity present significant challenges to adoption. The study concludes that while nanotechnology represents a promising innovation, its implementation requires site-specific validation, regulatory development, and integration with existing agricultural practices.

Keywords: nanotechnology nanopesticides, nanofertilizers, sustainable agriculture, feasibility

Publisher: Academy of Sciences of Albania
License: Creative Commons Attribution License (CC BY 4.0)
Citation: **Cara M, Gashi F, Cara O, Hoxhallari K, Isak N, Xhaxhiu K. 2026.** Feasibility assessment of nanopesticides and nanofertilizers for sustainable agriculture in Albania**.** *Albanian Journal of Natural and Technical Sciences* (*AJNTS),* **2 (30),**
Journal URL: https://journals-akad.gov.al/magazines/1
Classification: Research
Subject Category Applied Sciences subject areas: Agronomy & Agroecology

1. INTRODUCTION

Global agricultural systems are under increasing pressure to meet rising food demand while operating within finite land and environmental constraints. Approximately 36.8% of global land is currently used for agriculture, yet available agricultural land is declining despite continued population growth (FAO, 2022). Simultaneously, population expansion, urbanization, and climate change are intensifying demand for food production, placing additional strain on already stressed agricultural systems (Duro *et al.* 2020).

These dynamics highlight the urgent need to improve productivity while ensuring long-term environmental sustainability. Modern agriculture has addressed these pressures primarily through the intensive use of agrochemicals, including fertilizers and pesticides. While these inputs have contributed significantly to yield stabilization and increased food production, their widespread and often inefficient use has resulted in substantial environmental and health challenges. These include pesticide resistance, biodiversity loss, disruption of soil microbial communities, and contamination of food and water systems (Bombo *et al*. 2019; Gupta *et al.* 2024). Low nutrient-use efficiency (NUE) remains a critical issue, as a large proportion of applied inputs is lost through processes such as leaching, runoff, volatilization, and photodegradation (Mitra *et al*. 2021; Parven *et al*. 2025). A major limitation is their low use efficiency, with an estimated 60–70% of applied agrochemicals lost to processes such as leaching, runoff, volatilization, and degradation (Popp *et al.* 2013). These inefficiencies increase production costs while exacerbating environmental pollution and health risks (Devi *et al.* 2022; Zhou *et al*. 2025). Consequently, maximizing input-use efficiency has become a key priority

in sustainable agricultural strategies aligned with global food security goals (FAO, 2022).

In response to these challenges, nanotechnology has emerged as a promising approach to enhance agricultural productivity and sustainability through the development of nano-enabled agrochemicals. By exploiting properties such as high surface-area-to-volume ratios, tunable surface charge, and controlled-release mechanisms, nano-enabled systems may improve the delivery, stability, and performance of active ingredients (Fraceto *et al*. 2016; Manjunatha *et al*. 2016; Baker *et al*. 2017; Sharma *et al*. 2019). These systems include nanopesticides and nanofertilizers that utilize nanocarriers, encapsulation techniques, and advanced materials to enhance solubility, bioavailability, and targeted delivery (Agostini *et al*. 2012; Chaud *et al*. 2021). Nanopesticides can improve pest management by protecting active compounds from environmental degradation and increasing their efficacy against target organisms (Yadav *et al*. 2020), while nanofertilizers enable controlled and targeted nutrient release, thereby improving NUE and mitigating environmental losses (Abdalla *et al*. 2022; Yadav *et al*. 2023). Advanced materials such as carbon nanotubes, graphene, and quantum dots have also been explored for their potential to enhance nutrient uptake and crop physiological performance (Gaur *et al*. 2021).

Despite these advantages, important uncertainties remain regarding the environmental behaviour and safety of nano-enabled agrochemicals. Their high reactivity and mobility may increase the risk of bioaccumulation, ecosystem disruption, and unintended human exposure, particularly under conditions of insufficient regulatory oversight (Wu *et al*. 2025). The performance and safety of these materials are strongly influenced by physicochemical characteristics such as particle size, surface charge, and composition, which may also determine their capacity to cross biological barriers and induce cytotoxic or genotoxic effects (Prasad *et al*. 2017; Zielińska *et al*. 2020). In addition, challenges related to production costs, scalability, and the lack of standardized regulatory frameworks continue to constrain their widespread adoption (Parisi *et al*. 2015).

Although research on nano-enabled agrochemicals is expanding rapidly, their feasibility in smallholder-dominated and transition economies remains insufficiently explored. Albania represents a relevant case study, characterized by fragmented landholdings, heterogeneous production systems, and increasing pressure to align with European Union sustainability standards. These unique structural and institutional

conditions may significantly modulate the adoption rates and field performance of advanced agricultural technologies.

Consequently, this study evaluates the feasibility of nano-enabled agrochemicals, specifically nanopesticides and nanofertilizers, in Albania by assessing their agronomic performance, environmental implications, economic viability, and regulatory readiness within smallholder farming systems.

2. MATERIALS AND METHODS

2.1. Study design

This study was conducted as a structured narrative review to evaluate the feasibility of nano-enabled agrochemicals, specifically nanopesticides and nanofertilisers, within the context of sustainable agriculture in Albania. The methodological approach integrates qualitative evidence synthesis with a multi-dimensional feasibility framework, focusing on agronomic, environmental, economic, and regulatory aspects.

2.2. Data Collection and Literature Selection

A comprehensive literature search was executed across major academic databases, including Web of Science, Scopus, ScienceDirect, and Google Scholar, covering peer-reviewed publications from 2010 to 2025. Search strings were constructed using Boolean operators combining primary keywords (*nanopesticides, nanofertilizers, nano-agrochemicals, agricultural nanotechnology, environmental impact, toxicology, risk assessment, and sustainable agriculture*) with context-specific geographic and structural descriptors (*Albania, Mediterranean agriculture, and smallholder farming systems*).

Following the initial database retrieval, a two-stage screening process based on title, abstract, and full-text relevance was implemented. Studies were included if they directly evaluated the application of nano-enabled agrochemicals in agricultural systems, with specific emphasis on agronomic performance, environmental fate, economic viability, or regulatory oversight. High priority was assigned to peer-reviewed journal articles, institutional reports, and European Union (EU) regulatory frameworks. Conversely, studies were excluded if they focused on non-agricultural applications of nanotechnology (e.g., biomedical, cosmetic, or industrial sectors) or lacked explicit relevance to technological feasibility

assessments. To maximize regional validity and contextual interpretability, localized literature focusing on Albania and broader Mediterranean agroecosystems was intentionally integrated into the final selection pool.

2.3. Data analysis and Feasibility Framework

A thematic qualitative synthesis was applied to analyse the selected literature. Extracted data were systematically categorized into four predefined analytical feasibility domains:

i. Agronomic Feasibility: Evaluated via indicators such as crop yield performance, pest-control efficacy, and nutrient-use efficiency (NUE).
ii. Environmental Feasibility: Examined via nanoparticle environmental fate, soil-water persistence, bioaccumulation potential, and ecotoxicity profiles.
iii. Economic Feasibility: Assessed based on input-cost dynamics, farm-level productivity gains, and adoption barriers within smallholder farming systems.
iv. Regulatory Feasibility: Evaluated by assessing the maturity and adequacy of existing oversight frameworks, emphasizing European Union chemical and agricultural regulations and their transposition alignment for Albania as an EU-candidate country.

Synthesized findings were contextually contextualized against Albania's specific agricultural baseline, accounting for regional agro-climatic variability, soil heterogeneity, smallholder-dominated farm structures, and localized institutional constraints.

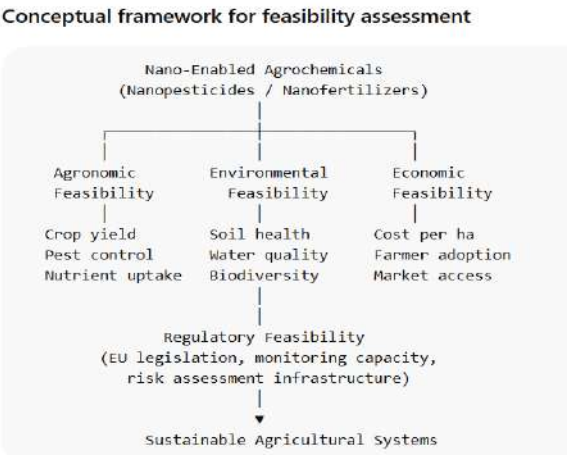

Fig. 1. Conceptual framework for feasibility assessment (Source: Author's compilation).

Conceptual framework synthesized from the literature to structure the assessment of nano-enabled agrochemicals across agronomic, environmental, economic, and regulatory dimensions.

3. Literature Synthesis

3.1. Feasibility Assessment Framework

The feasibility of nano-enabled agrochemicals is evaluated across four dimensions, agronomic, environmental, economic, and regulatory, based on a synthesis of existing literature rather than primary data. This section synthesizes findings from the literature on nano-enabled agrochemicals across four dimensions: agronomic, environmental, economic, and regulatory feasibility.

3.2. Agronomic Feasibility

Agronomic feasibility is assessed through indicators commonly reported in the literature, including yield response, pest-control effectiveness, and nutrient-use efficiency. Pest-control efficiency evaluates the reduction of pest pressures through direct or indirect mechanisms (Saito *et al*. 2021; Al-Shammary *et al*. 2024; Akchaya *et al*. 2025).

Evidence suggests that nanofertilizers can improve nutrient-use efficiency through mechanisms such as controlled release, enhanced solubility, and increased plant uptake (Kah *et al*. 2013;*DeRosa et al*. 2010). These mechanisms are associated with yield improvements and reduced fertilizer application rates under controlled experimental conditions (DeRosa *et al*. 2010). Similarly, nanopesticides have demonstrated improved pest-control performance due to enhanced stability, targeted delivery, and reduced degradation of active ingredients (Kah & Hofmann, 2014; Servin and White, 2016).

However, the available evidence is largely derived from laboratory studies or small-scale trials, with limited validation under large-scale or long-term field conditions (Chen and Yada, 2011). Reported outcomes vary considerably depending on agro-ecological factors such as soil properties, climate, crop species, and management practices (Nair *et al*. 2010). Soil characteristics such as pH, organic matter content, and microbial activity influence nanoparticle behaviour and nutrient dynamics (Navarro *et al*. 2008; Prasad *et al*. 2017).

The literature reports inconsistent agronomic outcomes. While some studies indicate significant yield improvements (Ghormade *et al*. 2011). Others show minimal or no advantage over conventional inputs. In addition, interactions between nanomaterials and soil–plant systems remain insufficiently understood, particularly regarding their effects on plant physiology, microbial communities, and nutrient cycling (Liu and Lal, 2015; Raliya *et al*. 2015). Potential phytotoxic effects and negative impacts on beneficial soil microorganisms have also been reported, especially at higher concentrations or with repeated applications (Navarro *et al*. 2008; Tourinho *et al*. 2012).

Overall, the literature reports variable agronomic outcomes, with performance influenced by environmental conditions, crop systems, and management practices.

3.3. Environmental Feasibility and the Role of Advanced Nanocarriers

Several studies indicate that nano-enabled formulations may mitigate environmental contamination through controlled-release mechanisms and improved delivery efficiency, thereby reducing losses from leaching, runoff, and volatilization (Kah *et al*. 2013; Servin *et al*. 2015).

Within this framework, advanced nanocarriers, particularly graphene-based derivatives, have attracted increasing attention due to their unique physicochemical properties. The agronomic and environmental performance of graphene-based nanofertilizers and nanopesticides depends heavily on the specific graphene derivative utilized. Graphene oxide (GO) has demonstrated superior functionality compared to other forms of graphene, primarily due to its hydrophilicity, high surface area, and abundant oxygen-containing functional groups (Du *et al*. 2015). These characteristics enhance interactions with water, nutrients, and active compounds, improving dispersion, adsorption capacity, and controlled-release behaviour. Consequently, GO-based nanocarriers can facilitate targeted delivery of agrochemicals, improve nutrient-use efficiency, and reduce environmental losses (DeRosa *et al*. 2010; Kah and Hofmann, 2014).

However, despite these advantages, important concerns remain regarding the environmental and biological safety of graphene-based nanomaterials. The increasing use of nanotechnology in agriculture raises concerns about potential toxicity, particularly because these materials may

enter the food chain (Fatima *et al*. 2021). Although mitigation strategies such as surface functionalization—including amine modification—have been shown to attenuate nanotoxicity (Lee *et al*. 2011). Substantial uncertainties remain concerning their long-term chronic safety (Tourinho *et al*. 2012).

More broadly, the environmental benefits of nano-enabled systems are not consistently observed across all studies and appear to be highly dependent on environmental conditions and application practices (Kah *et al*. 2019). Even with optimized use, agrochemicals and their metabolites may persist in soils and migrate into groundwater or surface water systems, where they contribute to contaminant loads and affect ecological processes (Hegde *et al*. 2016). Persistent residues can alter soil microbial community structures and impair nutrient cycling pathways, while cumulative exposure in aquatic environments poses ecotoxicological risks across multiple trophic levels (Carpenter *et al*. 2011; Hegde *et al*. 2016).

The incorporation of advanced nanocarriers introduces further complexity into environmental risk assessments. Due to their nanoscale dimensions and high surface reactivity, nanoparticles can exhibit enhanced mobility within soil pore water and aquatic systems, facilitating interactions with biological membranes and elevating the risk of unintended ecological impacts (Navarro *et al*. 2008; Servin *et al*. 2015). Interfaces within the soil–plant–microbe continuum significantly modulate nanoparticle behaviour; for instance, plant root exudates can dynamically alter the physicochemical properties of GO, including its hydrodynamic diameter and carbon-to-oxygen (C:O) ratio—thereby modifying its transport dynamics, bioavailability, and phytotoxicity (Du *et al*. 2015). In addition, nanomaterials may transform within environmental systems, altering their behaviour, bioavailability, and toxicity over time (Lowry *et al*. 2012).

Their potential for bioaccumulation, long-term persistence, and disruption of soil microbial communities highlights the need for careful evaluation of chronic environmental impacts (Servin *et al*. 2015; Kah *et al*. 2019). Evidence from ecotoxicological assays using standard terrestrial model bioindicators, such as *Lepidium sativum* L., demonstrates that graphene oxide can significantly modulate plant phenotypic growth and alter soil physicochemical properties, highlighting the narrow threshold between the agronomic benefits and ecotoxicological risks of these advanced materials (Begum *et al*. 2011). These findings contribute to a more comprehensive understanding of the dual role of engineered

nanocarriers as both efficiency-enhancing delivery tools and potential environmental stressors. Furthermore, the multi-year persistence of nanomaterials increases the risk of chronic soil accumulation following repeated agronomic applications, potentially triggering long-term ecological cascades that are not immediately detectable via short-term assays (Laxmi *et al*. 2023). While certain studies suggest that minimized chemical losses improve macro-environmental outcomes, counter-evidence indicates that nanoparticle interfaces with soil biota and plant rhizospheres can disrupt micro-nutrient cycling and overall ecosystem stability (Raliya *et al*. 2015), underscoring the high variability and unpredictability of localized environmental responses.

These uncertainties are highly critical within the Albanian agroecological context, where baseline environmental vulnerabilities such as accelerated soil erosion, agricultural runoff, and surface water contamination are already pronounced (Kopali, 2012; Eugen Skura, 2017) The physical transport of surface-adsorbed nanoparticles through active erosion and complex hydrological pathways could drastically elevate exposure risks and bioconcentration rates within vulnerable aquatic ecosystems, such as the Adriatic coastal lagoons and regional river basins. Moreover, localized constraints in technical monitoring capacity and institutional regulatory oversight could impede the empirical tracking, risk assessment, and field management of these advanced materials under real-world smallholder farming configurations (Parisi *et al*. 2015).

From a sustainability paradigm, these dynamics underscore the necessity of adopting a precautionary and adaptive risk-management framework. Although nano-enabled agrochemicals exhibit clear potential to lower input application rates and maximize utilization efficiency, their holistic environmental feasibility remains strictly contingent upon multi-season ecotoxicological evaluations, harmonized regulatory oversight, and structural integration with existing agroecological practices, such as Integrated Pest Management (IPM) (Kah *et al*. 2018; Laxmi *et al*. 2023). Within this framework, specialized applications such as incorporating graphene oxide (GO) matrices into nanofertilizer systems to modulate nutrient delivery kinetics and stimulate systemic plant defence mechanisms remain highly promising, yet their commercial deployment must remain conditional upon rigorous lifecycle assessments and the establishment of verified safe-usage thresholds (Saraiva *et al*. 2025).

In synthesis, the global literature presents divergent empirical evidence regarding environmental outcomes, balancing verified reductions

in chemical losses against critical uncertainties involving nanoparticle environmental fate, long-term persistence, and multi-trophic ecological interactions (Servin *et al*. 2015; Kah *et al*. 2018).

3.4. Economic Feasibility

Economic feasibility is evaluated based on reported impacts on productivity, input efficiency, and cost–benefit performance.

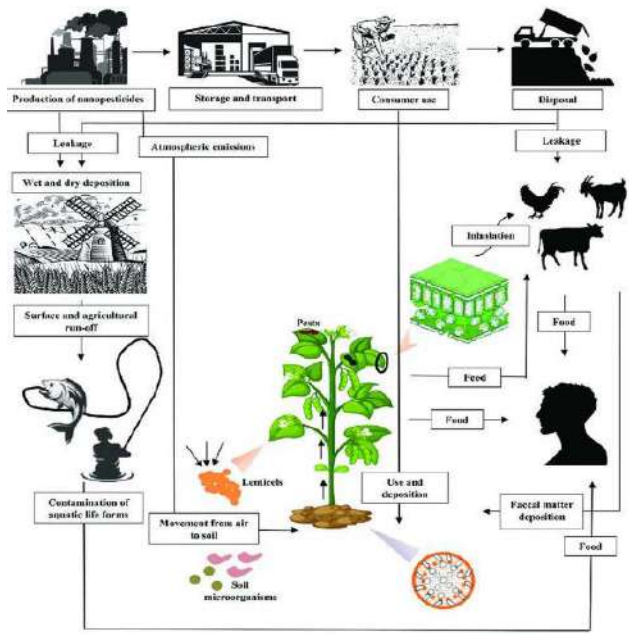

Fig. 2: Lifecycle of nanomaterials in agriculture, adapted from Shekhar *et al*. 2021.

Figure 2 illustrates the environmental pathways of nano-agrochemicals from synthesis and production through agronomic application, environmental dispersion, and subsequent entry into soil matrices, hydrological systems, and trophic networks.

The consensus in the literature indicates that nano-enabled formulations can increase active ingredient efficacy by 20–30% (Kah *et al.* 2019), while simultaneously reducing conventional fertilizer application rates by 30–50% and synthetic pesticide requirements by 40–80%, depending heavily on the specific nanocarrier matrix and field conditions

(Bist *et al*. 2025; Fraceto *et al*. 2016). These optimization metrics directly translate into lowered farm-level input costs and enhanced net profitability.

However, nano-formulations frequently incur higher initial capital expenditures due to manufacturing complexities and specialized industrial formulation processes (Parisi *et al*. 2015). Microeconomic cost–benefit analyses indicate that the net economic advantages of these technologies remain strictly contingent upon manufacturing efficiency, market scalability, and commercial availability (Su *et al*. 2022). Consequently, prominent adoption barriers within smallholder farming configurations include upfront financial constraints, restricted access to advanced inputs, and perceived uncertainty regarding return on investment (ROI). Additional institutional factors, such as localized market structures, evolving regulatory compliance requirements, and technical knowledge gaps, further modulate the overall economic feasibility of these advanced systems.

In synthesis, reported economic outcomes exhibit high variance, governed by a dynamic trade-off between industrial production costs, field-level efficiency gains, and socio-economic adoption conditions.

Table 1: Cost Comparison Between Nanotechnology-Based and Conventional Agriculture

Cost Component	Conventional Agriculture	Nanotechnology-Based Agriculture	Interpretation / Feasibility Insight
Fertilizer Input Cost	High due to large quantities required and repeated applications	Lower total input due to reduced dosage (up to 50% less in some cases) (Su *et al*. 2022).	Nanofertilizers reduce the overall cost per hectare despite a higher unit price
Application Frequency	Frequent applications are required due to nutrient loss (leaching, volatilization)	Reduced frequency due to controlled release mechanisms (Nair *et al*. 2010; Kah *et al*. 2019)	Lower labour and operational costs
Nutrient Use Efficiency (NUE)	Low efficiency (30–50% uptake typical for N	High efficiency due to targeted delivery and slow release	Improved efficiency reduces waste and cost losses

	fertilizers) (Navarro *et al*. 2008)	(Prasad *et al*. 2017; Ahmed *et al*. 2023)	
Pesticide Cost	High due to repeated spraying and resistance development	Potentially lower due to enhanced efficacy and reduced application rates (Chaud *et al*. 2021; *Kah et al*. 2019)	Cost savings depend on formulation efficiency
Labor and Machinery Costs	Higher due to multiple field operations	Reduced due to fewer applications and precision delivery systems *(Fraceto et al*. 2016)	Important advantage in smallholder systems
Environmental Cost (Externalities)	High (soil degradation, water pollution, eutrophication) *(Laxmi et al*. 2023)	Lower due to reduced chemical losses and targeted use (Su *et al*. 2022)	Long-term economic benefits through sustainability
Initial Technology Cost	Low (widely available inputs and infrastructure)	High (R&D, production, and formulation costs)	Major barrier to adoption
Yield Output / Return	Moderate, but dependent on high input use	Comparable or higher yield with lower input	Improves cost–benefit ratio
Overall Cost–Benefit Ratio	Moderate efficiency with high input dependency	Potentially higher profitability, but varies across reported conditions (Su *et al*. 2022)	Requires optimization and local validation

**Source: Author's compilation*

3.5. Regulatory Feasibility Framework

3.5.1. European Regulatory Framework

The regulation of nano-enabled agrochemicals in Europe is governed by a multilayered legislative framework designed to safeguard human health, animal welfare, and environmental integrity. Pre-market risk assessments of engineered nanomaterials are conducted by centralized

regulatory authorities, primarily the European Food Safety Authority (EFSA) and the European Chemicals Agency (ECHA), focusing heavily on substance-specific toxicity, environmental fate, and multi-pathway exposure scenarios (EFSA, 2011; ECHA, 2022).

Downstream food security is further managed by Regulation (EC) No 1935/2004, which mandates that nanomaterials utilized in food-contact materials must not migrate into food matrices at levels that jeopardize human health (European Commission, 2004). For livestock applications, nutritional feeds and additives are regulated under Regulation (EC) No 767/2009 (European Commission, 2009a). Plant nutrition and soil conditioners are governed by the more recent Regulation (EU) 2019/1009, which defines specific safety, purity, and labelling requirements for fertilizing products entering the single market (European Commission, 2019). Additionally, the Biocidal Products Regulation (EU) No 528/2012 enforces distinct evaluations for any active substances exhibiting nanoscale dimensions (European Commission, 2012).

To standardize nomenclature, the European Commission's Recommendation on the definition of a nanomaterial (2022/C 229/01) provides a definitive metric based entirely on particle-size distribution (European Commission, 2022). Beyond primary legislative acts, EFSA and ECHA have published technical guidance documents emphasizing that nanoforms necessitate a case-by-case risk assessment. This requirement stems from their distinct physicochemical properties, such as elevated specific surface reactivity, modified bioavailability, and high bioaccumulation potential (Hardy *et al*. 2018; ECHA, 2022).

Despite this comprehensive architecture, critical limitations remain within the literature, notably the persistent absence of harmonized, nano-specific testing protocols and high methodological variability in cross-border risk assessments.

3.5.2. Regulatory Implications for Albania

As an EU-candidate country, Albania is progressively harmonizing its domestic agricultural and environmental legislation with the European Union *acquis Communautaire*, with particular emphasis on chapters concerning food safety, veterinary and phytosanitary policy, and chemical management.

Consequently, the future adoption of nano-enabled agrochemicals in Albania remains strictly bound to the institutional transposition of EU

benchmarks, specifically Regulation (EC) No 1107/2009 and Regulation (EU) 2019/1009, alongside the formal adoption of EU nanomaterial criteria (European Commission, 2009b; 2019). Codifying unambiguous definitions, establishing standardized risk-assessment protocols, and enforcing transparent labelling mandates will be critical to achieving regulatory symmetry with European trading partners.

However, institutional capacity represents a primary operational bottleneck. The effective oversight of nano-agrochemicals demands specialized expertise in advanced fields such as nanotoxicology, environmental modelling, and high-resolution analytical chemistry (EFSA, 2011; ECHA, 2022). Currently, Albania faces structural constraints regarding state laboratory infrastructure, technical enforcement capabilities, and specialized human resources, which could severely limit the systematic tracking and monitoring of nanomaterials within regional agricultural systems (FAO, 2022).

Furthermore, Albania's agricultural sector is characterized by fragmented, smallholder-dominated farm structures that historically show limited access to advanced agricultural inputs and technological training. In transitional economies, these socio-economic matrices represent well-documented barriers to technology adoption (Popp *et al*. 2013; Parisi *et al*. 2015). This dual fragmentation complicates both the market deployment and the enforcement of nano-enabled agrochemicals, raising the risk of sub-optimal application, environmental over-loading, or non-compliance with statutory safety levels. Without dedicated agronomic extension services and targeted vocational training, smallholders may lack the specific skills needed to mitigate operational exposure risks (Nair *et al*. 2010; Prasad *et al*. 2017).

To circumvent these vulnerabilities, a phased, evidence-based integration strategy is highly recommended. Controlled pilot field trials and localized academic collaborations can yield essential empirical data regarding the field performance, mobility, and degradability of nano-agrochemicals under specific Mediterranean soil and climate dynamics (Ahmed *et al*. 2023; Kah *et al*. 2019). Simultaneously, targeted capacity-building initiatives for producers, agronomists, and inspectorate bodies are required to anchor safe-handling practices.

Fostering institutional linkages with centralized European bodies, such as EFSA and ECHA, would significantly accelerate Albania's regulatory transposition, providing direct access to validation protocols, peer-reviewed hazard data, and administrative best practices. Ultimately,

while nano-enabled agrochemicals offer strategic pathways to optimize input efficiency and regional sustainability, their deployment in Albania depends entirely on building parallel regulatory frameworks, robust analytical infrastructure, and localized risk-mitigation strategies.

Table 2. Integrated feasibility assessment of nano-enabled agrochemicals in Albania

Feasibility Dimension	Key Advantages	Key Limitations	Overall Feasibility
Agronomic	Improved nutrient-use efficiency; enhanced pest control	Variable performance under field conditions; limited long-term data	Moderate (site-specific)
Environmental	Reduced chemical losses; targeted delivery	Uncertain long-term impacts; nanoparticle persistence	Conditional
Economic	Reduced input use; potential yield increase	High initial cost; limited accessibility for smallholders	Moderate to low
Regulatory	Strong EU framework	Limited national capacity; lack of nano-specific guidelines	Low to moderate

**Source: Author's compilation*

3.6. Contextual Feasibility in Albania

3.6.1. Agro-Environmental Constraints and Variability

Albania is characterized by pronounced agro-environmental heterogeneity driven by the confluence of Mediterranean, Atlantic, and continental macroclimatic influences, combined with a highly complex topography (Kopali, 2012). This complex geographic matrix results in substantial spatial variation in temperature regimes, precipitation patterns, and seasonal microclimatic dynamics over relatively short physical distances, directly modulating crop phenology and the efficacy of applied inputs.

Edaphic conditions further amplify this systemic variability. Divergences in parent geology, historic land use, and active degradation processes have led to highly heterogeneous soil profiles. Soil degradation, particularly accelerated erosion, remains a primary structural constraint to regional agricultural productivity. Steep terrain gradients, high-intensity

rainfall events, and unsustainable land-use practices, such as historic deforestation and overgrazing, significantly accelerate topsoil loss and alter localized nutrient dynamics (Eugen Skura, 2017).

These baseline environmental stressors are critical when determining the environmental fate and performance of nano-enabled agrochemicals. Nanoparticle mobility, surface adsorption, and localized release kinetics are fundamentally governed by soil physicochemical characteristics, including pH gradients, soil organic matter (SOM) fractions, cation exchange capacity (CEC), and microbial community profiles (Navarro *et al*. 2008; Prasad *et al*. 2017).

From an analytical feasibility paradigm, this environmental heterogeneity exerts a dual effect:

Efficiency Gains: Engineered controlled-release and targeted-delivery systems can significantly optimize input-use efficiency (IUE) within agroecosystems prone to severe nutrient leaching, run-off, and spatial soil variations.

Performance Uncertainty: Conversely, this environmental variance introduces high unpredictability, as nanomaterial transport, bioavailability, and degradation rates may fluctuate dramatically across distinct agro-ecological zones (Nair *et al*. 2010).

Consequently, agronomic and environmental feasibility remains inherently site-specific, requiring rigorous, localized field validation before wide-scale technology deployment.

3.6.2. Structural And Management Constraints in Smallholder Systems

The agricultural landscape in Albania is heavily dominated by smallholder farming configurations, with typical holding sizes ranging from 1.0 to 1.2 hectares, which are frequently fragmented into multiple, non-contiguous plots (FAO, 2022). This highly fragmented structural baseline is historically correlated with low levels of mechanization, restricted capital access for advanced inputs, and high intra-regional variance in crop management practices. The farm-level adoption of frontier agricultural technologies remains fundamentally bound to capital liquidity, specialized technical knowledge, and the reach of institutional agronomic extension services (Parisi *et al*. 2015).

Within these structural parameters, nano-enabled agrochemicals present distinct operational advantages balanced against severe

implementation constraints. While their advanced delivery properties can technically maximize nutrient-use efficiency and plant protection efficacy (Fraceto *et al*. 2016; Kah *et al*. 2019), their optimized execution relies entirely on precise, calibrated application techniques and advanced user literacy.

Non-standardized, highly variable pesticide and fertilizer application methods remain prevalent within the domestic sector (FAO, 2022). Under uncalibrated application regimes, the intrinsic benefits of advanced nano-enabled systems, such as targeted delivery, cannot be fully realized. This operational disconnect indicates that the commercial feasibility of nano-agrochemicals in Albania is strictly contingent upon parallel, institutional investments in knowledge transfer, robust vocational advisory networks, and farm-level managerial capacity building.

3.6.3. Emerging Research and Innovation in Albania

Empirical evidence confirms that research and development (R&D) concerning nano-enabled agrochemicals in Albania is currently in its infancy. Domestic initiatives remain predominantly confined to ex-situ laboratory experiments or preliminary, small-scale trials evaluating nano-formulated essential micronutrients, specifically iron (Fe), molybdenum (Mo), and boron (B) (based on preliminary industry information and personal communication, 2026).

However, peer-reviewed, published data regarding long-term field-scale performance, real-world environmental fate, and microeconomic cost-benefit metrics under specific Albanian soil-climate dynamics remain virtually non-existent. This critical data gap severely constrains the capacity to conduct comprehensive risk and feasibility assessments, reflecting broader national challenges in translating fundamental benchtop chemistry into scalable, applied agronomic innovations.

The trajectory of emerging agricultural technologies is inextricably linked to national research infrastructure, institutional funding, and established academy-to-farm knowledge transmission pathways. In the Albanian context, nano-enabled agrochemicals remain positioned in a preliminary, speculative phase; their transition into viable commercial tools depends entirely on future multi-season field validation, dedicated institutional support, and structural alignment with regional agroecological management paradigms.

Current evidence indicates that research on nano-enabled agrochemicals in Albania is at an early stage. Existing activities are primarily experimental, including preliminary work on nano-formulated micronutrients such as iron (Fe), molybdenum (Mo), and boron (B) (based on preliminary industry information and personal communication, 2026).

However, published data on field-scale performance, environmental behaviour, and economic outcomes under Albanian conditions remain limited. This gap constrains the ability to assess real-world feasibility and reflects broader challenges associated with translating laboratory findings into applied agricultural systems.

The development of emerging agricultural technologies is closely associated with research capacity, infrastructure, and knowledge transfer mechanisms. In the Albanian context, current evidence suggests that nano-enabled agrochemicals remain in a preliminary evaluation phase, with feasibility dependent on future field validation, institutional support, and integration into existing agricultural systems.

4. DISCUSSIONS

This review demonstrates that the feasibility of nano-enabled agrochemicals in Albania is shaped by a complex interplay between technological performance, environmental kinetics, regulatory capacity, and farm-level structural conditions. Rather than representing a universally applicable solution, nanotechnology emerges as a highly context-dependent innovation whose real-world efficacy remains strictly contingent upon localized agro-ecological and socio-economic variables (Nair *et al*. 2010; Kah *et al*. 2019).

From a technological perspective, nano-enabled agrochemicals facilitate a paradigm shift toward precision-based agricultural systems by maximizing input-use efficiency and enabling site-directed delivery. However, their agronomic performance depends heavily on the alignment between specialized formulation architectures and regional agro-climatic profiles, underscoring the necessity of site-specific adaptation over uniform, homogenous deployment strategies.

Environmental considerations introduce a critical trade-off between macro-efficiency gains and long-term sustainability risks. While engineered controlled-release mechanisms can significantly mitigate immediate active ingredient losses, major uncertainties regarding nanoparticle environmental persistence, physical transformations, and

multi-trophic interactions within the soil–water–plant continuum remain unresolved bottlenecks (Navarro *et al*. 2008; Prasad *et al*. 2017). This emphasizes the necessity of adopting a precautionary risk-management approach supported by continuous environmental monitoring networks and robust lifecycle assessment frameworks.

Regulatory feasibility further conditions practical implementation outcomes. Although legislative alignment with the European Union *acquis communautaire* provides a structured governance blueprint, the global absence of harmonized, nano-specific risk assessment protocols limits operational clarity. In Albania, these systemic constraints are further intensified by localized institutional bottlenecks, including deficits in specialized nanotoxicological expertise and high-resolution analytical monitoring infrastructure required for effective market surveillance (Parisi *et al*. 2015). Consequently, regulatory readiness must be viewed not merely as a matter of legislative transposition, but as a function of practical institutional capacity.

At the farm level, the overwhelming dominance of smallholder systems heavily modulates socio-economic adoption potential. Highly fragmented landholdings, limited capital liquidity, and restricted access to advanced agronomic knowledge drastically reduce the probability of autonomous technology adoption. Empirical evidence suggests that the successful uptake of frontier agricultural inputs within smallholder configurations depends entirely on integrated institutional support mechanisms, including localized extension services, targeted financial incentives, and structured academy-to-farm knowledge transfer pathways (Fraceto *et al*. 2016).

Crucially, the current research landscape in Albania reflects a pronounced translational gap between ex-situ experimental studies and field-scale validation. While preliminary laboratory findings indicate clear isolated benefits, the total absence of long-term, real-world field data limits the empirical robustness of current feasibility frameworks. This translational gap represents a primary barrier to evidence-based commercialization, distinguishing holistic multi-dimensional feasibility assessments from purely fundamental technological evaluations.

In synthesis, the viability of nano-enabled agrochemicals in Albania must be conceptualized as a system-dependent phenomenon emerging from the reciprocal interactions of technological, environmental, regulatory, and socio-economic domains. Rather than functioning in isolation, these four axes operate as an interconnected matrix that

determines real-world applicability, highlighting the need for an integrated, systems-based evaluation framework that positions agricultural innovations within their broader institutional and environmental contexts.

5. CONCLUSIONS

This study provides a structured synthesis of current empirical evidence regarding the feasibility of nano-enabled agrochemicals—specifically nanopesticides and nanofertilizers—within the framework of sustainable agriculture. The analysis demonstrates that these advanced technologies offer clear, localized advantages in maximizing input-use efficiency, optimizing targeted crop protection, and reducing diffuse environmental losses compared to conventional, unformulated agrochemical systems. However, this theoretical potential is not consistently realized across divergent agro-ecological and socio-economic matrices.

The findings indicate that feasibility is inherently conditional, governed by the dynamic intersection of agronomic performance, environmental fate, microeconomic viability, and institutional regulatory capacity. While engineered nanocarriers and responsive delivery systems represent substantial technological milestones, their field-level effectiveness remains highly variable, and critical uncertainties persist regarding their multi-season environmental persistence, ecotoxicological impacts on functional soil microbiomes, and systemic trophic-level responses.

Within the specific context of Albania, these baseline challenges are significantly amplified by profound agro-environmental heterogeneity, fragmented smallholder farm structures, and localized constraints in regulatory enforcement and laboratory infrastructure. Consequently, the direct, uncalibrated transfer of globally reported agronomic benefits to the domestic sector cannot be assumed. Instead, the strategic deployment of nano-enabled agrochemicals requires precise tailoring to local edaphic and climatic conditions, supported by rigorous empirical field validation and context-specific risk modelling.

From a strategic perspective, nano-enabled inputs should not be pursued as standalone, silver-bullet solutions, but rather integrated as complementary tools within broader, sustainable agricultural frameworks, such as Integrated Pest Management (IPM) and conservation agriculture. Their responsible, safe implementation depends strictly on the parallel

maturation of domestic regulatory frameworks, targeted investments in state analytical infrastructure, and the establishment of monitoring protocols capable of tracking nanoscale-specific environmental risks.

A phased, evidence-based integration trajectory is therefore essential for Albania. National priority must be assigned to long-term, field-scale validation trials, continuous environmental fate monitoring, and microeconomic cost–benefit assessments under real-world farming configurations. Strengthening cross-sectoral collaborations between academic research institutions, state regulatory bodies, and agricultural stakeholder networks will be critical to reduce current scientific uncertainties and supporting informed, data-driven policymaking. Ultimately, nano-enabled agrochemicals represent a highly promising but transitional innovation; their long-term role in sustainable agriculture will be determined by the precision with which scientific evidence, regulatory governance, and practical farm-level execution can be harmonized to ensure parallel agronomic profitability and ecotoxicological safety.

Ethics. This research did not involve human participants, animal subjects, or any endangered biological material requiring specific ethical clearance or institutional approval.

Author Contributions. M.C. and F.G. conception and study design; F.G.: literature review, the data collection, and original draft; O.C., K.H., N.I., K.X.: data organizing, literature screening, and critical structural revision of the manuscript, M.C.: study supervision, project run, and acquired funding.

All authors have read and approved the final version of the manuscript.

Data sources. Tables 1 and 2, as well as Figure 1, are original and were prepared by the authors. Figure 2 was adapted from Shekhar *et al.* (2021), and the source has been cited accordingly in the text.

Funding. The authors gratefully acknowledge the financial support of the NanoAlb/NanoBalkan project, *"Advancing Agriculture through Nanotechnology-Supported Diagnosis and Management of Plant Pathogens (ANA_DIAMA)"*, funded by the Academy of Sciences of Albania, within the framework of which this study was conducted.

Conflict of Interest. The authors declare no conflict of interest regarding the publication of this manuscript.

Acknowledgments. The authors gratefully acknowledge the Academy of Sciences of Albania and NanoAlb/NanoBalkan – Regional

Center of Nanotechnology for providing institutional support and a collaborative scientific environment that facilitated this work.

REFERENCES:

Abdalla Z, El-Sawy S, El-Bassiony AE-M, Jun H, Shedeed S, Okasha A, Bayoumi Y, El-Ramady H, Prokisch J. 2022. Smart fertilizers vs. nano-fertilizers: A pictorial overview. *Environment, Biodiversity and Soil Security*, **6(2022):** 191–204. https://doi.org/10.21608/jenvbs. 2022.153990.1184.

Agostini A, Mondragón L, Coll C, Aznar E, Marcos MD, Martínez-Máñez R, Sancenón F, Soto J, Pérez-Payá E, Amorós P. 2012. Dual enzyme-triggered controlled release on capped nanometric silica mesoporous Supports. *Chemistry Open*, **1(1):** 17–20. https://doi.org/10.1002/open.201200003.

Ahmed T, Noman M, Gardea-Torresdey JL, White JC, Li B. 2023. Dynamic interplay between nano-enabled agrochemicals and the plant-associated microbiome. *Trends in Plant Science*, **28 (11):** 1310–1325. https://doi.org/10.1016/j.tplants.2023.06.001.

Akchaya K, Parasuraman P, Pandian K, Vijayakumar S, Thirukumaran K, Mustaffa MRAF, Rajpoot SK, Choudhary AK. 2025. Boosting resource use efficiency, soil fertility, food security, ecosystem services, and climate resilience with legume intercropping: a review. *Frontiers in Sustainable Food Systems*, **9**. https://doi.org/10.3389/fsufs.2025.1527256.

Al-Shammary AAG, Al-Shihmani LSS, Fernández-Gálvez J, Caballero-Calvo A. 2024. Optimizing sustainable agriculture: A comprehensive review of agronomic practices and their impacts on soil attributes. *Journal of Environmental Management*, **364**, 121487. https://doi.org/10.1016/j.jenvman. 2024.121487.

Baker S, Volova T, Prudnikova SV, Satish S, Prasad MNN. 2017. Nanoagroparticles emerging trends and future prospect in modern agriculture system. *Environmental Toxicology and Pharmacology*, **53**: 10–17. https://doi.org/10.1016/j.etap.2017.04.012.

Begum P, Ikhtiari R, Fugetsu B. 2011. Graphene phytotoxicity in the seedling stage of cabbage, tomato, red spinach, and lettuce. *Carbon*, **49(12):** 3907–3919. https://doi.org/10.1016/j.carbon. 2011.05.029.

Bist DR, Chapagaee P, Kunwar A, Pant BD, Khatri L, Mandal A. 2025. Nanotechnology in Agriculture: A review of innovations in

crop protection and food security. *Advances in Agriculture*, **2025**(1). https://doi.org/10.1155/aia/8892001.

Bombo AB, Pereira AES, Lusa MG, de Medeiros Oliveir E, de Oliveira JL, Campos EVR, de Jesus MB, Oliveira HC, Fraceto LF, Mayer JLS. 2019. A mechanistic view of interactions of a nanoherbicide with target organism. *Journal of Agricultural and Food Chemistry*, **67(16):** 4453–4462. https://doi.org/10.1021/acs.jafc.9b00806.

Carpenter SR, Stanley EH, Vander Zanden MJ. 2011. State of the world's freshwater ecosystems: physical, chemical, and biological changes. *Annual Review of Environment and Resources*, **36(1):** 75–99. https://doi.org/10.1146/annurev-environ-021810-094524.

Chaud M, Souto EB, Zielinska A, Severino P, Batain F, Oliveira-Junior J, Alves T. 2021. Nanopesticides in Agriculture: Benefits and challenge in agricultural productivity, toxicological risks to human health and environment. *Toxics*, **9(6):** 131. https://doi.org/10.3390/toxics9060131

Chen H, Yada R. 2011. Nanotechnologies in agriculture: New tools for sustainable development. *Trends in Food Science & Technology*, **22 (11):** 585–594. https://doi.org/10.1016/j.tifs.2011.09.004.

DeRosa MC, Monreal C, Schnitzer M, Walsh R, Sultan Y. 2010. Nanotechnology in fertilizers. *Nature Nanotechnology*, **5(2):** 91–91. https://doi.org/10.1038/nnano.2010.2.

Devi PI, Manjula M, Bhavani RV. 2022. Agrochemicals, environment, and human health. *Annual Review of Environment and Resources*, **47(1):** 399–421. https://doi.org/10.1146/annurev-environ-120920-111015.

Du J, Hu X, Mu L, Ouyang S, Ren C, Du Y, Zhou Q. 2015. Root exudates as natural ligands that alter the properties of graphene oxide and environmental implications thereof. *RSC Advances*, **5(23):** 17615–17622. https://doi.org/10.1039/C4RA16340K.

Duro JA, Lauk C, Kastner T, Erb K-H, Haberl H. 2020. Global inequalities in food consumption, cropland demand and land-use efficiency: A decomposition analysis. *Global Environmental Change*, **64**, 102124. https://doi.org/10.1016/j.gloenvcha.2020.102124.

EFSA. 2011. Guidance on the risk assessment of the application of nanoscience and nanotechnologies in the food and feed chain. *EFSA Journal*, **9**(5). https://doi.org/10.2903/j.efsa.2011.2140

Skura E, Kristo I. 2017. Modeling of rainfall factor in soil erosion risk in Albania. *Albanian Journal of Agricultural Sciences*, **16(3):** 127–132. https://drive.google.com/file/d/0B_i7_HlsPT6HNDZPSl9lWHl6T2M/view?pli=1&resourcekey=0-U5nXrGgOGj9-aQ3S0GhwTg.

European Chemicals Agency (ECHA). 2022. Guidance on information requirements and chemical safety assessment: Appendix R7-1 for nanomaterials applicable to Chapter R7a endpoint specific guidance: Version 4.0. December 2022. ECHA. https://op.europa.eu/en/publication-detail/-/publication/3c73bc0e-8caa-11ed-999b-01aa75ed71a1/language-en

European Commission (EC). 2004. Regulation - 1935/2004 - EN - EUR-Lex on materials and articles intended to come into contact with food. https://eur-lex.europa.eu/legal-content/EN/TXT/?uri=CELEX:32004R1935.

European Commission (EC). 2005. Regulation - 396/2005 - EN - EUR-Lex on maximum residue levels of pesticides in or on food and feed. https://eur-lex.europa.eu/legal-content/EN/TXT/?uri=CELEX:32005R0396.

European Commission (EC). 2009a. Regulation - 767/2009 - EN - EUR-Lex on the placing on the market and use of feed. https://eur-lex.europa.eu/legal-content/EN/TXT/?uri=CELEX:32009R0767.

European Commission (EC). 2009b. Regulation - 1107/2009 - EN - EUR-Lex concerning the placing of plant protection products on the market. https://eur-lex.europa.eu/legal-content/EN/TXT/?uri=CELEX:32009R1107.

European Commission (EC). 2012. Regulation (EU) No 528/2012 concerning the making available on the market and use of biocidal products. https://eur-lex.europa.eu/legalcontent/EN/TXT/PDF/?uri=CELEX:32012R0528.

European Commission (EC). 2019. Regulation - 2019/1009 - EN - EUR-Lex. https://eur-lex.europa.eu/legal-content/EN/TXT/?uri=CELEX:32019R1009

European Commission (EC). (2022). Commission recommendation of 10 June 2022 on the definition of nanomaterial (2022/C 229/01). https://eur-lex.europa.eu/legal-content/EN/TXT/PDF/?uri=CELEX:32022H0614(01

FAO. (2022). Analysis of agriculture and rural development policy in Albania. FAO.

https://www.researchgate.net/publication/369092808_Analysis_of_Agriculture_and_Rural_Development_Policy_in_Albania

Fatima F, Hashim A, Anees S. 2021. Efficacy of nanoparticles as nanofertilizer production: a review. *Environmental Science and Pollution Research*, **28 (2):** 1292–1303. https://doi.org/10.1007/s11356-020-11218-9

Fraceto LF, Grillo R, de Medeiros GA, Scognamiglio V, Rea G, Bartolucci C. 2016. Nanotechnology in agriculture: Which innovation potential does it have? *Frontiers in Environmental Science*, **4**. https://doi.org/10.3389/fenvs.2016.00020.

Gaur M, Misra C, Yadav AB, Swaroop S, Maolmhuaidh FÓ, Bechelany M, Barhoum A. 2021. Biomedical applications of carbon nanomaterials: Fullerenes, quantum dots, nanotubes, nanofibers, and graphene. *Materials*, **14(20)**: 5978. https://doi.org/10.3390/ma14205978.

Ghormade V, Deshpande MV, Paknikar KM. 2011. Perspectives for nano-biotechnology enabled protection and nutrition of plants. *Biotechnology Advances*, **29(6):** 792–803. https://doi.org/10.1016/j.biotechadv.2011.06.007.

Gupta A, Saharan BS, Sadh PK, Duhan JS. 2024. Green to green: harnessing bio-fertilizers for sustainable pulse production and food security. *Discover Plants*, **1(1):** 73. https://doi.org/10.1007/s44372-024-00079-y.

Hardy A, Benford D, Halldorsson T, Jeger MJ, Knutsen HK, More, S., Naegeli, H., Noteborn, H., Ockleford C, Ricci A, Rychen G, Schlatter JR, Silano V, Solecki R, Turck D, Younes M, Chaudhry Q, Cubadda F, Gott D, Mortensen A. 2018. Guidance on risk assessment of the application of nanoscience and nanotechnologies in the food and feed chain: Part 1, human and animal health. *EFSA Journal*, **16(7).** https://doi.org/10.2903/j.efsa.2018.5327.

Hegde K, Brar SK, Verma M, Surampalli, RY. 2016. Current understandings of toxicity, risks and regulations of engineered nanoparticles with respect to environmental microorganisms. *Nanotechnology for Environmental Engineering*, **1(1): 5.** https://doi.org/10.1007/s41204-016-0005-4

Kah M, Hofmann T. 2014. Nanopesticide research: Current trends and future priorities. *Environment International*, **63**, 224–235. https://doi.org/10.1016/j.envint.2013.11.015.

Kah M, Beulke S, Tiede K, Hofmann T. 2013. Nanopesticides: State of knowledge, environmental fate, and exposure modeling. *Critical Reviews in Environmental Science and Technology*, **43(16):** 1823–1867. https://doi.org/10.1080/10643389.2012.671750.

Kah M, Kookana RS, Gogos A, Bucheli TD. 2018. A critical evaluation of nanopesticides and nanofertilizers against their conventional analogues. *Nature Nanotechnology*, **13(8):** 677–684. https://doi.org/10.1038/s41565-018-0131-1.

Kah M, Tufenkji N, White JC. 2019. Nano-enabled strategies to enhance crop nutrition and protection. *Nature Nanotechnology*, **14(6):** 532–540. https://doi.org/10.1038/s41565-019-0439-5.

Kopali A, Peculi V, Teqja Z, Rota E. 2012. A study on agroclimatic characterization of Albanian territory. *Albanian Journal of Agricultural Sciences*, **11(3):** 173–177. 10.13140/RG.2.1.2527.9200

Laxmi V, Singhvi N, Ahmad N, Sinha S, Negi T, Gupta V, Mubashshir M, Ahmad A, Sharma S. (2023). Emerging field of nanotechnology in environment. *Indian Journal of Microbiology*, **63(3):** 244–252. https://doi.org/10.1007/s12088-023-01092-7.

Lee DY, Khatun Z, Lee J-H, Lee Y, In I. 2011. Blood-compatible graphene/heparin conjugate through noncovalent chemistry. *Biomacromolecules*, **12(2):** 336–341. https://doi.org/10.1021/bm101031a.

Liu R, Lal R. 2015. Potentials of engineered nanoparticles as fertilizers for increasing agronomic productions. *Science of The Total Environment*, **514**: 131–139. https://doi.org/10.1016/j.scitotenv.2015.01.104.

Lowry GV, Gregory KB, Apte SC, Lead JR. 2012. Transformations of nanomaterials in the environment. *Environmental Science & Technology*, **46(13):** 6893–6899. https://doi.org/10.1021/es300839e.

Manjunatha SB, Biradar DP, Aladakatti YR. 2016. Nanotechnology and its applications in agriculture: A review. *Journal of Farm Sciences*, **29(1):** 1-13. https://www.researchgate.net/publication/303665019_Nanotechnology_and_its_applications_in_agriculture_A_review

Mitra B, Chowdhury AR, Dey P, Hazra KK, Sinha AK, Hossain A, Meena RS. 2021. Use of agrochemicals in agriculture: Alarming issues and solutions. In *Input Use Efficiency for Food and*

Environmental Security (pp. 85–122). Springer Nature Singapore. https://doi.org/10.1007/978-981-16-5199-1_4.

Nair R, Varghese SH, Nair BG, Maekawa T, Yoshida Y, Kumar DS. 2010. Nanoparticulate material delivery to plants. *Plant Science*, **179(3):** 154–163. https://doi.org/10.1016/j.plantsci.2010.04.012

Navarro E, Baun A, Behra R, Hartmann NB, Filser J, Miao A-J, Quigg A, Santschi PH, Sigg L. 2008. Environmental behavior and ecotoxicity of engineered nanoparticles to algae, plants, and fungi. *Ecotoxicology*, **17(5):** 372–386. https://doi.org/10.1007/s10646-008-0214-0.

Parisi C, Vigani M, Rodríguez-Cerezo E. 2015. Agricultural nanotechnologies: What are the current possibilities? *Nano Today*, **10(2):** 124–127. https://doi.org/10.1016/j.nantod.2014.09.009.

Parven A, Meftaul IM, Venkateswarlu K, Megharaj M. 2025. Herbicides in modern sustainable agriculture: environmental fate, ecological implications, and human health concerns. *International Journal of Environmental Science and Technology*, **22(2):** 1181–1202. https://doi.org/10.1007/s13762-024-05818-y.

Popp J, Pető, K, Nagy J. 2013. Pesticide productivity and food security. A review. *Agronomy for Sustainable Development*, **33(1):** 243–255. https://doi.org/10.1007/s13593-012-0105-x.

Prasad R, Bhattacharyya A, Nguyen QD. 2017. Nanotechnology in Sustainable Agriculture: Recent Developments, Challenges, and Perspectives. *Frontiers in Microbiology*, **8**. https://doi.org/10.3389/fmicb.2017.01014.

Raliya R, Nair R, Chavalmane S, Wang, W-N, Biswas P. 2015. Mechanistic evaluation of translocation and physiological impact of titanium dioxide and zinc oxide nanoparticles on the tomato (*Solanum lycopersicum* L.) plant. *Metallomics*, **7(12):** 1584–1594. https://doi.org/10.1039/C5MT00168D.

Saito K, Six J, Komatsu S, Snapp S, Rosenstock T, Arouna A, Cole S, Taulya G, Vanlauwe B. 2021. Agronomic gain: Definition, approach, and application. *Field Crops Research*, **270**, 108193. https://doi.org/10.1016/j.fcr.2021.108193.

Saraiva R, Ferreira, Q, Rodrigues GC, Oliveira M. 2025. Graphene oxide and its viability as a constituent in nanofertilizers. *Frontiers in Nanotechnology*, **7**. https://doi.org/10.3389/fnano.2025.1580066.

Servin A D, White JC. 2016. Nanotechnology in agriculture: Next steps for understanding engineered nanoparticle exposure and risk. *NanoImpact*, **1**, 9–12. https://doi.org/10.1016/j.impact.2015.12.002

Servin A, Elmer W, Mukherjee A, De la Torre-Roche R, Hamdi H, White JC, Bindraban P, Dimkpa C. 2015. A review of the use of engineered nanomaterials to suppress plant disease and enhance crop yield. *Journal of Nanoparticle Research*, **17(2):** 92. https://doi.org/10.1007/s11051-015-2907-7.

Sharma S, Jaiswal S, Duffy B, Jaiswal AK. 2019. Nanostructured materials for food applications: Spectroscopy, microscopy and physical properties. *Bioengineering*, **6(1):** 26. https://doi.org/10.3390/bioengineering6010026

Shekhar S, Sharma S, Kumar A, Taneja A, Sharma B. 2021. The framework of nanopesticides: a paradigm in biodiversity. *Materials Advances*, **2(20):** 6569–6588. https://doi.org/10.1039/D1MA00329A

Su Y, Zhou X, Meng, H., Xia, T., Liu, H., Rolshausen, P., Roper, C., McLean, J. E., Zhang, Y., Keller AA, Jassby D. 2022. Cost–benefit analysis of nanofertilizers and nanopesticides emphasizes the need to improve the efficiency of nanoformulations for widescale adoption. *Nature Food*, **3(12):** 1020–1030. https://doi.org/10.1038/s43016-022-00647-z

Tourinho PS, van Gestel CAM, Lofts S, Svendsen C, Soares AMVM, Loureiro S. 2012. Metal-based nanoparticles in soil: Fate, behavior, and effects on soil invertebrates. *Environmental Toxicology and Chemistry*, **31**(8), 1679–1692. https://doi.org/10.1002/etc.1880.

Wu C, Shen X, Feng W, Li P, Chen Y. 2025. Agricultural nanotechnology. *Coordination Chemistry Reviews*, **543**: 216906. 10.1016/j.ccr.2025.216906.

Zielińska A, Costa B, Ferreira MV, Miguéis D, Louros JMS, Durazzo A, Lucarini M, Eder PV, Chaud M, Morsink M, Willemen N, Severino P, Santini A, Souto EB. 2020. Nanotoxicology and Nanosafety: Safety-by-Design and Testing at a Glance. *International Journal of Environmental Research and Public Health*, **17(13):** 4657. https://doi.org/10.3390/ijerph17134657.

Zhou W, Li M, Achal V. 2025. A comprehensive review on environmental and human health impacts of chemical pesticide usage. *Emerging Contaminants*, **11(1):** 100410. https://doi.org/10.1016/j.emcon.2024.100410.

WHEN PRESSURES ACCUMULATE: UNDERSTANDING DAIRY FARM DECLINE IN CENTRAL ALBANIA

Anila BOSHNJAKU[1], Engjell SKRELI [2], Fidel GJURGJI[3]

[1,2]Department of Economics and Rural Development Policies, Faculty of Economics and Agribusiness, Agricultural University of Tirana, Albania
[3]Department of Applied Integrated Studies, Faculty of Professional Studies, University, Aleksander Moisiu, Durres, Albania

Author for correspondence: aboshnjaku@ubt.edu.al

AB, 0009-0004-1159-4323 ; ES, 0000-0002-7556-763X; FGj, 0009-0006-4899-6291

ABSTRACT

Dairy farming remains a vital livelihood for rural households in Albania; however, the sector faces increasing sustainability challenges. This study investigates the factors shaping dairy farm viability in central Albania using a grounded theory approach. Data were collected through three focus group discussions with dairy farmers in Lushnja, Berati, and Tirana and analyzed using open, axial, and selective coding supported by constant comparison. The findings indicate that sustainability is undermined by interconnected pressures, including input insecurity, rising feed costs, inadequate veterinary and advisory services, infrastructure deficiencies, bureaucratic constrains, market instability, compliance risks related to quality standards, and labor shortages. These pressures accumulate over time, progressively constraining farmers' adaptive capacity. The study identifies *accumulated pressure and trajectory toward farm exit* as the central analytical constructs, conceptualizing farm exit as a gradual outcome of prolonged structural vulnerability rather than an isolated economic decision.

Keywords: dairy farming sustainability, farmer exit, grounded theory
Relevant JEL Codes: Q12, Q18, O13

Publisher: Academy of Sciences of Albania
License: Creative Commons Attribution License (CC BY 4.0)
Citation: Boshnjaku A, Skreli E, Gjurgji F. 2026. When pressures accumulate: Understanding dairy farm decline in central Albania. *Albanian Journal of Natural and Technical Sciences* (AJNTS), **2 (30),**
Journal URL: https://journals-akad.gov.al/magazines/1
Classification: Research
Subject Category Applied / Social Sciences subject areas: Agricultural Economics & Rural Development

1. INTRODUCTION

Dairy farming plays a central role in Albania's agricultural economy, providing income and employment for a substantial proportion of rural households and contributing significantly to national food security. Despite its importance, the sector has undergone profound structural change over the past two decades. Official statistics report a marked decline in livestock numbers, reflecting increasing vulnerability within the production system. Between 2000 and 2023, the number of cows decreased by 48%, sheep by 31%, and goats by 36%. This contraction has intensified in recent years, with the period 2019–2023 alone recording declines of 27% for cows, 20% for sheep, and 24% for goats (INSTAT, 2024). These trends raise serious concerns regarding the long-term sustainability of dairy farming in Albania.

The observed decline is associated with persistent multifaceted challenges faced by dairy farmers. Existing research has largely focused on macroeconomic trends, offering limited insight into farmers' lived experiences. While agricultural challenges are embedded within interconnected systems of production and governance (Gereffi *et al*. 2005), these dynamics remain insufficiently explored in central Albania. To better understand these complex interactions from the perspective of those directly affected, the central research question guiding this analysis is: *What factors influence the sustainability of dairy farming in central Albania, and how do farmers navigate these challenges?* In addressing this question, we introduce *accumulated pressure* as a processual construct that differs from traditional frameworks. Unlike *vulnerability*, which is often conceptualized a static condition, or *risk*, which typically emphasizes exposure to discrete events, accumulated pressure captures the temporal and cumulative intensification of multiple constraints. It extends beyond the 'cost-price squeeze' framework by emphasizing how institutional barriers and market instability interact to progressively narrow a farmer's adaptive space. Consequently, farm exit is reframed as a gradual trajectory emerging from interlocking pressures rather than a response to a single shock

To explore these complexities, a *grounded theory approach* (Strauss and Corbin, 1998) is employed as the guiding methodology. This inductive strategy allows theoretical explanations to emerge directly from empirical data, ensuring that the findings remain closely grounded in the farmers' narratives without imposing predefined conceptual models. Throughout

the analytical process, constant comparison was applied during open, axial, and selective coding to refine categories across three central regions—Lushnja, Berati, and Tirana.

By conceptualizing sectoral decline through the lens of accumulated pressure, this paper offers a data-driven explanation of agricultural contraction in transition contexts and advances a process-oriented understanding of vulnerability. The study contributes theoretically by developing an inductively grounded explanation of dairy farm decline centered on accumulated structural strain. Rather than treating constraints as isolated variables, the analysis demonstrates how economic, institutional, and market pressures interact and intensify over time, progressively eroding adaptive capacity. Farm exit is thus conceptualized not as a single decision triggered by a single shock, but as the outcome of a prolonged trajectory shaped by interlocking pressures. While grounded in farmers' narratives, the proposed framework also refines broader institutional and value-chain perspectives.

The remainder of the paper is organized as follows. Section 2 outlines the research design and grounded theory methodology. Section 3 presents the results of the coding process. Section 4 discusses the findings in relation to existing literature and their implications, and Section 5 concludes.

2. MATERIAL AND METHODS

2.1. Data

Data for this study were collected through focus group discussions with dairy farmers in the Albanian regions of Berati, Lushnja, and Tirana. The focus group meetings were organized in the framework of the EU funded project, *Farm to Fork Academy for Green Western Balkans*, implemented by Albanian Network for Rural Development. Prior to the data collection, a semi-structured discussion guide was developed to ensure thematic consistency across locations while retaining sufficient flexibility to explore participants' experiences in depth. The guide covered key domains, including access to production resources, feed procurement, veterinary and advisory services, water availability, farmer collaboration, market access, and government support mechanisms. Approximately 40 participants were involved in the study, primarily small-scale farmers, alongside representatives of medium- and large-scale operations to capture structural variation within the sector. To ensure the inclusion of diverse and

potentially underrepresented perspectives, the sample comprised approximately 20% women and 10% young farmers. This composition was intended to reflect demographic diversity while foregrounding groups often facing additional constraints withing agricultural systems.

Three focus group discussions were conducted, each consisting of a heterogeneous mix of dairy producers in order to capture variation in production conditions, market integration, and resource endowments. Each session lasted approximately 90 minutes and was facilitated by the research team using open-ended questions and follow-up probes to stimulate interaction, and the construction of meaning among participants. All discussions were audio-recorded with participants' informed consent and subsequently transcribed verbatim. The transcripts constituted the primary qualitative dataset used for coding and analysis.

Theoretical saturation was reached after the third focus group. Analysis of the third session generated only marginally new insight that the principal themes and categories had already been substantially developed during the first two discussions. The data from the final session primarily reinforced existing categories had already been substantially developed during the first two discussions. The data from the final session primarily reinforced existing categories and added analytical depth rather than introducing novel conceptual dimensions. Accordingly, it was determined that additional focus groups were unnecessary, as further data collection was unlikely to yield significant theoretical advancement. Saturation was thus defined as the point at which new data no longer contributed substantively to category development or to the refinement of emerging theoretical relationships.

2.2. Grounded Theory Approach

This study employed a grounded theory methodology to explore the challenges faced by dairy farmers and to develop a theoretically grounded explanation understanding of the factors influencing dairy farming sustainability. Grounded theory is an inductive methodological approach designed to generate theory directly from empirical data rather than to test pre-existing hypotheses. The analytical process followed the three-stage coding procedure proposed by Strauss and Corbin (1998): open coding, axial coding, and selective coding. Throughout all stages, the constant comparative method was systematically applied to ensure that emerging

categories remained closely anchored in the data and were progressively refined through iterative analysis.

Open Coding

The first stage of the analysis involved open coding. During this phase, the data were disaggregated into discrete units of meaning and labeled with conceptual codes that captured their substantive content. Examples of open codes included *feed procurement challenges*, *water scarcity*, and *subsidy delays* (a detailed presentation of open codes in the Results section). Each relevant of text was examined line by line and assigned a code representing its core meaning. Codes were derived both from participants' verbatim expressions and from analytically interpreted segments reflecting underlying processes or conditions. Constant comparison was applied throughout this stage by systematically comparing newly generated codes with previously identified ones. This iterative procedure facilitated conceptual clarification, reduced redundancy, and supported the development of a comprehensive and internally coherent set of open codes.

Axial Coding

Following the development of open codes, the analysis progressed to axial coding, in accordance with the paradigm model proposed by Strauss and Corbin. This stage focused on identifying relationships among open codes and organizing them into higher order categories and subcategories. Axial coding aimed to specify conditions, interactions, and consequences associated with each emerging category. In line with the paradigm model, categories were examined in relation to: casual conditions, contextual conditions, intervening conditions, action/interaction strategies, and consequences. For example, the axial category *Access to Resources* incorporated casual conditions such as feed procurement constrains, contextual conditions including geographical isolation, and consequences such as reduced milk productivity due to limited input availability. The constant comparative method was again employed to refine relationships between categories and to ensure analytical consistency between open and axial levels of coding.

Selective Coding

The final stage of analysis involved selective coding, as outlined by Strauss and Corbin (1998). At this stage, all axial categories were systematically evaluated to identify the core category — that is, the category with the greatest integrative and explanatory power.

Through iterative comparison and theoretical reflection, one central category was identified because it most effectively integrated the various causal conditions, contextual influences, action strategies, and consequences into a coherent explanatory process. This core category provided the organizing framework for the emerging theory and linked the subordinate categories into a unified conceptual structure.

The process of selective coding ensured theoretical integration and parsimony, while maintaining fidelity to the empirical data. The resulting theoretical explanation thus remains grounded in participants' experiences and reflects the dynamic and process-oriented nature of sustainability challenges within the dairy farming sector.

Constant Comparison Approach

Throughout all stages of data analysis, the constant comparative method was systematically applied. This analytical procedure involves continuously comparing newly coded data with previously coded segments in order to refine conceptual categories, clarify their properties and dimensions, and specify relationships among them. Rather than treating coding as a linear process, constant comparison operates iteratively across and withing transcripts. Incidents were compared with other incidents, codes with codes, and categories with emerging categories. This recursive examination enabled the identification of similarities, variations, and patterns withing the data, thereby strengthening conceptual coherence and reducing analytical redundancy.

3. RESULTS

3.1 Open Coding: Empirically Grounded Concepts

The open coding phase generated a wide range of conceptually rich codes that captured dairy farmers lived experiences, perceived constraints, and everyday coping strategies. Using constant comparison across the three consultation meetings, recurring patterns were identified while preserving contextual variation. Given space limitations, this section

presents selected open codes, illustrated with representative quotes that best exemplify the underlying concepts.

One of the most salient open codes was *feed purchase challenges*, which farmers described as both a structural and seasonal constraint. Participants emphasized their dependence on purchased feed due to limited land productivity and lack of irrigation, particularly during winter months. Feed was consistently framed as the single largest cost item in dairy production:

"...we are forced to buy all the feed; everything we give to the cows, we buy it" (*"...të gjithë ushqimin e blejmë, çfarëdo që u japim lopëve..."*)

Closely linked to feed issues, the open code *economic struggles* permeated nearly all narratives. Farmers described low and unstable incomes, rising input costs, and an inability to cover basic production expenses. These struggles were not depicted as temporary shocks but as persistent conditions shaping everyday decision-making:

"We cannot cover the costs anymore; this is why farms are shutting down" (*"Nuk arrijmë të mbulojmë shpenzimet, prandaj fermat po mbyllen"*)

Economic pressure was frequently associated with the open code risk of farm closure, particularly among small-scale producers. Several participants explicitly articulated dairy farming as an increasingly unsustainable livelihood:

"If this continues like this, we won't be able to keep the farms" (*"Nëse vazhdojmë kështu, nuk do të mund t'i mbajmë fermat"*)

Another recurrent open code concerned *veterinary care and animal health constraints*. Farmers reported irregular access to veterinary services, shortages of medicines, and delayed interventions, especially in remote areas. Veterinary services were often described as symbolic rather than functional:

"Before, there was veterinary support; now it exists only on paper" (*"Më parë kishte mbeshtetje veterinare, tani është vetëm si figurë"*)

These limitations were perceived as directly affecting milk quality and livestock survival, thereby reinforcing economic vulnerability.

Water scarcity emerged as a distinct and context-specific open code, particularly in upland and peri-urban areas. Participants highlighted the lack of water for irrigation, hygiene, and animal consumption, often linking water shortages to increased dependence on purchased feed:

"The land has no water, so we buy feed instead of producing it" (*"Tokat janë pa ujë, prandaj detyrohemi ta blejmë ushqimin"*)

Market-related challenges were captured under the open code market instability, encompassing price volatility, lack of transparency, and weak bargaining power. Farmers emphasized their inability to plan production or investments due to unpredictable prices:

"Prices change all the time; today it's one price, tomorrow another" (*"Çmimet ndryshojnë vazhdimisht, sot një, nesër tjetër"*)

As a response to these market constraints, many participants reported engaging in informal business practices, including selling milk without invoices or formal contracts. Informality was framed less as a preference and more as a necessity imposed by market and regulatory barriers:

"Many times we sell without invoices because otherwise we cannot sell at all" (*"Shpesh shesim pa fatura, sepse ndryshe nuk shesim dot"*)

Another prominent open code was limited government support, which farmers consistently described as insufficient, fragmented, or poorly targeted. While some participants acknowledged small per-head subsidies, these were widely perceived as inadequate relative to production costs:

"The state helps us a little, but it doesn't really change anything" (*"Shteti na ndihmon pak, por nuk na zgjidh asgjë"*)

This perception was closely connected to bureaucratic and regulatory barriers, including difficulties in accessing support schemes, obtaining permits, or investing in infrastructure such as barns:

"The state does not help us because everything gets stuck in bureaucracy" (*"Shteti nuk na ndihmon sepse gjithçka ngec në burokraci"*)

Finally, the open code *collective action and cooperation* captured both aspirations and frustrations related to farmer organization. While participants widely recognized the potential benefits of cooperatives, many described fragmentation and lack of institutional facilitation:

"We know we should unite, but everyone is left on their own" (*"E dimë që duhet të bashkohemi, por secili mbetet vetëm"*)

In sum, the open coding phase revealed a dense set of interrelated challenges, where economic pressure, resource scarcity, institutional gaps, lack of burgeoning power and informal practices coexisted and mutually reinforced one another. These empirically grounded open codes provided the analytical basis for axial coding, where relationships among categories were systematically examined.

3.2. Axial coding

Structural input insecurity and cost–price squeeze

Causal conditions underlying this phenomenon consist of persistent dependence on purchased feed, rising and volatile input prices, and limited on-farm fodder production capacity, further intensified by water scarcity. Collectively, these factors expose dairy farms to external market fluctuations and reduce their cost to control autonomy. This phenomenon unfolds within a context characterized by small-scale production, strong seasonal variation, particularly winter feed shortages, and constrained household purchasing power. Intervening conditions such as informal supplier credit arrangements, absence of formal contracts, and restricted access to financial services shape farmers' capacity to absorb cost shocks. In response, farmers adopt action and interaction strategies including partial self-sufficiency in fodder production, substitution toward lower-quality or cheaper feed inputs, and maintenance of long-term trust-based relationships with suppliers. The consequences are rising unit production costs, narrowing profit margins, shortened planning horizons, and declining capacity for reinvestment.

Fragile animal health and technical support systems

The emergence of weak animal health management is driven by causal conditions including irregular veterinary availability, delayed service provision, shortages of medicines, and the erosion of public extension support. This dynamic operates within a context of small- and medium-scale herds, where animal illness or milk contamination rapidly translate into income loss. Intervening conditions, particularly limited laboratory diagnostics, fee-based private veterinary services, and uneven

technical expertise, mediate farmers' access to preventive care. As a result, action and interaction strategies are predominantly reactive rather than preventive, relying heavily on experiential knowledge, informal monitoring, and selective engagement of private veterinarians when financially feasible. These responses generate consequences such as heightened animal mortality risk, unstable milk quality, increased exposure to penalties, and reduced confidence in adopting compliance-oriented upgrading practices.

Infrastructure deficits and blocked farm upgrading

This axial phenomenon is shaped by causal conditions related to the absence of adequate barns, cooling systems, storage facilities, and energy infrastructure necessary for modernization. The problem is situated within a context of rural investment scarcity and uneven territorial access to support mechanisms. Intervening conditions, including high initial investment costs, administrative uncertainty, and dependence on project-based assistance, influence farmers' upgrading decisions. Consequently, action and interaction strategies involve maintaining suboptimal facilities, improvising cooling and storage arrangements, and postponing capital investments. The resulting consequences include technological stagnation, limited compliance with hygiene and welfare standards, and restricted integration into higher-value market channels.

Institutional and bureaucratic barriers to formalization

Barriers to formalization arise from causal conditions such as complex permitting procedures, inconsistent municipal approvals, and fragmented administrative authority. These barriers operate within a context marked by contradictory policy signals that simultaneously promote modernization while obstructing its implementation. Intervening conditions, including weak advisory services and limited effectiveness of state subsidies, further discourage engagement with formal regulatory frameworks. Farmers therefore adopt action and interaction strategies centered on postponement of investment, avoidance of permit-dependent construction, and continuation of semi-formal operational practices. The consequences are persistent informality, declining institutional trust, and long-term underinvestment.

Market instability and informal commercialization pathways

Market vulnerability is driven by causal conditions including volatile milk prices, lack of stable contracts, and asymmetrical bargaining power between producers and buyers. This unfolds within a context of fragmented distribution systems, weak cold-chain infrastructure, and inconsistent enforcement of quality standards. Intervening conditions—notably limited storage capacity and restricted access to certification and testing—mediate farmers' market participation. In response, action and interaction strategies include diversification of sales outlets, direct household marketing, acceptance of lower prices to maintain liquidity, and reliance on informal social networks. These strategies produce consequences such as chronic low margins, limited scalability, reinforcement of informality, and persistent income volatility.

Quality and food safety risk exposure

This axial phenomenon originates from causal conditions in which strict food-safety requirements coexist with insufficient technical and infrastructural capacity to meet them. It occurs within a context of unequal producer organization, where some farmers operate within collective quality systems while others function individually. Intervening conditions, including availability of cooling tanks, laboratory testing, veterinary supervision, and training, strongly shape compliance capacity. As a result, farmers' action and interaction strategies diverge. Organized producers implement routine quality monitoring, whereas others rely on rapid sales and informal mitigation practices. The consequences include unequal exposure to sanctions, segmentation of markets, and exclusion of less-resourced producers from higher-value supply chains.

Labor constraints and household over-reliance

Labor scarcity emerges from causal conditions such as limited availability of hired workers, high wage costs, and low levels of mechanization. This dynamics within a context of household-based production characterized by gendered task allocation and aging rural populations. Intervening conditions, including low profitability, migration trends, and infrastructural deficiencies, intensify labor pressures. Farmers respond through action and interaction strategies that include limiting herd size, intensifying reliance on family labor, and engage in collective labor-

sharing arrangements during peak periods. The resulting consequences are physical exhaustion, constrained growth potential, weakened intergenerational succession, and increased vulnerability to farm exit.

Collective organization as a conditional resilience mechanism

Collective action develops from causal conditions associated with weak individual bargaining power and limited institutional representation. This phenomenon is embedded within a context in which producer organization frequently emerges through donor- or project-based facilitation rather than through permanent public structures. Intervening conditions such as leadership capacity, mutual trust, access to training, and continuity of external support determine organizational effectiveness. Farmers engage in action and interaction strategies including shared feed production, coordinated labor arrangements, participation in training activities, collective quality monitoring, and inter-group product redistribution. The consequences include enhanced resilience for organized farmers, uneven regional development, and structural dependence on external facilitation mechanisms for sustained collective functioning.

Accumulated pressure and trajectory toward farm exit

The integration of preceding axial categories reveals a cumulative process shaped by interacting causal conditions that intensify over time. These include rising input costs, fragile animal health and advisory services, infrastructural stagnation, bureaucratic barriers to formalization, labor shortages, and persistent market instability. This process unfolds within a context characterized by small-scale farms with limited financial reserves, restricted access to credit, and minimal capacity to absorb prolonged shocks. Intervening conditions, notably inadequate and inconsistently implemented government support measures, along with the absence of stabilizing market institutions- further amplify systematic vulnerability. As pressures accumulate, farmers' action and interaction strategies gradually shift from development-oriented investment toward short-term survival. These strategies include cost minimization, increasing reliance on informal commercialization channels, postponement or cancellation of capital investment, reduction of heard size, and dependence on immediate coping mechanisms rather than long-term planning. The

consequences of this adaptive shift are manifested in declining motivation, erosion of long-term viability, weakened intergenerational continuity, and the emergence of increasingly explicit trajectories toward partial or complete farm exit.

3.3. Selective coding

Following Strauss and Corbin's (1998) selective coding procedures, all axial categories were evaluated as potential selective codes. While each captured a significant dimension of farmers' challenges, none individually integrated the full range of economic, institutional, market, and household dynamics observed across regions. Through constant comparison, *accumulated pressure and trajectory toward farm exit* demonstrated the greatest integrative capacity, linking casual conditions, action/interaction strategies, and consequences into a coherent and processual explanation. Unlike the other axial categories, which primarily represented domain-specific mechanisms, this category accounted for their cumulative and temporal interaction. It was therefore selected as the core (selective) category, as it most comprehensively explains the central process underlying dairy farm decline. A central finding of this analysis is that farmers' vulnerability cannot be attributed to any single structural domain. Rather, the axial categories (refer to Axial codes) operate as interdependent pressure fields. Each domain generates strain through distinct causal conditions and consequences; however, their explanatory power lies in how they interact and reinforce one another over time. Input dependence amplifies exposure to volatile markets; infrastructural stagnation constrains compliance and upgrading; bureaucratic uncertainty discourages investment; labor shortages intensify household burdens; and weak technical services heighten production risk. It is not the presence of these pressures individually, but their cumulative and mutually reinforcing interaction, that produces systemic unsustainability. The grounded theory therefore reframes dairy sector decline not as a collection of isolated sectoral deficiencies, but as a structured process of pressure accumulation unfolding across interconnected domains.

Within this framework, farm exit emerges not as an abrupt economic decision, but as a gradual trajectory shaped by prolonged structural strain. Farmers rarely discontinue production following a single adverse event. Instead, repeated exposure to rising costs, regulatory obstruction, market

volatility, infrastructural limitations, and physical exhaustion progressively narrow their adaptive capacity. Coping strategies initially buffer shocks however, as pressures intensify and converge, these adaptative responses lose their effectiveness. Farm exit thus represents the terminal phase of a long-term erosion process in which continued engagement becomes increasingly untenable.

The selective code clarifies the meaning of farmers' adaptive behaviors within this dynamic of pressure accumulation. Practices such as informal milk marketing, partial feed self-sufficiency, herd reduction, delayed capital investment, reliance on family labor, and dependence on project-based support do not represent resistance to modernization. Rather, they constitute rational survival strategies enacted within structurally constrained environments. These strategies temporarily stabilize operations, yet they simultaneously reproduce vulnerability by postponing upgrading, limiting formal integration, and reinforcing informality. Short-term adaptation therefore coexists with long-term stagnation, revealing a paradox in which survival practices sustain production while deepening systematic exposure.

Variation across farmers reflects limited and uneven forms of cooperation. Where collective activities exist, primarily informal, pressure accumulation may temporarily decelerate, although structural constraints remain intact. In the absence of such cooperation, pressures converge more rapidly, accelerating trajectories toward farm exit. These differences stem less from individual managerial capacity than from unequal access to institutional mediation underscoring the structural nature of vulnerability.

From a theoretical perspective, the findings demonstrate that structural vulnerability—not farm-level inefficiency—constitutes the organizing principle of the dairy farming system. By identifying accumulated pressure as the integrating mechanism across domains, the grounded theory shifts analytical attention from discrete production constraints to the temporal interaction of institutional, market, infrastructural, and household conditions. This processual lens explains why interventions addressing single domains often fail to generate sustainable transformation: they do not alter the cumulative dynamic through which pressures converge and intensify.

In sum, *accumulated pressure and trajectory toward farm exit* functions as the selective code because it integrates all axial categories, explains the logic of farmers' coping strategies, accounts for differentiated trajectories within the sector, and captures the central process driving dairy

farm decline. Sustainability challenges in the Albanian dairy sector therefore emerge not from isolated failures, but from the structured and temporal convergence of multiple interlocking pressures that progressively constrain adaptive capacity.

4. DISCUSSION

This study contributes to understanding dairy farming sustainability in Central Albania by developing a grounded theory that conceptualizes farmers' challenges as an interrelated process of *accumulated pressure leading toward farm exit*. Rather than identifying isolated constraints, the findings reveal how economic, institutional, and market-related factors interact over time, progressively undermining farm viability. This integrative perspective advances both theoretical and applied discussions on agricultural vulnerability in transition economies.

Theoretical Implications

From a theoretical standpoint, the study extends existing frameworks on smallholder vulnerability and rural livelihoods by emphasizing accumulation dynamics rather than static constraints. While livelihood theory (Ellis, 2000) highlights exposure to risk and limited asset buffers, the present findings demonstrate how vulnerability intensifies through the interaction of multiple pressures operating simultaneously. The selective code refines this perspective by conceptualizing farm exit as a processual outcome rather than a discrete decision event.

The findings further resonate with Dercon and Christiaensen's (2011) analysis of uninsured consumption risk and technology adoption. When households operate under persistent uncertainty and lack effective risk-buffering mechanisms, they rationally avoid adopting potentially profitable but risky investments. This behavioral adaptation generates underinvestment and may contribute to poverty traps. The accumulation dynamic identified in this study reflects a similar mechanism: as structural pressures intensify and financial buffers weaken, farmers shift from development-oriented strategies toward short-term survival. Investment postponement, herd reduction, and infrastructural stagnation are therefore not symptoms of inefficiency, but rational responses to prolonged systemic risk exposure.

The study also contributes to institutional and political economy theories of agriculture. Consistent with new institutional economics (North, 1990), high transaction costs, regulatory uncertainty, and weak enforcement structures shape farmers' incentives more strongly than technical inefficiency. Furthermore, the findings align with global value chain theory (Gereffi *et al*. 2005) by illustrating how asymmetrical bargaining power, unstable prices, and uneven compliance capacity marginalize small producers within fragmented markets.

Importantly, the results also confirm Ostrom's (2009) theory of collective action. Ostrom demonstrates that durable local institutions, supported by clearly defined rules, monitoring systems, and mutual accountability, can mitigate resource-related pressures and reduce collective vulnerability. In the Albanian dairy sector, however, collective initiatives appear largely project-dependent and lack institutional continuity. In the absence of stable governance arrangements, pressures remain individualized rather than institutionalized. Consequently, farmers must absorb input volatility, market asymmetries, and compliance risks at the household level, accelerating the accumulation of vulnerability over time.

By integrating these perspectives, the grounded theory offers a multi-level explanation linking farm-level adaptive behavior to broader governance arrangements, institutional configurations, and market structures. The concept of accumulated pressure thus bridges livelihood vulnerability, institutional economics, value chain governance, and collective action theory into a coherent processual framework.

Practical and Policy Implications

The results carry important practical implications for agricultural development policy. First, they indicate that addressing single constraints, such as feed subsidies or equipment provision, is insufficient when structural pressures remain unaddressed. Effective intervention requires coordinated action across feed and water systems, veterinary and diagnostic services, infrastructure investment, and market governance mechanisms.

Second, the findings suggest that informality should be understood as an adaptive response to structural constraints rather than a behavioral failure. Policies aimed solely at enforcement are therefore unlikely to succeed without parallel investment in compliance capacity, including

cold-chain infrastructure, advisory services, and simplified administrative procedures.

Third, collective organization emerges as a critical yet under-institutionalized resilience mechanism. Strengthening farmer organizations through stable long-term public support, rather than short-term support, could enhance bargaining power, facilitate service provision, improve quality compliance, and reduce the accumulation of structural pressures.

Limitations

The study is based on qualitative focus group data, which prioritizes in depth qualitative interpretative analysis over statistical representativeness. While appropriate for grounded theory development, the findings cannot be quantitatively generalized to the entire dairy sector. In addition, focus group dynamics may have influenced the articulation of sensitive issues such as indebtedness, informality, or exit intentions.

The research is also context-specific, reflecting Albania's institutional and market environment. Caution is therefore required when transferring conclusions to other national or regional settings without careful contextual adaptation.

Directions for Further Research

Future research should adopt mixed-method and longitudinal designs to examine how structural pressures accumulate over time and how policy interventions alter exit trajectories. Quantitative studies could test the prevalence and relative weight of the identified pressures domains, while comparative research across regions, farm scales, and governance environments would strengthen theoretical generalization. Further investigation should also explore gender roles, youth participation, and succession dynamics, which emerged implicitly in the data but warrant deeper analysis.

Overall, the study demonstrates that sustainable transformation of the Albanian dairy sector requires systemic rather than fragmented solutions. By conceptualizing vulnerability as an accumulated process shaped by institutional and market governance, the grounded theory provides a robust foundation for future research and policy design.

5. CONCLUSIONS

The findings of this study extend beyond the specificities of Central Albania, offering a critical lens through which to interpret the broader decline of smallholder dairy systems in transition economies. By identifying *accumulated pressure and trajectory toward farm exit as a central phenomenon*, this research demonstrates that *sectoral decline constitutes a processual outcome of interlocking structural vulnerabilities*—where economic, institutional, and market pressures converge to systematically erode a producer's adaptive capacity over time. This accumulation dynamic suggests that in environments characterized by regulatory uncertainty and market asymmetry, *short-term survival strategies*—such as informalization, labor intensification, and investment postponement—*paradoxically deepen long-term fragility*. Consequently, this study provides a robust theoretical framework for international policymakers and scholars alike, showing that *sustainable agricultural transformation cannot be achieved through fragmented, single-domain interventions*. Safeguarding the viability of smallholder systems requires *systemic, coordinated governance that addresses the temporal and cumulative nature of structural strain.*

Data accessibility. All data generated or analyzed during this study are included in this published article.

Conflict of interest declaration.The authors declare that they have no competing interests.

Declaration of AI use. Artificial intelligence (AI) tools (ChatGPT, OpenAI) were used solely to proof reading. All scientific content, analyses, interpretations, and conclusions are the original work of the authors.

Author contributions. A.B.: - Ideation, conceptualization, resources, data interpretation, writing –original draft preparation, supervision, review editing, and corresponding author; E.S.: - Conceptualization, methodology, data interpretation, writing – original draft preparation, review editing; F. Gj.: -Data interpretation, resources, writing – original draft preparation.

All authors have read and agreed to the published version of the manuscript

REFERENCES

Charmaz K. 2014. *Constructing grounded theory* (2nd ed.). Sage Publications.

Dercon S, Christiaensen L. 2011. Consumption risk, technology adoption and poverty traps: Evidence from Ethiopia. *Journal of Development Economics*, **96(2):** 159–173. https://doi.org/10.1016/j.jdeveco.2010.08.003.

Ellis F. 2000. *Rural livelihoods and diversity in developing countries*. Oxford University Press.

Gereffi G, Humphrey J, Sturgeon T. 2005. The governance of global value chains. *Review of International Political Economy*, **12(1):** 78–104. https://doi.org/10.1080/09692290500049805.

Institute of Statistics of Albania (INSTAT). 2024. *Livestock statistics in Albania 2000–2023*.

North DC. 1990. *Institutions, institutional change and economic performance*. Cambridge University Press.

Ostrom E. 2009. *Governing the commons: The evolution of institutions for collective action*. Cambridge University Press.

Strauss A, Corbin J. 1998. *Basics of qualitative research: Techniques and procedures for developing grounded theory* (2nd ed.). Sage Publications.

Annex: Conceptual framework

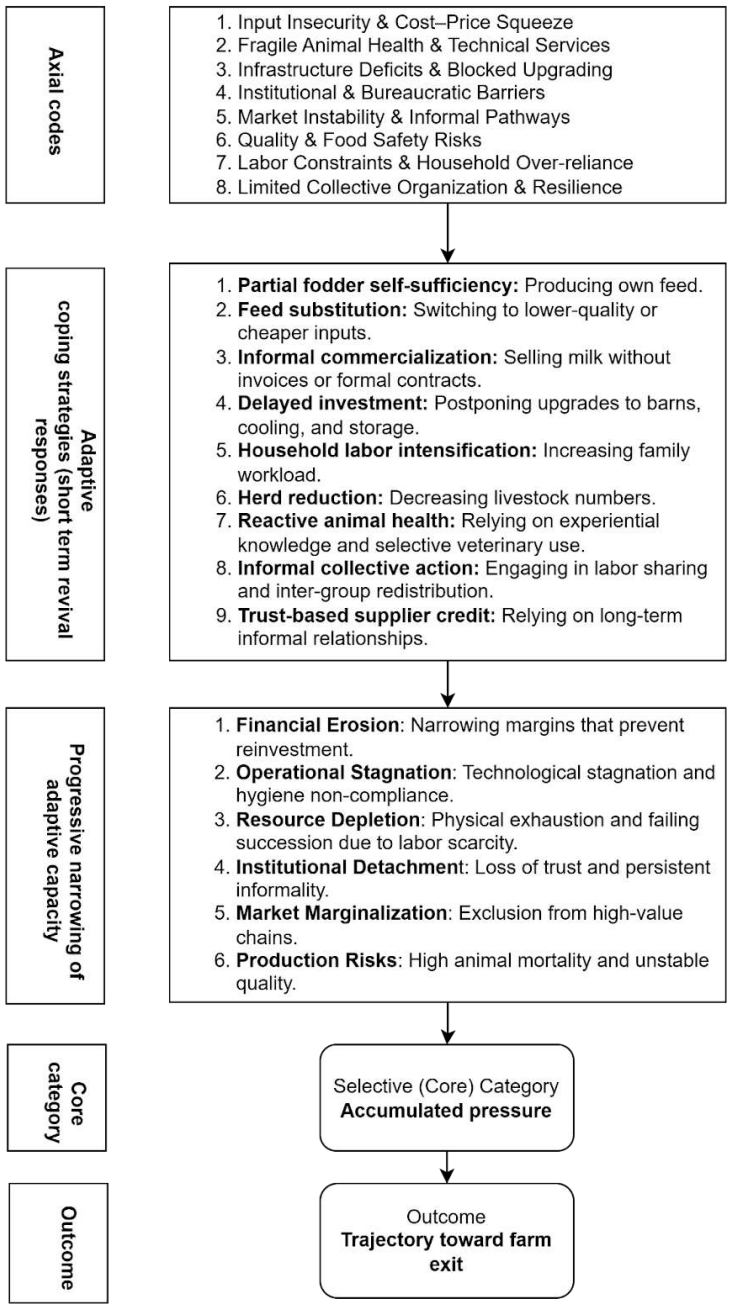

EVALUATING WORD-LEVEL READING METRICS ACROSS EYE-TRACKING AND MOUSE-TRACKING METHODS

Alba HAVERIKU[1] and Elinda KAJO MEÇE[1]

[1]Department of Computer Engineering, Faculty of Information Technology**,** Polytechnic University of Tirana, Albania

Author for correspondence: alba.haveriku@fti.edu.al

AH, 0000-0003-2246-8408**; EKM,** 0009-0002-7353-476X

ABSTRACT

Eye-tracking is a foundational methodology for investigating the cognitive and linguistic processes underlying reading behavior. However, the high financial costs associated with high-precision oculomotor equipment and laboratory configurations highlight the necessity for more accessible experimental alternatives. This study evaluates and compares word-level reading metrics derived from eye-tracking and mouse-tracking datasets collected from native Albanian speakers reading identical texts. The findings reveal a robust correlation between the metrics yielded by both methodologies, particularly concerning total reading duration. These results underscore the viability of affordable kinematic tracking tools for linguistic and cognitive research in resource-constrained environments.

Keywords: eye-tracking, mouse-tracking, Albanian language, psycholinguistics, reading metrics

Publisher: Academy of Sciences of Albania
License: Creative Commons Attribution License (CC BY 4.0)
Citation: **Haveriku A, Kajo Meçe E. 2026.** Evaluating word-level reading metrics across eye-tracking and mouse-tracking methods. *Albanian Journal of Natural and Technical Sciences* (*AJNTS),* **2 (30),**
Journal URL: https://journals-akad.gov.al/magazines/1
Classification: Research
Subject Category Formal sciences + Applied Sciences subject areas: Human-Computer Interaction (HCI) + Psycholinguistics

1. INTRODUCTION

Eye-tracking experiments capture ocular fixations and saccades to provide high-fidelity insights into visual attention across domains such as human-computer interaction (HCI), healthcare, and cognitive psychology. Integrating gaze data has also advanced various subfields of natural language processing (NLP) by providing granular, feature-rich information on reading behaviour and text comprehension. Traditionally, high-precision, laboratory-grade eye-trackers have been the predominant instrumentation utilized to guarantee empirical validity, yet these systems remain cost-prohibitive and scale-limited.

Recent research has consequently explored lower-cost diagnostic alternatives. These include webcam-based eye-tracking (Xu *et al*. 2015; Zhang *et al*. 2015; Ribeiro *et al*. 2023), mouse-tracking paradigms (Wilcox *et al*. 2024) and mobile applications (Huang *et al*. 2015; Krafka *et al*. 2016; Taban *et al*. 2018). Mouse-tracking records spatial cursor coordinates and dwell times as participants interact with on-screen text. Although cursor kinematics offer lower spatial and temporal resolution than direct gaze data, they effectively approximate cognitive processing loads during reading (Wilcox *et al*. 2024), particularly regarding the distribution of macro-attention and localized processing difficulties.

This study builds upon our previous work in this area by comparing two different datasets (Haveriku *et al*. 2025a) collected from native Albanian speakers reading texts in Albanian (Haveriku *et al*. 2025b). This article extends that research paradigm by evaluating the empirical validity of mouse-tracking as a low-cost proxy for traditional eye-tracking methods. Crucially, this study yields new insights into the spatial-temporal alignment between gaze paths and mouse trajectories in native Albanian readers, offering practical design implications for reading research utilizing accessible tracking infrastructures.

Our primary objective is to quantify the degree to which mouse-tracking metrics reflect established eye-movement patterns, thereby assessing the ecological validity of using low-cost alternatives for reading research.

The primary contributions of this article are:

- A comparative validation of word-level reading time measures extracted from parallel eye-tracking and mouse-tracking experiments.
- A formal evaluation of word-level correlations between gaze and cursor metrics using a Bayesian correlation analysis framework.

- An analytical decomposition of the structural limitations inherent to mouse-tracking alongside proposed trajectories for future research.

The remainder of this paper is organized as follows: Section 2 details the architecture of the datasets and the experimental paradigm; Section 3 presents the comparative analysis of the reading measures; Section 4 discusses the empirical implications within the context of low-cost tracking modalities; and Section 5 concludes the paper.

2. METHODS

2.1. Eye-tracking and Mouse-tracking datasets

The study sample comprised 76 native Albanian speakers. Of these, 25 participants (aged 20 to 40) participated in the eye-tracking experiment, while 51 participants (aged 20 to 45) completed the reading tasks via mouse-tracking (Haveriku *et al*. 2025a). All participants read standardized Albanian text passages displayed on a computer monitor. The eye-tracking corpus included 13 texts in total, whereas the mouse-tracking paradigm utilized a subset of three texts (Haveriku *et al*. 2025b), selected from the primary pool. Each textual passage ranged from 100 to 500 words and was segmented across multiple screens. To guarantee active cognitive engagement, participants were required to complete one or more comprehension questions immediately following each text. The eye-tracking trials were conducted in a controlled laboratory environment using an EyeLink Portable Duo system operating at a sampling rate of 1000 Hz. Conversely, the mouse-tracking experiments were deployed as an online utility on standard personal computers, recording spatial cursor coordinates and hover durations as participants read the identical three texts. Because the primary objective of this study is to compare word-level reading metrics across both experimental modalities, subsequent analyses are restricted exclusively to these three shared texts (Table 1).

Table 1. Features of common texts between the eye and mouse tracking experiments

	Wiki Moon	***Broken April***	***Caveman***
Typology of text	Encyclopaedic text	Literature	Scientific text
Number of sentences	5	29	17
Number of tokens	118	611	434

***Hëna* (WikiMoon):** An encyclopaedic text adapted from Wikipedia detailing the physical characteristics of Earth's natural satellite. The text features specialized scientific terminology and is presented on a single screen, with comprehension queries appearing immediately upon completion.

***Prilli i Thyer* (*Broken April*):** A selected excerpt from the third chapter of the novel by Ismail Kadare, presented in the original Albanian. The text features rich descriptive syntax detailing landscapes and the internal psychological states of the characters Besian and Diana. Due to its length, the excerpt was distributed across ten consecutive screens, followed by comprehension questions.

***Njeriu i Shpellave* (*Caveman*):** A scientific text outlining prominent archaeological discoveries made by an international research team. The prose is characterized by high terminological density and complex, hypotactic syntactic structures. It is presented across eight consecutive screens followed by trailing comprehension questions.

Figures 1 and 2 depict the distribution of experiment durations stratified by participant age groups across both empirical modalities.

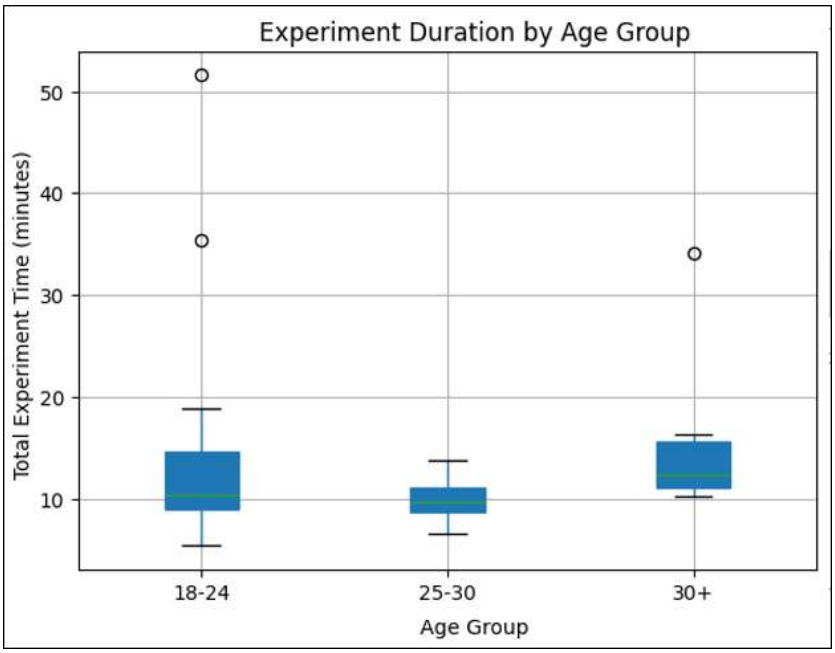

Fig. 1: Experiment duration by age group in the mouse tracking experiments.

Figure 1 presents the age distribution for the participant in the mouse tracking experiments, visually showing three outlier values, which were not considered in the later analysis. Meanwhile, Figure 2 presents the experiment duration by age group for the participants in the eye-tracking experiments.

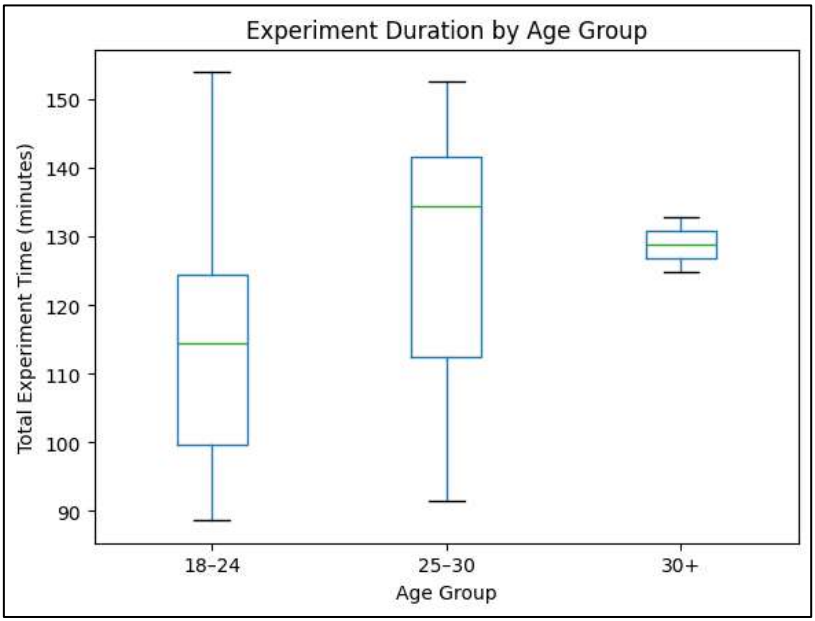

Fig. 2: Experiment duration by age group in the eye tracking experiments.

Figures 3 and 4 illustrate the structural topology of the raw data payloads captured during the initial phase of the mouse-tracking and eye-tracking regimes, respectively. This raw data undergoes systematic preprocessing pipelines to extract the standardized, word-level reading metrics evaluated in later sections.

	Index	Word	mousePositionX	mousePositionY	wordPositionTop	\
0	104.0	kryesor	576.0	393.0	391.162506	
8	15.0	mesatare	549.0	165.0	151.162506	
9	15.0	mesatare	552.0	161.0	151.162506	
10	15.0	mesatare	552.0	161.0	151.162506	
11	15.0	mesatare	552.0	161.0	151.162506	
...	...	...	...	...	...	
8257	49.0	në	971.0	233.0	231.162506	
8258	49.0	në	971.0	233.0	231.162506	
8259	49.0	në	971.0	233.0	231.162506	
8260	50.0	Finlandë.	991.0	236.0	231.162506	
8261	50.0	Finlandë.	1014.0	246.0	231.162506	

	wordPositionLeft	wordPositionBottom	wordPositionRight
0	532.287537	411.162506	596.300041
8	505.262512	171.162506	585.300011
9	505.262512	171.162506	585.300011
10	505.262512	171.162506	585.300011
11	505.262512	171.162506	585.300011
...	...	...	...
8257	961.600037	251.162506	986.625036
8258	961.600037	251.162506	986.625036
8259	961.600037	251.162506	986.625036
8260	986.625000	251.162506	1060.675003
8261	986.625000	251.162506	1060.675003

Fig. 3: Raw data from the mouse tracking experiments.

```
MSG 2031819 start_recording_PRACTICE_trial_1_stimulus_Enc_WikiMoon_13_page_1
MSG 2031824 RECCFG CR 1000 0 0 L
MSG 2031824 ELCLCFG BTABLER
MSG 2031824 GAZE_COORDS 0.00 0.00 1308.00 1001.00
MSG 2031824 THRESHOLDS L 67 228
MSG 2031824 ELCL_WINDOW_SIZES 176 188 0 0
MSG 2031824 CAMERA_LENS_FOCAL_LENGTH 27.00
MSG 2031824 PUPIL_DATA_TYPE RAW_AUTOSLIP
MSG 2031824 ELCL_PROC CENTROID (3)
MSG 2031824 ELCL_PCR_PARAM 5 3.0
MSG 2031825 !MODE RECORD CR 1000 0 0 L

START   2031827     LEFT    SAMPLES EVENTS
PRESCALER   1
VPRESCALER  1
PUPIL   AREA
EVENTS  GAZE    LEFT    RATE    1000.00 TRACKING    CR  FILTER  0
SAMPLES GAZE    LEFT    RATE    1000.00 TRACKING    CR  FILTER  0   INPUT
INPUT   2031827 0
2031827    75.2    92.2   836.0     0.0 ...
2031828    76.1    93.6   830.0     0.0 ...
2031829    73.9    92.6   829.0     0.0 ...
2031830    74.5    92.2   832.0     0.0 ...
2031831    75.0    92.6   824.0     0.0 ...
```

Fig.4: Raw ASCII format from the eye-tracking experiments.

For each lexical token across the texts, the eye-tracking dataset tracks multiple oculomotor metrics capturing visual attention and parsing behaviour: *first fixation duration (FFD)*, *total fixation duration (TFD)*, *gaze duration (GD)*, *go-past time*, *second-pass duration*, *re-reading time*, *absolute fixation count*, *ordered fixation arrays*, and *saccadic kinematics*.

For the mouse-tracking dataset, analogous metrics were derived from spatial cursor trajectories and regional dwell times to serve as cognitive processing proxies. The formalized cursor metrics include: *first hover duration*, *total hover duration*, *gaze-proxy duration*, *downstream response intervals*, and *structural fixation proxies* (comprising re-visit counts, cursor regressions, and intra-word cursor micro-movements).

These unified metrics enable a direct, parallel comparison between the eye-tracking and mouse-tracking data architectures, facilitating a precise evaluation of how robustly cursor kinematics mirror ocular attention patterns during natural reading.

2.2. Data Processing

Data from both experimental paradigms were preprocessed to ensure absolute structural alignment, pairing each lexical item by unique text identifier (`text_id`) and screen position (`page_number`) across all participants. To compile the definitive analytical matrix, individual participant log files were programmatically parsed and concatenated into a centralized relational data frame, yielding a unified eye-tracking dataset containing word-level reading measures. The raw mouse-tracking payloads were compiled using an identical pipeline. During this phase, mouse-tracking screen configurations were mapped directly to the baseline eye-tracking text architecture to ensure exact spatial-temporal correspondence across the three shared texts. This pipeline produced two highly structured data tables consisting of participant tokens, text conditions, page arrays, word-level indices, and their corresponding spatio-temporal metrics.

The subsequent phase involved computing aggregate mean reading measures at the distinct *text-page-word* intersecting node. Utilizing the synchronized token alignment, the two matrices were merged into a single database containing aligned records for the four target dependent variables: *first fixation duration*, *total fixation duration*, *gaze duration*, and *go-past time*.

To formally evaluate the degree of association between the laboratory oculomotor metrics and the online kinematic proxies, we

executed a Bayesian correlation analysis, adopting the statistical framework established for English-language corpora by Wilcox *et al.* (2024). This Bayesian approach offers robust inferential depth by estimating the joint posterior probability distribution of the correlation coefficient. Independent estimation models were executed for each individual reading metric. Posterior parameter sampling was completed via Markov Chain Monte Carlo (MCMC) algorithms utilizing 2000 tuning (burn-in) iterations. For each metric, the posterior mean (ρ) and its corresponding 95% highest density interval (HDI) or credible interval (CI) were derived (Behseta *et al*. 2009).

3. RESULTS AND COMPARISONS

A Bayesian correlation analysis was conducted to systematically evaluate the empirical validity of mouse-tracking kinematic metrics as low-cost proxies for laboratory-grade oculomotor data. Table 2 compiles the estimated posterior mean correlation coefficients (ρ) along with their corresponding 95% credible intervals (CIs) across each experimental text register and reading time measure. All modeled parameters yielded consistently positive correlation profiles, demonstrating that cursor trajectories preserve structural information regarding cognitive processing loads during reading. The varying distribution of these correlation profiles across the different text styles is illustrated dynamically in the widget below.

Table 2. Correlation between eye-tracking and mouse-tracking reading measures

		Total Duration	**First Duration**	**Gaze Duration**	**Go-past Time**
Text 1 *Wiki Moon*	*Posterior mean ρ 95% CI*	0.621 [0.573,0.672]	0.539 [0.481,0.596]	0.314 [0.235,0.395]	0.490 [0.422, 0.551]
Text 2 *Broken April*	*Posterior mean ρ 95% CI*	0.621 [0.57,0.67]	0.541 [0.482,0.599]	0.314 [0.230,0.391]	0.492 [0.429, 0.553]
Text 3 *Caveman*	*Posterior mean ρ 95% CI*	0.401 [0.339,0.459]	0.331 [0.266,0.400]	0.191 [0.113,0.264]	0.146 [0.072, 0.224]

Total duration reflects the sum of all fixation or hover intervals dedicated to a target word, capturing both initial processing and subsequent re-reading. As demonstrated in Table 2, this metric yielded the most robust and resilient cross-modal

agreement, with posterior means spanning from ρ = 0.401 to ρ = 0.621. This indicates that while real-time cursor tracking lacks the extreme temporal sensitivity of a 1000Hz oculomotor system, it remains a highly stable proxy for capturing global, cumulative cognitive processing loads at the word level. First fixation duration isolates the immediate temporal footprint of the reader's initial encounter with a word, serving as a reliable index of early lexical access and orthographic decoding before any regressive movements occur. The correlation coefficients for first fixation duration remain remarkably stable across Text 1 (ρ= 0.539) and Text 2 (ρ = 0.541). However, there is a pronounced performance drop in Text 3 (ρ=0.331). This systematic variance suggests that mouse-tracking kinematics successfully parallel early ocular engagement when reading linear, predictable prose, but uncouple during the initial processing of dense technical vocabulary or complex morphology. Gaze duration—the cumulative duration of all fixations on a word during the first pass before moving onward—exhibits a structural trend identical to first fixation duration. As visualized in Figure 5, the correlation remains stable for the informational and literary registers (ρ= 0.314) but drops significantly within the scientific text (ρ= 0.191).

A matching degradation profile is evident in the go-past time metric, which drops from a robust baseline (ρ≈0.490 in Texts 1 and 2) down to its lowest observed validity in Text 3 (ρ=0.146). Because go-past time encapsulates the total time spent from first entering a word until moving past it to the right—including any immediate regressive attempts to repair syntax—this minimal correlation highlights a core boundary condition of mouse tracking: manual cursor control is too slow to capture the rapid, automated oculomotor adjustments readers use to resolve local structural ambiguities in complex text.

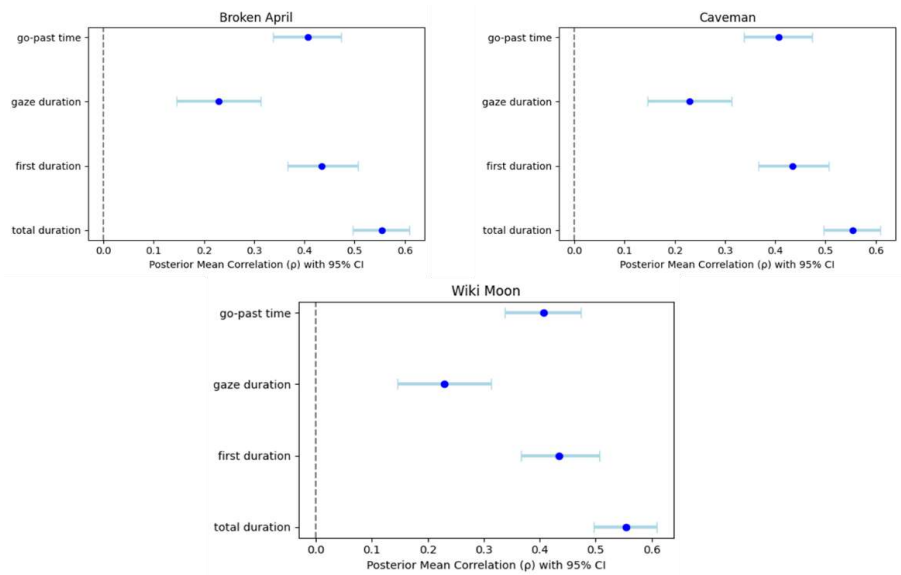

Fig. 5: Correlation between eye-tracking and mouse-tracking reading measures.

4. CONCLUSIONS AND FUTURE WORK

In this study we presented a comparison of word level reading measures obtained from eye- This study presented a comparative validation of word-level reading metrics obtained from parallel eye-tracking and mouse-tracking experiments conducted in the Albanian language. By analyzing word-by-word reading times across three identical text registers, we investigated the efficiency with which hand-cursor kinematics mirror the oculomotor tracking of latent cognitive processes during reading. Our empirical findings indicate a moderate-to-strong cross-modal correlation that is fundamentally modulated by text typology. For the informational (*WikiMoon*) and narrative literary (*Broken April*) texts, the correlations were consistently robust, particularly within the total reading duration metric. Conversely, the scientific exposition text (*Caveman*) exhibited a pronounced compression of correlation coefficients across all investigated dimensions, implying that cursor tracking accuracy is sensitive to specific structural and syntactic variables that alter typical hand-eye coordination patterns. Despite these boundary conditions, the collective results demonstrate that mouse-tracking constitutes an ecologically valid, highly scalable, and cost-effective methodology for approximating global reading behaviour.

Future research vectors should expand upon these findings by incorporating a broader array of computational reading metrics and testing them against a more typologically diverse typographic corpus. Expanding the participant sample sizes across both experimental cohorts will further minimize stochastic noise and enhance external validity. Another important methodological direction involves integrating mid-tier hardware paradigms, such as Pupil Core glasses, to evaluate alternative systems that bridge the precision gap between standard mouse cursors and laboratory-grade EyeLink infrastructure. Finally, a promising linguistic path is to incorporate automated text feature extractions—specifically isolating parts of speech, morphosyntactic alignment, and structural dependency length. This will systematically determine whether the cross-modal alignment between eye and mouse movements varies predictably across distinct grammatical constructions in the Albanian language.

Ethics. Informed consent was obtained from all individual participants included in the study prior to data collection and subsequent publication.

Originality and authorship. This work is based entirely on original datasets, experimental paradigms, and intellectual frameworks developed exclusively by the authors.

Author contributions. **A. H.:** Ideation, conceptualization, methodology, data interpretation, resources, writing—original draft preparation, and corresponding author; **E. KM.:** Ideation, conceptualization, methodology, data interpretation, resources, review and editing, supervision.

All authors have read and agreed to the published version of the manuscript.

Conflict of interest. The authors declare no conflicts of interest.

Declaration of AI use. We confirm that no AI-assisted technologies were used to create this article.

REFERENCES:

Behseta S, **Berdyeva T, Olson CR, Kass RE. 2009.** Bayesian correction for attenuation of correlation in multi-trial spike count data. *Journal of Neurophysiology*, **101 (4):** pp. 2186–2193. PMID: **19129297**. PMCID: PMC2695642. DOI: 10.1152/jn.90727.2008.

Haveriku A, Bedulla S, Meçe EK. 2025a. Understanding reading patterns of Albanian native readers through mouse tracking analysis. *The 39th International Conference on Advanced Information Networking and Applications (AINA-2025)*. 245. Springer, Cham. doi: https://doi.org/10.1007/978-3-031-87763-6_38.

Haveriku A, Kote N, Çepani A, Çerpja A, Trandafili E, Meçe EK. 2025b. Leveraging mouse tracking data for part-of-speech and syntactic dependency prediction in Albanian. In: *Proceedings of the 2025 symposium on Eye Tracking Research and Applications* (*ETRA '25*), ACM, New York, 2025, Article 115, pp. 1–5. doi: 10.1145/3715669.3726840.

Huang Q, Veeraraghavan A, Sabharwal A. 2015. TabletGaze: Unconstrained appearance-based gaze estimation in mobile tablets. In arXiv:1508.01244.

Krafka K, Khosla A, Kellnhofer P, Kannan H, Bhandarkar S, Matusik W, Torralba A. 2016. Eye Tracking for Everyone. *EEE Conference on Computer Vision and Pattern Recognition (CVPR),* In: https://gazecapture.csail.mit.edu/.

Ribeiro T, Brandl S, Søgaard A, Hollenstein N. 2023. WebQAmGaze: A MultilingualWebcam Eye-Tracking-While-Reading Dataset. *Computation and Language (cs.CL)*. In: https://arxiv.org/pdf/2303.17876v2.pdf.

Taban RA, Croock MS, Korial AE. 2018. Eye tracking based mobile application. *International Journal of Advanced Research in Computer Engineering & Technology (IJARCET),* **7(6):** 365- 374. http://dx.doi.org/10.12785/ijcds/070605.

Wilcox EG, Ding C, Sachan M, Jäger LA. 2024. Mouse tracking for reading (MoTR): A new naturalistic incremental processing measurement tool. *Journal of Memory and Language, 138*, 104534. https://doi.org/10.1016/j.jml.2024.104534.

Xu P, Ehinger KA, Zhang Y, Finkelstein A, Kulkarni SR, Xiao J. 2015. TurkerGaze: Crowdsourcing saliency with webcam based eye tracking. In arXiv:1504.06755.

Zhang X, Sugano Y, Fritz, M, Bulling A. 2015. Appearance-based gaze estimation in the wild. In: *Proceedings of the IEEE Conference on Computer Vision and Pattern Recognition (*CVPR), Boston, MA, USA, pp. 4511–4520. doi: 10.1109/CVPR.2015.7299081.

PREDICTING ACADEMIC PERFORMANCE IN HIGH SCHOOL USING GRADES AND EXAM SCORES WITH MACHINE LEARNING

Paola Shasivari[1], Aida Shasivari[2] and Aleksander Xhovani[3]

[1,2,3]Department of Informatics Engineering, Faculty of Information Technology, Polytechnic University of Tirana, Albania

PSh, 0000-0003-4874-9523, ASh, 0009-0007-5689-6503

ABSTRACT

Predicting academic performance is crucial for optimizing educational strategies and ensuring equitable student success. This study leverages machine learning to analyze a dataset from Ismail Qemali High School in Albania, encompassing three years of academic records, including core subject grades, elective choices, stream assignments, and Matura exam results. The research investigates the role of stream-specific curricula and electives in shaping overall grade point average (GPA) and Matura performance. By applying random forest, gradient boosting, and neural network models, the study evaluates predictive accuracy and feature importance. Key findings highlight the significance of mathematics, physics, and aligned electives in driving performance. The gradient boosting model emerges as the most effective predictor, offering actionable insights for educators. This paper demonstrates the potential of machine learning to guide stream selection, optimize elective choices, and improve student outcomes.

***Keywords*:** academic performance prediction, machine learning in education, Matura exam, educational data mining, predictive modelling, feature importance

Publisher: Academy of Sciences of Albania
License: Creative Commons Attribution License (CC BY 4.0)
Citation: **Shasivari P, Aida Shasivari A, Aleksander Xhovani A. 2026.** Predicting academic performance in high school using grades and exam scores with machine learning**.** *Albanian Journal of Natural and Technical Sciences* (*AJNTS),* **2 (30),**
Journal URL: https://journals-akad.gov.al/magazines/1
Classification: Research
Subject Category Formal sciences + Applied Sciences subject areas: Data science, artificial intelligence (AI), and education technology

1. INTRODUCTION

Predicting academic performance has become an essential tool for educators and policymakers, enabling the development of targeted strategies to improve student outcomes. High school serves as a critical phase in shaping future success, and understanding the factors that contribute to academic performance is paramount. The integration of machine learning into educational data mining offers a robust approach to uncovering these factors. Previous studies have demonstrated the efficacy of machine learning techniques in identifying key predictors of performance, such as prior grades, curriculum alignment, and demographic variables (Hussain & Khan, 2021; Chen and Ding, 2023).

This study leverages a dataset from Ismail Qemali High School, a prominent institution with over 2,000 student records spanning three academic years (Grades 10–12). The dataset includes core subject grades, elective choices, stream assignments, and Matura exam results. By employing machine learning techniques, this study seeks to predict academic outcomes, such as grade point average (GPA) and Matura success, while exploring the influence of stream-specific curricula and elective choices. The findings contribute to a growing body of research that highlights the importance of personalized educational pathways in enhancing student success (Nachouki and Mehdi, 2021; Badal and Sungkur, 2022).

Machine learning methods have been particularly effective in educational contexts, where complex interactions between predictors can be uncovered through algorithms. Using the Ismail Qemali High School dataset as a case study, this research demonstrates how machine learning provides actionable insights into the academic progression of students. The outcomes of this work include predictive models that guide stream selection, optimize elective choices, and improve overall student performance.

Although previous studies have successfully applied machine learning techniques to predict academic performance, most research focuses on university datasets or general educational indicators without considering stream-specific curricula and elective alignment in secondary education. Furthermore, limited research has explored educational data from Albania, particularly in the context of high school academic pathways and Matura examinations. This study addresses this gap by analysing how core subjects, electives, and stream assignments jointly influence GPA and

academic outcomes using machine learning models on a real-world Albanian high school dataset.

2. Related Work

Educational data mining (EDM) has emerged as a pivotal research area, leveraging machine learning to uncover patterns in student performance. Studies such as those by Conijn *et al*. (2017) and Helal *et al*. (2018) demonstrate the effectiveness of classification models in predicting academic success. Techniques ranging from decision trees to neural networks have been employed, emphasizing the role of predictors like prior grades, attendance, and demographic variables.

Chen and Ding (2023) explored the potential of ensemble learning models to improve predictive accuracy, emphasizing their iterative approach to optimizing outcomes. Alshanqiti and Namoun (2020) expanded on this by introducing hybrid regression techniques that integrated feature selection strategies with regression models, achieving higher prediction rates for student performance metrics. These findings highlight the effectiveness of advanced techniques in identifying factors affecting academic success.

In addition to prediction-focused studies, Al-Alawi *et al*. (2021) emphasized the importance of contextualizing machine learning applications within specific educational systems. Their work showed that tailored datasets improve the relevance and applicability of predictive insights. Similarly, Mehdi and Nachouki (2022) highlighted the influence of electives and curriculum alignment on student outcomes. These works collectively underscore the need for contextualized and feature-specific modelling approaches.

The study by Mehdi and Nachouki (2022) further demonstrated the potential of data-driven decision-making in guiding educational strategies. Their findings align with the current study's objective to develop machine learning models that capture the dynamics between core subjects, electives, and stream assignments. Through these combined perspectives, the present study integrates key advancements in machine learning and applies them to a high school context.

3. Dataset Description

The dataset contains 2,143 student records collected across three academic years (Grades 10–12), consisting of 12 primary academic features and one target variable (overall GPA). Grades are represented on a 4–10 scale according to the Albanian educational system. After preprocessing and the removal of incomplete records, 2,031 valid instances remained for modelling. The dataset includes the academic and demographic features detailed in Table 1:

Table 1. Description of academic features and target variables

Feature	Description
Mathematics Grades	Grades achieved in core mathematics courses across three years.
Physics Grades	Grades achieved in core physics courses across three years.
Biology Grades	Grades achieved in core biology courses.
Chemistry Grades	Grades achieved in core chemistry courses.
History Grades	Grades achieved in core history courses.
Language Grades	Grades achieved in Albanian and English language courses.
Elective Grades	Grades achieved in elective courses, such as advanced mathematics, sociology, and literature.
Stream Assignments	The academic stream selected by the student (e.g., Engineering, Medical, Law).
Matura Scores	Results of mandatory Matura examinations (mathematics, English, Albanian) and elective exams.

- **Core Subjects:** Grades for mathematics, physics, biology, chemistry, history, and languages.
- **Electives:** Stream-specific electives, such as advanced mathematics, sociology, and advanced literature.
- **Streams:**
    - *Engineering:* Focuses on advanced mathematics and physics.
    - *Medical:* Emphasizes biology and chemistry.
    - *Law:* Highlights history and advanced literature.

  - *Economics:* Centres on advanced mathematics and advanced English.
  - *Arts:* Includes sociology and psychology.
- **Matura Results:** Scores in three mandatory subjects (mathematics, English, and Albanian) and one elective subject.
- **Overall GPA:** Aggregated academic performance across all years.

This dataset provides a meaningful foundation for exploratory predictive modelling, aligning with prior research that demonstrates the importance of standardized exams and GPA as indicators of academic success (Rahman *et al.* 2021; Mehdi and Nachouki, 2022). Engineering represented 28% of students, followed by Medical (24%), Economics (20%), Law (16%), and Arts (12%). Moreover, the dataset reflects the diverse academic pathways offered at Ismail Qemali High School, making it a representative case study for examining educational outcomes.

4. MATERIALS AND METHODS

Data Preprocessing and Validation

Missing numerical values were replaced using median imputation, while incomplete categorical records were removed to preserve consistency. Stream assignments and electives were encoded using label encoding. Numerical features were standardized using a standard scaler before training the neural network model. Five-fold cross-validation was applied to reduce variance and improve model reliability. The dataset was divided into 80% training data and 20% testing data using random sampling with a fixed random seed to ensure reproducibility.

Features were selected based on both educational relevance and prior literature. Core subjects, such as mathematics and physics, were included because previous studies identified them as strong indicators of academic success in STEM-oriented educational pathways. Although stream distributions were not perfectly balanced, exploratory analysis showed that all streams contained sufficient observations for model training.

Predictive Modelling and Analysis

The methodology integrates machine learning pipelines with exploratory data analysis (EDA) and feature engineering. The random forest regressor was applied to model nonlinear relationships through an ensemble of decision trees, improving robustness and reducing variance.

The gradient boosting regressor was utilized due to its iterative optimization process, which improves prediction accuracy by minimizing residual errors. Finally, a multilayer neural network regressor was implemented to capture complex nonlinear interactions among the academic features.

EDA emphasized correlations between grades and overall GPA, with mathematics and physics showing the highest influence. Visualizations, including scatter plots and box plots, guided model selection and feature prioritization.

5. RESULTS AND ANALYSIS

Model Performance

The performance of the machine learning models was evaluated using metrics such as Mean Absolute Error (MAE), Mean Squared Error (MSE), and R^2 Score (Table 2):

Table 2: Performance evaluation of machine learning models

Model	MAE	MSE	R^2 Score
Random Forest	1.038	1.441	-0.048
Gradient Boosting	1.027	1.416	-0.030
Neural Network	1.040	1.422	-0.035

Insights from Model Tuning

- **Random Forest:** The model's performance was optimized by setting the number of estimators to 100 and utilizing a maximum depth of 10 for the decision trees. While effective at handling nonlinear relationships, it exhibited slight overfitting on the training data.
- **Gradient Boosting:** Hyperparameters including the learning rate (0.1), number of estimators (150), and maximum depth (5) were tuned to optimize predictive accuracy. The model emerged as the most effective predictor due to its iterative approach to minimizing residual errors.
- **Neural Network:** A three-layer architecture consisting of 64, 32, and 16 nodes, respectively, was implemented using rectified linear

unit (ReLU) activation functions. Regularization techniques, such as a dropout layer with a rate of (rate 0.2) were utilized to mitigate overfitting; however, the model's predictive capacity was slightly constrained by the small sample size of the dataset.

Feature Importance and Insights

Feature analysis revealed that mathematics grades were the strongest predictor of overall GPA, followed closely by physics and elective grades. The significance of curricular alignment—such as advanced mathematics electives taken by Engineering stream students—was evident in higher GPA clusters.

Exploratory scatter plots highlighted these relationships, displaying a positive correlation between higher elective performance and superior academic outcomes. Furthermore, students enrolled in the Engineering and Economics streams consistently displayed the highest overall GPA trends, driven primarily by strong performance in mathematics and specialized electives.

Scatter Plot Analysis

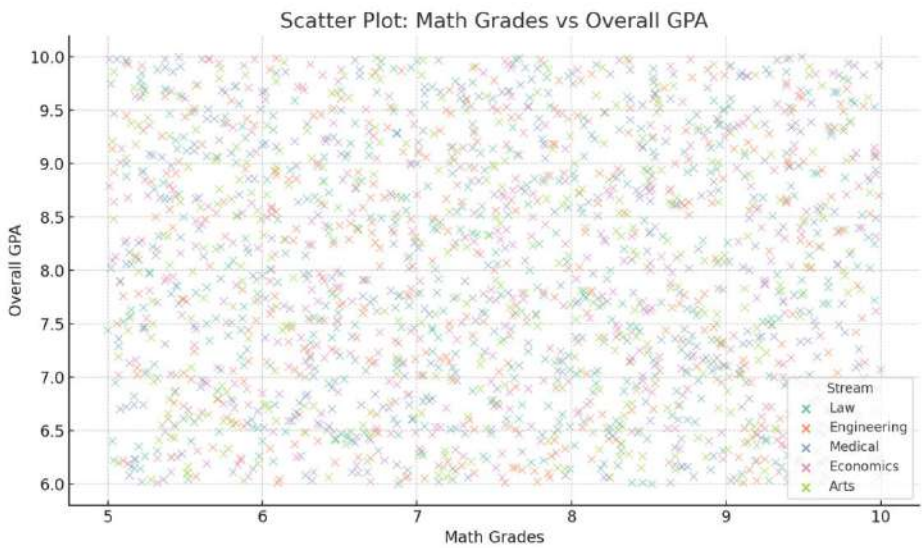

Fig.1. Math Grade VS Overall GPA.

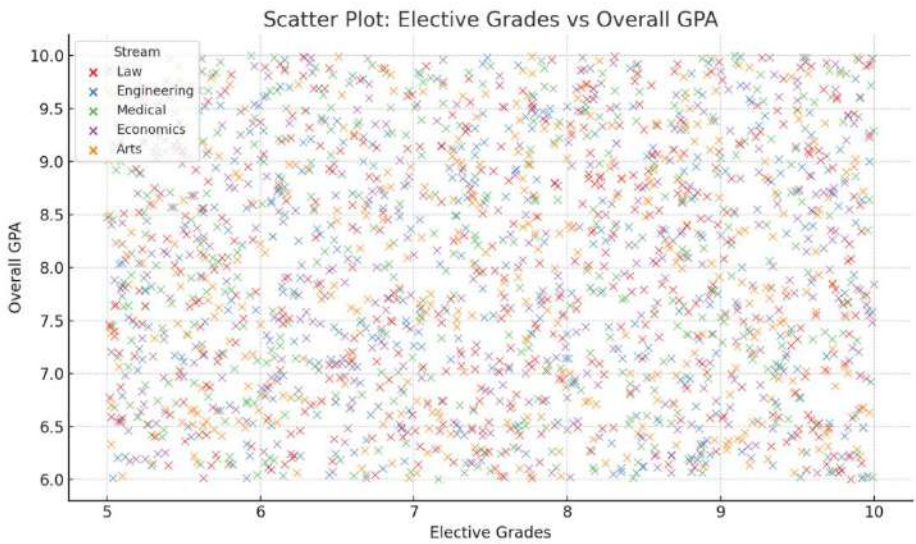

Fig.2: Elective Grade VS Overall GPA.

- **Mathematics Grades vs. Overall GPA:** The scatter plot (Figure 1) suggests a moderate positive correlation between mathematics grades and overall GPA, particularly for students in the Engineering and Economics streams. These streams exhibit prominent clusters in the upper-right quadrant of the plot, indicating a pattern of consistent academic excellence.
- **Elective Grades vs. Overall GPA:** This visualization (Figure 2) underscores the role of elective selections in shaping overall GPA. Streams with tightly aligned electives, such as advanced mathematics in Economics, demonstrate superior performance, emphasizing the critical importance of elective optimization.

Visualizing Performance Trends

Box plots (Figure 3) reveal that Engineering students achieved the highest median GPA (8.5), followed closely by Economics students at 8.2. Conversely, the Arts and Law streams exhibit greater variability in their distributions, reflecting the influence of less-aligned elective choices on overall academic outcomes.

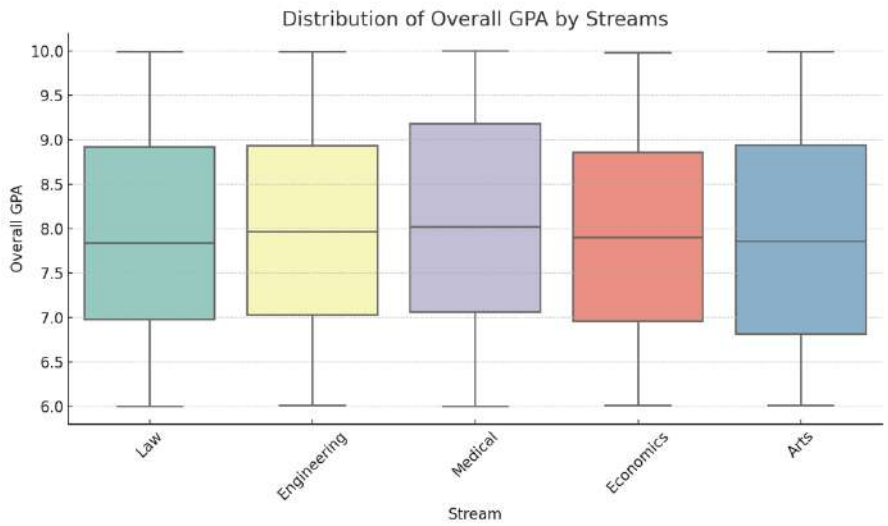

Fig.3. Distribution of Overall GPA by Streams.

Calculations and Additional Metrics

Through regression analysis, the gradient boosting model identified that for every unit increase in mathematics grades, overall GPA improved by approximately 0.4 units, a notable observed relationship. Similarly, elective grades contributed to a 0.3- unit improvement in GPA for students in aligned streams. These insights provide quantitative backing for curriculum adjustments and academic planning.

Although the gradient boosting model achieved the lowest MAE and MSE values among the evaluated approaches, all models produced negative.

Although the gradient boosting model achieved the lowest MAE and MSE values among the evaluated approaches, all models produced negative R^2 scores. A negative R^2 indicates that the models performed worse than a baseline predictor using the mean GPA value. This suggests that, despite identifiable feature-level relationships, the overall predictive capability of the models remains limited. Possible causes include dataset variability, limited sample diversity, unobserved educational factors, and the relatively small feature space. Consequently, these findings indicate that the proposed framework should currently be interpreted as exploratory rather than fully predictive.

6. INSIGHTS AND RECOMMENDATIONS

Key Insights from Machine Learning Models

The gradient boosting model emerged as the most accurate predictor, with a Mean Absolute Error (MAE) of 1.027. This suggests that the model's GPA predictions are, on average, within one grade point of the actual values. The Random Forest and Neural Network models, while effective, exhibited slightly higher errors, indicating comparatively lower prediction error among the evaluated models.

Feature Importance

Feature importance analysis identified mathematics grades as the most influential factor associated with GPA outcomes, followed closely by physics and elective grades. Students enrolled in quantitatively oriented streams, such as Engineering and Economics, generally demonstrated higher GPA trends. These findings suggest that curriculum alignment and subject specialization significantly influence academic performance.

Table 3. Feature importance percentages and estimated impact on overall GPA

Feature	Feature Importance	GPA Impact (per unit increase)
Mathematics Grades	40%	+0.4
Physics Grades	25%	+0.3
Elective Grades	20%	+0.3
English Grades	15%	+0.2

Recommendations

Technical streams, such as Engineering and Economics, may benefit from a stronger emphasis on mathematics and physics electives supported through tutoring initiatives and targeted academic assistance. Additional mentoring programs may also support streams experiencing greater GPA variability, such as Arts and Law.

Aligning electives with students' academic strengths may contribute to improved educational outcomes. Structured guidance and counselling

initiatives should assist students in selecting electives consistent with their academic interests and career goals.

Curriculum development strategies may benefit from incorporating insights derived from feature importance analysis, particularly regarding the vital role of mathematics and physics in foundational academic achievement.

7. CONCLUSION AND FUTURE WORK

This study explored the application of machine learning techniques for analysing academic performance using secondary school records. By analysing core subject grades, elective choices, and stream assignments, the proposed models highlight potential factors associated with academic performance, with mathematics, physics, and stream-aligned electives emerging as the most relevant features. Among the evaluated approaches, the gradient boosting model achieved the best predictive performance, demonstrating a lower prediction error relative to the alternative models. Ultimately, the findings emphasize the importance of curriculum alignment and data-driven educational planning within secondary education frameworks (Mehdi and Nachouki, 2022).

Future Work

Future research should expand the dataset by incorporating additional student cohorts and data from multiple educational institutions to improve model generalizability. Further studies may also include a broader set of variables, such as attendance records, behavioural indicators, and extracurricular activities, to better capture the multidimensional factors influencing academic performance. Finally, longitudinal analyses across multiple graduation cycles may provide deeper insight into evolving educational trends and support more robust predictive modelling approaches. These directions will contribute significantly to improving the practical applicability and reliability of machine learning frameworks within secondary education research.

Ethics. This study did not involve human participants, clinical data, or animal subjects.

Data sharing statement: The datasets generated and analysed during the current study are not publicly available due to legal and ethical

restrictions protecting the privacy of minors (high school students). De-identified data may be made available from the corresponding author upon reasonable request, subject to approval from the participating institution and institutional ethics committee.

Authors' contributions. All authors contributed equally to this work, including the experimental design, data collection, analysis, and manuscript preparation. All authors have read and approved the final version of the manuscript for submission.

Funding. This research received no external funding.

AI Statement. The authors state that no generative AI or AI-assisted technologies were used in the writing, data analysis, or creation of figures for this manuscript.

Declaration of interest. The authors declare that they have no known competing financial interests or personal relationships that could have appeared to influence the work reported in this paper.

REFERENCES:

Alshanqiti A, Namoun A. 2020. Predicting student performance and its influential factors using hybrid regression and multi-label classification. *IEEE Access*, **8:**203827-203844. **E- ISSN:** 2169-3536 10.1109/ACCESS.2020.3036572.

Badal YT, Sungkur RK. 2022. Predictive modelling and analytics of students' grades using machine learning algorithms. *Education and Information Technologies*, **28(3):**3027-3057 PMID: 36097545 PMCID: PMC9452868. DOI:10.1007/s10639-022-11299-8.

Chen S, Ding Y. 2023. A machine learning approach to predicting academic performance in Pennsylvania's schools. *Social Sciences*, **12(3):**118 doi: https://doi.org/10.3390/socsci12030118.

Conijn R, Snijders C, Kleingeld A, Matzat U. 2017. Predicting student performance from LMS data: A comparison of 17 blended courses using Moodle LMS. *IEEE Transactions on Learning Technologies.* Doi Bookmark. 10.1109/TLT.2016.2616312.

Helal S, Li J, Liu L, Ebrahimie E, Dawson S, Murray DJ, Long Q. 2018. Predicting academic performance by considering student heterogeneity. *Knowledge-Based Systems*, **161**:134-146. Doi: 10.1016/j.knosys.2018.07.042.

Hussain S, Khan MQ. 2021. Student-Performulator: Predicting Students' Academic Performance at Secondary and Intermediate Level Using

Machine Learning. *Annals of Data Science*, **10(3):**637-655. Doi: 10.1007/s40745-021-00341-0.

Mehdi R, Nachouki M. 2022. A neuro-fuzzy model for predicting and analyzing student graduation performance in computing programs. *Education and Information Technologies*, **28(3):**2455-2484 Doi:10.1007/s10639-022-11205-2 .

Nachouki M, Mehdi RAK. 2021. Particle Swarm Model for Predicting Student Performance in Computing Programs. *Lecture Notes in Networks and Systems*, 84-96 doi: 10.1007/978-3-030-82196-8_7.

Rahman M, Ahmed MI, Hossain MS. 2021. Analysis of Student's Achievement through Educational Data Mining. 2021 International Conference on Information Systems and Advanced Technologies (ICISAT):1-5 doi: 10.1109/ICISAT54145.2021.9678406 .

ARTIFICIAL INTELLIGENCE IN ACADEMIC FEEDBACK: A CORRELATIONAL ANALYSIS OF CHATGPT USE AND STUDENT PERCEPTIONS IN ALBANIAN HIGHER EDUCATION

Eda Tabaku[1], Anna Maria Kosova [2], Robert Kosova[3], Elvi Shqopa[4]
[1,4] Department of Computer Science, University, Aleksandër Moisiu, Durrës, Albania
[2]Faculty of Research and Development, Polis University, Tirana, Albania
[3]Department of Mathematics, University, Aleksandër Moisiu, Durrës, Albania
Author for correspondence: robertkosova@uamd.edu.al
RK, 0000-0001-7407-5441; AMK, 0009-0001-6998-5085;ET, 0009-0000-4876-6927

ABSTRACT

This research explores the relationship between the frequency of university students' use of ChatGPT as an intelligent academic feedback tool and their perceptions of feedback effectiveness. Data were collected from 350 students studying in the Faculty of Information Technology and the Faculty of Business Studies at the University, Aleksandër Moisiu, Durrës, Albania, during the second semester of the 2024-2025 academic year. A 15-item questionnaire based on a Likert scale was administered online through Google Forms. Because the data were not normally distributed, the relationship between ChatGPT use frequency and perceived feedback effectiveness was analyzed using Spearman's rank correlation coefficient. Results revealed a strong positive correlation between ChatGPT frequency use and perceived feedback usefulness. The results suggest that ChatGPT may serve as a valuable supplementary tool in formative assessment by supporting task improvement and self-directed learning. However, further longitudinal and discipline-specific research is required to better understand the broader educational implications of generative artificial intelligence in higher education.

Keywords: artificial intelligence; ChatGPT; academic feedback; higher education; learning; student perception; correlation; Albania

Publisher: Academy of Sciences of Albania
License: Creative Commons Attribution License (CC BY 4.0)
Citation: **Tabaku E, Kosova AM, Kosova R, Shqopa E. (2026).** Artificial intelligence in academic feedback: A correlational analysis of ChatGPT use and student perceptions in Albanian higher education. *Albanian Journal of Natural and Technical Sciences* (*AJNTS),* **2 (30)**
Journal URL: https://journals-akad.gov.al/magazines/1
Classification: Research
Subject Category: Applied + Social Sciences subject areas Educational Technology (EdTech) / Psychometrics

1. INTRODUCTION

Tan (2023) has said that the modern educational environment is rapidly evolving into an artificial intelligence (AI)-powered landscape with new possibilities to transform the pedagogy and automate essential administrative and instructional processes. The implementation of smart technologies into the system of higher education has also driven the emergence of new types of relations between students and the teaching system—specifically, knowledge accessibility, academic support, and support of self-directed learning (Alam and Mohanty, 2023). The latest examples of this trend are the development of generative large language models (LLMs), including Generative Pre-trained Transformer (ChatGPT), which are increasingly functioning as intelligent agents in education due to their capacity to generate contextualized, coherent, and personalized responses (Al Amri *et al.* 2025; Yigci *et al.* 2025).

An intelligent agent is defined as a system that observes its environments through sensors, processes the received information, and executes autonomous decisions to achieve preset objectives. These agents share three core behavioural characteristics: autonomy, adaptability, and proactivity. Within the learning environment, an intelligent agent engages with the student, processes the contextual data, and provides an answer with a significant meaning without human intervention, thereby assisting in more personalized and effective learning (Sánchez-Prieto *et al*. 2024). As a deep transformer-based AI trained on large-scale corpora, ChatGPT satisfies the criteria of an intelligent agent by automatically responding to user input while dynamically adjusting its content, style, and complexity to the target context.

Academic feedback—defined as the structured remarks and guidance provided to students regarding their academic performance—is a fundamental attribute to the learning process. Ilić *et al.* (2021) stress that the effective feedback must be specific, clear, timely, deep, and transferable and learning-oriented. However, empirical research indicated that conventional higher education feedback structures are frequently superficial, ineffective, and infrequent, particularly when exacerbated by high student-to-staff ratios and heavy institutional workloads (Nyanjom *et al*. 2023). This systematic dilemma requires scalable, sustainable solutions capable of accessible, sufficient, and sustained formative services. To this extent, conversational AI systems such as ChatGPT can serve as a vital complementary system.

ChatGPT operates as a versatile pedagogical tool because of its ability to address open-ended questions, clarify conceptual explanations, refine text, and recreate academic writing revisions. The main constraints of human feedback include the fact that it takes a long time to provide formative commentary, which is both an integration of its potential to provide feedback in real time and a delay in responding (Ahmedtelba, 2025). However, deploying intelligent agents for academic feedback involves some risks. There have been concerns about the overuse of technology, the lack of critical thinking ability, and the simplification of the academic discourse. Indeed, the accuracy of ChatGPT's outputs remains highly variable in scenarios demanding advanced linguistic nuances, deep subject-matter expertise, or rigorous critical evaluation (Baskara, 2025).

Theoretically, the Technology Acceptance Model (TAM) provides a robust framework for evaluating student adoption of the ChatGPT platform. Prior applications of TAM to educational AI have determined that the ease-of-use views of ChatGPT are generally high, but the perceived utilities are highly diverse based on the task and discipline (Ratten and Jones, 2023). Moreover, the self-regulated learning theory suggests that AI-generated feedback can successfully augment metacognitive monitoring, allowing students to cyclically assess their performance and develop greater academic autonomy (Rosales-Marquez *et al*. 2023).

Feedback effectiveness is an inherently multi-dimensional concept in nature. Chen (2025) says the students' reception of feedback depends heavily on messages' clarity, timeliness, relevance, and communication tone. In the context of AI-driven feedback, these dynamics are further mediated by the nature of the student-tool interaction, prompt specificity, and the student's independent interpretative capacity. Assessing ChatGPT's efficacity as a feedback agent therefore requires considering both its technical attributes and its pedagogical-communicative dimensions (Hooda *et al*. 2022).

Empirical data capturing student perceptions of and attitudes toward ChatGPT are expanding rapidly. Abdalgane *et al.* (2026) observed that students highly value the immediacy and articulateness of AI-generated responses, particularly during writing and problem-solving tasks. Similarly, Vinnikova *et al.* (2025) found that ChatGPT is predominantly utilized for academic consultation, verification, and structural orientation. However, the perceived utility of AI feedback is strongly moderated by a

student's baseline digital competencies, disciplinary mastery, and individual learning styles (Dringó-Horváth *et al*., 2025). These divergent variables underscore the critical need for university students and ChatGPT usage (Dorobăț and Corbea, 2025)

1.1 Literature review: Contextualizing Albanian scholarly contributions

Within the expanding global body of literature, Albanian researchers have focused heavily on the domestic higher education landscape, a context characterized by evolving digital infrastructures, progressive smart-campus initiatives, and highly variable student exposure to technology-enhanced learning (Stana *et al*. 2024; Tabaku and Duci, 2025).

Çerkini *et al*. (2025) investigated the attitude of 554 university students across public and private institutions in Kosovo towards AI practices, issues, and institutional policy in a system transitioning to e-learning. The results showed that students who lacked a formal AI education or institutional advice experienced significantly greater technical and operational difficulties when interacting with AI platforms. Conversely, positive perceptions of institutional AI frameworks were strongly correlated with higher rates of adoption. Crucially, the researchers reported no statistically significant differences across gender or age demographics, suggesting uniform baseline access and acceptance during cross-institutional digital transitions.

Concurrently, by Hoxhalli *et al*. (2025) explored the first-year undergraduate students' functional attitudes and ethical perceptions regarding ChatGPT. While the researchers identified a high baseline familiarity with AI systems (95.7%), usage frequencies varied considerably: 45.16% of respondents utilized the tool occasionally, 24.73% weekly, 17.20% daily, and 12.90% reported never using it. Furthermore, the cohort expressed pronounced ethical anxieties, specifically highlighting the risks of structural plagiarism, cognitive over-reliance, and the potential erosion of independent critical thinking skills.

To quantify these educational impacts, Guga and Binjaku (2025) deployed an experimental design to evaluate the direct effects of ChatGPT on learning performance. Students were instructed to acquire specific curricular concepts exclusively through ChatGPT interaction; their subsequent assessment scores were then evaluated against their cumulative grade point averages (GPAs). Descriptive statistics revealed a relatively

low performance threshold when the AI tool was utilized in isolation (M = 5.94/10). Furthermore, correlational analysis indicated that performance during ChatGPT-assisted learning did not statistically depend on a student's baseline academic history (p = 0.683; r = 0.157). The authors concluded that outcomes in AI-mediated learning environments are not predetermined by prior academic achievement but are instead mediated by secondary operational variables, such as prompt engineering quality and task complexity.

Synthesizing these regional perspectives reveals a high overall adoption rate and a generally receptive attitude toward AI integration among Albanian student cohorts. However, empirical consensus regarding AI's pedagogical efficacy remains fragmented, ethical frameworks are still nascent, and institutional support mechanisms remain incomplete. These systemic gaps underscore the critical necessity of investigating how distinct, real-time feedback patterns correlate with objective student evaluations of feedback quality, clarity, and utilitarian applicability (Kosova *et al*. 2025; Xhako *et al*. 2025).

2. MATERIALS AND METHODS

2.1 Research Design

This study employs a quantitative, non-experimental, cross-sectional, and correlational design. The primary objective was to investigate the magnitude and direction of the relationship between two composite variables, the frequency of ChatGPT usage and perceived feedback effectiveness, without the implementation of an intervention or the manipulation of experimental conditions.

Research Question: Is there a statistically positive relationship between the frequency of ChatGPT usage for academic feedback and the student perception of academic feedback effectiveness among university students at University, Aleksandër Moisiu, Durrës (UAMD)?

Hypothesis (H1): There is a significantly positive relationship between the frequency of using ChatGPT as an academic feedback source and student attitudes toward feedback effectiveness (H1: $\rho > 0$, $p < .05$).

2.2 Participants and Sampling

The study involved 350 undergraduate students enrolled in the second semester of the 2024–2025 academic year at the Faculty of Information Technology and the Faculty of Business Studies at UAMD.

The sample included 116 female participants (33.1%) and 234 male participants (66.9%), with ages ranging from 18 to 27 years (M = 21.3, SD = 2.1). In terms of academic progression, 38.0% of participants were in their second and 34.6% in their third year, ensuring a broad range of academic experience. Participation was strictly voluntary; all subjects were provided with a detailed study briefing and submitted informed consent prior to data collection.

Data were collected via a 15-item structured online questionnaire administered through Google Forms consisting of two subscales:

- Subscale 1 (8 items): measured the frequency and specific types of academic feedback that students received from ChatGPT.
- Subscale 2 (7 items): Evaluated student-involved perceptions of feedback across five qualitative dimensions: clarity, applicability, reliability, and supplementary value.

Both subscales utilized a five-point Likert-type scale, ranging from 1 (Strongly Disagree/Never) to 5 (Strongly Agree/Always).

2.3 Data Analysis Procedures

Statistical processing was conducted using Python (v3.10) for data cleaning and organization (Pandas library) and JAMOVI (v2.6.44) for inferential statistics. The analytical workflow followed four logical steps.

1. Descriptive analysis: Individual items and composite scores were calculated using means (*M*), standard deviations (*SD*), and range (minimum/maximum) values. Composite scores were generated by calculating the arithmetic mean of constituent items, resulting in continuous scores (theoretical range 1.00 - 5.00).
2. Normality testing: Distributional normality was assessed using the Kolmogorov-Smirnov test, which was selected over the Shapiro-Wilk test due to its superior power for large sample sizes. (n=350).
3. Inferential correlation**:** Following the rejection of the normality assumption for both composite variables ($p < .001$), the non-parametric Spearman rank-order correlation coefficient (ρ) was employed. To ensure robustness, 95% confidence intervals were generated using bootstrapping (1,000 iterations). Effect sizes were interpreted according to Cohen's (1988) benchmarks: weak ($\rho < .30$), moderate ($.30 \leq \rho < .60$), and strong ($\rho \geq .60$).
4. Level Diagnostics: Spearman correlations were calculated between individual usage items and the composite perception score to

identify specific patterns driving feedback satisfaction. Internal consistency for both subscales and the aggregate instrument was verified using Cronbach's alpha (α), applying the threshold criteria where $\alpha \geq 0.70$ is acceptable $\alpha \geq 0.80$ is good (Nunnally, 1978). The significance level for all statistical tests was set at $\alpha = 0.05$.

3. RESULTS AND DISCUSSIONS

3.1 Instrument reliability and psychometric evaluation

To ensure the empirical viability of the research instrument, internal consistency was evaluated prior to inferential testing. The aggregate 15-item scale demonstrated high reliability, yielding an overall Cronbach's alpha (α) of 0.92 (Table 1).

Table 1. Internal Consistency and Scale Descriptive Statistics (n = 350)

Scale	Number of Items	Cronbach's α	Mean (M)	SD
ChatGPT Use	8	0.91	3.24	0.80
Perceived Feedback Effectiveness	7	0.89	2.76	0.74
Full Instrument (15 items)	15	0.92	—	—

Note. α = coefficient of alpha Cronbach; M = composite scale mean; SD = standard deviation.

At the subscale level, both the *ChatGPT use* dimension ($\alpha = 0.91$) and the *Perceived Feedback Effectiveness* dimension ($\alpha = 0.89$) comfortably exceeded the standard psychometric threshold of 0.70 established by Nunnally (1978). This confirms that the internal indicators are highly stable and reliable, providing a sound baseline for assessing student behaviours and attitudes.

3.2 Distributional Normality and Model Selection

The distributional properties of the two primary composite scores were evaluated using the Kolmogorov–Smirnov test to guide the choice between parametric and non-parametric inferential models.

Table 2. Kolmogorov–Smirnov Normality Test Results for Composite Variables (n = 350)

Variable	Test	Statistic (D)	df	p-value
ChatGPT Use (composite)	Kolmogorov–Smirnov	0.071	350	< .001
Perceived Feedback Effectiveness (composite)	Kolmogorov–Smirnov	0.058	350	< .001

Note. Significance threshold α = .05. Both distributions deviate significantly from normality, warranting non-parametric analysis.

The results revealed significant departures from normality for both the *ChatGPT Use* composite (D = 0.071, $p < .001$) and the Perceived Effectiveness composite ($D = 0.058$, $p < .001$). Because the assumption of normality was rejected, parametric testing was deemed inappropriate. Consequently, the non-parametric Spearman rank-order correlation coefficient (ρ) was selected as the primary inferential tool, ensuring robust calculations that are less sensitive to distributional skewness.

3.3 Evaluation of ChatGPT Usage Patterns

Descriptive analysis of the *ChatGPT Use* subscale revealed an overall composite sample mean of 3.24 (SD=0.80) (Table 3).

Table 3. Descriptive Statistics for the ChatGPT Use Subscale (n = 350)

Item	**Mean**	**SD**	**n**
I use ChatGPT frequently for academic tasks.	3.20	1.26	350
I use ChatGPT to get feedback on my written assignments.	2.91	1.44	350
I use ChatGPT to improve my answers before submission.	3.23	1.33	350
I use ChatGPT to clarify theoretical concepts or academic doubts.	3.57	1.29	350

I use ChatGPT to check the structure or format of my assignments.	3.31	1.49	350
I use ChatGPT to get specific suggestions for improvement.	3.57	1.33	350
I use ChatGPT to identify errors in completed assignments.	3.60	1.48	350
I use ChatGPT as a supplement to professor feedback.	2.54	1.34	350
Scale mean (use subscale).	3.24	0.80	350

Note. SD = standard deviation. Scale: 1 = Never; 2 = Rarely; 3 = Sometimes; 4 = Often; 5 = Very Often. The scale mean is the arithmetic mean of all 8 items.

An item-level analysis indicated that student interactions are highly targeted. The highest mean scores were recorded for localized diagnostic and corrective tasks: identifying specific errors in completed drafts (M = 3.60, SD = 1.48), clarifying complex theoretical concepts (M = 3.57, SD = 1.29), and eliciting structured suggestions for structural revisions (M = 3.57, SD = 1.33).

As illustrated in Figure 1, the sample exhibits a clear functional tilt toward self-directed diagnostic adjustments. Conversely, using the AI tool to directly supplement formal instructor feedback yielded the lowest score (M=2.54, SD=1.34) This indicates that students do not view generative AI as a bridge to institutional evaluation pathways but rather as an independent workspace for real-time text and conceptual troubleshooting.

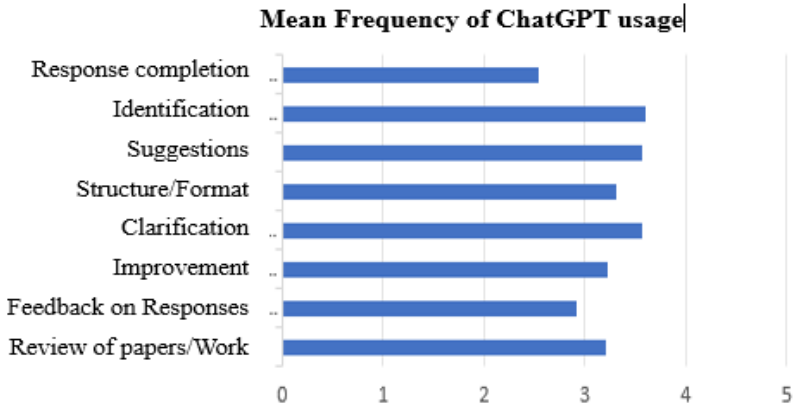

Fig. 1. Mean frequency of ChatGPT use by task.

3.4 Student perceptions of AI feedback efficacy

The composite mean for the *Perceived Feedback Effectiveness* subscale was 2.76 (SD = 0.74), positioning the aggregate cohort opinion slightly below the scale midpoint (Table 4).

Table 4. Descriptive Statistics for the Perceived Feedback Effectiveness Subscale (n = 350)

Item	Mean	SD	n
ChatGPT's feedback helps me understand my mistakes.	2.91	1.34	350
ChatGPT's suggestions are applicable to my academic tasks.	2.86	1.14	350
The use of ChatGPT supports my independent learning.	2.71	1.18	350
I trust the quality and accuracy of feedback provided by ChatGPT.	2.49	1.17	350
ChatGPT complements the feedback I receive from my instructor.	2.29	1.13	350
ChatGPT's comments are clear and understandable.	3.00	1.31	350
ChatGPT's responses are aligned with my questions.	3.09	1.04	350
Scale mean (perception subscale)	2.76	0.74	350

Note. Scale: 1 = Strongly Disagree; 5 = Strongly Agree.

Item-level metrics revealed that students rate the structural and linguistic execution of the model favourably, specifically highlighting prompt-to-response alignment (M = 3.09, SD = 1.04) and the clarity of explanations (M = 3.00, SD = 1.31). However, trust in the accuracy of the output (M = 2.49, SD = 1.17) and the platform's capacity to complement instructor guidance (M = 2.29, SD = 1.13).

As visualized in Figure 2, there is a clear conceptual divide between operational utility and deep pedagogical trust. Students appreciate the clear formatting and immediate responsiveness of the AI, but they remain cautious regarding its authority and accuracy. This caution is reflected in

the lower scores for items measuring trust and instructional complementarity.

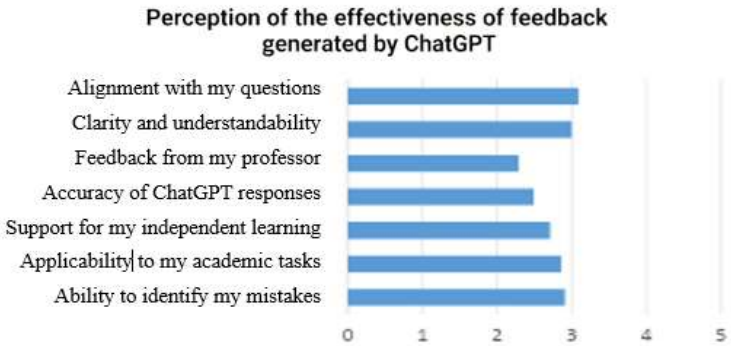

Fig. 2: Perception of the effectiveness of feedback

3.5 Bivariate and item-level inferential analysis

To test the primary research hypothesis (H_1), a bidirectional Spearman rank-order correlation was calculated using the two aggregate composite dimensions. Results are presented in Table 5.

Table 5. Spearman Rank-Order Correlation Between ChatGPT Use and Feedback Effectiveness (perceived) (n = 350)

Variables	ρ	p-value	95% CI (lower)	95% CI (upper)	n
ChatGPT Use × Perceived Effectiveness	0.665	< .001	0.603	0.721	350

Note. ρ = Spearman rank-order correlation coefficient; CI = confidence interval (bootstrap, 1,000 iterations); significance threshold α = .05.

A statistically significant, strong positive correlation was confirmed between the variables ($\rho = 0.665$, $p < .001$, 95% CI [0.603, 0.721]), providing robust empirical validation for H_1. As shown in the scatter plot (Figure 3), despite normal variance among moderate users, a clear linear trajectory indicates that increased exposure and frequent interaction with

the platform strongly co-vary with higher student ratings of its formative assessment capabilities.

To analyse the specific factors driving this relationship, item-level Spearman correlations were evaluated between individual usage items and the overall perception score.

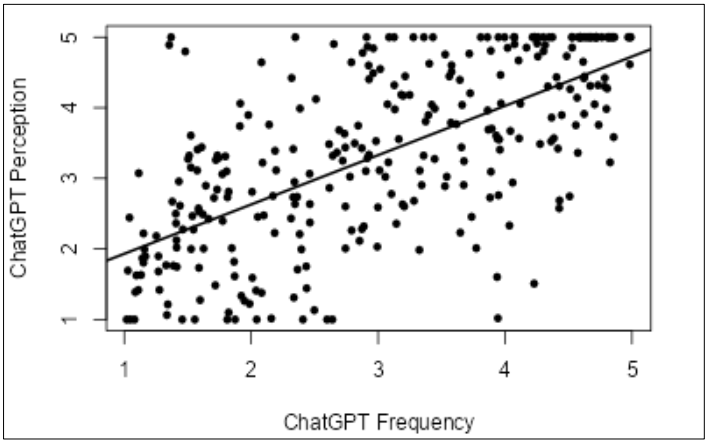

Fig. 3. Correlation between the degree of ChatGPT usage and the feedback effectiveness perception.

The item-level matrix reveals a precise functional hierarchy. Active diagnostic tasks show the strongest relationships with positive effectiveness perceptions, led by error identification (ρ=0.61), suggestion-seeking (ρ=0.58), and real-tim

e concept clarification (ρ=0.57). Conversely, using the platform as a supplement to formal instructor guidance produced the weakest relationship

Table 6. Item-Level Spearman Correlations Between Individual Use Patterns and Perceived Effectiveness of Feedback (n = 350)

Item (Use subscale)	ρ with perception	p-value	Interpretation
Identify errors in completed assignments.	0.61	< .001	Moderate–Strong
Get specific suggestions for improvement.	0.58	< .001	Moderate

Clarify theoretical concepts / academic doubts	0.57	< .001	Moderate
Improve answers before submission.	0.55	< .001	Moderate
Check the structure or format of assignments.	0.49	< .001	Moderate
Get feedback on written assignments.	0.47	< .001	Moderate
Frequent general academic use	0.44	< .001	Moderate
Supplement to professor feedback.	0.38	< .001	Weak–Moderate

Note. All correlations are significant at $p < .001$. Strength thresholds: weak < 0.30; moderate 0.30–0.59; strong ≥ 0.60 (Cohen, 1988).

3.6 Synthesis and theoretical interpretation

The strong positive correlation (ρ=0.665) between usage frequency and perceived effectiveness supports a learning-curve framework. As students interact more frequently with large language models, they likely develop greater prompt-engineering literacy. This evolving skill allows them to move past superficial queries and extract highly customized, contextual, and actionable feedback tailored to their specific coursework needs.

The item-level hierarchy further refines this interpretation by highlighting the role of student agency. Active diagnostic interactions—where a student provides a draft and runs specific, targeted queries—yielded the strongest correlation coefficients. This pattern aligns directly with self-regulated learning theory (Rosales-Marquez *et al.* 2023), demonstrating that students use generative AI primarily as an independent workspace for metacognitive monitoring and error tracking before submitting their assignments for final evaluation.

Conversely, the drop in scores for instructor-supplementary items (M = 2.54, ρ = 0.38) shows that students maintain a sharp distinction between the operational convenience of automated text editing and the pedagogical

authority of human instructors. While students rely on ChatGPT to clean up mechanics and clarify unfamiliar terms, they do not view it as a substitute for the specialized judgment, contextual grading, or institutional validation provided by faculty members.

3.7 Contextual evaluation within Albanian higher education

These patterns carry distinct regional implications within the current Albanian higher education landscape, specifically at the University, Aleksandër Moisiu, Durrës. The moderate baseline usage score (M = 3.24) paired with a cautious perception mean (M = 2.76) shows that while Albanian undergraduate students are actively adopting generative AI tools, they maintain a degree of critical scepticism. This cautious approach matches recent findings by Tabaku and Duci (2025), who observed that Albanian consumers regularly embrace AI platforms for immediate functional tasks but are highly hesitant to rely on automated systems for high-stakes evaluations or tasks requiring deep institutional trust.

This cautious behaviour is further shaped by local institutional frameworks. At the time of data collection, UAMD had no formalized institutional AI policies or regulatory guidelines governing the use of generative tools in student assignments. This regulatory vacuum helps explain the wide variance in individual usage styles (SD = 1.48 for error identification), as students are left to navigate these platforms independently. This pattern reflects the broader technological trends documented by Kosova and Krasniqi (2025), who characterized the current digital transition in Albania's academic and professional sectors as an informal, decentralized diffusion process driven by individual initiative rather than institutional mandate.

3.8 Study Limitations and Future Directions

Several limitations should be considered when interpreting these results:

- **Design constraints:** The cross-sectional, non-experimental design prevents drawing causal inferences. The observed correlations can be explained by two competing pathways: regular platform interaction may improve a student's prompt skills and lead to better feedback experiences, or students who already hold positive views

of technology may simply use the tool more frequently. Experimental or longitudinal designs are needed to isolate these developmental paths.

- **Methodological bias:** Data collection relied entirely on self-reported questionnaires, which are vulnerable to social desirability and recall biases. Students may over- or under-report their AI usage based on perceived faculty approval or academic integrity concerns. Future research should integrate objective telemetry, such as platform interaction logs, alongside self-reports.
- **Sampling limitations:** This study utilized non-probability purposive sampling within a single public institution (UAMD), focusing on two specific faculties (Information Technology and Business Studies). While appropriate for this exploratory phase, these constraints limit the generalization of findings to the broader Albanian student population. Collaborative multi-institutional studies covering humanities, medical sciences, and arts tracks are required to build a nationally representative dataset.
- **Construct scope:** This study measured *perceived* feedback effectiveness rather than *actual learning* outcomes. While positive student perceptions are necessary for tool adoption, they do not automatically translate into improved academic performance, deeper conceptual mastery, or higher grade point averages. Future research should pair perception scales with objective performance diagnostics to measure the true impact of AI feedback on student learning outcomes.

5. CONCLUSIONS

This study investigated the association between the frequency of ChatGPT usage as an academic feedback tool and undergraduate students' perceptions of its effectiveness among a sample of 350 students from the University, Aleksandër Moisiu, Durrës, Albania. The empirical evidence supported the central hypothesis (H_1), revealing a statistically significant, strong positive correlation (ρ=0.665, p<.001) between usage frequency and perceived feedback effectiveness. This primary result suggests that as students gain regular exposure to the platform, they likely develop the tactical prompting skills necessary to extract more valuable formative utility from generative artificial intelligence.

Descriptively, while students maintained a moderate level of overall baseline engagement with the platform (M=3.24), their aggregate evaluation of its systemic feedback effectiveness sat slightly below the scale midpoint (M=2.76). Item-level analyses clarified this divergence by uncovering a distinct functional hierarchy. Students responded most favourably to highly targeted, task-corrective, and metacognitive support functions—such as localized error identification, real-time conceptual clarification, and structured suggestions for structural revisions. These self-directed behaviours strongly align with self-regulated learning (SRL) theory, demonstrating that students treat the language model as a useful workspace for independent editing and conceptual debugging.

Conversely, the lowest scores were consistently recorded for items measuring trust in output accuracy and the tool's capacity to complement formal instructor guidance. This drop reveals a clear epistemic boundary in the student mindset: undergraduates value ChatGPT as a highly responsive, automated task-level assistant, but they do not view it as a legitimate or authoritative replacement for human instruction. They actively utilize its operational speed to clean up mechanics, yet they continue to reserve primary pedagogical authority for faculty members.

These insights offer several clear practical implications for higher education institutions:

- **Institutional Frameworks:** University administrations should develop explicit, structured pedagogical guidelines that formally position generative AI platforms as formative, supplementary toolkits rather than direct replacements for faculty evaluation.
- **Literacy Initiatives:** Explicit digital and AI literacy programs should be integrated into the curriculum. These initiatives are especially vital for students with limited prior exposure, ensuring that student engagement with automated systems remains critical, reflective, and anchored in academic integrity.
- **Optimizing Faculty Bandwidth:** Instructors can strategically leverage ChatGPT's comparative advantages—namely its absolute immediacy and 24/7 availability—by encouraging students to use it for initial mechanical and structural editing. This shift can free up valuable faculty bandwidth, allowing instructors to focus their feedback on higher-order conceptual depth, nuanced disciplinary critiques, and the relational dimensions of academic mentoring.

To build upon these exploratory findings, future research should move past cross-sectional designs and deploy experimental or longitudinal frameworks. Such approaches are necessary to determine whether the perceived feedback utility documented here actually translates into objective, measurable learning gains over time. Additionally, mixed-method studies incorporating qualitative data on specific student prompting strategies would help clarify the exact mechanisms driving the correlation between usage and perceived value. Finally, multi-institutional comparative research across Albania and the broader Western Balkan region is needed to test the generalizability of these dynamics, providing a valuable regional benchmark as evolving large language models continue to reshape the global higher education landscape.

Acknowledgements

The authors express their sincere gratitude to the undergraduate students from the Faculty of Information Technology and the Faculty of Business Studies, University, Aleksandër Moisiu, Durrës, Albania for their voluntary participation and cooperation throughout the data collection process.

Authors' contribution. E. T.: conceptualization, methodology, data collection, formal analysis, and writing—original draft preparation. A. M. K.: literature review; validation; writing, review, and visualization. R. K.: statistical consultation, validation, and writing—review and editing; E. Sh.: data collection and formal analysis.

All authors have read and agreed to the published version of the manuscript.

Declaration of generative AI use. The authors declare that generative Artificial Intelligence (AI) tools or large language models were not utilized in the conceptualization, drafting, or formal writing of this manuscript. Standard statistical analysis programs and word-processing software were used exclusively for data processing and structural formatting.

Ethical considerations. This study was conducted in accordance with institutional guidelines for research involving human participants. Participation was entirely voluntary, and data anonymization was strictly maintained. Formal ethical approval from an institutional human subjects or animal welfare committee was not required for this non-invasive, survey-based research design.

Data availability statement. The anonymized dataset and statistical outputs supporting the findings and conclusions of this study are available from the corresponding author upon reasonable request.

Funding. This research received no specific grant or financial support from any funding agency in the public, commercial, or not-for-profit sectors.

Conflict of interest. The authors declare that they have no known competing financial interests or personal relationships that could have appeared to influence the work reported in this paper.

REFERENCES

AbdAlgane M, Ali R, Othman K, Ibrahim I, Alhaj M, Ali, E, Allehyani F. 2026. Exploring AI-generated texts vs. human-written texts in EFL academic writing: A case study of Qassim University in Saudi Arabia. *World*, **16(2):** 114-131. https://doi.org/10.5430/wjel.v16n2p114 .

Ahmedtelba E. 2025. Critical integration of generative AI in higher education: Cognitive, pedagogical, and ethical perspectives. *London Journal of Research in Humanities and Social Sciences*, **25(13):** 1-12. https://doi.org/10.34257/LJRHSSVOL25IS13PG1.

Al Amri H, Atta A, Nawaz N. 2025. Lost in translation revisited: Timely teacher feedback and the academic writing performance of Omani EFL undergraduates. *Journal of Arts and Linguistics Studies*, **3(4):** 5303-5331. https://doi.org/10.71281/jals.v3i4.475.

Alam A, Mohanty A. 2023. Educational technology: Exploring the convergence of technology and pedagogy through mobility, interactivity, AI, and learning tools. *Cogent Engineering*, **10(2):** 2283282. https://doi.org/10.1080/23311916.2023.2283282

Baskara FR. 2025. ChatGPT and google Gemini in EFL education: A qualitative exploration of pedagogical efficacy among Indonesian Sophomores. *Journal of Languages and Language Teaching* (JOLLT), **13(1):** 436-447. https://doi.org/10.33394/jollt.v13i1.9926.

Çerkini B, Bajraktari, Çibukçiu B, Ramadani F, Zejnullahu F, Hajdini L. 2025. Artificial intelligence in higher education: Student perspectives on practices, challenges, and policies in a transitional

context. *Frontiers in Education*, **10**: 1700056. https://doi.org/10.3389/feduc.2025.1700056.

Chen, Q. (2025). Students' Perceptions of AI-Powered Feedback in English Writing: Benefits and Challenges in Higher Education. *International Journal of Changes in Education*. https://doi.org/10.47852/bonviewIJCE52025580

Cohen J. 1988. *Statistical Power Analysis for the Behavioural Sciences* (2nd ed.). Hillsdale, NJ: Lawrence Erlbaum Associates, Publishers.

Dorobăț I, Corbea AMI. 2025. Assessing ChatGPT Adoption in Higher Education: An empirical analysis. *Electronics*, **14(23):** 4739. https://doi.org/10.3390/electronics14234739.

Dringó-Horváth I, Rajki Z, Nagy JT. 2025. University teachers' digital competence and AI literacy: Moderating role of gender, age, experience, and discipline. *Education Sciences*, **15(7):** 868. https://doi.org/10.3390/educsci15070868.

Guga I, Binjaku A. 2025. Artificial intelligence in e-learning: An empirical study of ChatGPT as a learning tool. *Karshi Multidisciplinary International Scientific Journal*, **2(2):** 60–64. https://doi.org/10.22105/kmisj.v2i2.89.

Hooda M, Rana C, Dahiya O, Rizwan A, Hossain MS. 2022. Artificial intelligence for assessment and feedback to enhance student success in higher education. *Mathematical Problems in Engineering*, **2022(1):** 5215722. https://doi.org/10.1155/2022/5215722.

Hoxhalli G, Plasari E, Fata I, Baholli I. 2025. Student attitudes and perceptions towards the use of ChatGPT: A study on the ethics and effectiveness of AI in education. *In Proceedings of the International Scientific Conference: Technology & Business Update* (pp. 232–246). Tirana Business University College. https://philarchive.org/archive/KUMCAO-3.

Ilić M, Milić M, Jovičić A. 2021. Characteristics of effective academic feedback in higher education: A systematic review. *Teaching in Higher Education*, **26(7):** 924–940. https://doi.org/10.1080/13562517.2021.1892043.

Kosova AM, Krasniqi M. 2025. The Evolution of Price: From Ancient Value Concepts to Artificial Intelligence. *Interdisciplinary Journal of Research and Development*, **12(3):** 306-315. https://doi.org/10.56345/ijrdv12n333.

Kosova R, Xhafaj E, Gjikaj N, Kosova AM. 2025. Optimizing Survey Data: Factor Reduction with SPSS in STEM Education. *Interdisciplinary Journal of Research and Development*, **12(2 S1):** 8. https://doi.org/10.56345/ijrdv12n2s102.

Nunnally JC. 1978. *Psychometric theory* (2nd ed.). McGraw-Hill.

Nyanjom J, Goh, E, Yang ECL. 2023. Integrating authentic assessment tasks in work integrated learning hospitality internships. *Journal of Vocational Education & Training*, **75(2):** 300-322. https://doi.org/10.1080/13636820.2020.1841821.

Ratten V, Jones P. 2023. Artificial intelligence in education: Perceived usefulness, ease of use, and technology acceptance. *The International Journal of Management Education*, **21(2):** 100796. https://doi.org/10.1016/j.ijme.2023.100796.

Rosales-Marquez A, Cruz-Flores R, Gordillo-Mejía A. 2023. Self-regulated learning and AI-mediated academic feedback: Theoretical convergences and empirical perspectives. *Frontiers in Education*, **8:** 1096640. https://doi.org/10.3389/feduc.2023.1096640.

Sánchez-Prieto JC, Huang, F, Olmos-Migueláñez S, García-Peñalvo FJ, Teo T. 2024. Factors influencing the perception of AI feedback effectiveness: Clarity, timing, and applicability. *Computers in Human Behaviour*, **152**, 107889. https://doi.org/10.1016/j.chb.2023.107889.

Stana A, Kosova R, Rista A. 2024. Benefits of using ICT tools in higher education institutions in Albania. *In 2024 5th international conference on communications, information, electronic and energy systems* (CIEES), (pp. 1-6). IEEE. https://doi.org/10.1109/CIEES62939.2024.10811268.

Tabaku E, Duçi E. 2025. Optimizing High Availability in Educational Systems Using Xen Paravirtualization. *Journal of Educational and Social Research*, **15(2):** 205. https://doi.org/10.36941/jesr-2025-0054.

Tan S. 2023. Harnessing artificial intelligence for innovation in education. In *Learning intelligence: Innovative and digital transformative learning strategies: Cultural and social engineering perspectives* (pp. 335-363). Singapore: Springer Nature Singapore. https://doi.org/10.1007/978-981-19-9201-8_8 .

Vinnikova N, Bondarenko L, Karpenko A, Mankovska I. 2025. ChatGPT in educational and scientific activities of Grinchenko University: A diagnostic section. *In Environment, Technology,*

Resources. Proceedings of the International Scientific and Practical Conference (**3**, pp. 349-359). https://doi.org/10.17770/etr2025vol3.8514.

Xhako D, Hyka N, Gjevori, A, Muda V, Duro C, Demirneli M, Hoxhaj S. 2025. The level of AI application in university STEM study programs: A comprehensive review. *International Journal of Innovative Technology and Interdisciplinary Sciences*, **8(4):** 1244-1283. https://doi.org/10.15157/ijitis.2025.8.4.1244-1283.

Yigci, D, Baysura OD, Özbay F, Kesli EC. 2025. ChatGPT as a generative AI agent in educational contexts: Contextualized, coherent, and personalized responses. *Education and Information Technologies*, **30(1):** 1201–1225. https://doi.org/10.1007/s10639-024-12750-4.

ISSN 2074-0867
EISSN 3135-1115